ISAS - INTERNATIONAL SCHOOL FOR ADVANCED STUDIES

Cosmologies with a dynamical vacuum energy

CANDIDATE
Francesca Perrotta

SUPERVISORS
Prof. Luigi Danese
Prof. Sabino Matarrese

Thesis submitted for the degree of *"Doctor Philosophiæ"*.
Academic Year 1999/2000

SISSA - SCUOLA INTERNAZIONALE SUPERIORE DI STUDI AVANZATI
TRIESTE
Via Beirut 2-4

TRIESTE

Cosmologies with a dynamical vacuum energy

CANDIDATE
Francesca Perrotta

SUPERVISORS
Prof. Luigi Danese
Prof. Sabino Matarrese

Thesis submitted for the degree of *"Doctor Philosophiæ"*.
Academic Year 1999/2000

"We shall not cease from exploration and the end of all our exploring will be to arrive where we started and know the place for the first time."

T. S. Eliot

Abstract

The possibility of a nonzero cosmological constant has been invoked several times in the past, both for theoretical and observational motivations. It has been often discarded by particle physicists, due to the huge difficulties in justifying a value of vacuum energy tiny enough to allow the universe to survive more than 10^{-41} s after the Big Bang. At present, the cosmological constant problem is still, probably, the most ununderstood issue of the physics.
However, in recent times, it has again come into vogue, and again as a consequence of a number of observational evidences. Despite their apparent simplicity, the results of observations of more than 40 distant type 1A supernovae seem to converge on the astonishing evidence that the present expansion of the universe is accelerating; this fact, together with many other experimental evidences of a low-density universe, and with the most recent CMB data indicating that the universe is very near to the flatness, has opened again the difficult question of what is the unobserved energy component that would balance a low-density universe with a flat one.
At the same time, a new branch of cosmology has been opened, involving scalar fields as candidates for such "missing" energy. Motivated by the difficulties of cosmological constant models and by the most recent observational case of an accelerating universe, many alternative scenarios have been proposed: amongst them, the Quintessence scenarios, which are the subject of this thesis.
In these models, the "missing energy" should reside in a dynamical scalar field rather than in a pure vacuum state; the dynamics of the field plays an important role, since the field energy density can adjust in a way that it comes to dominate at late times.
The most important and distinctive feature of a scalar field vs. a cosmological constant, is that a field will develop fluctuations, that interact gravitationally with those of matter. To obtain the correct predictions of their impact on the Cosmic Microwave Background radiation and on the evolution of perturbations, the formalism of linear perturbation theory must be widely used.
In this thesis we will focus on some basic issues connected with the attempt to build predictions on the cosmological impact of such scalar fields, following the results discussed in refs. [173, 174, 10, 15].
The first chapter is introductory and aims at giving an overview of the current observational evidences from which the case of a positive non-zero vacuum energy arises, motivating the consideration of the cosmological constant problem. In Chapter 2, the gauge-invariant formalism of linear cosmological perturbation theory is described, with particular attention to quantities such as the gravitational potentials, entropy and curvature perturbations, which are used in the following of the thesis.
In Chapter 3 we recall some basic ideas on the mechanisms that generated the observed Cosmic Microwave Background of radiation, whose small but detectable anisotropies contain a large amount of information on the history of the Universe. In particular, CMB anisotropies turned out to be a very rich ground of investigation for discriminating between Quintessence and cosmological constant scenarios.
These chapters set the framework for the results that will be presented in the following chapters, containing the original work of the thesis.
In Chapter 4, focusing on scalar-type perturbations, we settled the analytical initial conditions that must be imposed on the components of cosmic fluid involving a minimally-coupled scalar field, in order to produce purely adiabatic or purely isocurvature initial conditions on super-horizon scales. Thus, an interesting comparison with the "standard" pure CDM flat model is performed. The distinctive imprints of Quintessence on large scale structure and on CMB anisotropies, both of polarization and temperature, are extensively analyzed.
Chapter 5 extends the concept of Quintessence to a larger class of scalar fields, having an explicit coupling with the Ricci scalar in the Lagrangian. These more general models, here named "Extended Quintessence", are shown to enrich the phenomenology with respect to the simple minimally-coupled

Quintessence. In fact, the predictions for the CMB anisotropies show new distinctive features, directly related to the presence of a non-zero coupling of the field with the gravitational sector of the Lagrangian and, ultimately, with the time-variation of the gravitational constant.
A problem of "fine tuning" is however inherent both to cosmological constant and quintessence models: in order to have today an amount of vacuum energy comparable with that of matter, the vacuum energy density should have been initially vanishingly small.
A way out to such fine tuning problem is possible in Quintessence scenarios, where one can select a subclass of models which admit "tracking solutions". This means that the present value of scalar field energy density, once fixed, can be determined starting from a very wide set of initial conditions, even though the tracking solutions are not perfect attractors and do not solve the problem of why the field energy density should have this value just today.
Chapter 6 considers tracking behaviors in Extended Quintessence scenarios and presents a description of the rich phenomenology that arises from the corresponding dynamics; in particular, we show that the coupling with the Ricci scalar can act initially as an effective potential pushing the field in the tracking trajectory ("R-boost"). The dependence of the phenomenology on the sign of the coupling constant is also described.
Finally, Chapter 7 presents the conclusions and faces the future observational perspectives, on the light of the most recent data from MAXIMA and BOOMERANG-98 balloon experiments and of the future satellite missions MAP and Planck.

Contents

Chapter 1

The missing energy problem

1.1 Introduction

One of the great developments of the 1980's was the creation of a "Standard" Cold Dark Matter model (sCDM) of Cosmology, based on ideas arising from Particle Physics, with energy density contribution in matter $\Omega_m = 1$, no cosmological constant and a near-Zel'dovich spectrum of primordial fluctuations [25]. This model brings together the idea of inflation [99, 144, 5] and the picture of large scale gravitational collapse [168] .
For many years, such cosmology has been regarded as the most attractive one; however, in the last decade, observational cosmology has made tremendous strides, and the standard CDM model proved unable to simultaneously match a series of observational evidences on different scales. Matching its predictions to COBE measurements of the microwave background, one finds that the amplitude of fluctuations on $8h^{-1}$ Mpc scales (where h is the Hubble constant today in units of 100 km/s/Mpc) do not match those observed (measured through rich galaxy cluster abundance). Furthermore, not only the amplitude, but also the scale dependence of the fluctuation spectrum in the sCDM differs from the measured galaxy correlation function [165].
These failings of sCDM have led to many attempts to improve it, while keeping its basic features intact; the latter are associated with its theoretical motivation from inflation. On one hand, all simple inflationary models predict that the universe is flat, i.e. its curvature is zero or negligibly small. Meanwhile, the inflationary paradigm is the only known solution to the horizon and flatness problem: if $\Omega_{total} \neq 1$, the canonical prediction of inflation would be incorrect and we would have to understand how inflation, or another theory, might address the fine tuning required to solve the flatness problem without actually restricting in a flat universe today. On the other hand, in recent times, a growing evidence for a low-density universe has come from many independent sources: the recent trends in cosmology push towards a value of $\Omega_m \sim 0.3$, a value suggested from many independent estimates on various scales. Dynamical estimates of the mass density on the scale of galaxy clusters suggest that $\Omega_m = 0.2 \pm 0.1$ for the matter that clusters gravitationally [39]. Other independent observations appear to converge to the evidence that we are living in a low-density universe.
Furthermore, the most recent CMB data [138] from BOOMERANG indicate that the universe is actually very near to the flatness, according to the inflationary paradigm.
These observational evidences motivated a revival of the cosmological constant; the cosmological constant, indicated with Λ, was originally introduced [72] in order to allow static homogeneous solutions to Einstein's equations in the presence of matter, and then it turned out to be unnecessary when the expansion of the universe was discovered [114]. However, the cosmological constant has had a very long and tortured history ever since, being periodically invoked by cosmologists as an explanation of a set of observations, and then quickly forgotten when the observational case evaporated.
Detailed reviews on the effects of Λ in cosmology can be found in [40, 188, 65, 52].
We are now in a situation that at least suggests the presence of a vacuum energy component in the universe; first, a cosmological constant would be one way to resolve the discrepancy between the low observed value of Ω_m and $\Omega_{total} = 1$ as predicted from inflation.

A second motivation for the cosmological constant revival has been the need to have the age of the Universe, t_0, exceeding the age of globular clusters in our galaxy; the limits on t_0 are holding at about 13 Gyr or more [119], and when combined with current estimates of the Hubble expansion parameter $H_0 \approx 65.2 \pm 1.3$km/sec/Mpc [182], give rise to an observed value of the "expansion-age" parameter $H_0 t_0 \simeq .9$, significantly higher than that predicted by the sCDM. Preserving the flatness of the Universe, its age could be enhanced by lowering the matter content in models involving a component whose equation of state is different from matter and radiation, for example models including a cosmological constant.
Most importantly, quite strong evidence for a positive cosmological constant comes from the analysis of high-redshift type 1A Supernovae [171, 172, 89, 182], that placed a constraint on the difference $\Omega_m - \Omega_\Lambda$ [140] through the measure of the "deceleration parameter". The surprising result is that the sCDM is strongly ruled out by the Supernovae data, that instead appear to favor a positive cosmological constant at a quite high confidence level.
If this result is confirmed, we should be currently entering a period of cosmological inflation, that is typically interpreted as evidence for a cosmological constant.
Despite the apparent successes of the cosmological constant models, they still face several difficulties on their own. At the present, no one can explain why the vacuum energy density of the universe, $\rho_\Lambda \equiv \Lambda/8\pi G$ should be of the order $(10^{-3}eV)^4$, as it must be to have a cosmological impact ($\Omega_\Lambda \sim 1$); instead, on dimensional grounds, one would expect it to be many orders of magnitude larger, of order m_{Pl}^4 or perhaps m_{SUSY}^4. A vacuum energy density of order $(10^{-3}eV)^4$ appears to require cancelation between large numbers to very high precision. In addition, it implies that we are observing the universe just at the special epoch when $\Omega_m \sim \Omega_\Lambda$. The unnatural size of Λ suggested by the data gives rise to the question of whether the data supports some other form of energy density as well: we might plausibly assume that some as yet not understood physical mechanism sets the ultimate vacuum energy of the Universe to zero, but we are faced with figuring out how to explain "missing-energy" values of as much as 70 or 80 percent of critical density.
Motivated by the difficulties of the cosmological constant models, alternative scenarios were proposed in the last years, in which the residual energy density is assumed to reside in the potential energy of some classical scalar field. As far back as ten years ago, Ratra and Peebles [178] considered a cosmology where the scalar field energy density becomes dominant at the present cosmological epoch, finding asymptotically stable equilibrium solutions in which the scalar field energy density dominates the dynamics. The most recent models that involve scalar fields as candidates for the dominant energy component of the present epoch of the universe are often named "Quintessence" models [178, 177, 221, 82, 54, 51, 8, 249, 115, 173, 174, 37, 10, 231, 189, 104, 229] and are a continuation of the original ideas of a "dynamical" vacuum energy [178, 177, 232, 229, 162, 181, 48, 43, 85].
In Quintessence scenarios, the "missing energy" is then associated with the evolution of a scalar field according to its equation of motion: the "quantum-mechanical" vacuum energy is still assumed to be zero, and hence the energy density associated to a Quintessence field is something very different from a "pure" vacuum energy. However, a Quintessence field can mimic a cosmological constant when its kinetical energy is negligible with respect to the potential energy, so that its equation of state approaches -1; such conditions are verified whenever the field is slowly rolling down its classical potential (in a manner analogous to the inflaton field in slow-rolling inflation scenarios), making the potential energy very slowly changing. By this mechanism, a self-interacting scalar field that is presently relaxing towards the minimum of its potential is one way to provide acceleration to the cosmic expansion.
More generally, the "missing energy" can be described in terms of an unspecified equation of state that is different from that of matter and radiation [107, 37, 217]: indeed, the growing evidence of an accelerating Universe from Supernovae testifies that the dominant material in the Universe is characterized by an equation of state that satisfies $\rho + 3p < 0$.
We will refer to Quintessence denoting any component whose properties are well described in terms of the dynamics of a scalar field; furthermore, we assume that such a field couples to ordinary matter only through gravity.
Due to the strongly relativistic nature of such component, the characteristic scale of clustering pro-

cesses for a scalar field is just the horizon, [178] giving a further similarity with a cosmological constant in the undetectability of quintessence energy concentrations on scales smaller than the horizon. The interesting feature of the "quintessence" component is just that, contrary to the cosmological constant, it is time-varying and spatially inhomogeneous, so that it can develop fluctuations which can be relevant in the perturbation growth and can leave a characteristic signature in the CMB and in large scale structure.
We wish to outline the importance of these fluctuations on the light of the future MAP and Planck satellite missions [155],[156], that will allow a determination with very high accuracy of the level of primordial anisotropies imprinted on the last scattering surface: the evolution of the CMB photons is sensitive to the history of the universe, allowing a comparison of CMB observations with Quintessence predictions that could help to discriminate between different models, with a large improvement on current knowledge.

We will now introduce the background equations in FRW cosmologies and review the experimental evidence that leads to the necessity of reconsidering the presence of a substantial vacuum energy component.

1.2 The FRW background equations

In modern cosmology, the universe is described as a perturbed Friedmann-Robertson-Walker (FRW) one. This means that the unperturbed spacetime is spatially homogeneous and isotropic, so that the background metric is assumed to be

$$ds^2 = g_{\mu\nu}dx^\mu dx^\nu = a^2\gamma_{\mu\nu}dx^\mu dx^\nu \ , \tag{1.1}$$

where $a(t)$ is the cosmic scale factor, and the signature is (–,+,+,+). We used units so that $c = 1$. The conformal time τ, defined by $d\tau = dt/a(t)$, corresponds to the metric component $\gamma_{00} = 1$; space and time do not mix ($\gamma_{0i} = 0$) and the purely spatial part (denoted by latin indexes) in spherical coordinates is

$$\gamma_{ij}dx^i dx^j = \frac{dr^2}{1-Kr^2} + r^2(d\theta^2 + \sin^2\theta d\phi^2) \ , \tag{1.2}$$

where K is the spatial curvature that is positive (negative) for a closed (open) universe; for $K = 0$, $\gamma_{\mu\nu}$ takes the form of the ordinary Minkowski metric.
Putting $d\chi = dr/\sqrt{1-Kr^2}$, the metric 1.1 assumes the form

$$ds^2 = a^2d\tau^2 - a^2[d\chi^2 + r^2(\chi)(d\theta^2 + \sin^2\theta d\phi^2)] \quad . \tag{1.3}$$

In the above,

$$r(\chi) = \text{sinn}\ \chi = \begin{cases} \sin(\chi) & \text{if K=1} \quad \text{closed} \\ \chi & \text{if K=0} \quad \text{flat} \\ \sinh(\chi) & \text{if K=–1} \quad \text{open} \end{cases} \tag{1.4}$$

The metric and fluid evolution are determined by the Einstein equations [71],

$$G_{\mu\nu} = 8\pi G T_{\mu\nu} \tag{1.5}$$

The cosmological constant Λ is a dimensionful parameter with units of $(\text{length})^{-2}$ that enters as a possible additional term in the equations of General Relativity (GR):

$$R_{\mu\nu} = -\frac{1}{2}Rg_{\mu\nu} + \Lambda g_{\mu\nu} = 8\pi G T_{\mu\nu} \quad . \tag{1.6}$$

In the FRW spacetime, the energy-momentum tensor of the background matter has a perfect fluid form,

$$T_{\mu\nu} = (\rho + p)u_\mu u_\nu + p g_{\mu\nu} \tag{1.7}$$

where the time-dependent pressure and energy density, p and ρ, respectively, include also the cosmological constant, if present, and $u^\mu = (a^{-1}, 0, 0, 0)$. The Hubble expansion rate of the universe, H, is given at any time by

$$H = \frac{1}{a}\frac{da}{dt} , \tag{1.8}$$

Its value at the present time t_0 is denoted by H_0.
In this thesis, we often make use of the conformal Hubble constant, expressed in terms of the derivative with respect to the conformal time,

$$\mathcal{H} = \frac{1}{a}\frac{da}{d\tau} . \tag{1.9}$$

The background equations, which follow from the Arnowitt-Deser-Misner energy constraint and the Raychaudhury equation respectively, are

$$\left(\frac{\dot{a}}{a}\right)^2 = \frac{8\pi G}{3}a^2\rho - K + \frac{\Lambda a^2}{3}, \tag{1.10}$$

$$\dot{\mathcal{H}} - \mathcal{H}^2 = -4\pi G a^2(\rho + p) + K \quad , \tag{1.11}$$

where the overdot means conformal time derivative.
From these equations we can derive the conservation equation

$$\frac{\dot{\rho}}{\rho} + 3\,(1+w)\,\mathcal{H} = 0 \, , \tag{1.12}$$

where $w = p/\rho$ expresses the fluid equation of state. Let us define

$$\Omega_M \equiv \frac{8\pi G\rho_{M0}}{3H_0^2} \quad , \quad \Omega_\Lambda \equiv \frac{\Lambda}{3H_0^2} \quad , \quad \Omega_K \equiv -\frac{K}{a_0^2 H_0^2} \quad .$$

1.3 Evidence for a low density universe

1.3.1 Cluster evolution

Structure formation proceeds by gravitational collapse of small amplitude perturbations into larger and larger ones. The homogeneity of the CMB tells us that at early times fluctuations had very small amplitude: then, the linear perturbation theory is expected to work very well for fluctuations on the largest scales, because they have only recently entered the horizon and thus only recently they have started to collapse. For smaller scales, nonlinearities begin to be important; the scale for this crossover today is $\simeq 10h^{-1}Mpc$. Let us briefly describe the qualitative effects of a cosmological constant on linear perturbation theory.
A cosmological constant corresponds to an energy density which is smooth; that is, it doesn't clump or change on any scale. Thus, for a given Ω_K, increasing the cosmological constant contribution decreases Ω_m, the matter available for gravitational collapse. Consequently structure grows more slowly in a universe with larger Ω_Λ for fixed Ω_K. In the limit that the energy density from nonrelativistic matter is subdominant, the expansion of the universe prevents structure from growing. In other words, universe would expand faster than the perturbations can collapse, as can be seen directly by looking at the equations governing the growth of density perturbations (see, e.g. [163, 52],).
In a universe in which there is not a precisely critical density of matter, small density fluctuations on large scales cease to grow due to gravity once either the total density begins to deviate significantly from that associated with a flat universe, or when the density in a cosmological constant term begins to dominate over the density of matter. Thus if the universe is Λ- dominated or curvature dominated, large scale structure formation should have ceased, and vice versa for a flat matter dominated universe. The difference is significant: the probability of finding a rich cluster at a redshift of 0.7 is perhaps 100 times smaller for a flat CDM universe than for a universe in which the growth of large structures stopped some time ago [86, 161, 11, 12, 225]. Indeed, normalizing to the rich cluster abundance seen

today at 8 $h^{-1}Mpc$, σ_8, for a fixed Ω_K, a high-Ω_Λ universe has earlier cluster formation. Observations are compared with theory, using Press-Schechter or N-body calculations in order to determine the expected mass distribution, and then the mass is related to the X-ray temperature: the latter is one of the most uncertain steps . The numerically calculated cluster number evolution can then be compared to current data [73, 222, 179, 23, 103, 80, 97]. The deepest complete X-ray sample available is that from the Einstein Medium Sensivity Survey (EMSS) [76]. Although the statistics and uncertainties are not yet good enough to determine Ω_m precisely [53, 222] the measured abundance of rich clusters summarized in [13, 38] seem to converge to an evidence that rules out the flat CDM model; Eke et al [73], using just X-ray temperature data, conclude that $\Omega_m \sim 0.45 \pm 0.2$.
Future X-ray and optical surveys, such as CHANDRA [45] and XMM will allow an improved determination of cluster properties.

1.3.2 Gravitational lenses

Gravitational lensing of quasars by intervening galaxies measures the volume of space back to a given redshift, assuming constant comoving density of lensing objects. As a consequence, the number of multiply imaged QSOs found in lens surveys is sensitive to Ω_Λ. The current situation with the data is as follows. For $\Omega_k = 0$, the analysis of surveys for multiply imaged quasars give a 2σ upper limit $\Omega_\Lambda < .66$ [130, 131, 150]. Using radio selected lenses to reduce possible systematics errors [79], Falco et al. find $\Omega_\Lambda < .73$ at 2σ . Combining the radio and optical data they find $\Omega_\Lambda < .62$ at 2σ for their most conservative model. This limit could perhaps be weakened if there were significant extinction by dust or rapid evolution of the lensing galaxies, but there is much evidence that these galaxies have little dust [205, 143, 191]. The errors should improve significantly with the observations such as the CASTLe survey [96].
Models of gravitational lensing must, however, explain not only the observed probability of lensing, but also the relative probability of showing a specific image separation; the analysis of Chiba & Yoshii [50], that use new models of the evolution of elliptical galaxies, gives $\Omega_\Lambda = 0.7^{+0.1}_{0.2}$, but Kochaneck et al. [132] show that the available evidence disfavors the models of Chiba and Yoshii.

Another constraint on Λ from simulations is a claim that the number of long arcs in clusters is in accord with observations for an open CDM model with $\Omega_m = 0.3$ but an order of magnitude too low in a ΛCDM model with the same Ω_m [18]. This apparently occurs because clusters with dense cores form too late in such models. These results are not altered by the inclusion of cluster galaxies [154, 84]. Since this is a potentially powerful constraint, it deserves to be better understood and checked in the future.

1.3.3 Galaxy peculiar velocities

The large-scale peculiar velocities of galaxies correspond via gravity to mass density fluctuations about the mean, and depend also on the mean density itself. Two catalogs of galaxies have been analyzed for these velocities: the Mark III catalog [239, 245] of about 3000 galaxies within a distance of $\sim 70h^{-1}$ Mpc, and the SFI catalog [29] of about 1300 spiral galaxies in a similar volume.
Combining the results in these catalogs, Zehavi & Dekel [247] quote the constraint $\Omega_m h_{65}^{1.3} n^2 \simeq 0.58 \pm 0.12$ in the case of a flat cosmology, where the error corresponds to a 90% confidence range. Taking the index n of the mass-density fluctuation spectrum to be $n = 1.0 \pm 0.1$ [28] gives $\Omega_m = 0.55 \pm 0.14$ at 68% confidence range.
A different method for estimating the matter density field, modulo an assumption about biasing, is to compare peculiar velocity data obtained from distance indicators such as Tully-Fisher, and from redshift surveys. Through this method, the quantity $\beta \equiv f(\Omega_m)/b$ is obtained, where $f \equiv d\ln\delta_m/d\ln a \sim \Omega_m^{0.6}$ and b is a linear bias parameter. A number of recent results [59, 56, 239, 240] suggest a low matter density, but strong constraints on Ω_m cannot be rigorous due to the incomplete understanding of bias.
A particularly simple way to deduce a lower limit on Ω_m from the POTENT peculiar velocity data was proposed by Dekel & Rees [62], based on the fact that high-velocity outflows from voids are not

expected in low-Ω models; data on just one nearby void indicates that $\Omega_m \geq 0.3$ at the 97% C. L.

1.3.4 The CMB anisotropies

One of the most powerful cosmological probes is the CMB anisotropy, the imprint of the recombination epoch on the celestial sphere. As we shall see in detail in chapter 3, the temperature fluctuations on the sky can be decomposed into spherical harmonics, and the amount of anisotropy correspondent to a multipole l is expressed through the *power spectrum*; each multipole moment corresponds to angular separations on the sky of order $\simeq 180°/l$. Even though the dependence of the spectrum on the cosmological parameters is rather complicated, the location of the first acoustic peak (an increase in power due to acoustic oscillations of the cosmic fluid at recombination [235]) is strictly connected with the overall geometry of the universe: the positive (negative) curvature of the universe makes the photons trajectories converge (diverge), projecting the same physical scale on smaller (larger) angles in the sky, with respect to a flat universe. Since the first acoustic peak is nearly at the horizon scale at recombination $\propto H_{rec}^{-1}$, that is mostly determined by the microphysics, the geometric effect dominates on the observed location of the peak, which can be related to the total energy density parameter by [112, 120, 125]:

$$l_{peak} \sim 220\Omega^{-1/2} \quad .$$

So, the first acoustic peak measures the angular diameter distance to the last scattering surface.
The most recent data from MAXIMA and BOOMERANG balloon flights indicate that the peak is located at $l \simeq 200$, favoring a flat universe [60, 101, 138, 14]. Further data will be available in the next years, from the MAP and Planck satellites [155],[156]. CMB anisotropies are complementary to the supernovae results: while the supernovae results at $z \sim .5$ measure $\Omega_m - \Omega_\Lambda$, the location of the first peak measures their sum; the two approaches lead to confidence contours that are nearly orthogonal in the plane $\Omega_m - \Omega_\Lambda$. Combining these results is a promising tool [237, 211, 212, 89, 145, 216]. The region of overlap of the constraints from the 1998 BOOMERANG [138] flight and supernovae is in the vicinity of $(\Omega_m, \Omega_\Lambda) = (0.3, 0.7)$.

1.3.5 Type 1A Supernovae

At present, one of the most promising techniques for measuring Ω_m and Ω_Λ on cosmological scales uses high-redshift type 1a Supernovae (SNe 1a); they are excellent probes, being the brightest supernovae, with a nearly uniform intrinsic luminosity ($M \sim -19.5$, comparable to the brightness of the entire host galaxy [32]).
Plausibly, SNe 1a are optimal Standard Candles : since they occur when an accreting white dwarf passes the Chandrasekhar limit and undergoes a detonation explosion, the physics of this process is nearly independent on the evolutionary status of the host galaxy; the Chandrasekhar limit is a nearly-universal quantity, so the resulting explosion luminosity will be.
Thus, the spread in the SNe 1a intrinsic brightness appears to be relatively small.
Furthermore, there is a strong relation between the width of the light curve and the absolute luminosity of the supernova, that allows in principle an accurate determination of the luminosity distance d_L via the distance modulus

$$m - M = 5\log_{10}[d_L(Mpc)] + 25 \quad .$$

with d_L the luminosity distance

$$d_L = R_0(1+z)\text{sinn}\int_0^z \frac{dz'}{R_0 H_0 E(z')}$$

Thus the curve for $d_L(z)$ versus z measures cosmological parameters . Using a method pioneered by Perlmutter et al. [170], two groups have independently claimed to measure the redshift-distance relation out to redshift 0.5, probing for cosmic deceleration or acceleration. The combined results have indicated high confidence for a positive nonzero cosmological constant. The first seven high redshift

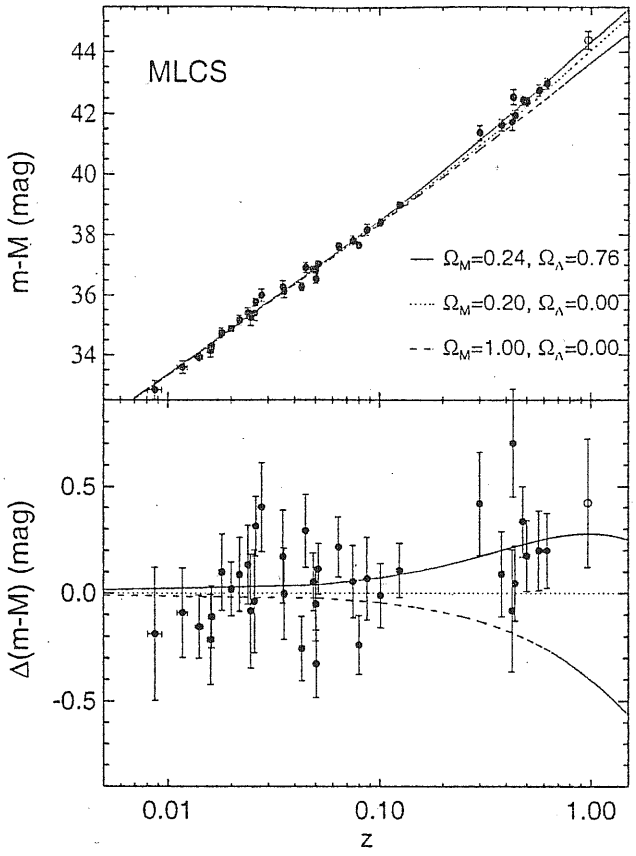

Figure 1.1: Hubble diagram (distance modulus vs. redshift) from the High-Z Supernova Team. The lines represent predictions from the cosmological models with the specified parameters. The lower plot indicates the difference between observed distance modulus and that predicted in an open-universe model.

SNe 1a analyzed by the Supernovae Cosmology Project, with redshifts in the range $0.35 \leq z \leq 0.65$, gave for a flat universe $\Omega_m = 1 - \Omega_\Lambda = 0.94^{+0.34}_{-0.28}$ or equivalently $\Omega_\Lambda = 0.06^{+0.68}_{-0.34}$ (< 0.51 at the 95% confidence level), consistent with a near critical density universe [170]; although the first seven SNe 1a seemed to disfavor the cosmological constant, the further discovery in 1997 of a Supernova explosion at z=0.83, and its photometric analysis, suggested that we may live in a low mass-density universe [171].

The results from the first 7 supernovae were overturned in 1998, when the analysis of 42 type 1a Supernovae at redshifts between 0.18 and 0.83 allowed to fit the SNe magnitude-redshift diagram with more data, up to larger redshifts. The surprising result was that the data were strongly inconsistent with $\Lambda = 0$: for a flat cosmology, the Supernova Cosmology Project estimated $\Omega_m = 0.28^{+0.09}_{-0.08}$ (1 sigma statistical) $^{+0.05}_{-0.04}$ (identified systematics).

Figure 1.3.5 shows the results for $m - M$ vs. z for the High-Z Supernova Team [90, 192, 182, 89], while figure (1.3.5) shows the equivalent results for the analysis of 42 high-z supernovae by the Supernova Cosmology Project (SCP) [171, 172].

These data can be converted into limits on Ω_m and Ω_Λ , assuming that the energy density of the universe is dominated by matter and vacuum components. Results are shown in Fig. 1.3.5 and in Fig. 1.3.5.

Both teams seem to favor a positive cosmological constant, ruling out both a flat CDM universe and an open universe with zero cosmological constant. Even more remarkably, the favored region, for a flat universe, is precisely in the range favored by other constraints, such as those from large scale structure .

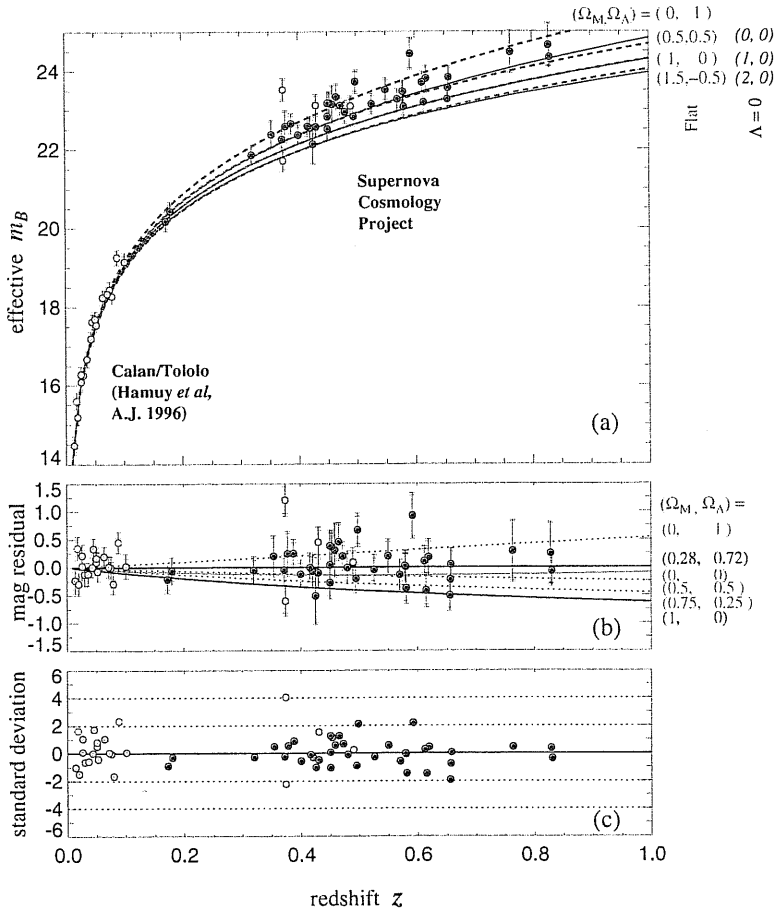

Figure 1.2: Hubble diagram from the Supernova Cosmology Project. The bottom plot shows the number of standard deviations of each point from the best-fit curve.

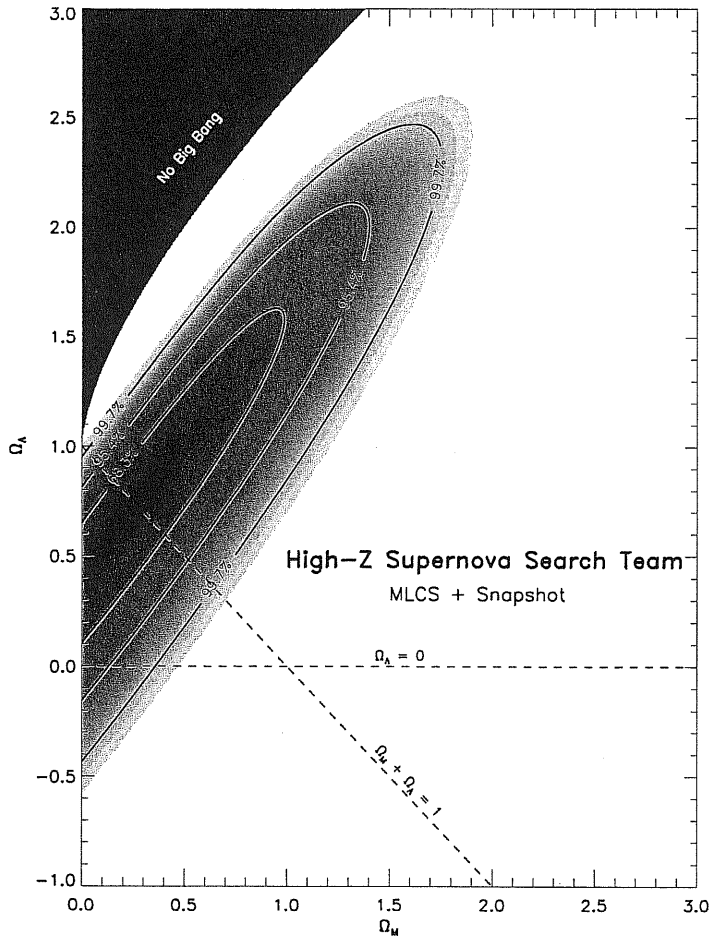

Figure 1.3: Constraints in the Ω_m-Ω_Λ plane from the High-Z Supernova Team.

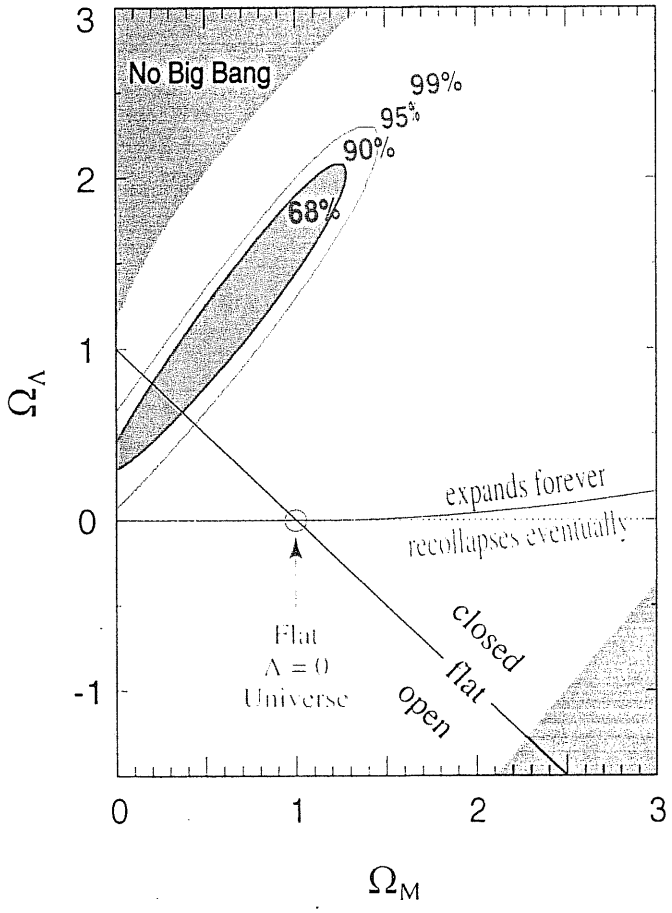

Figure 1.4: Constraints in the Ω_m-Ω_Λ plane from the Supernova Cosmology Project [171, 172].

The importance of such results leads to the question of what confidence level we should have with respect them; possible systematics errors which have been studied include extinction [2, 3, 4, 201, 210] and evolution [68, 185], selection effects, weak lensing [106, 126], the width-brightness relation used for calibration [175, 184, 100] and sample contamination [183].
All these effects have been carefully taken into account by the supernovae teams, and are thought to be unimportant, though the main concerns about the interpretation of the data are evolutionary effects and dimming by dust.
A specific evolution concern is that the rest frame rise-times of distant supernovae may be longer than nearby ones [184]; on the other hand, a direct comparison between nearby supernovae and the SCP sample shows that they are rather consistent with each other [6]: Spectra of high and low redshift supernovae have been compared with good agreement, and the distribution of faint and bright supernovae appears similar over a variety of redshifts and environments.
Other than evolution, the leading concern about the reliability of the SNe results is obscuration by dust; while the ordinary astrophysical dust would obscure preferentially the blue light, causing reddening, spectral measurements revealed that there is very little reddening seen in either the far or near SNe. There are models which predict this [102], [2, 3, 4, 201, 210], invoking a kind of "grey "dust that would cause much less reddening than the ordinary one: it could in principle provide an alternative explanation for the fact that the high-redshift supernovae are observed to be dimmer than expected in a critical-density cosmology. But this hypothetical grey dust is, in turn, severely constrained by observations of the cosmic far-infrared background [4]. New insights will be probably gained when data on $z > 1$ SNe is collected: at such redshifts, the dust scenario predicts considerably more dimming than the Λ cosmology.
In conclusion, the possibility of extinction by dust for SNe 1a cannot be ruled out, but it is hard to place it in a coherent picture.
As so much relies upon SNe 1A being standard candles, these questions are crucial. It remains to be seen if further data taken at high redshift will confirm these results, and more importantly confirm the assumption that the evolution is negligible for such supernovae.

1.3.6 Power spectrum

Structure formation begins and ends with matter dominance, and is characterized by the horizon scale at the cross-over from radiation to matter dominance; predicting the power spectrum of matter density fluctuations requires an assumption on the correct theory and a specification of a number of cosmological parameters [164, 58, 17, 122, 44, 24, 91]. In the context of the ΛCDM class of models, two additional constraints are available on Ω_m. The spectrum shape parameter $\Gamma \simeq \Omega_m h \simeq 0.25 \pm 0.05$, implying $\Omega_m \simeq 0.4 \pm 0.1$.
Measuring the amplitude of the power spectrum of fluctuations at redshift $z \sim 3$ from the Lyman α forest gives $\Omega_m = 0.34 \pm 0.1$ [226, 55]. Broadhurst & Jaffe [35] used a set of Lyman galaxies at $z \sim 3$ finding a constraint of the form $\Omega_m = 0.20 \pm 0.10 + 0.34\Omega_\Lambda$.
Measurements of the Lyman α forest are promising because they probe the power spectrum on smaller scales at a redshift before the development of non-linearities, allowing a direct comparison with the linear power spectrum.

1.3.7 Cluster dynamics

The traditional method to estimate the mass density of the universe is to "weigh" a cluster of galaxies, divide by its luminosity and extrapolate the result to the universe as a whole, assuming that clusters are representative samples of the universe. Studies applying the virial theorem to clusters dynamics have obtained values around $\Omega_m = 0.2 \pm 0.1$ [39, 63, 12].

1.3.8 Cluster baryons vs. Big Bang Nucleosynthesis

Recent observations of the deuterium fraction in primordial hydrogen clouds illuminated by the light of distant quasars [219] suggest that $D/H = 3.4 \pm 0.3 \times 10^{-5}$; if this value reflects the primordial abundance, then Big Bang Nucleosynthesis [193, 36] with three light neutrinos gives $\Omega_b h^{-2} = 0.019 \pm 0.002$.
When compared with observations of the baryon fraction on large scales today, this seems to rule out the possibility of a flat universe.
X-ray observations of galaxy clusters, the largest bound structures known in the Universe, suggest that baryons exist in these systems in the form of hot X-ray emitting gas. White et al. [234] emphasized that X-ray observations of the baryon abundance in clusters can be used to determine Ω_m, if clusters are a fair sample of both baryons and dark matter as they are expected to be based on simulations [78] The baryon fraction estimated from cluster observations [77, 233, 87], also taking into account the stellar fraction [146], results in [224] $f_{baryon} = (0.067 \pm 0.008)h^{-3/2}$ [157, 158].
The fair sample hypothesis implies that

$$\Omega_m = \frac{\Omega_b}{f_{baryon}}$$

so that, using $h = 0.65 \pm 0.08$, the constraint on Ω_m would be $\Omega_m = 0.25h^{-1/2} = 0.3 \pm 0.1$.

1.4 The cosmological constant problem

The Friedmann equation 1.11 that, according to GR, governs the expansion factor of the universe a(t), includes Λ as a source of the universe dynamics; this equation implies that we must have

$$1 = \Omega_M + \Omega_\Lambda + \Omega_K \quad . \tag{1.13}$$

Now, it is an observational question whether a nonzero cosmological constant is required to achieve consistency in equation 1.13; this is the cosmological constant problem from an astronomer's point of view.
Since vacuum energy influences the evolution of the universe, from the absence of excessive changes with respect to the usual Friedman model one may deduce that $|\Omega_\Lambda| = |\rho_{vac}/\rho_c| \leq 1$. Here $\rho_c = 3H_0^2 m_{Pl}^2/8\pi \approx 10^{-29}\mathrm{g/cm}^3 \approx 10^{-47}\mathrm{GeV}^4$ is the present value of the critical energy density. So we can conclude that

$$|\rho_{vac}| < 10^{-47}\mathrm{GeV}^4 \tag{1.14}$$

There is a continuous discussion, if Ω_Λ is zero (or unnoticeably small) or it may be close to unity so that its effects on universe evolution are significant. In the previous section, we treated such observational problems quite extensively .
On the other hand, to a particle physicist, the word "vacuum " has a different meaning than to an astronomer, denoting the ground state (state of lowest energy) of a theory rather than the "empty space".
The cosmological constant defines a length scale; while in cosmology there is no preferred choice for what this scale might be, if one sees at Λ as measure of the energy density of the vacuum, interpreted as the ground state of a theory, it is possible to consider the scales of various contributions to Λ.
The classical action for a single scalar field with potential energy $V(\phi)$ is

$$S = \int d^4x\sqrt{-g}\left[\frac{1}{2}g^{\mu\nu}\partial_\mu\phi\partial_\nu\phi - V(\phi)\right] \quad .$$

In this theory, the ground state would be characterized by $\partial_\mu\phi = 0$ (i.e., no kinetic and gradient energy contributions); correspondingly, the potential will be minimized by a value ϕ_0 of ϕ, and the energy-momentum tensor of the field,

$$T_{\mu\nu} = \frac{1}{2}\partial_\mu\phi\partial_\nu\phi + \frac{1}{2}(g^{\sigma\rho}\partial_\sigma\phi\partial_\rho\phi)g_{\mu\nu} - V(\phi)g_{\mu\nu}$$

reduces to $T_{\mu\nu} = -V(\phi_0)g_{\mu\nu}$, and the vacuum energy of the system is represented by $V(\phi_0)$; since there is no reason in principle why $V(\phi_0)$ should vanish, the vacuum energy-momentum tensor can be written as $T_{\mu\nu} = -\rho_{vac}g_{\mu\nu}$.
The vacuum can therefore be thought of as a perfect fluid with

$$p_{vac} = -\rho_{vac} \quad . \tag{1.15}$$

Setting $\rho_{vac} = \rho_\Lambda \equiv \frac{\Lambda}{8\pi G}$, one can identify the cosmological constant with the energy of the vacuum . In general, the ground state must be Lorentz invariant; as a consequence, the energy-momentum tensor of vacuum must be proportional, in any locally inertial frame, to the diagonal Minkowski metric, resulting in a perfect fluid having equation of state 1.15; this is the only equation of state that causes ρ_{vac} to remain constant under an adiabatic expansion of its volume. In contrast to the classical scalar field system, a "bare " cosmological constant Λ_0 would enter the action of GR as

$$S = \frac{1}{16\pi G}\int d^4x\sqrt{-g}(R - 2\Lambda_0) \quad ,$$

i.e. Λ_0 could be thought of as a constant term in the Lagrange density of the theory. Classically, then, the cosmological constant is the sum of a bare term and the potential energy of the lowest energy density of a scalar field.
Quantum mechanics adds another contribution, namely the zero-point energies of vacuum fluctuations.
It was realized in 1967 by Zel'dovich [248] that quantum field theory generically demands that cosmological constant, or vacuum energy, is non-vanishing, as a consequence of the Heisenberg uncertainty principle, that allows particle-antiparticle pairs spontaneously to appear and disappear. It is very well known from quantum mechanics that the ground state energy of harmonic oscillator is not zero, due to the uncertainty principle: a similar phenomenon takes place in quantum field theory because any quantized field represents a collection of oscillators with all possible frequencies.
As an example, let us consider a scalar field ϕ (i. e. a spinless boson) of mass m. For this system, the vacuum energy is obtained putting the system in a box of volume L^3, summing the contribution from each mode of the field, and letting L go to infinity [22]; for periodic boundary conditions,

$$E_0 = \frac{1}{2}\hbar L^3 \int \frac{d^3k}{(2\pi)^3}\omega_k$$

Correspondingly, the ground state energy of this system is given by the expression [42, 228, 67, 65]

$$\rho_{vac} = \lim_{L\to\infty}\frac{E_0}{L^3} = \hbar\frac{k_{max}^4}{16\pi^2} \tag{1.16}$$

As the cutoff k_{max} approaches infinity, ρ_{vac} becomes divergent. If there is a symmetry between bosons and fermions, such that for each bosonic state there exist a fermionic state with the same mass and vice versa, then the energy of vacuum fluctuations of bosons and fermions would be exactly compensated, giving zero net result [248, 94, 223, 230]; however, supersymmetry is not exact and such compensation is not complete: the masses of bosons and corresponding fermions are different, and one is able to cancel out only the leading divergent term. Supersymmetric theories with spontaneous symmetry breaking ensure also the compensation of the quadratically and logarithmically divergent terms, by canceling out the zero point energies of particles of different spin; however, the predicted finite contribution to the vacuum energy, that must be nonzero, should be

$$\rho_{vac}^{SUSY} \simeq m_{SUSY}^4 \quad ,$$

where m_{SUSY} is the scale of supersymmetry breaking. From the experiments, we are confident that $m_{SUSY} \geq 100\text{GeV}$, and the correspondent contribution to ρ_{vac} should be $\geq 10^8\text{GeV}$, i. e. 55 orders of magnitude larger than the permitted upper bound (1.14).

In general, the divergence in 1.16 can be eliminated by discarding the very high-momentum modes, estimating k_{max} as the energy scale up to which we trust our low-energy theory.
As in classical mechanics, the absolute value of the vacuum energy has no measurable effects in quantum field theory; however, GR postulates that gravitation couples universally to all energy and momentum, including that of vacuum (furthermore, we note that since gravity is the only force for which this is true, the only manifestation of the cosmological constant would be through its gravitational influence).
From this point of view, the net cosmological constant will be the sum of independent contributions, from the bare cosmological constant, from the potential energies of scalar fields, and the zero-point "virtual " fluctuations of each field.
For what concerns the vacuum fluctuations, the natural cut off should be chosen at the energy limit that we believe correspond to the validity of the theory. For example, it is widely believed that the Planck energy $E^* \simeq 10^{19}$ GeV marks a point where conventional field theory breaks down due to quantum gravitational effects. Choosing $k_{max} = E^*/\hbar$ as the cut off scale, we obtain from eq. 1.16

$$\rho_{vac} \simeq 10^{74}\mathrm{GeV}^4\hbar^{-3} \simeq 10^{92}\mathrm{g/cm}^3 \quad . \tag{1.17}$$

Compared with (1.14), the vacuum energy contribution in (1.17) is larger than the observational bound by $\simeq 120$ orders of magnitude.

In theories with spontaneous symmetry breaking, the source of vacuum energy is the potential energy of the scalar (Higgs) field of the theory; in the course of the universe cooling down, a phase transition took place [128, 129], changing the amount of energy corresponding to the "minimum" of the potential.
In the broken-symmetry phase of the Weinberg-Salam electroweak model, the electroweak phase transition would predict a contribution to the vacuum energy today of order

$$\rho_\Lambda^{EW} \simeq (200\mathrm{GeV})^4 \simeq 10^{10}\mathrm{GeV}^4 \quad .$$

This contribution should add to those from any other, yet unknown, phase transition in the early universe, such as those that would come from the GUT at $M_{GUT} \simeq 10^{16} GeV$:

$$\rho_\Lambda^{GUT} \simeq 10^{60}\mathrm{GeV}^4 \quad .$$

There exist some other contributions which, though smaller than these, are still huge when compared with the bound (1.14): it is an experimental fact that vacuum state in quantum chromodynamics (QCD) is filled by non-perturbative quark (or chiral) condensate [92] and gluon condensate [198], that contributes with $\simeq 10^{-3} - 10^{-4}\mathrm{GeV}^4$. Compared with (1.14), this allows to conclude that there must exist some mysterious agent that is able to compensate their vacuum energy with the accuracy of 10^{-44}.
The impressive discrepancy between the observational bound on the vacuum energy, and the value expected from particle theory, is known as the "cosmological constant problem" .

In the absence of a recognized symmetry principle protecting its value, no theoretical reason for making the cosmological constant zero or small has been found. One could postulate that a bare cosmological constant, opposite in sign and exactly equal in magnitude to the zero-point energy, conspires to cancel out the 'net' vacuum energy, but given the large number of elementary particle fields, this would be an extreme case of fine-tuning. For this reason, a large part of the particle physics community has been pushed towards a different point of view, i.e. that the cosmological constant is zero, due to some mechanism that is not yet understood. The Quintessence models have been proposed in order to alleviate the theoretical problems of the cosmological constant, with the necessity to explain the observational evidences of a nearly flat [138] and accelerating universe. Such models are the subject of this thesis.

1.5 Quintessence

The difficulties faced by cosmological constant models motivated the proposal of several alternative scenarios; amongst them, the so-called "quintessence" models, which are the subject of this thesis,

propose that the "missing energy" could reside in the potential and kinetic energy of a dynamical scalar field, rather than in a pure vacuum state. This "dark energy" candidate is a time-varying, spatially inhomogeneous component with negative pressure, that interact only gravitationally with matter. For the purposes of our investigation, we model Quintessence as a field evolving in its potential: if the potential is sufficiently flat at late times, the consequent slow-rolling motion can mimic a cosmological constant that decreases with time. We assume that the field is only very weakly coupled to matter, therefore there is no creation of matter or radiation: the decrease in the potential energy of the field as it rolls down the potential is simply converted to kinetic energy.
Assuming that the fundamental vacuum energy is zero, the effective vacuum energy is simply stored in the potential of a scalar field, so that at any epoch, it will be dominated by the heaviest fields which have not yet relaxed to their vacuum state; at late times, these fields must be very light.
The key differences between a quintessence and the "true" vacuum energy are that the field equation of state $w = pressure/density$ is larger than -1, whereas vacuum energy density has w precisely equal to -1, and that the former is generally time-dependent. This results in different predictions for the expansion rate. Furthermore, the quintessence is spatially inhomogeneous, resulting in a direct imprint of quintessence fluctuations on the CMB and large scale structure.

Scalar fields in cosmology are ubiquitous; both the cosmology of weakly coupled scalar fields and their theoretical motivations have been much studied since the advent of the idea of inflation.
However, the definition of Quintessence is different from that of an inflaton field: indeed, Quintessence needs not to participate to the inflationary phase, i.e. it may not to be the same field as the inflaton. Only, this field has an energy density that survives the inflation and can come to dominate the entire energy density today. We note also that if the scalar field were to dominate early enough (like the canonical Hot Dark Matter, the almost massless neutrino, does) it would suppress growth of baryonic structures on small scales, because the Universe expands faster than the perturbation can collapse. This is the reason why it is generally assumed that the Universe has only recently become dominated by the scalar field energy density.

Much work has already been done, since the pioneering idea of Ratra and Peebles [178]. However, this thesis contains a rather large amount of original work.
As soon will become clear, the development of linear perturbation theory is an essential tool for the study of the perturbation evolution even in Quintessence scenarios. We devote Chapter 2 to the development of the necessary formalism, while Chapter 3 deals with the features of the Cosmic Microwave Background of radiation and of its anisotropies; this is a rather qualitative description, that should help to understand both the importance of CMB observations and the cosmological role of a dynamical vacuum energy on the overall geometry and dynamics of the universe.
The following chapters contain the original work, which follows refs. [173, 174, 10, 15]. In chapter 4, we consider the problem of the initial conditions and behaviour of the perturbations in scalar field cosmology with general potential.
We use the general definition of adiabatic and isocurvature conditions to set the appropriate initial values for the perturbation in the scalar field and in the ordinary matter and radiation components. In both the cases of initial adiabaticity and isocurvature, we solve the Einstein and fluid equation at early times and on superhorizon scales to find the initial behaviour of the relevant quantities. In particular, in the isocurvature case, we consider models in which the initial perturbation arises from the matter as well as from the scalar field itself, provided that the initial value of the gauge invariant curvature is zero.
We extend the standard Boltzmann code, modifying the CMBFAST to include all these cases, and we show the predicted power spectrum of the CMB temperature and polarization anisotropies, as well as the matter power spectrum containing the evolutionary history of matter perturbation. The comparison with the standard pure CDM model is performed.
In Chapter 5, these results are generalized to a larger class of Quintessence models; indeed, we consider Quintessence cosmologies in the context of scalar-tensor theories of gravity, where the scalar field ϕ, which is assumed to provide most of the cosmic energy density today, is non-minimally coupled to the

Ricci curvature scalar R. We named such models 'Extended Quintessence' cosmologies. It turns out that the role of Quintessence is now not only to provide the time and space variation of the cosmological constant, but also to act as a source of time variation of the Newton's constant.
We investigate two classes of models, where the gravitational sector of the Lagrangian is $F(\phi)R$ with $F(\phi) = \xi\phi^2$ (Induced Gravity, IG) and $F(\phi) = 1 + \xi\phi^2$ (Non-Minimal Coupling, NMC). It turned out that new distinctive features, due the coupling with the Ricci scalar, arise in these models and are visible in the CMB anisotropies power spectrum, allowing a comparison with "simple" (minimally coupled) Quintessence scenarios.
One of the main advantages of Quintessence (and Extended Quintessence) on the cosmological constant, resides in the dynamics: the dynamics of the scalar field plays an important role, because it can adjust in a way that the scalar field energy density becomes dominant at the present time.
However, the existence of a considerable amount of vacuum energy in the Universe, as observations seem to imply, brings together two fundamental problems. The first regards the fact that we are right now in the phase in which the vacuum energy is starting to dominate over matter, and is often called the "coincidence" problem. The second is a "fine tuning" one: the vacuum (or the Quintessence) energy density should have been vanishingly small at the initial time, in order to have today an amount of vacuum energy comparable with that of matter.
It has been shown that in Quintessence scenarios it exists a possible way out to the fine tuning problem; in fact, one can select a subclass of models which admit "tracking solutions": this means that the observed amount of scalar field energy density today can be reached starting from a very wide set of initial conditions.
In Chapter 6, we extended the tracking phenomenology to non-minimally coupled scalar fields ("Tracking Extended Quintessence"); in this scenario, considering inverse-power law potentials of the field, we analyzed the background and perturbation evolution, pointing out observable effects on CMB and Large Scale Structure. Finally, Chapter 7 is devoted to the conclusions and comments on the future detection perspectives.

In the next Chapter, we will introduce the most important tool for the study of Quintessence cosmologies: the linear perturbation theory.

Chapter 2

Linear perturbation theory

This chapter is a review of the cosmological perturbation theory that is the basis for what will be treated in the next chapters. We introduce the perturbations of metric and matter quantities in a gauge-invariant formalism, and then we write the perturbed Einstein equations in the synchronous and conformal Newtonian gauges. The notation of Kodama & Sasaki has been respected as far as possible. For a complete exposition, we refer to [133, 160, 148].

2.0.1 Perturbing the FRW metric

The most general perturbation to the metric (1.1) may be written as

$$\tilde{g}_{\mu\nu} = a^2(\gamma_{\mu\nu} + h_{\mu\nu}) \ , \tag{2.1}$$

where $h_{\mu\nu}(x)$ is the perturbation tensor, whose role is of fundamental importance for the whole cosmological linear perturbation theory. The linear theory of perturbations is valid as long as $h_{\mu\nu}(x) \ll \gamma_{\mu\nu}(x)$; the strong evidence of CMB homogeneity, resulting in fluctuations of the order $\delta T/T \simeq 10^{-5}$, allows us to assume the validity of the linear approximation starting from the very early universe at least to the epoch of decoupling between matter and radiation. As we shall see, the linearity condition will be extremely helpful in trying to solve the Einstein equations for the coupled system composed of metric and fluid. Indeed, it is known that, in general, perturbations of various quantities relative to both metric and fluid, can be decomposed into three types of components, of scalar type, vector type and tensor type, respectively. A perturbation is of scalar, vector or tensor type, depending on the transformation properties under rotations of the spatial coordinate system. As showed in [133], in a FRW spacetime, in the linear regime, scalar, vector and symmetric second-rank tensor equations can be decomposed into independent sets of equations relative to components of each type only. Therefore, the Einstein equations that describe the linear evolution of each type of perturbation components can be studied separately ([133],[160], [16],[74]). Each of these components can be conveniently expanded in a complete and orthonormal set of harmonic functions, that satisfies the equation

$$\nabla^2 Y^{(m)} = \gamma^{ij} Y^{(m)}_{k\,|ij} = -k^2 Y^{(m)}_k \ , \tag{2.2}$$

where $|$ stays for covariant differentiation with respect to the metric γ_{ij}, while $-k^2$ represents an eigenvalue of the Laplace operator ∇^2. The eigenmodes $Y^{(m)}_k$ may be of scalar ($m = 0$), vector ($m = \pm 1$) and tensor ($m = \pm 2$) type; we will omit the indices k indicating the specific eigenfunction, since different modes do not couple. To help the visualization of this expansion basis, it is useful to give a specific representation for the eigenmodes; assuming flatness for the background FRW metric and choosing a specific orthonormal basis so that the polar axis coincides with $\hat{k}$, $\hat{e}_1$, $\hat{e}_2$, $\hat{e}_3{=}\hat{k}$, a convenient expression for the eigenmodes in (2.2) is

$$Y^{(0)} = \exp(i\vec{k}\cdot\vec{x}) \ , \tag{2.3}$$

$$Y^{(\pm 1)}_i = -\frac{i}{\sqrt{2}}(\hat{e}_1 \pm i\hat{e}_2)_i \exp(i\vec{k}\cdot\vec{x}) \ , \tag{2.4}$$

$$Y_{ij}^{(\pm 2)} = -\sqrt{\frac{3}{8}}(\hat{e}_1 \pm i\hat{e}_2)_i \times (\hat{e}_1 \pm i\hat{e}_2)_j \exp(i\vec{k}\cdot\vec{x}) \ , \tag{2.5}$$

These functions are completely defined by the following conditions on trace and divergence:

$$Y_i^{(\pm 1)\ |i} = 0 \ , \ Y_{ij}^{(\pm 2)\ |i} = 0 \ , \ Y_i^{(\pm 2)\ i} = 0 \ . \tag{2.6}$$

Scalar quantities can be expanded in terms of the set Y^0 of harmonic functions; divergenceless vectors are expanded by $Y^{\pm 1}$, while divergenceless and traceless second rank symmetric tensors are expanded by the set $Y^{(\pm 2)}$. On the other hand, the scalar part of vectors, likewise the scalar and vector part of tensors, can be expanded in terms of the following functions, derived from the $Y^{(m)}$:

$$Y_i^{(0)} = -\frac{1}{k}Y_{|i}^{(0)} \quad \text{(scalar part of vector)} \ , \tag{2.7}$$

$$Y_{ij}^{(0)} = \frac{1}{k^2}Y_{|ij}^{(0)} + \frac{1}{3}\gamma_{ij}Y \quad \text{and} \quad \gamma_{ij}Y \quad \text{(scalar parts of tensor)} \ , \tag{2.8}$$

$$Y_{ij}^{(\pm 1)} = -\frac{2}{k}\left(Y_{i|j}^{(\pm 1)} + Y_{j|i}^{(\pm 1)}\right) \quad \text{(vector part of tensor)}; \tag{2.9}$$

These harmonic functions are the basis for the development of the metric and fluid perturbations; by a spatial transformation, the components of the perturbed metric tensor g_{00},g_{0i}, g_{ij} transform as a scalar, a vector and a tensor, respectively, so that the most general linear perturbation of the FRW metric (2.1) can be written as follows:

$$h_{00} = -2A^{(0)}Y^{(0)} \tag{2.10}$$

$$h_{0i} = -B^{(0)}Y_i^{(0)} - B^{(1)}Y_i^{(1)} - B^{(-1)}Y_i^{(-1)} \tag{2.11}$$

$$\begin{aligned} h_{ij} = {} & 2H_L^{(0)}\gamma_{ij}Y^{(0)} + 2H_T^{(0)}Y_{ij}^{(0)} + 2H_T^{(1)}Y_{ij}^{(1)} + \\ & + 2H_T^{(-1)}Y_{ij}^{(-1)} + 2H_T^{(2)}Y_{ij}^{(2)} + 2H_T^{(-2)}Y_{ij}^{(-2)} \ , \end{aligned} \tag{2.12}$$

where the coefficients $A^{(0)}, B^{(0)}, B^{(\pm 1)}, H_L^{(0)}, H_T^{(0)}, H_T^{(\pm 1)}, H_T^{(\pm 2)}$ are independent functions of time. The function $A^{(0)}$ is usually interpreted as the amplitude of perturbation in the lapse function, defined as the ratio of the proper-time distance to the coordinate-time distance between two neighboring constant time hypersurfaces. In the next section, we will develop in spherical harmonics the perturbations of the stress-energy tensor, in order to relate perturbations through the Einstein equations.

2.0.2 Perturbing the stress-energy tensor

For writing down the linearized Einstein equations, the first step is to choose a convenient set of variables that will represent the perturbed state of the matter; usually, the algebraically independent components of the energy-momentum tensor are chosen as such variables. Let us denote with a tilde the perturbed quantities; we will indicate with $\tilde{u}^\mu$ the time-like eigenvector, with unit norm, of the energy-momentum tensor, and the proper density $\tilde{\rho}$ as the corresponding eigenvalue:

$$\tilde{T}_\nu^\mu u^\nu = -\rho u^\mu \quad , \quad u^\mu u_\mu = -1 \ . \tag{2.13}$$

Density and isotropic pressure transform as scalars, while the spatial velocity of the fluid, $v^i \equiv \frac{u^i}{u^0}$, transforms as a vector that vanishes in the unperturbed state; using the harmonic functions previously defined, one has the following perturbed quantities:

$$\tilde{\rho} = \rho[1 + \delta Y^{(0)}] \ , \ \tilde{p} = p[1 + \pi_L Y^{(0)}] \ , \ \tilde{v^i} = v^{(0)}Y^{(0)i} + v^{(\pm 1)}Y^{(\pm 1)^i} \tag{2.14}$$

From eq.(2.10)-(2.12) and from the normalization condition on the 4-velocity, one has, to the first order,

$$\tilde{u}_i = a(v^{(0)} - B^{(0)})Y_i^{(0)} + a(v^{(\pm 1)} - B^{(\pm 1)})Y_i^{(\pm 1)} \quad ; \quad \tilde{u}_0 = -a(1 + AY^{(0)}) \ . \tag{2.15}$$

In the perturbed energy-momentum tensor one can separate out the spatial stress tensor $\tilde{\tau}_{\mu\nu}$ orthogonal to $\tilde{u}^\mu$, as follows:

$$\tilde{T}^\mu_\nu = \tilde{\rho}\tilde{u}^\mu\tilde{u}_\nu + \tau^\mu_\nu \tag{2.16}$$

The unperturbed state of the matter is described by the non-zero components of the energy-momentum tensor $T_{\mu\nu}$, namely $T^0_0 = -\rho$ and $T^j_i = p\delta^j_i$, while the most general perturbation to the stress energy tensor, obtained from (2.16), is:

$$\delta T^0_0 = -\rho \cdot \delta \cdot Y^{(0)} \ , \tag{2.17}$$

$$\delta T^i_0 = -(\rho + p)((v^{(0)} - B^{(0)})Y^{(0)\ i} + (v^{(\pm 1)} - B^{(\pm 1)})Y^{(\pm 1)\ i}) \ , \tag{2.18}$$

$$\delta T^j_i = p\pi^{(0)}_L\delta^j_i + p\pi^{(0)}_T Y^{(0)\ j}_i + p\pi^{(\pm 1)}_T Y^{(\pm 1)\ j}_i + \\ + p\pi^{(\pm 2)}_T Y^{(\pm 2)\ j}_i \ , \tag{2.19}$$

Thus, in general, a perturbation in the stress-energy tensor can be described by ten functions of time, namely $\delta, \pi_L, \pi^{(0)}_T, \pi^{(\pm 1)}_T, \pi^{(\pm 2)}_T, v^{(0)}, v^{(\pm 1)}$.
In particular, scalar perturbations, that will be used in this thesis, can be described by four metric functions and four matter functions, some of which can be eliminated using the gauge freedom implicit in the perturbed Einstein equations.

2.1 Gauge transformations and the gauge invariant formalism

To implement the relativistic perturbation theory, it is necessary to treat the question of gauge freedom; indeed, a perturbation of the physical spacetime can only be defined with respect to a hypothetical unperturbed background. Changing the correspondence between the perturbed world and the unperturbed background also changes the values of the perturbations introduced in the previous sections; a gauge choice, consisting in fixing the constant-time hypersurfaces and a spatial grid on these surfaces, is not unique, and should be performed before making any interpretations regarding perturbation evolution. Due to the freedom in the choice of a gauge, one could change the correspondence between the perturbed and the unperturbed world: this will be accompanied by a gauge transformation in a perturbed quantity, which will be different from a genuine coordinate transformation even though, formally, it can be expressed as a coordinate transformation too.
Once a gauge is fixed, the difference between quantities at the same coordinate values (in the perturbed and unperturbed world) is interpreted as a perturbation of this quantity. However, this may give rise to "unphysical" modes, in the sense that perturbations could appear in a particular gauge just as a consequence of the particular time slicing, for example, rather than coming from a pure physical effect. This ambiguity is generally resolved by measuring the perturbation in different coordinate systems (i.e., in different gauges), to remove the ambiguity. Obviously, since there is a one-to-one mapping between gauges whose coordinate are completely fixed, measurements of observable quantities will give the same results; differences arise only if the coordinate system is not entirely fixed, as is the case for the *synchronous gauge*, to be defined in the next subsection.
Let us now formalize the properties of the perturbations under gauge transformations. In the passive approach, one could consider a physical space-time manifold $\mathcal{M}$ with some coordinate system x^μ. The "background" model is defined by assigning to all functions Q (scalars, vector or tensors) on $\mathcal{M}$ a previously given function $Q^0(x^\mu)$, that must be intended as a fixed function of the coordinates. In a second coordinate system $\bar{x}^\mu$ the background functions $Q^0(\bar{x}^\mu)$ will have the same functional dependence on $\bar{x}^\mu$, and the perturbation δQ of the quantity Q in the system of coordinates x^μ is defined as

$$\delta Q(p) = Q(x^\mu(p)) - Q^0(x^\mu(p))$$

for any point p of the manifold with coordinates $x^\mu(p)$. Similarly, in the second system of coordinates, the perturbation of Q is

$$\delta\bar{Q}(p) = \bar{Q}(\bar{x}^\mu(p)) - Q^0(\bar{x}^\mu(p)) \quad .$$

Here, $\bar{Q}(\bar{x}^\mu(p))$ is the value of Q in the new coordinate system at the same point p of $\mathcal{M}$ and $Q^0(\bar{x}^\mu(p)$ is the same function of $\bar{x}^\mu$ as $Q^0(x^\mu(p)$; the gauge transformation $\delta Q(p) \to \delta\bar{Q}(p)$ is associated with the change of variables $x^\mu \to \bar{x}^\mu$. In the active approach, the correspondence between the physical space-time and the background space-time is determined by the relation between the coordinate systems fixed on the two, say x^μ and x_b^μ respectively; the system of coordinates x^μ can be viewed as induced by a diffeomorphism $\mathcal{D}$ on the background, such that $\mathcal{D} : x_b^\mu \to x^\mu$; let us denote as $Q(x^\mu(p))$ a function evaluated on a point p of the physical space; we define the perturbation δQ as

$$\delta Q(p) = Q(p) - Q^0(\mathcal{D}^{-1}(p)) \tag{2.20}$$

where Q^0 is defined on the background space-time. A second diffeomorphism $\bar{\mathcal{D}} : x_b^\mu \to \bar{x}^\mu$ induces a different set of coordinates on the physical space, and a different perturbation

$$\delta\bar{Q}(p) = \bar{Q}(p) - Q^0(\bar{\mathcal{D}}^{-1}(p)) \tag{2.21}$$

where $\bar{Q}$ is the value of Q in $\bar{x}^\mu$ coordinates. In this approach, one could interpret the gauge transformation $\delta Q(p) \to \delta\bar{Q}(p)$ as it originates from the change of correspondence $\mathcal{D} \to \bar{\mathcal{D}}$, to which we associate the coordinate transformation $x^\mu \to \bar{x}^\mu$ on the perturbed space-time. For infinitesimal coordinate transformations, $\bar{x}^\mu = x^\mu + \zeta^\mu$. The most general gauge transformation can be therefore treated as a coordinate change and, making use of the expansion in Laplace operator eigenmodes, one has:

$$\begin{aligned} \bar{\tau} &= \tau + TY^{(0)} \ , \\ \bar{x}^i &= x^i + L^{(0)}Y^{(0)i} + L^{(\pm1)}Y^{(\pm1)\,i}, \end{aligned} \tag{2.22}$$

where $L^{(0)}, L^{(\pm1)}$ and T are arbitrary functions of time. The metric perturbation $h_{\mu\nu}$ is not invariant under this change of coordinates; indeed, this transformation will reflect in a change of the metric tensor as follows:

$$\bar{\tilde{g}}_{\mu\nu}(\bar{x}) = \tilde{g}_{\rho\sigma}(x)\frac{\partial x^\rho}{\partial\bar{x}^\mu}\frac{\partial x^\sigma}{\partial\bar{x}^\nu} \ . \tag{2.23}$$

In order to compare perturbations at points having the same coordinates, the quantities in the frame with space-time grid x^μ are expanded around $\bar{x}^\mu$, and it is simple to obtain the following gauge transformations in the metric perturbations:

$$\begin{aligned} \bar{A}^{(0)} &= A^{(0)} - \dot{T} - \frac{\dot{a}}{a}T \ , \\ \bar{B}^{(0)} &= B^{(0)} + \dot{L}^{(0)} + kT \ \ , \ \ \bar{B}^{(\pm1)} = B^{(\pm1)} + \dot{L}^{(\pm1)} \ , \\ \bar{H}_L^{(0)} &= H_L^{(0)} - \frac{k}{3}L^{(0)} - \frac{\dot{a}}{a}T \ , \\ \bar{H}_T^{(0)} &= H_T^{(0)} + kL^{(0)} \ , \ \bar{H}_T^{(\pm1)} = H_T^{(\pm1)} + kL^{(\pm1)} \ , \ \bar{H}_T^{(\pm2)} = H_T^{(\pm2)} \ . \end{aligned} \tag{2.24}$$

With the same procedure, we obtain the link between perturbations of the stress energy tensor in the two frames related by the transformations (2.22):

$$\begin{aligned} \bar{\delta} &= \delta + 3(1+w)\frac{\dot{a}}{a}T \ , \ \bar{\pi}_L^{(0)} = \pi_L^{(0)} + 3c_s^2\frac{1+w}{w}\frac{\dot{a}}{a}T \ , \\ \bar{v}^{(0)} &= v^{(0)} + \dot{L}^{(0)} \ , \ \bar{v}^{(\pm1)} = v^{(\pm1)} + \dot{L}^{(\pm1)} \ , \\ \bar{\pi}_T^{(0)} &= \pi_T^{(0)} \ , \ \bar{\pi}_T^{(\pm1)} = \pi_T^{(\pm1)} \ , \bar{\pi}_T^{(\pm2)} = \pi_T^{(\pm2)} \ . \end{aligned} \tag{2.25}$$

From now on, we will concentrate on scalar type gauge transformations and we will omit the index $^{(0)}$ from the amplitude of metric and matter scalar perturbations. The gauge transformations are therefore

$$\tilde{\tau} = \tau + TY^{(0)} \ , \ \tilde{x}^i = x^i + LY^{(0)i} \ .$$

To first order, the quantities describing the perturbed metric become

$$\bar{A} = A - \dot{T} - \frac{\dot{a}}{a}T \ ,$$

$$\bar{B} = B + \dot{L} + kT \ ,$$

$$\bar{H}_L = H_L - \frac{k}{3}L^{(0)} - \frac{\dot{a}}{a}T \ ,$$

$$\bar{H}_T = H_T + kL \ . \tag{2.26}$$

It is possible to construct two independent gauge-invariant quantities by means of linear combinations of (2.26) that eliminate the dependence on the two functions T and L. An example of such combinations is given by the Bardeen's invariants Φ and Ψ:

$$\Phi = H_L + \frac{1}{3}H_T + \frac{1}{k}\frac{\dot{a}}{a}\left(B - \frac{1}{k}\dot{H}_T\right) \ , \tag{2.27}$$

$$\Psi = A + \frac{1}{k}\frac{\dot{a}}{a}\left(B - \frac{1}{k}\dot{H}_T\right) + \frac{1}{k}\left(\dot{B} - \frac{1}{k}\ddot{H}_T\right) \ . \tag{2.28}$$

Any linear combination of Φ and Ψ and their time derivatives, whose coefficients are chosen as arbitrary function of time, is a gauge invariant quantity too.
The quantities Ψ and Φ have a deep physical meaning; in order to understand it, we will link them to fluid quantities. Let us consider the time slicing (i.e. the family of constant time hypersurfaces) associated with a given choice of time coordinate in the perturbed spacetime, and let V^μ be the time-like unit vector field normal to the constant time hypersurfaces; the covariant derivative of any time-like unit vector field can be decomposed as

$$V_{\mu;\nu} = \omega_{\mu\nu} + \sigma_{\mu\nu} + \frac{\theta}{3}P_{\mu\nu} - a_\mu V_\nu \ ,$$

where

$$P_{\mu\nu} \equiv g_{\mu\nu} + V_\mu V_\nu \ , \tag{2.29}$$

$$\omega_{\mu\nu} \equiv P^\alpha_\mu P^\beta_\nu (V_{\alpha;\beta} - V_{\beta;\alpha}) \ , \tag{2.30}$$

$$\theta \equiv V^\mu{}_{;\mu} \ , \tag{2.31}$$

$$\sigma_{\mu\nu} \equiv \frac{1}{2}P^\alpha_\mu P^\beta_\nu (V_{\alpha;\beta} + V_{\beta;\alpha}) - \frac{1}{3}\theta P_{\mu\nu} \ , \tag{2.32}$$

$$a_\mu \equiv V_{\mu;\nu}V^\nu \tag{2.33}$$

The quantities $\omega_{\mu\nu}, \theta, \sigma_{\mu\nu}$ and a_μ are the vorticity, expansion rate, shear and acceleration of the time-like unit vector filed V^μ respectively. The unit vector field $\tilde{V}^\mu$ normal to constant time hypersurfaces of the perturbed space is

$$\tilde{V}^0 = a^{-1}(1 - AY^{(0)}) \ , \ \tilde{V}^i = -BY^{(0)i} \tag{2.34}$$

and the quantities defined above can therefore be computed with the help of the perturbed Christoffel symbols, resulting in

$$\tilde{\omega}_{\mu\nu} = 0 \ , \tag{2.35}$$

$$\tilde{\theta} = 3\frac{\dot{a}}{a^2}[1 + \mathcal{K}_g Y^{(0)}] \ , \tag{2.36}$$

$$\tilde{\sigma_{00}} = \tilde{\sigma_{0i}} = 0 \ , \tilde{\sigma_{ij}} = ak\sigma_g Y^{(0)}_{ij} \ , \tag{2.37}$$

$$\tilde{a}_0 = 0 \ , \ \tilde{a}_j = -kA^{(0)}Y^{(0)}_j \tag{2.38}$$

where

$$\mathcal{K}_g \equiv -A + \frac{1}{3}\left(\frac{a^2}{\dot{a}}\right)B + \left(\frac{a}{\dot{a}}\right)\dot{H}_L \ , \tag{2.39}$$

$$\sigma_g \equiv k^{-1}\dot{H}_T - B \quad . \tag{2.40}$$

We see that in the unperturbed background, $\tilde{\theta}$ reduces to the expansion rate of the spatial volume per unit proper time, while the shear $\tilde{\sigma}_{\mu\nu}$ vanishes because of the spatial isotropy: this allows us to interpret $\mathcal{K}$ as the amplitude of the perturbation in the expansion rate and σ_g as that of the shear, while $A^{(0)}$ is the amplitude of the acceleration: in the Newtonian limit, it is generally interpreted as the conventional gravitational potential.
It can be shown (see [133]) that the perturbation in the intrinsic curvature of the constant time hypersurfaces, with respect to a flat unperturbed background, is given by:

$$\delta R = \frac{4k^2}{a^2}\mathcal{R}Y^{(0)} \tag{2.41}$$

where

$$\mathcal{R} = H_L + \frac{H_T}{3} \quad . \tag{2.42}$$

With the use of the definitions (2.27),(2.40), (2.42), we can express Φ and Ψ as linear combinations of $\mathcal{R}$ and σ_g:

$$\Phi = \mathcal{R} - k^{-1}(\dot{a}/a)\sigma_g \tag{2.43}$$

$$\Psi = A^{(0)} - k^{-1}(\dot{a}/a)\sigma_g - k^{-1}\dot{\sigma}_g \tag{2.44}$$

It is straightforward to assign a physical meaning to Φ and Ψ in a particular time slicing, namely that specified by the condition $\sigma_g = 0$ ("Newtonian slicing"): from eq. (2.43) it follows that Φ reduces, in that time slicing, to the amplitude of perturbation in the intrinsic curvature of the space; on the other hand, as we will see, the perturbed Einstein equations in the gauge-invariant formalism can be written in such a way that Ψ can be interpreted as the amplitude of perturbation in the gravitational potential. In order to write Einstein equations in the most simple form, it is useful to introduce two gauge invariant geometrical quantities,

$$\mathcal{A} = A - a^{-1}\frac{d}{d\tau}\left[\left(\frac{\dot{a}}{a}\right)^{-1} a\mathcal{R}\right] = A - a^{-1}\frac{d}{d\tau}\left[\left(\frac{a^2}{\dot{a}}\right)\left(H_L + \frac{H_T}{3}\right)\right] \tag{2.45}$$

$$\mathcal{B} = k(\frac{\dot{a}}{a})^{-1}\mathcal{R} - \sigma_g = B + (\frac{\dot{a}}{a})^{-1}k(H_L + \frac{H_T}{3}) - k^{-1}\dot{H}_T \tag{2.46}$$

Now, let us introduce gauge-invariant quantities for the matter variables. Under a gauge transformation, the spatial velocity perturbation, density perturbation, isotropic pressure perturbation and anisotropic perturbation transform respectively as

$$\bar{v} = v + \dot{L} \;\; ; \;\; \bar{\delta} = \delta + \frac{(1+w)}{3}\left(\frac{\dot{a}}{a}\right)T \;\; ,$$

$$\bar{\pi}_L = \pi_L + \frac{c_s^2}{w}3(1+w)\frac{\dot{a}}{a}T \;\; , \;\; \bar{\pi}_T = \pi_T \;\; ,$$

where $c_s^2 \equiv \dot{p}/\dot{\rho}$.
Therefore, we can construct two gauge-invariants from matter variables,

$$\Gamma \equiv \pi_L - \frac{c_s^2}{w}\delta \tag{2.47}$$

$$\Pi \equiv \pi_T \quad . \tag{2.48}$$

The gauge invariance of Γ, together with its vanishing for adiabatic perturbations, allows to give a gauge-invariant meaning to the concept of adiabatic perturbations: Γ will be interpreted as the amplitude of an entropy perturbation.

The most important gauge invariant quantities that can be constructed from matter variables are defined as follows:

$$V \equiv v - k^{-1}\dot{H}_T \quad \text{and} \quad \Delta = \delta + 3(1+w)(\dot{a}/a)k^{-1}(v-B) \tag{2.49}$$

From eq. (2.40), we see that in the Newtonian slicing $\sigma_g = 0$ the gauge invariant V has a direct physical meaning, reducing to $V = v - B$: since B is the amplitude of a perturbation in the shift vector, defined as the rate of deviation of a constant space-coordinate from a line normal to a constant time hypersurface, V represents the matter velocity relative to the normal line observers. On the other hand, the gauge invariant Δ represents the density contrast in the slicing such that the fluid four-velocity is orthogonal to constant time hypersurfaces. When Δ and V are used as the fundamental variables representing the perturbed state of matter, the Einstein equations can be written in a rather simple form; another useful variable that refers to the density contrast is represented by the combination:

$$\Delta_g \equiv \delta + 3(1+w)\mathcal{R} \ ; \tag{2.50}$$

in a flat slicing, i.e. in a slicing where the perturbation of the scalar curvature vanishes in the constant time hypersurfaces, Δ_g is just the density contrast.
Now, let us come to the linearized Einstein equations

$$\delta G^{\mu}_{\nu} = 8\pi G \delta T^{\mu}_{\nu} \quad , \tag{2.51}$$

that can be written in terms of the gauge-invariant quantities defined above: the time-time, longitudinal time-space, trace space-space and longitudinal traceless space-space components of the Einstein equations, in the Fourier space, are:

$$\delta G^0_0 = 8\pi G \delta T^0_0 \rightarrow 3\left(\frac{\dot{a}}{a}^2\right)\mathcal{A} - \frac{\dot{a}}{a}k\mathcal{B} = -\frac{8\pi G}{3}a^2\rho\Delta_g \tag{2.52}$$

$$\delta G^0_i = 8\pi G \delta T^0_i \rightarrow k\frac{\dot{a}}{a}\mathcal{A} + 4\pi G a^2(p+\rho)\mathcal{B} = -4\pi G a^2(p+\rho)V \tag{2.53}$$

$$\delta G^i_j = 8\pi G \delta T^i_j \rightarrow \text{trace part and traceless part}$$

The trace part gives:

$$\frac{\dot{a}}{a}\dot{\mathcal{A}} + \left\{2a\frac{d}{d\tau}\left(\frac{\dot{a}}{a}\right) + 3\left(\frac{\dot{a}}{a}\right)^2\right\}\mathcal{A} = 4\pi G a^2 p\left(\Gamma + \frac{c_s^2}{w}\Delta_g\right) - \frac{8\pi G}{3}a^2 p\Pi \tag{2.54}$$

and the traceless part:

$$\mathcal{A} + k^{-1}a^{-2}\frac{d}{d\tau}(a^2\mathcal{B}) = -8\pi G k^{-2}a^2 p\Pi \quad . \tag{2.55}$$

From the definition of Ψ and Φ, eq. (2.55) can be rewritten as

$$\Psi + \Phi = -8\pi G a^2 k^{-2} p\Pi \tag{2.56}$$

At this point, it is useful to note that, whenever the anisotropic stress can be neglected, equation (2.56) can be expressed, in a zero-curvature space, in the same form as the usual Newtonian Poisson equation for the gravitational potential induced by some energy density perturbation Δ:

$$\frac{1}{a^2}\nabla^2\Psi = 4\pi G\rho\Delta \ ; \tag{2.57}$$

this supports the interpretation of Ψ as the relativistic generalization of the Newtonian gravitational potential, as we anticipated above.
A further manipulation allows us to express equations (2.54) and (2.55) in terms of the matter variables only:

$$\dot{\Delta} - 3w\frac{\dot{a}}{a}\Delta = -(1+w)kV - 2\frac{\dot{a}}{a}w\Pi \ , \tag{2.58}$$

$$\dot{V} + \frac{\dot{a}}{a}V = k\left[\frac{{c_s}^2}{1+w}\Delta + \frac{w}{1+w}\Gamma\right] + k\Psi - \frac{2k}{3}\frac{w}{1+w}\Pi \quad . \tag{2.59}$$

The latter two equations could also be obtained by the fluid equation of motion

$$\delta(\tilde{T}^{\mu}_{\nu;\mu}) = 0 \quad . \tag{2.60}$$

These are the equations describing, in a gauge-invariant form, the temporal evolution of density and velocity fluid perturbations; we can see that fluid perturbation evolution depends on many contributions, of both geometrical and physical origin. The second term in the left-hand side of eq. (2.58) represents the adiabatic change in the density contrast generated from the cosmic expansion; analogously, the second term in the left-hand side of eq. (2.59) is of cosmological origin, representing the adiabatic slowing-down of velocity due to the universe expansion.

$$\ddot{\Delta} - \left\{3(2w - c_s^2) - 1\right\}\frac{\dot{a}}{a}\dot{\Delta} + 3\left\{\left[\frac{3}{2}w^2 - 4w - \frac{1}{2} + 3c_s^2\right]\left(\frac{\dot{a}}{a}\right)^2 + \frac{k^2c_s^2}{3}\right\}\Delta = \mathcal{S} \tag{2.61}$$

where

$$\mathcal{S} = -k^2w\Gamma - 2\frac{\dot{a}}{a}w\dot{\Pi} + \left\{3[(w^2 + c_s^2) - 2w]\left(\frac{\dot{a}}{a}\right)^2 + \frac{k^2}{3}c_s^2\right\}2\Pi \quad . \tag{2.62}$$

From eq. (2.61) we see that an entropy perturbation Γ and an anisotropic stress perturbation Π can act as sources for density perturbations.
This is quite important for the case in which a multi-component system is investigated. That is the subject of the next section; as we shall see, in most of realistic situations, the appearance of Π and Γ is a consequence of some intrinsic structure of matter; in particular, this is true for multi-component systems. Entropy perturbations can be generated if the different matter components are distributed nonuniformly in space but with uniform total energy density and hence uniform curvature at the beginning. Such perturbations are often called isocurvature perturbations. An example of entropy perturbations is an inhomogeneous distribution of baryons in a radiation background, with the energy density excess in baryons being initially compensated by a deficit in radiation energy. In traditional isocurvature models, the initial density balance comes at the expense of number density or "entropy" fluctuations between matter and radiation. In isocurvature scenarios, structure formation proceeds by such initial stress fluctuations between matter and radiation, which push the matter into gravitationally unstable configurations.
Instead, for adiabatic perturbations, the source term in 2.61 vanishes, and the equations become homogeneous; in the adiabatic scenario, conventional models for structure formation utilize such initial density fluctuations that then grow by gravitational instability. We will come back to these scenarios in chapter 4. Before to go on, we wish to observe that the terms "isocurvature" and "isothermal" fluctuations are often used interchangeably in the literature, even if they are not precisely equivalent. So long as an isocurvature mode is super-horizon sized, it must be characterized by zero total density perturbations, because causality precludes the super-horizon redistribution of energy density (it can be converted into an energy density perturbation once it enters the horizon). Using the fact that the total energy density perturbation must remain equal to zero on super-horizon scales, it is possible to relate the photon temperature fluctuation to the perturbations S_{Xi} in the ratio of the number density of each species Xi to the number density of photons [134]. The resulting temperature perturbation is proportional to the ratio of the energy density of each species to that of photons, and is negligible at early times, when radiation dominates: hence the name "isothermal" .
The two definitions are nearly coincident at early times, when a very little temperature fluctuation compensates for energy density perturbations in the fluid components.

2.2 Extension to a multi-component fluid

The formalism described above is useful when the energy density of the universe is dominated by a single fluid component. However, when the matter can be considered as a mixture of many fluid

components. The gauge-invariant fluid perturbation defined above are still meaningful, but they must be regarded as representing the state of matter as a whole, i.e. the average properties of the perturbed system. In a multi-component system, the energy-momentum tensor of the single component (denoted by an index "a") will not generally be conserved:

$$\tilde{T}^{\nu}_{(a)\mu;\nu} = \tilde{Q}_{(a)\mu} \tag{2.63}$$

However, since the total energy-momentum must obey the conservation law, the source terms $\tilde{Q}_{(a)\mu}$ appearing in the single-component energy-momentum divergences in eq. (2.63) must cancel,

$$\tilde{T}^{\nu}_{\mu;\nu} = \sum_a \tilde{T}^{\nu}_{(a)\mu;\nu} = 0 \implies \sum_a \tilde{Q}_{(a)\mu} = 0 \tag{2.64}$$

Since we assumed that for the single component

$$T^{\nu}_{(a)\mu} = (\rho_{(a)} + p_{(a)})u_\mu u^\nu + p_{(a)}\delta^\nu_\mu \ , \tag{2.65}$$

with $u^\mu = (a^{-1}, \mathbf{0})$, then the equation of motion in the unperturbed background will acquire a source term

$$\dot{\rho}_{(a)} = -3\frac{\dot{a}}{a}(p_{(a)} + \rho_{(a)}) + Q_{(a)} \tag{2.66}$$

where $Q_{(a)\mu} = (-aQ_{(a)}, \mathbf{0})$.

Now, let us consider the gauge-invariant perturbation variables that we can construct for each component. The relations with gauge-dependent ones are the same as those of the total matter. Again, the 4-velocity and the proper energy density of each fluid component are defined in terms of the eigenvector and the corresponding eigenvalue of the energy-momentum tensor,

$$\tilde{T}(a)^{\nu}_{\mu}\tilde{u}^{\nu}_{(a)} = -\tilde{\rho}_{(a)}\tilde{u}^{\mu}_{(a)} \ , \tag{2.67}$$

and equations (2.17),(2.18),(2.19) are still satisfied, by simply attaching the suffix (a) to each variable. Therefore the Einstein equations (2.51) remain the same by defining

$$\rho\delta = \sum_{(\alpha)} \rho_{(\alpha)}\delta_{(\alpha)} \ , \tag{2.68}$$

$$(\rho + p)v = \sum_{(\alpha)} (\rho_{(\alpha)} + p_{(\alpha)})v_{(\alpha)} \ , \tag{2.69}$$

$$p\pi_L = \sum_{(\alpha)} p_{(\alpha)}\pi_{L(\alpha)} \ , \tag{2.70}$$

$$p\pi_T = \sum_{(\alpha)} p_{(\alpha)}\pi_{T(\alpha)} \ , \tag{2.71}$$

where of course $\rho = \sum_{(\alpha)} \rho_{(\alpha)}$ and $p = \sum_{(\alpha)} p_{(\alpha)}$; also the total sound speed can be defined in terms of the ones from the single species as

$$c_s^2 = \sum_{(\alpha)} p_{(\alpha)} c^2_{s(\alpha)}/\rho \ . \tag{2.72}$$

For what concerns the perturbations of each single species, their gauge transformations are identical to that of v, δ, π_L and π_T, with the only difference coming from the exchange terms $Q_{(\alpha)\mu}$; restricting ourself to scalar gauge transformations,

$$\bar{v}_{(a)} = v_{(a)} + \dot{L} \ , \tag{2.73}$$

$$\bar{\delta}_{(a)} = \delta_{(a)} + 3(1 + w_{(a)})\frac{\dot{a}}{a}(1 - q_{(a)})T \ , \tag{2.74}$$

$$\bar{\pi}_{L(a)} = \pi_{L(a)} + \frac{3c^2_{(a)}}{w_{(a)}}(1 + w_{(a)})(1 - q_{(a)})\frac{\dot{a}}{a}T \ , \tag{2.75}$$

$$\bar{\pi}_{T(a)} = \pi_{T(a)} \tag{2.76}$$

where

$$q_{(a)} \equiv Q_{(a)} / \left(3\frac{\dot{a}}{a} h_{(a)}\right) \tag{2.77}$$

$$h_{(a)} \equiv \rho_{(a)} + p_{(a)} \tag{2.78}$$

The gauge invariant variables that can be constructed from these gauge-dependent quantities are

$$V_{(a)} \equiv v_{(a)} - k^{-1}\dot{H}_T \ , \tag{2.79}$$

$$\Delta_{(a)} \equiv \delta_{(a)} + 3(1+w_{(a)})(1-q_{(a)})\frac{\dot{a}}{a}k^{-1}(v_{(a)} - B) \ , \tag{2.80}$$

$$\Gamma_{(a)} \equiv \pi_{L(a)} - \frac{c^2_{(a)}}{w_{(a)}}\delta_{(a)} \ , \tag{2.81}$$

$$\Pi_{(a)} \equiv \pi_{T(a)} \tag{2.82}$$

We can observe that $\Delta_{(a)}$ is the density perturbation of the a-component relative the hypersurface representing the rest frame of the a-component, therefore it can be useful for describing of the intrinsic perturbations of the single component; however, a more intuitive expression of the total-matter gauge invariant density perturbation can be obtained by introducing the gauge invariant density perturbation $\Delta_{c(a)}$ of the single components in the total matter rest frame,

$$\Delta_{c(a)} \equiv \delta_{(a)} + 3(1+w_{(a)})(1-q_{(a)})\frac{\dot{a}}{a}k^{-1}(v - B) \ . \tag{2.83}$$

Finally, we are able to relate, in the gauge invariant formalism, the total matter perturbations to those relative to the single components:

$$\rho\Delta = \sum_a \rho_{(a)}\Delta_{c(a)} \tag{2.84}$$

$$= \sum_a \rho_{(a)}\Delta_{(a)} + \frac{a}{k}\sum_a Q_{(a)}V_{(a)} \ , \tag{2.85}$$

$$hV = \sum_a h_{(a)}V_{(a)} \ , \tag{2.86}$$

$$p\Gamma = p\Gamma_{int} + p\Gamma_{rel} \ , \tag{2.87}$$

$$p\Pi = \sum_a p_{(a)}\Pi_{(a)} \ , \tag{2.88}$$

where

$$p\Gamma_{int} \equiv \sum_a p_{(a)}\Gamma_{(a)} \ , \tag{2.89}$$

$$p\Gamma_{rel} \equiv \sum_a (c^2_{(a)} - c^2_s)\delta\rho_{(a)} =$$

$$= \sum_a (c^2_{(a)} - c^2_s)\rho_{(a)}\Delta_{c(a)} \tag{2.90}$$

$$c^2_s = \sum_a \frac{h_a}{h}(1-q_{(a)})c^2_{(a)} \ . \tag{2.91}$$

The gauge invariance of Γ_{rel} is a direct consequence of the gauge invariance of Γ and Γ_{int}; the latter is an intrinsic entropy perturbation of a fluid component, while the physical meaning of the relative entropy perturbation can be better understood by

$$p\Gamma_{rel} = \frac{1}{2}\sum_{a,b}\frac{h_{(a)}h_{(b)}}{h}(1-q_{(a)})(1-q_{(b)})(c^2_{(a)} - c^2_{(b)}) \times$$

$$\left[\frac{\Delta_{c(a)}}{(1+w_{(a)})(1-q_{(a)})} - \frac{\Delta_{c(b)}}{(1+w_{(b)})(1-q_{(b)})}\right]$$

$$= \frac{1}{2}\sum_{a,b}\frac{h_{(a)}h_{(b)}}{h}(c^2_{(a)}-c^2_{(b)})S_{(a)(b)} + \frac{1}{2N(1+w)}\sum_{a,b}\frac{1}{n}\left(\frac{\dot{a}}{a}\right)^{-1}(c^2_{(b)}-c^2_{(a)})(Q_{(b)}-Q_{(a)}) \ , \quad (2.92)$$

where N is the number of components and

$$S_{(a)(b)} \equiv \frac{\Delta_{c(a)}}{(1+w_{(a)})} - \frac{\Delta_{c(b)}}{(1+w_{(b)})} \ . \quad (2.93)$$

Equation (2.87) is of fundamental importance, since it shows that the total entropy perturbation has two contributions of different origin: the internal entropy of the single fluids adds to a relative entropy contribution, that originates from the differences in the dynamical properties of the single fluids, in particular the sound velocities. Most importantly, the extension of the formalism to a multi-component fluid implies that, generally, entropy perturbations will arise in any multi-component system. At the end of sect. 2.1, we already noted that entropy perturbations can act as sources for density perturbations (see eqs. 2.61 and 2.62); furthermore, by writing down the dynamical equations for the quantities $S_{(a)(b)}$, it is possible to show that, in a multi-component system, entropy perturbations can be (and, generally, are) inherited from purely adiabatic perturbations: they are coupled with each other, once the scale of the perturbation enters the horizon and sub-horizon causal dynamics has begun.

2.3 Gauge-dependent methods

For practical applications of perturbation theory, it is often necessary to fix the gauge in order to set the initial conditions on the perturbation variables or to interpret the results obtained.
In order to specify a gauge, we must fix the space-time coordinates; let us concentrate on scalar-type perturbations. The choice of the time slicing for the perturbed spacetime is given by imposing a constraint on one of the gauge-dependent variables whose change under the gauge transformations 2.22 is expressed only in terms of T, as is the case for $A, v-B, \mathcal{R}, \mathcal{K}_g$ and σ_g; for each time slicing, the gauge freedom associated to the spatial coordinates is eliminated by imposing a condition on a quantity whose change under the gauge transformations 2.22 involves only L.
In the following, we will review two typical gauge conditions, namely the *synchronous* and the *Newtonian* gauges, which will be used in this thesis.

2.3.1 The Conformal Newtonian gauge

As seen, the most general form of a metric perturbed by scalar fluctuations at a given Fourier mode $\vec{k}$ is

$$g_{00} = -a^2[1+2Ae^{ik\cdot x}] \ , \quad (2.94)$$
$$g_{0j} = a^2 B\ i\hat{k}_j e^{ik\cdot x} \ , \quad (2.95)$$
$$g_{ij} = a^2\{\delta_{ij}+[2H_L\delta_{ij}(-\hat{k}_i\hat{k}_j+\delta_{ij}/3)]e^{ik\cdot x}\} \ . \quad (2.96)$$

The choice of the gauge allows to eliminate two out of the four metric terms. In the Newtonian gauge, $B = H_T = 0$, and it is traditional to label the Newtonian potential $A = \Psi$ and the space curvature perturbation $H_L = \Phi$. From 2.43 and 2.44, we see that the coordinate frame here corresponds to zero-shear hypersurfaces where the expansion appears isotropic. Inside the horizon, the analysis of perturbations reduces to the standard Newtonian treatment, helping our physical intuition.
The first-order perturbed Einstein equations in this gauge are given by the following system:

$$-k^2\Phi + 3\frac{\dot{a}}{a}\left(-\dot{\Phi}+\frac{\dot{a}}{a}\Psi\right) = 4\pi G a^2\delta T^0_0(\mathrm{Con}) \quad (2.97)$$

$$k^2\left(\frac{-\dot{\Phi}+\dot{a}}{a\Psi}\right) = (\bar{\rho}+\bar{P})\theta(\mathrm{Con}) \tag{2.98}$$

$$-\ddot{\Phi}+\frac{\dot{a}}{a}(\dot{\Psi}+2\dot{\Phi})+\left(2\frac{\ddot{a}}{a}-\frac{\dot{a}^2}{a^2}\right)\Psi - \frac{k^2}{3}(\Phi+\Psi) \tag{2.99}$$

$$= \frac{4\pi}{3Ga^2\delta T_i^i(\mathrm{Con})}\ , \tag{2.100}$$

$$k^2(\Psi+\Phi) = -12\pi G a^2(\bar{\rho}+\bar{P})\sigma(\mathrm{Con}) \quad . \tag{2.101}$$

The label "Con" is used to specify the gauge. The variables θ and σ are defined as

$$(\bar{\rho}+\bar{P})\theta \equiv \delta T_j^0 \quad , \quad (\bar{\rho}+\bar{P})\sigma \equiv -(\hat{k}_i\cdot\hat{k}_j - \frac{1}{3}\delta_{ij})\Sigma_j^i$$

and $\Sigma_j^i \equiv T_j^i - \delta_j^i T_k^k/3$ denotes the traceless component of T_j^i. This σ is related to the anisotropic stress Π in 2.88 by $\sigma = 2\Pi\bar{P}/3(\bar{\rho}+\bar{P})$.
This gauge will be mostly used in chapter 3 for the description of the physics of CMB anisotropies.

2.3.2 The synchronous gauge

The gauge condition (i.e. the choice of the perturbed spacetime slicing) completely fixes the frame in which perturbations are measured. As we anticipated, ambiguities due to unphysical modes of perturbations can only arise if the coordinate system is not entirely fixed, as is the case for the *synchronous gauge*, in which the space-coordinates are specified by the condition that the lines of constant space-coordinates are orthogonal to the constant time hypersurfaces, that is $A = B = 0$. Given any initial system of coordinates x^μ it is always possible to find a coordinate transformation to the synchronous gauge $x^\mu \to x^\mu + \zeta^\mu$. To do this, one sets $\bar{A} = \bar{B} = 0$ in (2.24) and solves for τ and x^i; however, this does not completely fix the synchronous coordinates. It can be shown (see, e.g., [160]) that, under a residual transformation of τ and x^i, the synchronous-gauge conditions are maintained; this residual coordinate freedom in synchronous gauge leads to the appearance of unphysical modes that render the interpretation of synchronous gauge calculations difficult (see [176]). Gauge modes can be avoided by completely fixing the coordinates. The definition of Newtonian gauge already does so, while a synchronous coordinate system, defined by a set of freely falling observers, requires a further specification of this set through the initial conditions [148, 133, 160].
The components g_{00} and g_{0i} of the metric tensor in the synchronous gauge are by definition unperturbed; the line element is given by $ds^2 = a^2[-d\tau^2 + (\delta_{ij}+h_{ij})dx^i dx^j]$. Since we are interested here only on scalar-type perturbations, the metric perturbations can be parametrized as

$$h_{ij}(\mathbf{x},\tau) = \int d^3k e^{i\mathbf{k}\cdot\mathbf{x}}\left[\hat{\mathbf{k}}_\mathbf{i}\hat{\mathbf{k}}_\mathbf{j}h(\mathbf{k},\tau) + (\hat{\mathbf{k}}_\mathbf{i}\hat{\mathbf{k}}_\mathbf{j} - \frac{1}{3}\delta_{ij})6\eta(\mathbf{k},\tau)\right]\ , \tag{2.102}$$

with $\mathbf{k} = k\hat{k}$; here, $h \equiv 6H_L$ denotes the trace of h_{ij}, and $\eta \equiv -H_L - \frac{H_T}{3}$.
Note that the synchronous potentials h and η in k-space are related to the gauge-invariant variables $\mathbf{\Phi}_A$ of Bardeen (1980) and Ψ of Kodama and Sasaki (1984) by the relation

$$\mathbf{\Phi}_A = \Psi = \frac{1}{2k^2}\left[\ddot{h}+6\ddot{\eta}+\frac{\dot{a}}{a}\left(\dot{h}+6\dot{\eta}\right)\right]\ , \tag{2.103}$$

and to Φ_H of Bardeen (1980) and Φ of Kodama and Sasaki (1984) by

$$\mathbf{\Phi}_H = \Phi = -\eta + \frac{1}{k^2}\frac{\dot{a}}{a}[\dot{h}+6\eta] \quad . \tag{2.104}$$

An important gauge-invariant quantity that can be constructed from Ψ and related to h and η through 2.103 is

$$\zeta = \frac{2}{3}(\mathcal{H}^{-1}\dot{\mathbf{\Psi}}+\mathbf{\Psi})/(1+w)+\mathbf{\Psi} \quad . \tag{2.105}$$

As shown in [147], in the comoving gauge ζ takes on the physical meaning of a curvature perturbation. Now, let us come to the equations describing the evolution of perturbations in the synchronous gauge. The scalar metric perturbations are characterized by the two "potentials" $h(\mathbf{k},\tau)$ and $\eta(\mathbf{k},\tau)$ in the Fourier space k. The linearized Einstein equations in this gauge give the following system [148]:

$$k^2\eta - \frac{1}{2}\frac{\dot{a}}{a}\dot{h} = 4\pi G a^2 \delta T_0^0(Syn) \ , \tag{2.106}$$

$$k^2\dot{\eta} = 4\pi G a^2(\bar{\rho}+\bar{P})\theta(Syn) \ , \tag{2.107}$$

$$\ddot{h} + 2\frac{\dot{a}}{a}\dot{h} - 2k^2\eta = -8\pi G a^2 \delta T_i^i(Syn) \ , \tag{2.108}$$

$$\ddot{h} + 6\ddot{\eta} + 2\frac{\dot{a}}{a}(\dot{h}+6\dot{\eta}) - 2k^2\eta = -24\pi G a^2(\bar{\rho}+\bar{P})\sigma(Syn) \ . \tag{2.109}$$

Despite the difficulties related to the gauge modes, the evolution equations and their solutions are simplified in this gauge, so we will adopt it in this thesis, when dealing with a system including scalar fields. The conformal Newtonian gauge will be instead used in chapter 3, in order to have an easier physical intuition of the anisotropy formation processes.

2.3.3 Conclusions

In this chapter, the most important tools of the linear cosmological perturbation theory have been defined. In principle, once one has specified the background metric, the composition of the cosmic fluid together with the state equations relating pressure and energy density of each component and the initial conditions, the equations exposed above may be integrated to evolve the cosmological system in time; note that one can do this while the perturbations are small with respect to the unperturbed quantities, in other words in the linear regime. Unfortunately, at the present the universe is not in the linear regime on all the scales; non-linearity is evident on the scale of stars and galaxies, as the result of recent non-linear growth of the perturbations that, on a larger scale, are still in the linear regime; this is strongly supported by observations of the universe in its remote past, through the CMB, that reveals perturbations in linear regime on all scales. A general study of the physics of CMB will be the subject of the next chapter.

Chapter 3

The physics of the CMB: an overview

3.1 Physical foundations

Observations of the cosmic microwave background (CMB), a thermal sea of photons at $2.725 \pm 0.001K$ [83], is the cornerstone of the modern cosmology. The discovery of the CMB came in 1964, when Penzias and Wilson [169] detected it as an anomalous noise coming from all directions, consistent with the thermal emission of a $\simeq 3K$ blackbody spectrum.
This was interpreted as the relic radiation in the expanding universe by Dicke et al. [64], strongly supporting the Hot Big Bang paradigm: in the Hot Big Bang model, the universe was once hot and dense, and it has been expanding and adiabatically cooling ever since. When the universe was $\simeq 10^5$ years old, at a redshift of about 10^3 from us, its temperature was around $3000K$ (kT$\simeq 0.25eV$), so that the CMB photons were hot enough to ionize hydrogen. Before this epoch, the dominant interaction process was Compton scattering off free electrons; due to the high electron density in the early universe, the Compton mean free path was much smaller than the particle horizon at that time, making the universe opaque to radiation. The photons were tightly coupled to the electrons, which in turn were tightly coupled to the protons by Coulomb interactions: in some sense, electrons "glue" the baryons to the photons by Compton scattering and by electromagnetic interactions, so that the resulting dynamics involve a single photon-baryon fluid (tight coupling approximation). As a consequence, perturbations in number, and hence in energy density, of photons and baryons, were forced to evolve together. Furthermore, as we shall see analytically, scattering isotropizes the photons in the electron rest frame, resulting in a coupling between the electron velocity and the CMB dipole.
Since scattering does not change the net energy or photon number in the CMB photons to lowest order (in the Thomson limit, energy exchange only occurs to $O(T_e/m_e)$), spectral distortions to the blackbody do not arise in linear theory.
As the temperature drops below $3,000\ K$, the free electrons trapping the photons vanish as atomic hydrogen, setting the photons free, and the majority of them have interacted only gravitationally with matter since that time. The sphere surrounding us at $z^* \simeq 1000$ (which represent the position at which the photons seen today as CMB radiation last interacted directly with matter) is called the *last scattering surface.*

Soon after the CMB discovery it was realized that the presence of fluctuations at the last scattering epoch would necessarily induce angular anisotropy in the CMB intensity: as neutral hydrogen formed (recombination), the photons last scattered, leaving fluctuations in the CMB frozen in at z^*, unless the universe suffered reionization at high redshift.
These anisotropies were indeed discovered in 1992 by the DMR experiment performed by the satellite COBE [202]; such small variations in the CMB temperature across the sky, detected at the level of 10^{-5}, encode a wealth of cosmological information that can be extracted from a detailed knowledge of the CMB physics.

The fundamental ingredients needed for describing the evolution of CMB anisotropies are two:

relativistic kinetic theory and perturbation theory. Kinetic theory describes the properties of the CMB photons radiation transport in a perturbed metric; the metric is perturbed as a consequence of gravitationally unstable density fluctuations, that evolve according to relativistic perturbation theory, treated in chapter 2. These two mechanisms yield a complete system able to describe the formation of CMB anisotropies in any model where structure formation proceeds by gravitational instability.
Conceptually, relativistic kinetic theory is identical to the non-relativistic one, since the phase space distribution is still conserved along geodesics, save for a collision term due to scattering:

$$\frac{df}{dt} \equiv \frac{\partial f}{\partial t} + \frac{\partial f}{\partial x^i}\frac{dx^i}{dt} + \frac{\partial f}{\partial p}\frac{dp}{dt} + \frac{\partial f}{\partial \gamma^i}\frac{d\gamma^i}{dt} = C[f] \ , \tag{3.1}$$

where γ^i are the direction cosines of the photon momentum p. In curved spaces, the terms $\dot{\gamma}^i$ do not vanish due to the curving of the geodesics.
As the CMB photons decouple from the baryons, they free stream taking with them three different imprints of the region from which they last scatter, namely the peculiar gravitational potential, the radial peculiar velocity and the density fluctuations (primary effects):

- Photons last scattered in a potential well will experience a gravitational redshift as they climb out of it;
- Photons last scattered by matter whose peculiar velocity is towards or away from us will receive a Doppler shift;
- Photons emanating from an overdense region will have a higher temperature, simply because denser regions are intrinsically hotter; regions of compression and rarefaction at this epoch result in hot and cold spots respectively in the CMB.

Actually, the free-streaming of photons after last scattering can be perturbed by many line-of-sight effects of different origin: processes affecting the CMB photons, and occurring on their way from the last scattering surface to us, i.e. in the redshift range $0 < z < 10^3$, are called secondary effects. Amongst the various secondary effects, the gravitational ones are directly connected with the baryon content: even if the baryons, after recombination, have essentially lost their ability to interact with the CMB photons through Thomson scattering, they will continue to affect them gravitationally. Any time variation in the gravitational potential along the photon trajectories will reflect in an additional gravitational redshift (Early and Late Integrated Sachs-Wolfe effect).
Other mechanisms of secondary anisotropies can arise if the baryons become reionized; this may happen locally, for instance confined to hot clusters of galaxies (SZ effect) or globally, throughout all of space.
The temperature distribution that we can measure in the microwave sky is also affected by tertiary sources of anisotropies, as the extragalactic radio and IR point sources [27], local emission from the Solar System, atmosphere, noise, etc., and Galactic emissions, associated with dust, free-free emission from ionized gas [180], and synchrotron emission [139] from relativistic electron (see e.g. [33], [209] for reviews). Although these are of course not CMB fluctuations in the conventional sense, reliable parameter estimation from CMB data requires accurate knowledge of their properties (see [31], [105], [9], [213], [214], [215]).

The combination of all these effects results in temperature differences on the last scattering surface that appear to the observer today as anisotropies in the sky: looking at the anisotropies of the CMB radiation on various angular scales, one can extract information on the physical processes that characterize different epochs of the history of the universe.
Since the horizon at z^* subtends an angle $\leq 1^\circ$ in the sky, the scales smaller than one degree reflect the status of CMB when the photons were tightly coupled to the electrons; on the other hand, the anisotropies on larger angular scales will reflect the status of the perturbations that, at recombination, were still outside the horizon.
But much information on the physics of the photon-baryon fluid can also be obtained by the analysis

of the polarization pattern of the CMB radiation (see [123], [124], [135], [244], [236]). Indeed, Thomson scattering of temperature anisotropies at the last scattering epoch also generates a linear polarization pattern on the sky. The dependence of Thomson scattering cross section on polarization can be read off by the relation (see e.g. [46]):

$$\frac{d\sigma_T}{d\Omega} \propto |\hat{\epsilon} \cdot \hat{\epsilon}'| \quad , \tag{3.2}$$

where $\hat{\epsilon}$ ($\hat{\epsilon}'$) are the incident (scattered) polarization directions in the electron rest frame. This makes the scattered radiation peaked in the direction normal to, with polarization parallel to, the incident polarization. If the incoming radiation were isotropic, orthogonal polarization states from incident directions separated by 90° would balance, so that the outgoing radiation would be unpolarized. Conversely, if the incident radiation field possesses a *quadrupolar* variation in intensity or temperature, the result is a linear polarization of the scattered radiation. A reversal in sign of the temperature fluctuation corresponds to a 90° rotation of the polarization, which reflects the spin-2 nature of polarization; when developing the radiation field into spherical harmonics $Y_m^l(\theta, \phi)$, the orthogonality of spherical harmonics guarantees that no other moment can generate polarization from Thomson scattering, so that the polarization pattern can be simply read off from the quadrupole moments ($l = 2.m = 0, \pm 1, \pm 2$) of the CMB anisotropies.
The reason why we should be concerned with the polarized component of the CMB anisotropies is that polarization probes the epoch of last scattering directly, as opposed to temperature fluctuations which may evolve between last scattering and the present. Indeed, in the tight-coupling regime, Thomson scattering randomizes the photon directions in the electron's rest frame, destroying any quadrupole anisotropy: a quadrupole is produced at times near decoupling, as the free streaming of photons begins (see sec. 3.5); at later times, the number density of free electrons which can Thomson scatter has dropped to negligible levels, and no further polarization can be produced if no reionization occurred. In fact, as we shall see in detail in sect. 3.4, "primary" polarization is only produced as the radiation can free-stream, i.e. as a quadrupole moment can be produced without suppression by scattering. As a consequence of this, it is significant on scales that are within the horizon at recombination.
This localization in time of the polarization by Thomson scattering reduces the problem of understanding the CMB polarization patterns to understanding the quadrupolar temperature fluctuation at last scattering, and is a very powerful constraint for reconstructing the sources of anisotropies.
We note at this point that a further source of polarization is produced in reionized scenarios; such scenarios are motivated by the observations of the quasar spectra, because the light of quasars absorbed (and reemitted) by the neutral hydrogen in the intergalactic medium [98] shows that the Universe is in a very high state of ionization already by the redshifts of the most distant quasars, at $z \simeq 5$. While reionization suppresses temperature anisotropies on scales smaller than the horizon size at rescattering (the suppression is more dramatic for earlier reionization), it can produce more polarization, due to the fact that the differential optical depth for Thomson scattering becomes again non-vanishing, as it was before recombination. The non vanishing of the differential optical depth couples again photons to free electrons, generating quadrupole temperature anisotropies that are sources of polarization [153]. The effect of reionization on the CMB polarization is to produce significant "secondary" polarization on large scales (i.e. on the scales smaller than the horizon at rescattering), much above the characteristic scales of the acoustic peaks: the power spectrum of polarization anisotropies is boosted to smaller values of l in reionized scenarios, when compared with the standard one (no reionization), and it is easily distinguishable from it, allowing to obtain important hints on the history of the universe.
In this chapter we will review the main physical processes from which CMB anisotropies originate, and we will describe their imprint on the angular power spectrum. A more detailed discussion can be found in [109], [111], [112], [108], [113].

3.2 The Boltzmann equation

In order to describe in greater detail the physical mechanisms that are responsible for the observable anisotropies, we have to describe the evolution in time (denoted by η throughout this chapter) of the

spatial ($\vec{x}$) and angular ($\hat{n}$) distribution of the radiation under gravity and scatter processes; this is performed by the Boltzmann equation

$$\frac{d}{d\eta}\vec{T}(\eta,\vec{x},\hat{n}) = \dot{\vec{T}} + n^i\vec{T}_{|i} = \vec{C}(\vec{T}) + \vec{G}(h_{\mu\nu}) \ . \tag{3.3}$$

where the vector $\vec{T}(\eta,\vec{x},\hat{n}) = (\Theta, Q+iU, Q-iU)$ encapsulates the perturbation to the temperature $\Theta \equiv \delta T/T$ and the polarization (Stokes Q and U parameters). Q and V are the only Stokes parameters needed, since Thomson scattering cannot generate circular polarization.
The term $\vec{C}(\vec{T})$ accounts for collisions (here Compton scattering of the photons with electrons), while $\vec{G}(h_{\mu\nu})$ accounts for gravitational redshifts.
In eq. (3.3) we used the fact that $\dot{x}^i = n_i$ and that in a flat universe photons propagate in straight lines, $\dot{n}_i = 0$.

To examine the scattering, we will first perform computations in the electron rest frame: we indicate by $\hat{n}'$ and $\hat{n}$ the propagation directions of the incoming and outcoming radiation, respectively; we adopt spherical coordinates centered on the scattering point $\vec{x}$, in which the scattering plane is spanned by the angle θ with respect to the polar axis coincident with $\hat{n}$. Thus Q is the difference between the radiation components with polarization along $\hat{e}_\theta$ and $\hat{e}_\phi$ directions; U is the same difference in the $(\hat{e}_\theta + \hat{e}_\phi)/\sqrt{2}$ and $(\hat{e}_\theta - \hat{e}_\phi)/\sqrt{2}$ directions.

In the next two subparagraphs we shall give a brief description of the terms in this equation.

3.2.1 Metric and scattering sources

The gravitational term $\vec{G}$ in (3.3) is easily evaluated from the Euler-Lagrange equations of motion for a massless particle in a perturbed FRW background, and from the requirement that $|u|^2 = 1$, where u^μ is the four velocity of an observer that is at rest with respect to the Friedmannian expansion; the photon energy (frequency) is defined in the comoving frame by

$$\nu \equiv -p_\mu u^\mu = p, \tag{3.4}$$

where p^μ is the photon momentum. The linearly perturbed time derivative of equation (3.4) is

$$\frac{\dot{\nu}}{\nu} = -\frac{\dot{a}}{a} - \frac{1}{2}n^i n^j \dot{h}_{ij} - n^i \dot{h}_{0i} - \frac{1}{2}n^i h_{00|i} \ , \tag{3.5}$$

where $\hat{n}$ is as usual the photon propagation direction [112]. Since the shift in amplitude in (3.5) is independent of the frequency, it perturbes the whole CMB spectrum. The first term does not affect temperature perturbations Θ, since it is the ordinary isotropic expansion effect: it simply implies that in a Friedmannian unperturbed background the temperature of the Planckian spectrum is redshifted as $T \propto 1/a$ because of the cosmological expansion of the spatial metric. The second term has a similar origin and is due to stretching of the spatial metric. The third and fourth term are the frame dragging and time dilation effects.

Also, since different polarization states undergo the same gravitational effect, Q and U are not affected by gravitational terms. Thus the gravitational term in (3.3) is

$$\vec{G}(\vec{T}) = \left(\frac{1}{2}n^i n^j \dot{h}_{ij} + n^i \dot{h}_{0i} + \frac{1}{2}n^i h_{00|i}, 0, 0\right) \ . \tag{3.6}$$

Let us now come to evaluate the collisional term in (3.3).
It is known from optics [30] that the component of the radiation with polarization perpendicular to the scattering plane is diffused without power loss, while the parallel polarized component picks up a factor $\cos^2\beta$ where β is the scattering angle, $\cos\beta = \hat{n}' \cdot \hat{n}$; each component has its own temperature perturbation, indicated as Θ_+ and $\Theta_{||}$ respectively. The temperature perturbation is $\Theta = \Theta_{||} + \Theta_+$, while from the definition of the Stokes parameters, $Q = \Theta_{||} - \Theta_+$; the value of U is obtained by rotating around the photon propagation direction by 45^o. Therefore, indicating with *in* and *out* respectively

the quantities before and after the scattering process, the latter leaves unchanged the $(_+)$ polarization component,

$$\Theta_{+\ out} = \Theta_{+\ in}, \tag{3.7}$$

while reduces the $(_{||})$ one,

$$\Theta_{||\ out} = \Theta_{||\ in} \cos^2\beta. \tag{3.8}$$

Also, from the Thomson scattering geometry, it is easy to see that

$$U_{out} = U_{in}\cos\beta \ \ , \ \ Q_{out} = Q_{in} - \Theta_{||\ in}\sin^2\beta \ . \tag{3.9}$$

The relation between $\vec{T}_{out}$ and $\vec{T}_{in}$ follows from these equations; it is convenient to cast it in a matrix form:

$$\vec{T}_{out} = \mathrm{S}\vec{T}_{in} = \frac{3}{4}\begin{pmatrix} \cos^2\beta + 1 & -(1/2)\sin^2\beta & -(1/2)\sin^2\beta \\ -(1/2)\sin^2\beta & (\cos\beta+1)^2/2 & (\cos\beta-1)^2/2 \\ -(1/2)\sin^2\beta & (\cos\beta-1)^2/2 & (\cos\beta+1)^2/2 \end{pmatrix}\vec{T}_{in} \tag{3.10}$$

where S is the scattering matrix. The overall normalization is fixed by photon conservation in the scattering. This equation completely describes the scattering process in the electron rest frame; since we will be concerned with the Fourier expansion of all perturbations, it convenient to relate these scattering frame quantities to those in the frame defined by $\hat{k} = \hat{e}_3$, i.e. to the frame where the polar axis is aligned with the wavevector $\vec{k}$. This can be done with rotational algebra; the details can be found in [112]. Qualitatively, this transformation implies one should perform a first rotation from the $\hat{k}$ frame to the scattering frame; after scattering, a second rotation returns to the $\hat{k}$ frame. These rotations transform $\vec{T}$ as the product of a matrix, denoted by P, and a vector, $\mathrm{P}(\hat{n},\hat{n}')\cdot\vec{T}(\hat{n}')$.
Integrating over incoming angles, we take into account the scattering out of and into a given angle, and the collisional term in (3.3), in the electron rest frame, is

$$\vec{C}(\vec{T})_{rest} = -\dot{\tau}\vec{T}(\hat{n}) + \dot{\tau}\int\frac{d\hat{n}'}{4\pi}\mathrm{P}(\hat{n},\hat{n}')\vec{T}(\hat{n}') \ . \tag{3.11}$$

Note that the number of photons involved in collisions during an infinitesimal conformal time interval is represented by the differential optical depth $\dot{\tau} = n_e\sigma_T a(\eta)$, where n_e is the free electron number density and σ_T is the Thomson cross section.

The transformation from the electron rest frame into the background frame yields a Doppler shift $\hat{n}\cdot\vec{v}_B$ in the temperature of the scattered radiation, where $\vec{v}_B$ is the peculiar velocity of electrons (and baryons); with the help of spherical spin s harmonics algebra [112], the final result for the collisional term may be written as

$$\vec{C}(\vec{T}) = -\dot{\tau}\vec{I}(\hat{n}) + \frac{1}{10}\dot{\tau}\int\frac{d\hat{n}'}{4\pi}\sum_{m=-2}^{2}\mathrm{P}^{(m)}(\hat{n},\hat{n}')\vec{T}(\hat{n}') \ , \tag{3.12}$$

where the vector $\vec{I}$ describes the isotropization of photon distribution in the scattering frame, and is given by

$$\vec{I}(\hat{n}) = \vec{T}(\hat{n}) - \left(\int\frac{d\hat{n}'}{4\pi}\Theta(\hat{n}') + \hat{n}\cdot\vec{v}_B, 0, 0\right) \ , \tag{3.13}$$

with

$$\mathrm{P}^{(m)} = \begin{pmatrix} Y_2^{m*'}Y_2^m & -\sqrt{\frac{3}{2}}\,{}_2Y_2^{m*'}Y_2^m & -\sqrt{\frac{3}{2}}\,{}_{-2}Y_2^{m*'}Y_2^m \\ -\sqrt{6}\ Y_2^{m*'}\,{}_2Y_2^m & 3\ {}_2Y_2^{m*'}\,{}_2Y_2^m & 3\ {}_{-2}Y_2^{m*'}\,{}_2Y_2^m \\ -\sqrt{6}\ Y_2^{m*'}\,{}_{-2}Y_2^m & 3\ {}_2Y_2^{m*'}\,{}_{-2}Y_2^m & 3\ {}_{-2}Y_2^{m*'}\,{}_{-2}Y_2^m \end{pmatrix} \ , \tag{3.14}$$

where the primed harmonics have to be interpreted as functions of $\hat{n}'$ (spin s spherical harmonics definitions and properties are summarized in [112]).
In this way, the anisotropic behavior of the Thomson scattering is completely contained in the $P^{(m)}$ matrix; the form of this matrix shows that , as expected, polarization is generated through quadrupoles anisotropies in the temperature and vice versa.

3.3 Normal modes evolution

All the treatment developed so far regards each Fourier mode separately; since the temperature and polarization distributions depends both on the position $\vec{r}$ and on the direction of propagation of the photons, it is useful to expand them in modes which account for both the local angular and spatial variations. Since each eigenmode evolves independently in linear perturbation theory, each Fourier mode can conveniently be decomposed into angular moments by using the product of spin-weighted harmonics and plane waves [112], [241], [95]; for a flat space, we will use the following basis:

$$ {}_sG_l^m = (-i)^l \sqrt{\frac{4\pi}{2l+1}}\ {}_sY_l^m(\hat{n}_{\hat{k}}) \exp(i\vec{k}\cdot\vec{r}) \ , \tag{3.15} $$

with spin $s = 0$ describing scalar spherical harmonics and $s = \pm 2$ describing tensor spherical harmonics.
The expressions of the spatial modes for a curved background ($K \neq 0$) may be found in [108].
The notation $\hat{n}_{\hat{k}}$ has been used to point out that, for each $\vec{k}$ mode, all the quantities in (3.15) are expressed in the $\hat{k}$-frame.
Denoting by η the conformal time and expanding temperature and polarization distributions in the modes just defined, one has:

$$ \Theta(\eta,\vec{r},\hat{n}) = \int \frac{d^3k}{(2\pi)^3} \sum_l \sum_{m=-2}^{2} \Theta_l^{(m)}(\eta,\vec{k}) G_l^m(\vec{r},\vec{k},\hat{n}) \ , \tag{3.16} $$

$$ (Q \pm iU)(\eta,\vec{r},\hat{n}) = \int \frac{d^3k}{(2\pi)^3} \sum_{l\geq 2} \sum_{m=-2}^{2} (E_l^{(m)} \pm iB_l^{(m)})(\eta,\vec{k}) {}_{\pm 2}G_l^m(\vec{r},\vec{k},\hat{n}) \tag{3.17} $$

In the expansion (3.17), $E_l^{(m)}$ and $B_l^{(m)}$ represent polarization with *electric* $(-1)^l$ and *magnetic* $(-1)^{l+1}$ parity respectively, while the temperature has electric parity type only; since they corresponds to polarization states with Q and U interchanged, $E_l^{(m)}$ and $B_l^{(m)}$ represent polarization patterns rotated by 45°.
Note that the angular expansion is made on spin $s = 0$ harmonics for the temperature perturbation and on $s = \pm 2$ for the polarization one.
As we shall see, since in linear perturbation theory different perturbations modes do not mix, the $m = 0, \pm 1, \pm 2$ modes are stimulated by scalar, vector and tensor perturbations in the metric respectively.
Having found the source terms of the Boltzmann equation (3.3), we can rewrite it as a coupled system of equations that must be satisfied independently by the amplitudes of the normal modes of the temperature and polarization $\vec{T}_l^{(m)} = (\Theta_l^{(m)}, E_l^{(m)}, B_l^{(m)})$.
Concerning the gradient term $n^i \vec{T}_{|i}$ in (3.3), it has the effect of multiplying the intrinsic angular dependence of temperature and polarization distribution by a term $i\hat{n}\cdot\vec{k} = i\sqrt{4\pi/3}\ kY_1^0$; as a consequence, the Clebsh-Gordan relations will couple the $l, l \pm 1$ terms of the expansions (3.16) and (3.17), giving an infinite hierarchy of coupled l-moments that transmit power from sources at low multipoles up the l-chain as time progresses:

$$ \dot{\Theta}_l^{(m)} = k\left[\frac{{}_0k_l^m}{2l-1}\Theta_{l-1}^{(m)} - \frac{{}_0k_{l+1}^m}{2l+3}\Theta_{l+1}^{(m)}\right] - \dot{\tau}\Theta_l^{(m)} + S_l^{(m)} \ , \tag{3.18} $$

$$ \dot{E}_l^{(m)} = k\left[\frac{{}_2k_l^m}{2l-1}E_{l-1}^{(m)} - \frac{2m}{l(l+1)}B_l^{(m)} - \frac{{}_2k_{l+1}^m}{2l+3}E_{l+1}^{(m)}\right] - $$
$$ - \dot{\tau}\left[E_l^{(m)} + \sqrt{6}P^{(m)}\delta_{l,2}\right] \ , \tag{3.19} $$

$$ \dot{B}_l^{(m)} = k\left[\frac{{}_2k_l^m}{2l-1}B_{l-1}^{(m)} + \frac{2m}{l(l+1)}E_l^{(m)} - \frac{{}_2k_{l+1}^m}{2l+3}B_{l+1}^{(m)}\right] - \dot{\tau}B_l^{(m)} \ . \tag{3.20} $$

We have defined

$$ {}_sk_l^m = \sqrt{\frac{(l^2-m^2)(l^2-s^2)}{l^2}} \cdot \sqrt{1-\frac{l^2}{k^2+(|m|+1)K}K} \ , \tag{3.21} $$

where the second factor is present only in the $K \neq 0$ case: the quantity $\sqrt{k^2+(|m|+1)K}$ is a generalization of the wavenumber in curved backgrounds.
The term in square brackets in eq. (3.18) is the free streaming effect, independent on scattering as well as on gravitational sources: as the radiation free streams, gradients in the distribution produce anisotropies that are transferred down the hierarchy when $k\eta \geq 1$, as the result of the geometrical projection of fluctuations on the scale corresponding to k at a distance η which subtends an angle given by $l \simeq k\eta$ (see sec. 3.5)
The main effect of scattering comes through the term $\dot{\tau}\Theta_l^{(m)}$, and implies an exponential suppression of anisotropies with optical depth in the absence of sources.
The source terms $S_l^{(m)}$ account for gravitational and residual scattering effects: in Newtonian gauge, the sources of temperature fluctuations are given by

$$ S_0^{(0)} = \dot{\tau}\Theta_0^{(0)} - \dot{\Phi} \ , \quad S_1^{(0)} = \dot{\tau}v_b^{(0)} + k\Psi \ , \quad S_2^{(0)} = \dot{\tau}P^{(0)} \ , \tag{3.22} $$

$$ S_1^{(1)} = \dot{\tau}v_b^{(1)} + \dot{V} \ , \quad S_2^{(1)} = \dot{\tau}P^{(1)} \ , \quad S_2^{(2)} = \dot{\tau}P^{(2)} - \dot{H} \ , \tag{3.23} $$

where

$$ P^{(m)} = \frac{1}{10}\left[\Theta_2^{(m)} - \sqrt{6}E_2^{(m)}\right] \ . \tag{3.24} $$

Massless neutrinos obey equations of the same form of (3.18), without the Thomson scattering terms.
As we shall see in the next section, the presence of $\Theta_0^{(0)}$ in eq. (3.22) represent the fact that the scattering does not destroy an isotropic temperature fluctuation; the Doppler effect enters the dipole ($l = 1$) equation through the baryon velocity, while $P^{(m)}$ contains the anisotropic nature of Compton scattering, and involves the quadrupole moments of the temperature and E-polarization only.
In the next section, we will review the behaviour of the photon-baryon fluid under these evolution equation, with particular attention to scalar-type perturbations.

3.4 The tight coupling regime

As discussed in section 3.1, before recombination, Thomson scattering between photons and electrons and Coulomb interactions between electrons and baryons are so efficient, to make the mean free path for a photon ($1/\dot{\tau}$) much smaller than the effective horizon H^{-1}. Therefore photons and baryons are better described as a single entity, the photon-baryon fluid; this condition is known as tight coupling.
The evolution equations can be expanded in powers of the photon mean free path over the wavelength and over the horizon scale.
The zeroth order expansion of the polarization ($l = 2$) equations (3.20) gives

$$ E_2^{(m)} = -\frac{\sqrt{6}}{4}\Theta_2^{(m)} \ , \ B_2^{(m)} = 0 \ . \tag{3.25} $$

The lowest order in $k\dot{\tau}^{-1}$ of equations (3.18) becomes

$$ \Theta_2^{(m)} = \frac{4\sqrt{4-m^2}}{9}\frac{k}{\dot{\tau}}\Theta_1^{(m)} \ , \quad P^{(m)} = \frac{\sqrt{4-m^2}}{9}\frac{k}{\dot{\tau}}P^{(m)} \quad (m = 0, \pm 1) \ , $$

$$ \Theta_2^{(\pm 2)} = -\frac{4}{3}\frac{\dot{H}}{\dot{\tau}} \ , \quad P^{(\pm 2)} = -\frac{1}{3}\frac{\dot{H}}{\dot{\tau}} \ . \tag{3.26} $$

Combining (3.26) and (3.25), we see that polarization fluctuations are generally suppressed with respect to metric or temperature fluctuations, because they are proportional to the quadrupole moments in the temperature which are suppressed by scattering. As an immediate consequence of the tight

coupling approximation, the angular dependence of the radiation field at a given point can only possess a monopole (corresponding to temperature) and a dipole (corresponding to a Doppler shift from a peculiar velocity) component, and the radiation is unpolarized.
A quadrupole is subsequently produced at decoupling as free streaming of the photons begins: therefore, polarization can be sourced by scattering only as the optical depth decreases, but this also corresponds to a lower fraction of photons affected, so that polarization is, in almost all cosmological models, at a level of few percent of the temperature anisotropy.
The degree of linear polarization is then directly related to the quadrupole anisotropy in the photons when they last scattered [121], [124], [196]: the polarized fraction of the temperature anisotropy is generally small, since only the photons that last scattered in an optically thin region could have possessed a quadrupole anisotropy. This fraction depends on the duration of last scattering, and for the standard thermal history it is $\simeq 5-10\%$.
We are ready to write down the equations for scalar perturbations in a flat universe. From the $l=0,1$ scalar ($m=0$) components of the system (3.18), we obtain:

$$\dot{\Theta}_0^{(0)} = -\frac{k}{3}\Theta_1^{(0)} - \dot{\Phi} , \tag{3.27}$$

$$\dot{\Theta}_1^{(0)} = k[\Theta_0^{(0)} + \Psi - \frac{2}{5}\Theta_2^{(0)}] - \dot{\tau}(\Theta_1^{(0)} - v_B^{(0)}) \tag{3.28}$$

A comparison with the expressions of photon perturbations in the Newtonian gauge (eqs. 2.97-2.100) allows us to recognize in the equations above the continuity and Euler equations for the photons in flat space (see [242]), with the identifications

$$\delta_\gamma = 4\Theta_0^{(0)} , \quad v_\gamma^{(0)} = \Theta_1^{(0)} , \quad \pi_{T\gamma}^{(0)} = \frac{12}{5}\Theta_2^{(0)} . \tag{3.29}$$

Therefore, $\Theta_0^{(0)}$ is the isotropic temperature fluctuation, and $\Theta_1^{(0)}$ is interpreted as the amplitude of the photon dipole or bulk velocity. From eq. (3.26), it is easy to see that the anisotropic stress $\pi_{T\gamma}$, proportional to the quadrupole moment, is of the order $k/\dot{\tau}\Theta_1^{(0)}$; this correspond to the fact that since scattering makes the photons isotropic in the baryon rest frame, the anisotropic stress is negligible to the lowest order in $1/\dot{\tau}$ in the tight coupling approximation.
Aside from the velocity divergence source term in the continuity equation (3.27), there is a term dependent on the metric: this is due to the gravitational redshift effect of time dilation, analogous to the cosmological redshift: the presence of matter curves or stretches the space taking the wavelength of the photon with it. In the Euler equation, the Newtonian potential Ψ acts as a source of the dipole. Gradients in the potential also induce gravitational blue and red shifts as the photons fall into and climb out of potential wells ($\Psi < 0$). This is countered by photon pressure from $\Theta_0^{(0)}$, so that, as the temperature rises, so does the pressure which opposes the fall of a photon into the potential well, setting up acoustic oscillations in the fluid.
The baryon continuity and Euler equations take on a similar form,

$$\dot{\delta}_B = -kv_B^{(0)} - 3\dot{\Phi} , \tag{3.30}$$

$$\dot{v}_B^{(0)} = -\frac{\dot{a}}{a}v_B^{(0)} + k\Psi + \frac{\dot{\tau}}{R}\left(\Theta_1^{(0)} - v_B^{(0)}\right) , \tag{3.31}$$

$$\dot{v}_B^{(\pm 1)} = \dot{V} - \frac{\dot{a}}{a}\left(v_B^{(\pm 1)} - V\right) + \frac{\dot{\tau}}{R}\left(\Theta_1^{(\pm 1)} - v_B^{(\pm 1)}\right) . \tag{3.32}$$

where

$$R = \frac{\rho_B + p_B}{\rho_\gamma + p_\gamma} \simeq \frac{3\rho_B}{4\rho_\gamma} \text{ if } p_B \simeq 0 , \; p_\gamma = \frac{1}{3}\rho_\gamma , \tag{3.33}$$

The altered form of the coupling term in the baryon Euler equation, that picks up a factor $1/R$, follows from momentum conservation in Thomson scattering. The effective momentum density of a general fluid X is indeed $(\rho_X + p_X)v_X$; since $p_\gamma = \frac{1}{3}\rho_\gamma$ and $p_B \ll \rho_B$, conservation implies $\frac{4}{3}\rho_\gamma\Theta_1^{(m)} = \rho_B v_B^{(m)}$;

therefore, the baryon Euler equation is similar to eq. (3.28), correcting for the R factor.
The lowest order in $1/\dot{\tau}$ of equations (3.31) and (3.32) allows to write

$$v_b^{(0,\pm1)} = \Theta_1^{(0,\pm1)} \ , \tag{3.34}$$

so that when the optical depth to scattering is high, the photons become isotropic in the electron-baryon rest frame.
As shown above, the tight coupling approximation allows us to drop the viscosity term; then, eliminating the baryon velocity from the photon evolution equation, we obtain, to lowest order, the following equation for $\Theta_0^{(0)}$ ([167], [109]):

$$\frac{d}{d\eta}\left[(1+R)\,\dot{\Theta}_0^{(0)}\right] + \frac{k^2}{3}\Theta_0^{(0)} = -\frac{k^2}{3}(1+R)\Psi - \frac{d}{d\eta}\left[(1+R)\,\dot{\Phi}\right] \ . \tag{3.35}$$

If we ignore the time variation of the baryon-photon momentum ratio, this is the equation of a forced oscillator: the change in momentum of the photon-baryon fluid is determined by a competition between the pressure restoring and the gravitational driving forces. The effective dimensionless mass of the fluid is given by $m_{eff} = 1 + R$, accounting for the inertia of the baryons. Baryons also contribute gravitational mass to the system, resulting in the appearance of $m_{\rm eff}$ in the two gravitational terms on the right hand side; however, they do not contribute significantly to the restoring pressure: in the tight coupling regime, photons contribute pressure and baryons contribute inertia to the single photon-baryon fluid ([207], [110]).
As an illustrative simple example, let us first consider the unrealistic case of static potentials Ψ and Φ and of constant R; equation (3.35) then reduces to

$$\ddot{\Theta}_0^{(0)} + k^2 c_s^2 \Theta_0^{(0)} = -\frac{1}{3}k^2\Psi \tag{3.36}$$

where c_s is the sound speed in the photon-baryon fluid,

$$c_s = \frac{1}{\sqrt{3(1+R)}} \ .$$

Equation (3.36) describes a simple harmonic oscillator under the constant acceleration provided by gravitational infall, and the immediate solution is

$$\Theta_0^{(0)}(\eta) = [\Theta_0^{(0)}(0) + m_{eff}\Psi]\cos(kr_s) + \frac{1}{kc_s}\dot{\Theta}_0^{(0)}(0)\sin(kr_s) - m_{eff}\Psi \tag{3.37}$$

where r_s is the sound horizon at the time η,

$$r_s(\eta) = \int_0^\eta c_s(\eta)d\eta' \ . \tag{3.38}$$

The two initial conditions $\Theta_0^{(0)}(0)$ and $\dot{\Theta}_0^{(0)}(0)$ govern the form of acoustic oscillations, representing the adiabatic and isocurvature modes respectively, as we shall see.
Equation (3.37) implies, through the photon continuity equation, that

$$\Theta_1^{(0)}(\eta) = 3[\Theta_0^{(0)}(0) + m_{eff}\Psi]c_s\sin(kr_s) + 3k^{-1}\dot{\Theta}_0^{(0)}(0)\cos(kr_s) \tag{3.39}$$

In eqs. (3.37) and (3.39) lie the main acoustic and redshift effects dominating primary anisotropy formation.

3.4.1 Gravitational infall and redshift

In the early universe, photons dominate the fluid and $R \to 0$. In this limit, eq. (3.37), for the adiabatic mode, is that of an oscillator whose zero point has been displaced by gravity,

$$\Theta_0^{(0)}(\eta) = [\Theta_0^{(0)}(0) + \Psi]\cos(kr_s) - \Psi \ . \tag{3.40}$$

The zero point is the state at which gravity and pressure are balanced; a displacement $-\Psi$ yields hotter photons in the potential well, since gravitational infall increases the number density of photons as well as their energy through gravitational blueshift. However, the gravitational blueshift is precisely canceled out when the photons climb out of the potential well at last scattering, therefore the effective temperature perturbation is $\Theta_0^{(0)}(\eta) + \Psi = [\Theta_0^{(0)}(0) + \Psi]\cos(kr_s)$. Larger scales (lower k) oscillate more slowly, owing to the finite time sound takes to cross the potential fluctuation.
The phase of oscillation at last scattering epoch (η^*) is $\simeq kr_s^*$: at this time, different scales will be caught at different phases of their oscillation: the wavenumber that reaches its first compression by last scattering is $k_A = \pi/r_s^*$, and corresponds to the sound horizon at that time. If there is a spectrum of k-modes, there will be a harmonic series of temperature fluctuation peaks with $k_n = n\pi/r_s(\eta^*)$: odd peaks thus represent the compression phase, whereas even peaks represent the rarefaction phase. The scales larger than the horizon at recombination will not have evolved significantly, yielding an effective temperature fluctuation which directly reflects the primordial perturbations: this combination of the intrinsic temperature fluctuation and the gravitational redshift is the well known Sachs-Wolfe effect [187].
For shorter wavelength fluctuations, the harmonic series of temperature peaks is based on the sound horizon r_s^*, which is most sensitive to the expansion rate of the universe before last scattering, which in turn depends primarily on the ratio of matter to radiation in the universe. Because the latter is fixed by the CMB itself, the sound horizon is mainly determined by the matter density today, $\Omega_m h^2$. As it is evident from (3.37), sub-horizon scales are dominated by acoustic oscillations, with the dynamics frozen on super-horizon scales. Since the horizon scale at decoupling subtended approximatively 1^o in the sky, we expect to see oscillations on sub-degree scales, and not above. These sub-degree oscillations indeed determine the oscillatory behavior of CMB anisotropies on small angular scales; these in turn generate a sequence of peaks into the angular power spectrum (the sets of coefficients C_l defined by the spherical harmonics expansion of the two point correlation function, see sec. 3.7) as l goes into the sub-degree region, $l \geq 200$ from (3.57): such peaks are called *acoustic peaks* and are extremely popular in the literature since, as we shall see in sec. 3.7. the power spectrum of CMB anisotropies completely characterizes the underlying cosmological perturbations, if they are Gaussian.
On the other hand, vector perturbations lack pressure and do not generate acoustic oscillations; this is easily seen by looking at equations (3.32), (3.18) and (3.34):

$$\frac{d}{d\eta}\left(\frac{\Theta_1^{(\pm 1)} - V}{1+R}\right) = 0 \ . \tag{3.41}$$

It is easy to see that in absence of a source, the quantity in (3.41) is constant in the radiation dominated era, while it decays as a^{-1} in the matter dominated era.

3.4.2 Baryon drag

Though pressureless, the baryons contribute to the inertial and gravitational mass of the fluid; this lowers the frequency of the oscillations by decreasing the sound speed, but more importantly, also causes a greater gravitational compression of the fluid in a potential well, with respect to the case $R = 0$: the baryon dragging of photons into the potential wells produces a further displacement of the oscillation zero point. Since the redshift is not affected by the baryon content, this redshift remains even after last scattering, enhancing peaks from compression over those from rarefaction. If the potential and the baryon contribution were constant, the fluid will oscillate as

$$\Theta_0^{(0)} + \Psi = \frac{1}{3}\Psi(1+3R)\cos(kr_s) - R\Psi \ , \tag{3.42}$$

with compressional peaks a factor of $(1+6R)$ larger than the $\frac{1}{3}\Psi$ Sachs-Wolfe plateau; in reality, this effect is modified due to time evolution in the baryon content: for slow changes, the oscillation amplitude varies as $m_{eff}^{-1/4} \propto (1+R)^{-1/4}$, slowly decaying with time.

3.4.3 Doppler effect

Since the turning point are at the extrema, the fluid velocity oscillates 90 degrees out of phase with the density, as it is evident from eq. (3.39); its motion relative to the observer causes a Doppler shift, imprinting oscillations which are less prominent than, and out of phase with, the intrinsic temperature oscillations. The Doppler effect adds a smoother component to the anisotropy that makes the acoustic peaks rather less prominent for low-baryon content universes. Whereas the observer velocity causes a pure dipole anisotropy on the sky, the fluid velocity causes an r.m.s. spatial temperature variation on the last scattering surface from its line-of-sight component. In the absence of baryons, the velocity contribution is equal in amplitude to the temperature effect; but because the line-of sight restriction eliminates the face-on contribution, projection effects smooth Doppler features more strongly than temperature features. This implies that the peak structure of the anisotropy is due mainly to the intrinsic temperature.
Baryons increase the prominence of the peaks by decreasing the relative contribution of the Doppler effect: as the baryons increase the effective mass, the velocity decreases as the inverse square-root of the mass. Note also that, since velocity oscillations are symmetric around zero, they enhance the baryon drag effect.

3.4.4 Driving effects

Whenever the non-relativistic matter is not the dominant dynamical component, the potentials Φ and Ψ become time-dependent: for example, when radiation dominates, pressure and entropy alter the behaviour of the gravitational potentials. The effects of potential evolution can be separated into those that occur before last scattering and those occurring afterwards, affecting the CMB photons along their free-streaming trajectories.
As a simple example, consider adiabatic fluctuations, where the initial temperature $\Theta_0^{(0)}(0)$ is related through Poisson equation to curvature fluctuations $\Phi(0)$. Adiabatic fluctuations are fluctuations in the energy density that can be characterized in a gauge invariant manner as fluctuations in the local value of spatial curvature (see chapter 2). Because both the radiation and matter species participate in the fluctuation, the fluctuation in the local number density of any species relative to the entropy density, vanishes.
After horizon crossing, unless CDM dominates, the energy density perturbations decay with expansion, and can no longer maintain a constant gravitational potential. The decaying gravitational potential drives the first compression without a counterbalancing effect on the subsequent rarefaction stage, enhancing temperature fluctuations. Furthermore, the dilation effect from a decaying space curvature Φ also enhances the acoustic fluctuations. Since this effect only occurs for modes which cross the horizon before CDM domination, the amplitude of this boost is sensitive to the matter-radiation ratio of the universe.
The situation is rather different for isocurvature scenarios; isocurvature fluctuations correspond to fluctuations in the form of the local equation of state, with no fluctuations in the local curvature; instead, there is a non-zero entropy perturbation 2.47.
So long as an isocurvature mode is super-horizon sized, it must be characterized by zero curvature (and density) fluctuations, because causality precludes the re-distribution of energy density on scales larger than the horizon; once an isocurvature mode becomes sub-horizon sized, fluctuations in the local pressure can "push " energy density around and convert an isocurvature fluctuation into an energy density perturbation (see eq. 2.61). Curvature fluctuations are therefore zero outside the horizon, and grows by causal processes as the fluctuation crosses the horizon; the driving mechanism of isocurvature perturbations causes a phase shift in the acoustic oscillation which is typically $\phi \simeq \pi/2$:

such a phase shift can be measured by determining the locations of the peaks, allowing us to learn important properties of particle physics in the early Universe.

3.4.5 Silk damping

The photon-baryon fluid is imperfect because the photons random walk through the baryons with a mean free path λ_C given by Compton scattering: as the photons diffuse, hot and cold regions mix and the generation of viscosity and heat conduction in the fluid dissipates fluctuations through the Euler equation. To the first order in $k/\dot{\tau}$, the Euler equation becomes (3.28)

$$\frac{kR^2}{\dot{\tau}}\dot{\Theta}_0^{(0)} = (1+R)\dot{\Theta}_1^{(0)} - k\left[\Theta_0^{(0)} + (1+R)\Psi\right] + \frac{16}{45}\frac{k^2}{\dot{\tau}}\Theta_1^{(0)} \quad ; \tag{3.43}$$

The expansion $\dot{a}/a$ terms have been dropped under the assumption that the damping effect discussed here involves times much smaller than the expansion rate. Using the continuity equation (3.27), one gains an intuitive expression for (3.43):

$$\ddot{\Theta}_0^{(0)} + \frac{k^2}{3\dot{\tau}}\left[\frac{R^2}{(1+R)^2} + \frac{16}{15}\frac{1}{1+R}\right]\dot{\Theta}_0^{(0)} + \frac{k^2}{3(1+R)}\Theta_0^{(0)} = -\frac{k^2}{3}\Psi - \ddot{\Phi} \ , \tag{3.44}$$

which is a damped forced oscillator. Again the damping behavior is evident if we consider the case in absence of metric fluctuations. The acoustic amplitude for scalars damps as $\exp[-(k/k_D^{(m)})^2]$, where

$$\left[\frac{1}{k_D^{(0)}(\eta)}\right]^2 = \frac{1}{6}\int_0^\eta \frac{d\eta'}{\dot{\tau}}\frac{R^2 + 16(1+R)/15}{(1+R)^2} \ . \tag{3.45}$$

This severe damping is known as Silk damping (see [112] and references therein). Fluctuations are damped nearly exponentially as the diffusion length $\lambda_D \simeq \sqrt{N}\lambda_C$ overtakes the wavelength of the fluctuation mode. Note that the scale at which it occurs $1/k_D^{(m)}$ grows when the mean photon free path $\dot{\tau}^{-1}$ grows: at last scattering, the ionization fraction x_e decreases due to recombination, thus increasing the mean free path of the photons $\lambda_C \propto x_e^{-1}$.
Of course, these equations depend on the particular cosmological scenario adopted, but the general occurrence is that the CMB anisotropies under the Silk damping scales, that subtended about $10'$ on the sky, are severely damped. The diffusion scale $k_D = \lambda_D/2\pi$ can therefore be used as a probe of the ionization history and the baryon content.

3.5 The free-streaming and projection effects

As the universe drops below a temperature of around 0.1 eV, almost all free electrons are converted to neutral hydrogen; the rapid Thomson scattering ceases for lack of scatterers and the radiation decouples. At this point, the radiation propagates freely until the universe reionizes at some redshift greater than 5. As anticipated, during the tight coupling epoch the radiation field can only possess a monopole and a dipole component, and it is unpolarized: any higher multipole moment is rapidly damped away by the scattering, and is subsequently produced at decoupling, as the free streaming of photons begins.
A single Fourier mode of the radiation field can be described by the temperature distribution function $\Theta(k, \mu, \eta)$, where μ is the angle between the wave vector and the propagation direction; the free streaming of the photons is described by the Boltzmann equation 3.3, in which the collision term has been neglected:

$$\dot{\Theta} + ik\mu\Theta = 0 \ .$$

If the free streaming begins at time η^*, then the solution at a later time is simply

$$\Theta(k, \eta, \mu) = \Theta(k, \eta^*, \mu)\exp(-ik\mu(\eta - \eta^*)) \ . \tag{3.46}$$

We can reexpress the μ dependence as a multipole expansion

$$\Theta(k,\eta,\mu) = \sum_{l=0}^{\infty}(-i)^l\Theta_l(k,\eta)P_l(\mu) \quad ; \tag{3.47}$$

using the identity

$$e^{iz\cos(\phi)} = \sum_{n=0}^{\infty}(2n+1)i^n j_n(z)P_n(cos\phi)$$

the free streaming becomes

$$\frac{\Theta_l(\eta,k)}{2l+1} = \left\{[\theta_0+\Psi](\eta^*,k) + \theta_1(\eta^*,k)\frac{1}{k}\frac{d}{d\eta}\right\} j_l(k\Delta\eta) + \int_{\eta^*}^{\eta}(\dot{\Psi}-\dot{\Phi})j_l(k\Delta\eta) \quad , \tag{3.48}$$

where j_l is the usual spherical Bessel function and $\Delta\eta = \eta^* - \eta$. In eq. (3.48), we neglected diffusion damping.
Since j_l peaks at $l \simeq k\Delta$, the free streaming just projects the physical scale $k \simeq \lambda^{-1}$ onto am angular scale as $\theta \simeq \lambda/\Delta\eta$. Then, the total power in the lth multipole is then obtained by integration over k modes (cfr. sec. 4.106),

$$C_l = \frac{2}{\pi}\int k^3 \frac{|\Theta_l(\eta_0,k)|^2}{(2l+1)^2} d\ln k \quad .$$

Since free streaming merely represents a projection, the generalization to non-flat universes is made by replacing the comoving distance $\Delta\eta$ with the comoving angular diameter distance:

$$r_\theta = |K|^{-1/2}\sinh\left(|K|^{1/2}\Delta\eta\right) \quad \text{for} \quad K<0$$

$$r_\theta = |K|^{-1/2}\sin\left(|K|^{1/2}\Delta\eta\right) \quad \text{for} \quad K>0 \quad .$$

Putting this together, the acoustic peaks occur at

$$l_j = k_j\,|r_\theta(\eta^*)|$$

making evident that the dominant factor in the peak locations is the curvature of the universe, which can make the same physical scale subtends a much smaller (larger) angle on the sky.

3.6 Integral solutions

A formal integral solution to the Boltzmann equation (3.3) may be obtained by considering the properties of source projection

$$\frac{\Theta_l^{(m)}(\eta_0,k)}{2l+1} = \int_0^{\eta_0} d\eta' e^{-\tau(\eta_0,\eta')}\sum_{l'} S_{l'}^{(m)}(\eta')j_l^{(l'm)}(k,\eta_0-\eta') \ , \tag{3.49}$$

$$\frac{E_l^{(m)}(\eta_0,k)}{2l+1} = -\sqrt{6}\int_0^{\eta_0} d\eta'\dot{\tau}e^{-\tau(\eta_0,\eta')}P^{(m)}(\eta')\epsilon_l^{(m)}(k,\eta_0-\eta') \ , \tag{3.50}$$

$$\frac{B_l^{(m)}(\eta_0,k)}{2l+1} = -\sqrt{6}\int_0^{\eta_0} d\eta'\dot{\tau}e^{-\tau(\eta_0,\eta')}P^{(m)}(\eta')\beta_l^{(m)}(k,\eta_0-\eta') \ , \tag{3.51}$$

where η_0 is the present conformal time and $j_l^{(l'm)}$, $\epsilon_l^{(m)}$, $\beta_l^{(m)}$ contain the spatial curvature K and are combinations of the Bessel functions and their derivatives.
Here

$$\tau(\eta) \equiv \int_\eta^{\eta 0}\dot{\tau}(\eta')d\eta' \tag{3.52}$$

is the optical depth between η and the present.
In the context of our analysis of scalar perturbations, let us express the properties of the temperature angular decomposition; integrating by parts eq. (3.49), the integral solutions can be rewritten as

$$\frac{\Theta_l^{(0)}(\eta_0,k)}{2l+1} = \int_0^{\eta_0} d\eta e^{-\tau}\left[(\dot{\tau}\Theta_0^{(0)} + \dot{\tau}\Psi + \dot{\Psi} - \dot{\Phi})j_l^{(00)} + \dot{\tau}v_B^{(0)}j_l^{(10)} + \dot{\tau}P^{(0)}j_l^{(20)}\right] \ . \tag{3.53}$$

Notice how the sum $\Theta_0^{(0)} + \Psi$ acts as the effective temperature, accounting for the gravitational potential wells at last scattering; we can also recognize the Doppler effect coming from the baryon velocity. Most importantly, eq. (3.53) outlines that in the free-streaming trajectories of the CMB photons from last scattering surface to us, i.e. when optical depth is negligible, an important source of secondary anisotropies arises: it is just contained into the potential time variation in (3.53). The differential redshift from $\dot{\Psi}$ and dilation from $\dot{\Phi}$ must be integrated along the trajectory of photons, so that time variations of the metric fluctuations leads to additive anisotropies. This effect is the so called *integrated* Sachs-Wolfe (ISW) effect. It can be differently classified, depending on the origin of the potential time variation; the early ISW is the direct analogue of the acoustic driving effect of 3.4.4, save for the fact that the photons are in the free streaming rather than in the tight coupling regime: since the gravitational potentials cannot decay in the matter-dominated era, the early ISW arises only if the Universe is not completely matter-dominated at last scattering. Unfortunately, an analytical derivation of this effect is difficult because it cannot arise either in the tight coupling regime or in the weak coupling one.
For adiabatic models, the potential decays after horizon crossing if radiation dominates making an important pressure contribution. For isocurvature scenarios, it grows from zero to a maximum near sound horizon crossing and then decays due to radiation pressure [111]. Due to the later time of generation (the equivalence epoch), the early ISW could affect scales larger than the acoustic peaks, in particular scales that are inside the horizon at matter-radiation equality, even though it is cut off above the matter-radiation equality scale, $k_{eq} \ll k_A$. Therefore, the early ISW effect affects the anisotropies on scales just larger than the first acoustic peak, broadening the rise and shifting the location of the first peak to larger scales.
In some cosmological models, another source of time variation of the potential is related to the change in the cosmic equation of state: as an example, in open models, or in cosmological constant models, the universe enters a phase of rapid expansion once matter no longer dominates, making the potential decay. The opposing effects from decaying over densities and underdensities will cancel if the photon can travel across many wavelengths during the decay, so that this *late* ISW effect is suppressed below the horizon at the decay epoch, $k_{K\Lambda} = 2\pi/\tau_{K\Lambda}c$ (see [109]).

3.7 Power spectra

The CMB temperature anisotropies on the celestial sphere can be expanded in spherical harmonics [26] :

$$\Theta(\theta,\phi) = \frac{\delta T}{T}(\theta,\phi) = \sum_{lm} a_{lm}Y_l^m(\theta,\phi) \ . \tag{3.54}$$

A similar decomposition is also true for perturbations of the polarization field; the temperature two-point correlation function is

$$C^{\Theta\Theta}(\theta) = \langle\Theta(\hat{n})\Theta(\hat{n}')\rangle_{\hat{n}\cdot\hat{n}'=\cos\theta} \tag{3.55}$$

where the average is over all pairs of points on the sky separated by an angle θ ; of course, we can compute the two-point correlation function also between different fields. Indicating generically with $X, \tilde{X}$ the quantities Θ and $Q \pm iU$, the two-point angular correlation function of the $X, \tilde{X}$ fields anisotropies at an angular scale θ can be written in terms of their power spectrum (i.e. the $C_l^{X\tilde{X}}$),

$$C^{X\tilde{X}} =< X_{\hat{n}}\tilde{X}_{\hat{n}'} >_{\hat{n}\cdot\hat{n}'=\cos\theta}= \sum_l \frac{2l+1}{4\pi}C_l^{X\tilde{X}}P_l(\cos\theta) \ . \tag{3.56}$$

In (3.56), the quantities P_l are Legendre polynomials.
This expansion is useful since from the functional form of the Legendre polynomials, it can be shown that each $C_l^{X\tilde{X}}$ represents the amount of power at the scale

$$\theta \text{ (degrees)} \simeq \frac{180}{l} . \tag{3.57}$$

It can be shown (see [163]) that in a Gaussian theory the correlation function, also known as power spectrum, is the only thing we have to know to describe the perturbations. Theories for the origin of large-scale structure predict that the mass distribution in the universe is a single realization of a statistically isotropic random field. In other words, the Fourier components $\delta(\vec{k})$ of the fractional density perturbation field are random variables that have expectation values $\left\langle \delta(\vec{k}) \right\rangle = 0$ and covariance given by

$$\left\langle \delta(\vec{k})\delta(\vec{k}') \right\rangle = (2\pi)^3 \delta_D(\vec{k}+\vec{k}') P_s(k) \ . \tag{3.58}$$

Here $P_s(k)$ is the scalar power spectrum for the spatial mass distribution (density perturbations produce scalar perturbations to the spacetime metric). Statistical isotropy demands that the power spectrum depends only on the amplitude (and not the orientation) of $\vec{k}$.

Because the temperature perturbation and polarization of the CMB are due to density perturbations, the a_{lm}^X that follows from the decomposition of X as in (3.54) must be random variables with zero mean $\left\langle a_{lm}^X \right\rangle = 0$ and covariance given by

$$< a_{lm}^X a_{l'm'}^{\tilde{X}\,*} >= C_l^{X\tilde{X}} \delta_{ll'} \delta_{mm'} \ , \tag{3.59}$$

where now the average is taken over all possible configurations. The statistical independence of each lm mode is a consequence of statistical isotropy.

Under these hypothesis, and assuming that the whole sky average (3.56) coincides with the one in (3.59), one can obtain a simple relation between the coefficients C_l in (3.59) and the expansion coefficients in (3.16, 3.17); simply one can project the $\hat{k}-$frame spherical harmonics in (3.16) and (3.17) into a particular Y_l^m in (3.54); from the Gaussianity of the spectrum one obtains

$$C_l^{X\tilde{X}} = \frac{2}{\pi(2l+1)^2} \int \frac{dk}{k} \sum_{m=-2}^{2} k^3 X_l^{(m)*}(\eta,k) \tilde{X}_l^{(m)}(\eta,k) \ , \tag{3.60}$$

where X_l and $\tilde{X}_l$ stays for any of Θ_l, E_l or B_l.
Due to the opposite parity of $Theta_l^m, E_l^m$ (electric parity) and B_l^m (magnetic parity), $C_l^{EB} = C_l^{\Theta B} = 0$ if the physics that gives rise to temperature anisotropies and polarization is parity-invariant. In this case, the two-point statistics of the CMB temperature-polarization map are completely specified by the four sets of moments, $C_l^{\Theta\Theta}, C_l^{\Theta E}, C_l^{EE}, C_l^{BB}$.
Nonzero $C_l^{\Theta B}$ or C_l^{EB} would provide a signature of cosmological parity breaking.

Chapter 4

Scalar field cosmology

4.1 Introduction

Scalar fields were introduced in Quintessence cosmologies with the aim of resolving the "missing energy" problem, described in chapter 1.
Differently from the cosmological constant models, which are able to preserve the spatial flatness required from inflation but still retain serious unsolved theoretical issues, Quintessence models propose scalar fields as candidates for such missing energy. More generally, the definition of Quintessence refers here to any energy component whose properties are well described in terms of a scalar field evolving in a potential which couples to ordinary matter only through gravity.
As discussed in chapter 1, the Quintessence can mimic the behaviour of a cosmological constant when it slowly evolves in its potential; in this scenario, the "vacuum " energy resides in the potential energy of such a scalar field.
The most important difference with respect to the cosmological constant is that it is time-varying and spatially inhomogeneous, so that it can develop fluctuations which can be relevant in the perturbation growth and can leave a characteristic signature in the CMB and in large scale structure.
In this chapter, we model the Quintessence candidate as the scalar field associated with an ultralight pseudo Nambu-Goldstone boson [104]; it possesses a global spontaneous symmetry breaking scale $f \simeq 10^{18}$ GeV and an explicit breaking scale $M \sim 10^{-3}$ eV; such a field is taken to be acting at present like an effective cosmological constant and dominating the energy density of the Universe [51].
In order to find the possible observational imprints of Quintessence on the CMB anisotropies and on structure formation, it is necessary to apply linear perturbation theory, integrating the Einstein equations starting with the appropriate initial conditions. In this chapter we give a complete prescription for describing adiabatic and isocurvature initial conditions if an additional component is present in the form of a minimally-coupled scalar field; this can be acquired by giving the set of equations relating all the fluid components needed in the two cases. In order to do that, we need the background and perturbation equations, that we report in section 4.2.
Then, working in the formalism of the synchronous gauge, we present a generalization of the work of Ma and Bertschinger [148], aimed to find the super-horizon-scale behaviour of perturbations at early times, starting from initial zero entropy perturbations (adiabatic case) or initial zero curvature perturbations (isocurvature case). We express the gauge-invariant entropy and curvature perturbations in terms of synchronous perturbations of baryons, photons, massless neutrinos, cold dark matter and a minimally-coupled scalar field, as well as metric perturbations.
These results refer to the paper by Perrotta & Baccigalupi [173]. The results are then translated to the conformal Newtonian gauge in section (4.6).
In section 4.7 we numerically investigate the growth of entropy and curvature perturbations starting from different initial conditions, and we compare them with the corresponding behaviours in the standard CDM model. We also plot, and discuss, the pure adiabatic and pure isocurvature CMB anisotropies spectra, again making a comparison with standard CDM.

4.2 Einstein and conservation equations

Let us briefly discuss the effects on the homogeneous FRW cosmology coming from the additional contribution of an homogeneous, minimally coupled, real scalar field ϕ. Neglecting interactions of ϕ with other fields than gravity, the dynamics of the field will depend, of course, on the potential in which it evolves, as well on the global expansion of the universe. We assume that the field is forced to evolve in a potential $V(\phi)$.
For the rest of this thesis, we will concentrate on models with total $\Omega = 1$ (spatial curvature $K = 0$) and we work in conformal coordinates.
The Lagrangian describing the classical behavior of a minimally-coupled scalar field is given by the well-known expression

$$\mathcal{L} = -\frac{1}{2}\sqrt{-g}\left[g^{\mu\nu}\partial_\mu\phi\partial_\nu\phi + 2V(\phi)\right] , \tag{4.1}$$

and the scalar field energy density and pressure, associated to this Lagrangian, directly follow from expression of the stress-energy tensor of the scalar field,

$$T^\mu_\nu = \phi^{;\mu}\phi_{;\nu} - \frac{1}{2}(\phi^{;\alpha}\phi_{;\alpha} + 2V)\delta^\mu_\nu \ . \tag{4.2}$$

The contribution to the energy-momentum tensor from the scalar field corresponds to the non-zero elements

$$T^\phi_{00} = \rho_\phi \ \text{ and } \ T_{ij} = a^2 p_\phi \delta_{ij} \ . \tag{4.3}$$

From (4.2) we have

$$\rho_\phi = \frac{1}{2a^2}\dot{\phi}^2 + V(\phi) \ ; \quad p_\phi = \frac{1}{2a^2}\dot{\phi}^2 - V(\phi) \ . \tag{4.4}$$

The above quantities evolve according to the Friedmann equation, in which we separate the contributions of matter, radiation and scalar field to the total energy density ρ, putting the cosmological constant equal to zero: the system composed by the metric and the fluids is then described by the equation

$$\mathcal{H}^2 = \left(\frac{\dot{a}}{a}\right)^2 = \frac{8\pi G}{3}a^2\left[\rho_m + \rho_r + \rho_\phi\right] , \tag{4.5}$$

together with the conservation equations

$$\dot{\rho}_\phi = -3\mathcal{H}(\rho_\phi + p_\phi) \ . \tag{4.6}$$

$$\dot{\rho}_n + n\mathcal{H}\rho_n = 0 \ , \tag{4.7}$$

where ρ_n is the energy density contributed by radiation ($n = 4$) or nonrelativistic matter ($n = 3$) and $V' = dV/d\phi$. Note that, from (4.4), the scalar field conservation law (4.6) is equivalent to the second order Klein-Gordon equation of motion:

$$\ddot{\phi} + 2\mathcal{H}\dot{\phi} + a^2\frac{dV}{d\phi} = \frac{1}{a^2}\frac{d}{d\tau}(a^2\dot{\phi}) + a^2V'(\phi) = 0 \ . \tag{4.8}$$

One of the motivations that leads to the concept of Quintessence as a vacuum energy candidate is that the scalar field could mimic a cosmological constant if its kinetic energy is negligible with respect to the potential one. However, a substantial difference is that it admits perturbations around the homogeneous solution of (4.8); a number of studies have assumed a "smooth" (spatially uniform), time-dependent component with arbitrary equation of state, which does not respond to the inhomogeneities in the dark matter and baryon-photon-neutrino component [217, 199, 200, 231]. However, such scenario is ill-defined and unphysical; the notion of a smooth component is gauge-dependent: only if the energy density is constant in time and position is it gauge-invariant, but this only allows a cosmological constant. We should therefore include perturbations of the scalar field, and, as we shall see, the imprints on observable quantities such as the CMB anisotropies or the matter power spectrum make the scalar field distinguishable from the pure cosmological constant. In linear theory, they are

described by small fluctuations $\delta\phi$ and $\delta\dot{\phi}$ around the background values, driven by the equation of motion

$$\ddot{\delta\phi} + 2\frac{\dot{a}}{a}\dot{\delta\phi} - \nabla^2\delta\phi + a^2\frac{d^2V}{d\phi^2}\delta\phi + \frac{1}{2}\dot{\phi}\dot{h} = 0 \ . \tag{4.9}$$

The density, pressure and velocity perturbations for the scalar field are described as usual by the following quantities

$$\delta\rho_\phi = -\delta T^0_0 = \frac{\dot{\phi}\dot{\delta\phi}}{a^2} + V'\delta\phi \ , \tag{4.10}$$

$$\delta p_\phi = \frac{1}{3}\delta T^i_i = \frac{\dot{\phi}\dot{\delta\phi}}{a^2} - V'\delta\phi \ , \tag{4.11}$$

$$(\rho_\phi + p_\phi)\theta_\phi = \delta T^0_i = ka^{-2}\dot{\phi}\delta\phi \ , \tag{4.12}$$

$$p_\phi\pi_\phi = 0 \ , \tag{4.13}$$

$$\delta_\phi = \frac{\delta\rho_\phi}{\rho_\phi} \ , \quad \theta_\phi = \frac{k}{a^2}\frac{\dot{\phi}\dot{\delta\phi}}{\rho_\phi + p_\phi} = k\frac{\dot{\delta\phi}}{\dot{\phi}} \ ; \tag{4.14}$$

therefore, we define the differential ratio

$$\frac{\dot{\delta p_\phi}}{\dot{\delta\rho_\phi}} = \frac{\dot{\phi}\dot{\delta\phi} - a^2V'\delta\phi}{\dot{\phi}\dot{\delta\phi} + a^2V'\delta\phi} = c^2_\phi + \frac{p_\phi}{\dot{\delta\rho_\phi}}\Gamma_\phi \ , \tag{4.15}$$

that differs from the scalar field sound velocity

$$c^2_\phi = \frac{\dot{p}_\phi}{\dot{\rho}_\phi} \tag{4.16}$$

by the term Γ_ϕ describing the entropy contribution [133].

It is useful to describe radiation in terms of the coefficients characterizing the Legendre expansion of the temperature and polarization brightness functions, $\Delta_T(\mathbf{k},\hat{\mathbf{n}},\tau)$ and $\Delta_P(\mathbf{k},\hat{\mathbf{n}},\tau)$

$$\Delta_T(\mathbf{k},\hat{\mathbf{n}},\tau) = \sum_{l=0}^{\infty}(-i^l)(2l+1)\Delta_{Tl}(k,\tau)P_l(\hat{\mathbf{k}}\cdot\hat{\mathbf{n}}) \ , \tag{4.17}$$

$$\Delta_P(\mathbf{k},\hat{\mathbf{n}},\tau) = \sum_{\updownarrow=0}^{\infty}(-i^l)(2l+1)\Delta_{Pl}(k,\tau)P_l(\hat{\mathbf{k}}\cdot\hat{\mathbf{n}}) \ . \tag{4.18}$$

Their evolution is completely determined by the Boltzmann equations; denoting by σ_T the Thomson scattering cross section and by n_e the electron density, we have for photons:

$$\dot{\delta}_\gamma = -\frac{4}{3}\theta_\gamma - \frac{2}{3}\dot{h} \ , \tag{4.19}$$

$$\dot{\theta}_\gamma = k^2\left(\frac{1}{4}\delta_\gamma - \sigma_\gamma\right) + an_e\sigma_T(\theta_b - \theta_\gamma) \ , \tag{4.20}$$

$$2\dot{\sigma}_\gamma = \frac{8}{15}\theta_\gamma - \frac{3}{5}k\Delta_{\gamma 3} + \frac{4}{15}\dot{h} + \frac{8}{5}\dot{\eta} - \frac{9}{5}an_e\sigma_T\sigma_\gamma + \frac{1}{10}an_e\sigma_T(\Delta_{P0(\gamma)} + \Delta_{P2(\gamma)}) \ , \tag{4.21}$$

$$\dot{\Delta}_{Tl(\gamma)} = \frac{k}{2l+1}[l\Delta_{T(l-1)(\gamma)} - (l+1)\Delta_{T(l+1)(\gamma)}] - an_e\sigma_T\Delta_{Tl(\gamma)} \quad (l \geq 3) \ , \tag{4.22}$$

$$\begin{aligned}\dot{\Delta}_{Pl(\gamma)} &= \frac{k}{2l+1}[l\Delta_{P(l-1)(\gamma)} - (l+1)\Delta_{P(l+1)(\gamma)}] + \\ &+ an_e\sigma_T\left[\frac{1}{2}(\Delta_{T2(\gamma)} + \Delta_{P0(\gamma)} + \Delta_{P2(\gamma)})\left(\delta_{l0} + \frac{\delta_{l2}}{5}\right) - \Delta_{Pl(\gamma)}\right] \ ,\end{aligned} \tag{4.23}$$

where

$$\delta_\gamma = \Delta_{T0} \ , \quad \theta_\gamma = \frac{3}{4}k\Delta_{T1} \ , \quad \sigma_\gamma = \frac{1}{2}\Delta_{T2} \ . \tag{4.24}$$

The perturbed stress-energy tensor for radiation contributes with the following non-zero quantities:

$$\delta T_0^0 = -\rho_\gamma \delta_\gamma \ , \tag{4.25}$$

$$ik^i \delta T_i^0 = \frac{4}{3}\rho_\gamma \theta_\gamma \ , \tag{4.26}$$

$$\delta T_j^i = \frac{1}{3}\rho_\gamma \delta_\gamma + \Sigma_j^i \ , \tag{4.27}$$

$$(\hat{\mathbf{k}}_i \hat{\mathbf{k}}_j - \frac{1}{3}\delta_{ij})\Sigma_j^i = -\frac{4}{3}\rho_\gamma \sigma_\gamma \ . \tag{4.28}$$

The expansion (4.17) also applies for massless neutrinos; their evolution equations in the synchronous gauge are given by the following system:

$$\dot{\delta}_\nu = -\frac{4}{3}\theta_\nu - \frac{2}{3}\dot{h} \ , \tag{4.29}$$

$$\dot{\theta}_\nu = k^2\left(\frac{1}{4}\delta_\nu - \sigma_\nu\right) \ , \tag{4.30}$$

$$\dot{\Delta}_{T2(\nu)} = 2\dot{\sigma}_\nu = \frac{8}{15}\theta_\nu - \frac{3}{5}k\Delta_{T3(\nu)} + \frac{4}{15}\dot{h} + \frac{8}{5}\dot{\eta} \ , \tag{4.31}$$

$$\dot{\Delta}_{Tl(\nu)} = \frac{k}{2l+1}[l\Delta_{T(l-1)(\nu)} - (l+1)\Delta_{T(l+1)(\nu)}] \quad (l \geq 3) \ . \tag{4.32}$$

Pressureless Cold Dark Matter interacts only gravitationally with other particles and in the synchronous gauge its peculiar velocity is zero; setting $\theta_c = 0$, the evolution of CDM density perturbations is given by

$$\dot{\delta}_c = -\frac{1}{2}\dot{h} \ , \tag{4.33}$$

and the non-zero component of its perturbed stress-energy tensor is

$$\delta T_0^0 = -\rho_c \delta_c \ . \tag{4.34}$$

Taking into account the coupling between photons and baryons by Thomson scattering,

$$\dot{\delta}_b = -\theta_b - \frac{1}{2}\dot{h} \ , \tag{4.35}$$

$$\dot{\theta}_b = \frac{\dot{a}}{a}\theta_b + c_s^2 k^2 \delta_b + \frac{4\rho_\gamma}{3\rho_b} a n_e \sigma_T (\theta_\gamma - \theta_b) \ , \tag{4.36}$$

and the perturbed stress-energy tensor for baryons contributes by

$$\delta T_0^0 = -\rho_b \delta_b \ , \tag{4.37}$$

$$ik^i T_i^0 = \frac{4}{3}\rho_\gamma \theta_b \ . \tag{4.38}$$

All these ingredients are to be implemented in perturbed Einstein equations (2.106)-(2.109), that can be integrated once the appropriate initial conditions are fixed , which will be the content of the next sections.

4.3 Initial conditions and superhorizon evolution

In order to start the numerical integration of the evolution equations wrote down in the previous section, one has to impose appropriate initial conditions to the fluid and metric perturbations. Although a general perturbation need not to be either entropic or adiabatic, it can always be expressed as a linear superposition of adiabatic and isothermal components [163]. Also, it is useful to recall that isocurvature perturbations may be present in this kind of model [159]. We explore both these conditions in scalar field cosmology. In particular we search for the initial values of the field perturbations

$\delta\phi_0$ and $\delta\phi_{t0}$ (initial real time derivative) that realize initial adiabaticity and isocurvature, together with appropriate initial conditions on the other perturbed quantities. For this purpose, we will focus on the initial fluctuation of the real time derivative of the scalar field perturbation, since the conformal time derivative is always zero at $a = 0$ by definition ($\delta\dot{\phi} = a \cdot \delta\phi_t$). The same happens of course to the initial conformal time derivative of the background scalar field ϕ; if in general the latter has an initial non-vanishing kinetic energy, so that $\phi_{t0} = (d\phi/dt)_0 \neq 0$, its conformal time velocity $\dot{\phi}_0$ is zero since $\dot{\phi} = a \cdot \phi_t$.

In the following, we will need to use the scale factor behaviour at early times, when $a \ll 1$. We will often use the expansion of the scale factor in powers of the dimensionless parameter ϵ:

$$\epsilon = \sqrt{\frac{8\pi G \rho_c \Omega_r}{3}}\tau = H_0\sqrt{\Omega_r}\tau = \mathcal{C}\tau \ , \tag{4.39}$$

where ρ_c and H_0 are the present critical density and Hubble parameter respectively, and $\Omega_r = \Omega_\gamma + \Omega_\nu$ is the total radiation density contribution at the present. Indeed, as it can be easily verified, AS the scale factor $a \ll 1$ at early times, we can neglect the scalar field contribution in equation (4.5), which admits the simple solution

$$a(\epsilon) = \epsilon + \frac{1}{4}\frac{\Omega_m}{\Omega_r}\epsilon^2 + O(\epsilon^3) \ . \tag{4.40}$$

The expansion rate behaves as

$$\mathcal{H} = \mathcal{C}\left[\frac{1}{\epsilon} + \frac{1}{4}\frac{\Omega_m}{\Omega_r} - \frac{1}{16}\left(\frac{\Omega_m}{\Omega_r}\right)^2\epsilon + O(\epsilon^2)\right] \ . \tag{4.41}$$

Before continuing, it is worth reviewing some general results concerning the synchronous gauge behaviour of metric and density perturbations on superhorizon scales (we refer to the work of Ma and Bertschinger [148], although they did not include the scalar field component). We impose the initial condition at an early time, deep in the radiation era, when photons and baryons are tightly coupled and can be considered as a single coupled fluid; due to the large Thomson scattering opacity, the $l \geq 2$ moments of the photon temperature brightness function (4.22) (in particular, the shear σ_γ) and the polarization brightness function (4.23) are driven to zero. Similarly, to the lowest order in $k\tau$, one can ignore the $l \geq 3$ moments of the neutrino temperature brightness function. Thus, equations (4.19),(4.20), (4.29),(4.30) become:

$$\dot{\delta}_\gamma + \frac{4}{3}\theta_\gamma + \frac{2}{3}\dot{h} = 0 \quad , \quad \dot{\theta}_\gamma - \frac{1}{4}k^2\delta_\gamma = 0 \ , \tag{4.42}$$

$$\dot{\delta}_\nu + \frac{4}{3}\theta_\nu + \frac{2}{3}\dot{h} = 0 \quad , \quad \dot{\theta}_\nu - \frac{1}{4}k^2(\delta_\nu - 4\sigma_\nu) = 0 \ , \tag{4.43}$$

$$\dot{\sigma}_\gamma - \frac{2}{15}(2\theta_\gamma + \dot{h} + 6\dot{\eta}) = 0 \quad , \quad \dot{\sigma}_\nu - \frac{2}{15}(2\theta_\nu + \dot{h} + 6\dot{\eta}) = 0 \ . \tag{4.44}$$

When we impose initial conditions, at $\epsilon \ll 1$, to get starting values for numerical integration, all the $k-$modes are still outside the horizon, i.e. $k \ll aH = 1/\tau$ (the last equality holds in a radiation dominated universe). Our aim is to extract the analytical time-dependence of superhorizon-sized perturbations at early times, once the initial conditions are realized: thus we find the early time form of equations (2.106)-(2.109), (4.42)-(4.44), (4.9) and we find their solutions in successive powers of $k\tau$. To set-up the growth of perturbations, we must assume that at least a single perturbation is nonzero at initial time, in order to generate all the others.

4.4 Adiabatic initial conditions

The first necessary step in imposing adiabatic conditions is setting to zero the initial entropy perturbation; ultimately, the origin of this result is that there is initially a single curvature perturbation

(generated we suppose by inflation) and all later perturbations are inherited from it. The entropy exchange between any two fluid species a and b is ruled by the gauge invariant quantity

$$S_{ab} = \frac{\delta_a}{1+w_a} - \frac{\delta_b}{1+w_b} , \tag{4.45}$$

that must be set to zero initially [133]. The second requirement comes from setting to zero the first time derivative of S_{ab}; actually, S_{ab} obeys the following differential equation:

$$\dot{S}_{ab} = -kV_{ab} - 3\mathcal{H}\Gamma_{ab} , \tag{4.46}$$

where Γ_{ab} is defined as

$$\Gamma_{ab} = \frac{w_a}{1+w_a}\Gamma_a - \frac{w_b}{1+w_b}\Gamma_b , \tag{4.47}$$

Γ_a being the gauge-invariant amplitude of the entropy perturbation of the fluid species a. The quantity $V_{ab} = v_a - v_b$ is the gauge-invariant difference between the gauge-dependent velocity perturbations of the species a and b. In order to have adiabatic initial conditions, both these terms on the right hand side of equation (4.46) are initially set to zero. Thus, for each pair of fluid components, we impose

$$S_{ab} = \dot{S}_{ab} = 0 . \tag{4.48}$$

In particular, applying (4.48) to the scalar field and another component (that we leave unspecified and label with x), will relate the initial values of $\delta\phi$ and $\delta\dot{\phi}$ to the other energy component and metric perturbations. The first condition in (4.48) gives:

$$\phi_t\delta\phi_t + V'\delta\phi = \phi_t^2\frac{\delta_x}{1+w_x} . \tag{4.49}$$

Taking $\dot{S}_{\phi x} = a \cdot S_{\phi xt} = 0$ and using the Klein Gordon equation (4.8,4.9), we obtain

$$\delta\phi_t\left(1 - \frac{k^2\phi_t}{6a^2HV'}\right) = \frac{1}{6H}\left[-\frac{1}{2}\phi_t h_t - \left(\frac{\delta_x}{1+w_x}\right)_t\phi_t + \frac{\delta_x}{1+w_x}\left(6H\phi_t + 2V' - \frac{k^2\phi_t^2}{a^2V'}\right)\right] . \tag{4.50}$$

Combining them together we find:

$$\delta\phi = \frac{1}{V'}\left(\phi_t^2\frac{\delta_x}{1+w_x} - \phi_t\delta\phi_t\right) , \tag{4.51}$$

$$\delta\phi_t = \frac{1}{6H - k^2\phi_t/(a^2V')}\left[-\frac{1}{2}\phi_t h_t - \left(\frac{\delta_x}{1+w_x}\right)_t\phi_t + \frac{\delta_x}{1+w_x}\left(6H\phi_t + 2V' - \frac{k^2\phi_t^2}{a^2V'}\right)\right] . \tag{4.52}$$

The above expressions specify the general adiabatic conditions for the scalar field. Now, let us make a link to previous works. In [148] the adiabatic initial values and early time behaviours of the matter and the radiation components were found in the synchronous gauge; these results apply here too. Indeed, as can easily be seen from the Einstein equations, the contribution of the scalar field fluctuations is negligible at early times $a \ll 1$ with respect to the matter and radiation ones, by a factor a^3 and a^4 respectively. Thus the approximations and treatment developed in [148] is valid also here for what concerns the ordinary fluid components, i.e. photons, massless neutrinos, baryons and dark matter; the time-dependence of the resulting superhorizon-sized perturbations ($k\tau \ll 1$) is found by expanding the Einstein equations in powers of $k\tau$ and resolving the system of coupled differential equations to obtain the leading-order terms :

$$\delta_\gamma = \delta_\nu = \frac{4}{3}\delta_b = \frac{4}{3}\delta_c = -\frac{2}{3}\mathcal{N}(k\tau)^2 , \tag{4.53}$$

$$\theta_\gamma = \frac{15+4R_\nu}{23+4R_\nu}\,\theta_\nu = \theta_b = -\frac{1}{18}\mathcal{N}k^4\tau^3 , \quad \theta_c = 0 , \tag{4.54}$$

$$\sigma_\gamma = 0 \ , \ \sigma_\nu = \frac{4\mathcal{N}}{45 + 12R_\nu}(k\tau)^2 \ , \tag{4.55}$$

$$h = \mathcal{N}(k\tau)^2 \ , \ \eta = 2\mathcal{N} - \frac{5 + 4R_\nu}{90 + 24R_\nu}\mathcal{N}(k\tau)^2 \ , \tag{4.56}$$

where $R_\nu = \rho_\nu/(\rho_\nu + \rho_\gamma)$ and $\mathcal{N}$ is a normalization constant. Using these results, it is immediate to see from (4.51, 4.52) that, imposing adiabatic initial conditions, the initial values of $\delta\phi$ and $\delta\phi_t$ must be set to zero. Note that this result hold provided that the time derivative of the unperturbed scalar field does not diverge at the initial time, which we assumed throughout this thesis.
Adiabatic conditions can be strictly verified *only* at this initial time, due to the effect of the mutual coupling between total density perturbations and entropy perturbations which appear in a generic multi-component fluid. Starting from initial zero values and using (4.56), $\delta\phi$ and $\delta\dot{\phi}$ will evolve according to the (4.9) which can be easily integrated once dropped terms of highest order in τ; this gives the following behaviours at early times ($a \ll 1$):

$$\delta\phi = -\frac{1}{20}\phi_{t0}\ \mathcal{N}Ck^2\tau^4 \ , \tag{4.57}$$

$$\delta\dot{\phi} = -\frac{1}{5}\phi_{t0}\ \mathcal{N}Ck^2\tau^3 \ , \tag{4.58}$$

having considered the lowest terms in τ, thereby approximating the time derivative of ϕ with its value at the initial time ϕ_{t0} . We have inserted these inputs into the standard CMB code and in Section VII we shall expose some numerical results. Now, let us turn to the second class of initial conditions.

4.5 Isocurvature initial conditions

As anticipated at the end of section 2.1, entropy perturbations can and generically will arise in all multi-component systems. They also generate scalar-type metric perturbations. For entropy perturbations, the source term in eq. (2.61) does not vanish; we shall assume that at the initial time there are no adiabatic perturbations, and the entropy perturbations are defined imposing the initial condition $\Psi \to 0$ as $t \to 0$. Instead of distinguishing between adiabatic and entropy perturbations, fluctuations are often divided into isocurvature and adiabatic ones. The isocurvature initial conditions are defined by the initial condition that the gauge invariant curvature perturbation ζ, given by eq. (2.105), vanishes at the initial time; the definitions of isocurvature and entropy perturbations are coincident (or they differ by a term proportional to the decaying mode of Ψ).
Expressing ζ in terms of the metric perturbations h and η through eq. (2.103), the appropriate isocurvature initial conditions are then realized by the time growing solutions of the system (2.106)-(2.109) in which Ψ and $\mathcal{H}^{-1}\dot{\Psi}$ are zero initially. First, let us see that, if the variables describing all the perturbations are regular enough to be differentiable at least four times at $\tau = 0$, then the isocurvature initial conditions are simply imposed by setting the metric and radiation perturbations to zero initially.

$$\text{Isocurvature initial conditions} : h_0 = \eta_0 = \delta_\gamma = \theta_\gamma = \sigma_\gamma = \delta_\nu = \theta_\nu = \sigma_\nu = 0 \ . \tag{4.59}$$

This can be easily seen by using essentially the Einstein equation (2.109); multiplying both the members by a^4, deriving once and factoring out the present critical density ρ_c, it takes the following form:

$$a^2\frac{d^3}{d\tau^3}(h + 6\eta) + 4a\dot{a}\left(\ddot{h} + 6\ddot{\eta}\right) + \left(2\dot{a}^2 + 2a\ddot{a}\right)\left(\dot{h} + 6\dot{\eta}\right) - 4k^2a\dot{a}\eta - 2k^2a^2\dot{\eta} = -32\pi G\rho_c\left(\Omega_\gamma\dot{\sigma}_\gamma + \Omega_\nu\dot{\sigma}_\nu\right) \ . \tag{4.60}$$

Since by hypothesis h and η are differentiable four times in $\tau = 0$, $h + 6\eta$ admits the following early time expansion

$$(h+6\eta)(\tau) = \frac{d}{d\tau}(h+6\eta)_0\tau + \frac{1}{2}\frac{d^2}{d\tau^2}(h+6\eta)_0\tau^2 + \frac{1}{6}\frac{d^3}{d\tau^3}(h+6\eta)_0\tau^3 + \frac{1}{24}\frac{d^4}{d\tau^4}(h+6\eta)_0\tau^4 + O(\tau^5) \ , \tag{4.61}$$

since with the initial condition (4.59) its initial value is zero. At $\tau = 0$ the only term that survives in (4.60) is $\dot{a}^2(\dot{h} + 6\dot{\eta})$ since $\dot{a}_0^2 = 8\pi G\rho_c(\Omega_\gamma + \Omega_\nu)/3$. Then, by using equations (4.42,4.43,4.44) one obtains:

$$\left(\dot{h} + 6\dot{\eta}\right)_0 \frac{48\pi G}{5}\rho_c\left(\Omega_\gamma + \Omega_\nu\right) = 0 \Rightarrow \left(\dot{h} + 6\dot{\eta}\right)_0 = 0 \ . \tag{4.62}$$

In the same way, by differentiating (4.60) again one finds

$$\left(\ddot{h} + 6\ddot{\eta}\right)_0 = 0 \ . \tag{4.63}$$

Instead, it may be easily seen that $d^3(h + 6\eta)/d\tau^3$ can be different from zero; in fact, differentiating (4.60) three times would bring $d^3(h+6\eta)/d\tau^3 \propto k^2\dot{a}^2\dot{\eta}$ which may be different from zero by hypothesis (4.59). This means that, for $\tau \to 0$, $h+6\eta = O(\tau^3)$; since $\mathcal{H} = 1/\tau$ to the lowest order, this is evidently enough to make $\Psi_0 = (\mathcal{H}^{-1}\dot{\Psi})_0 = \zeta_0 = 0$, showing that the initial conditions (4.59) imply isocurvature.

It is evident that the initial condition (4.59) can be realized in several ways, depending on which matter component is initially perturbed, or, in other words, on which δ_x is initially different from zero. In the present case a further degree of freedom arises from the presence of the scalar field, and we will analyze separately two main situations: in the first case only one matter component (CDM or baryons) is initially perturbed; in the second case the initially perturbed component is only the scalar field.

4.5.1 Isocurvature conditions from matter perturbations

Let us consider first the case in which an initial density perturbation, with amplitude δ_{c0}, resides only on the CDM component. By integrating (4.33), one finds

$$\delta_c = \delta_{c0} - \frac{1}{2}h \ . \tag{4.64}$$

By hypothesis, this is the only initially perturbed quantity. All the others must to be set to zero at $\tau = 0$. Let us study the early time behaviour of the perturbations. Since all the modes are outside the horizon at early times, we first neglect all the terms proportional to k in the Einstein equations; then we expand all the quantities in powers of ϵ defined in (4.39) and we calculate the leading orders. In making this, we are assuming that all the perturbed quantities admit a Taylor expansion in $\tau = 0$ of course. By making use of the above criteria and of equations (4.40,4.41), the Einstein equation (2.106) becomes

$$\begin{aligned}&\left(1 + \frac{1}{4}\frac{\Omega_m}{\Omega_r}\epsilon + O(\epsilon^2)\right)\left(1 + \frac{1}{2}\frac{\Omega_m}{\Omega_r}\epsilon + O(\epsilon^2)\right)\epsilon\dot{h} = \\ &= \frac{8\pi G}{\mathcal{C}^2}\left(\Omega_\gamma\delta_\gamma + \Omega_\nu\delta_\nu + \Omega_c\delta_c\epsilon + \Omega_b\delta_b\epsilon + O(\epsilon^2)\right) \ ,\end{aligned} \tag{4.65}$$

and it is immediate to gain the early time behaviour of h:

$$h = \delta_{c0}\frac{\Omega_c}{\Omega_r}\epsilon - \frac{3}{8}\delta_{c0}\frac{\Omega_c\Omega_m}{\Omega_r^2}\epsilon^2 + O(\epsilon^3) \ . \tag{4.66}$$

From the arguments presented at the beginning of this section, up to the order ϵ^2 we have also

$$\eta = -\frac{1}{6}h \ . \tag{4.67}$$

Let us come now to the fluid perturbation quantities. As it is evident from the fluid equations, the θ and σ quantities are of higher order in $k\tau$ with respect to the purely metric perturbations h and η. Therefore, their early time behaviour can be written as follows:

$$\delta_\gamma = \delta_\nu = \frac{4}{3}\delta_b = -\frac{2}{3}h \ , \tag{4.68}$$

$$\theta_\gamma = \theta_\nu = \theta_b = -\frac{1}{12}\delta_{c0}\frac{\Omega_c}{\Omega_r \mathcal{C}}k^2\epsilon^2 + O(\epsilon^3) \ , \ \theta_c = 0 \ , \ \sigma_\nu = O(\epsilon^3) \ . \tag{4.69}$$

The behaviour of $h+6\eta$ is interesting even if of high order in τ, since it is directly related to the gauge invariant curvature by (2.105,2.103) and it can be obtained by solving equation (2.109):

$$h + 6\eta = \frac{\mathcal{I}_1}{3}\tau^3 \ , \tag{4.70}$$

where we have defined

$$\mathcal{I}_1 = \frac{4\delta_{c0}\Omega_c(\Omega_\nu - 5\Omega_r)\mathcal{C}k^2}{36\Omega_r + 24\Omega_\nu} \ . \tag{4.71}$$

Note that $h+6\eta \propto \tau^3$, according to the isocurvature nature of the present case, as we described in the beginning of this section. Also, (4.70) can be used to find the behaviour of σ_ν, by using again (2.109).

It remains to find the early time behaviour of the scalar field perturbation $\delta\phi$. This can be done by expanding $\delta\phi$ in powers of ϵ and looking at the perturbed Klein Gordon equation once the terms proportional to k^2 have been neglected. The inhomogeneous term is $-\frac{1}{2}\dot{\phi}\dot{h}$; $\dot{h}$ is of the order zero from (4.66), and $\dot{\phi} = a \cdot \phi_t$ is at least of the order ϵ; thereby, to the lowest order in ϵ, equation (4.9) is satisfied by

$$\delta\phi = -\frac{1}{24}\phi_{t0}\delta_{c0}\frac{\Omega_c}{\Omega_r}\frac{\epsilon^3}{\mathcal{C}} \ , \quad \delta\dot{\phi} = -\frac{1}{8}\phi_{t0}\delta_{c0}\frac{\Omega_c}{\Omega_r}\epsilon^2. \tag{4.72}$$

This completes the early time behaviour of all the perturbation quantities in this case of isocurvature initial conditions. All these relations can be easily generalized to the case in which the initial perturbed matter component is the baryonic one. In the next subsection we study the other interesting case: the initial perturbed fluid component is the scalar field itself.

4.5.2 Isocurvature conditions from scalar field perturbations

Let us suppose that at the initial time $a \to 0$ the only non-zero perturbed quantity is the scalar field, in a manner such that the total gauge-invariant energy density contrast is zero, all the other perturbations being zero. This means that at least one of the two quantities $\delta_{\phi 0}, \theta_{\phi 0}$ must be different from zero initially; from (4.14), the corresponding expressions for $\delta\phi_0$ and $\delta\phi_{t0}$ are

$$\delta\phi_0 = \frac{1}{V'(\phi_0)}\left[\frac{1}{2}\phi_{t0}^2\left(\delta_{\phi 0} - 2\frac{\theta_{\phi 0}}{k}\right) + V(\phi_0)\delta_{\phi 0}\right] \ , \ \delta\phi_{t0} = \frac{\phi_{t0}\theta_{\phi 0}}{k} \ . \tag{4.73}$$

In order to have isocurvature, for the other quantities we impose again the initial conditions (4.59). The relevant difference with respect to the previous situation lies in the slower rise of the metric and fluid perturbations starting from their initial zero values: they will grow according to (2.106)-(2.109) and (4.42-4.44), the whole perturbation-growth-machinery being initially driven only by the $O(\epsilon^4)$ contribution of the scalar field through the perturbed Einstein equations, while the perturbed Klein Gordon equation starts its dynamics from the conditions $\delta\phi_0 \neq 0$, $\delta\dot{\phi} = 0$ and generates the inhomogeneous term driving the evolution of h. From equation (2.106), together with (4.42-4.44), it is easy to find the early-time behaviour of the metric perturbation h:

$$h = \frac{3}{4}\left(\frac{\delta_{\phi 0}\ \rho_\phi}{\rho_c \Omega_r}\right)\mathcal{C}^4\tau^4 + O(\tau^5) \ . \tag{4.74}$$

Using the method applied in the previous sections, one finds the leading-order behaviours:

$$\delta_\gamma = \delta_\nu = \frac{4}{3}\delta_c = \frac{4}{3}\delta_b = -\frac{2}{3}h \propto \tau^4 \tag{4.75}$$

$$\theta_\nu, \theta_\gamma, \theta_b \ \propto \tau^5 \ , \quad \sigma_\nu \propto \tau^6 \ , \tag{4.76}$$

and, from (2.109), it can be seen that

$$h + 6\eta = \frac{\mathcal{I}_2}{6}\tau^6 \ , \tag{4.77}$$

where

$$\mathcal{I}_2 = \frac{k^2\mathcal{C}^4}{170\Omega_r + 8\Omega_\nu}\left(\frac{\delta_{\phi 0}\rho_\phi}{\rho_c\Omega_r}\right)\left(-\frac{2}{10}\Omega_\nu - \frac{125}{10}\Omega_r\right) . \tag{4.78}$$

From the above formulas we see that the perturbations regarding the metric and the ordinary fluid components rise very slowly; indeed we found a substantial failure of this model in providing a significant amount of perturbations. For this reason we will not consider this case in the numerical integrations of section VII.

It is interesting to find the behaviour of scalar field perturbation at early times, that moves it away from its initial value $\delta\phi_0$; this contains corrections in $(k\tau^2)$ together with a term proportional to τ^4, as can be verified by integration of (4.9):

$$\delta\phi = \delta\phi_0 + \delta\phi^{(2)}\tau^2 + \delta\phi^{(3)}\tau^3 + \delta\phi^{(4)}\tau^4 + \delta\phi^{(5)}\tau^5 + \delta\phi^{(6)}\tau^6 + O(\tau^7) , \tag{4.79}$$

where the expansion coefficients are given by

$$\delta\phi^{(2)} = -\frac{1}{6}\delta\phi_0\ k^2 \quad , \quad \delta\phi^{(3)} = \frac{1}{72}\frac{\Omega_m}{\Omega_r}\mathcal{C}k^2\delta\phi_0 ,$$

$$\delta\phi^{(4)} = \frac{1}{20}\delta\phi_0\left(\frac{k^4}{6} - \mathcal{C}^2V''\right) + \frac{1}{80}\left(\frac{\Omega_m}{\Omega_r}\right)^2\mathcal{C}^2\delta\phi^{(2)} - \frac{3}{40}\frac{\Omega_m}{\Omega_r}\mathcal{C}\delta\phi^{(3)} ,$$

$$\delta\phi^{(5)} = -\frac{1}{15}\frac{\Omega_m}{\Omega_r}\mathcal{C}\delta\phi^{(4)} + \left[\frac{1}{80}\left(\frac{\Omega_m}{\Omega_r}\right)^2\mathcal{C}^2 - k^2\right]\delta\phi^{(3)} ,$$

$$\delta\phi^{(6)} = -\frac{5}{84}\frac{\Omega_m}{\Omega_r}\mathcal{C}\delta\phi^{(5)} + \left[\frac{1}{84}\left(\frac{\Omega_m}{\Omega_r}\right)^2\mathcal{C}^2 - k^2\right]\delta\phi^{(4)} - \mathcal{C}^2V''\delta\phi^{(2)} - \frac{3}{2}\left(\frac{\delta_{\phi 0}\rho_\phi}{\rho_c\Omega_r}\right)\mathcal{C}^5\phi_{t0} . \tag{4.80}$$

We considered the expansion up to the sixth order in τ because, as we will see in the next section, going to the Newtonian gauge changes the last coefficient.

In the next section we extend the results of sections IV and V to the conformal Newtonian gauge.

4.6 Results in the Conformal Newtonian gauge

As is well known, the synchronous gauge is a coordinate system corresponding to observers at rest with respect to the collisionless matter component. These "Lagrangian coordinates" are defined by the rest frame of a set of preferred observers. More physical intuition can be achieved in the conformal Newtonian gauge, where the metric tensor is diagonal. Inside the horizon, the perturbation equations reduce to the standard non-relativistic Newtonian equations. In this section we write the results of section IV and V in the Newtonian gauge.

The connection between two gauges is realized in general by performing a coordinate transformation relating the two frames. The link between the perturbations in the two gauges is expressed at the same coordinate point instead of the same spacetime point; this is why in most cases it is interesting to know the difference of the fluctuations in the two gauges [133].

First we write down the relations between the genuine metric perturbed quantities. In the Newtonian gauge the perturbation to g_{00} exists and it is represented by the potential Ψ; the trace of g_{ij} is instead perturbed by Φ. Their relations with h and η are

$$\Psi = \frac{1}{2k^2}\left[\ddot{h} + 6\ddot{\eta} + \frac{\dot{a}}{a}\left(\dot{h} + 6\dot{\eta}\right)\right] , \tag{4.81}$$

$$\Phi = \frac{1}{2k^2}\frac{\dot{a}}{a}\left(\dot{h} + 6\dot{\eta}\right) - \eta . \tag{4.82}$$

They can be easily expressed for $\epsilon \ll 1$, $k\tau \ll 1$ by substituting directly the expressions for h and η contained in sections IV and V.

Now we concentrate on the transformations regarding fluids and the scalar field. They are contained in the stress energy tensor, which transforms as

$$T^{\mu\nu}(\tilde{x}) = \frac{\partial \tilde{x}^\mu}{\partial x^\rho}\frac{\partial \tilde{x}^\nu}{\partial x^\sigma}T^{\rho\sigma}(x) \ . \tag{4.83}$$

Using this, and taking care to compare the perturbations at the same coordinate point, the relations between the quantities in the two gauges (synchronous and Newtonian labeled as s and N respectively) for each fluid are:

$$\delta_s = \delta_N - \mathcal{T}\frac{\dot{\rho}}{\rho} \ , \tag{4.84}$$

$$\theta_s = \theta_N - k^2\mathcal{T} \ , \tag{4.85}$$

$$p_s = p_N - p\mathcal{T} \ , \tag{4.86}$$

$$\sigma_s = \sigma_N \ , \tag{4.87}$$

where

$$\mathcal{T} = \frac{\dot{h}+6\dot{\eta}}{2k^2} \tag{4.88}$$

is the lapse between the synchronous and the Newtonian time coordinate. Regarding the scalar field, we compute the Newtonian gauge expression of the amplitude fluctuation $\delta\phi$ by using the transformation

$$\delta\phi_s = \delta\phi_N - \dot{\phi}\mathcal{T} \ . \tag{4.89}$$

In the following subsections we write the behaviour of the fluid quantities in the $\epsilon \ll 1$, $k\tau \ll 1$ regime and in the Newtonian gauge, dropping the N subscript.

4.6.1 Adiabaticity

The leading orders for matter and radiation perturbations are

$$\delta_\gamma = -\frac{40\mathcal{N}}{15+4R_\nu} = \delta_\nu = \frac{4}{3}\delta_b = \frac{4}{3}\delta_c \ , \tag{4.90}$$

$$\theta_\gamma = \theta_\nu = \theta_c = \theta_b = \frac{10\mathcal{N}}{15+4R_\nu}k^2\tau \ , \tag{4.91}$$

$$\sigma_\nu = \frac{4\mathcal{N}}{45+12R_\nu}k^2\tau^2 \ . \tag{4.92}$$

The scalar field perturbation amplitude is

$$\delta\phi = \mathcal{N}\tau^2\phi_{t0}\frac{10}{15+4R_\nu} \ . \tag{4.93}$$

Note that in this case the scalar field perturbations faster grow in time ($\propto \tau^2$) than in the synchronous gauge ($\propto \tau^4$); as we point out below, this is not a feature of the isocurvature initial conditions.

4.6.2 Isocurvature from matter

Matter and radiation behave as

$$\delta_\gamma = \delta_\nu = \frac{4}{3}\delta_b = -\frac{2}{3}\delta_{c0}\frac{\Omega_c}{\Omega_r}\mathcal{N}\tau - \frac{2\mathcal{I}_1}{k^2}\tau \ . \tag{4.94}$$

$$\delta_c = \delta_{c0} - \frac{1}{2}\delta_{c0}\frac{\Omega_c}{\Omega_r}\mathcal{C}\tau - 3\frac{\mathcal{I}_1\tau}{2k^2} \ , \tag{4.95}$$

$$\theta_\gamma = \theta_\nu = \theta_b = -\frac{1}{12}\delta_{c0}\frac{\Omega_c}{\Omega_r}k^2\mathcal{C}\tau^2 + \frac{\mathcal{I}_1\tau^2}{2} \ , \ \theta_c = \frac{\mathcal{I}_1\tau^2}{2} \ . \tag{4.96}$$

$$\sigma_\nu = O(\epsilon^3) \ . \tag{4.97}$$

The scalar field amplitude is given by

$$\delta\phi = -\frac{1}{24}\phi_{t0}\delta_{c0}\frac{\Omega_c}{\Omega_r}\mathcal{C}^2\tau^3 + \frac{\mathcal{I}_1\mathcal{C}\tau^3}{2k^2}\phi_{t0} \ , \tag{4.98}$$

and shows that the gauge change does not touch the order of the leading power in τ, although it modifies its numerical coefficient.

4.6.3 Isocurvature from scalar field

Matter and radiation behave as

$$\delta_\gamma = \delta_\nu = \frac{4}{3}\delta_b = -\frac{1}{2}\left(\frac{\delta_{\phi 0}\rho_\phi}{\rho_c\Omega_r}\right)\mathcal{C}^4\tau^4 - 2\frac{\mathcal{I}_2}{k^2}\tau^4 \ , \tag{4.99}$$

$$\delta_c = -\frac{3}{8}\left(\frac{\delta_{\phi 0}\rho_\phi}{\rho_c\Omega_r}\right)\mathcal{C}^4\tau^4 - \frac{3\mathcal{I}_2\tau^4}{2k^2} \ , \ \theta_c = \frac{\mathcal{I}_2\tau^5}{2} \ , \tag{4.100}$$

$$\theta_\gamma = \theta_\nu = \theta_b \propto \tau^5 \ , \ \sigma_\nu \propto \tau^6 \ . \tag{4.101}$$

The scalar field amplitude is given by

$$\delta\phi = \delta\phi_0 + \delta\phi^{(2)}\tau^2 + \delta\phi^{(3)}\tau^3 + \delta\phi^{(4)}\tau^4 + \delta\phi^{(5)}\tau^5 + \left(\delta\phi^{(6)} + \frac{\mathcal{I}_2}{2k^2}\phi_{t0}\right)\tau^6 + O(\tau^7) \ ; \tag{4.102}$$

therefore, in this isocurvature case, the behaviour of $\delta\phi$ is affected by the gauge change only at high orders in τ, leaving the leading terms unperturbed.

In the next section we will numerically solve the linear cosmological perturbation equations with the initial conditions sets developed in sections IV and V.

4.7 Numerical integrations and discussion

In order to obtain the anisotropies power spectra in temperature and polarization, as well as the matter power spectrum today, we have to integrate with the proper initial conditions the equations described above.

As we have seen in chapter 3, expanding the temperature and polarization anisotropies in multipole moments gives rise to a hierarchy of coupled differential equations, where power is transferred from lower to higher multipoles. To test a model up to a given angular scale θ, one should solve the system 3.18-3.20 up to $l \sim 1/\theta$: for a detailed prediction of the CMB spectra on small angular scales, this would require the integration in time of a very large system of differential equations, with the cost of a large computational time.

We found convenient to modify the existing code CMBFAST [197], based on the *line of sight approach* to the CMB anisotropies. This method is based on the integration, along the photon past light cone, of the formal integral solutions of the Boltzmann equation implemented with the perturbed fluid equations, i.e. the integral solutions given by eqs. 3.49, 3.50 and 3.51. This approach has the main advantage to clearly express the integrand in eqs. 3.49-3.51 as the product of a cosmological source term, independent on the multipole moment l, and a geometrical one, independent on the cosmology: the latter can therefore be computed once and stored in a file to be used in any cosmological model. On the other hand, the source terms in the integrals are given by eqs. 3.22, 3.23 and 3.24 and can be easily computed, for each Fourier mode k, at any time. For scalar perturbation, the source terms expressed in the synchronous gauge, for a flat universe, are given by:

$$S_0^{(0)} = \dot{\tau}\frac{\delta_\gamma}{4} - \dot{h} \ , \ S_1^{(0)} = \dot{\tau}\theta_b^{(0)} \ , \ S_2^{(0)} = \dot{\tau}P^{(0)} + \frac{2}{3}(\frac{\dot{h}}{2} + 3\dot{\eta}) \ , \tag{4.103}$$

and, again,

$$P^{(0)} = \frac{1}{10}\left[\frac{5}{12}\sigma_\gamma - \sqrt{6}E_2^{(0)}\right] . \tag{4.104}$$

Such source terms evolve in time, following the evolution of the photons and baryons perturbations, as well as the metric perturbations. As we can see, the introduction of a scalar field enters only implicitly in the source terms, both through the background, which is now described by two equations (namely, the Friedmann equation and the Klein-Gordon one) and the metric perturbation evolution (because the metric perturbations h and η contain all the perturbed fluid quantities, including the scalar field). By inserting the Klein Gordon equation and its perturbed form into the numerical code, and including the scalar field and its fluctuations in the Einstein equations, the correct evolution of the remaining quantities is immediately obtained, and the correct values for the source terms 4.103 are recovered .

To check the accuracy of our integrations, beyond the internal checks of the integration routines, we compared flatter and flatter quintessence potentials (thus approaching the "true" cosmological constant behavior) with the spectra corresponding to the cosmological constant case, finding a complete agreement. In chapter 6 we will see a further improvement of this code, to recover cases in which the quintessence field is coupled with the Ricci scalar. Also in this case, we verified that, as the coupling parameter goes to zero, we recover the standard quintessence scenario.
Before going to the results, we must finally comment about the initial conditions for the background values of the quintessence field and its derivatives; in fact, for a given value of Ω_ϕ today, the starting values of ϕ and $\dot{\phi}$ at $\tau = 0$ are not unique; in particular, there exist particular trajectories, named "tracking solutions", which have attractive properties, that will be considered in chapter reftra. These solutions are generally characterized by comparable values of the kinetic and potential energies of the field along the trajectory. Here, instead, we consider the trajectories for which, starting with initial null velocity, the field reaches today a given value of Ω_ϕ with nearly vanishing kinetic energy. Therefore, the case considered here can be regarded as the limit of tracking solutions for vanishing Quintessence kinetic energy.

We performed the numerical integration applying our considerations to a scalar field model based on ultra-light pseudo-Nambu-Goldstone bosons; the potential associated to this field has the form [104]:

$$V(\phi) = M^4[\cos(\phi/f) + 1] \tag{4.105}$$

Our working point corresponds to the parameter choice $f = 1.885 \times 10^{18}$ GeV and $M = 10^{-3}$ eV, assuming an initial kinetic energy equal to the potential one. The starting values of the scalar field and its initial time derivative are obtained by requiring that the present contribution is $\Omega_\phi = 0.6$, fixing $H_0 = 70$ km/sec/Mpc and $\Omega_b = 0.05$. Furthermore, we have taken the primordial power spectrum to be exactly scale-invariant.

Even though the main cosmological consequences of this kind of scalar fields have been analyzed by many authors (see [51, 221]), here we use the formulas developed in the previous sections to accurately compare the pure adiabatic and pure isocurvature regimes. Also we give particular emphasis on the behaviour of entropy and curvature perturbations, again comparing their evolution starting from isocurvature (from CDM) and adiabatic initial conditions; each case is compared with a pure CDM model with the same background parameters. The comparison of Quintessence cosmologies with the cosmological constant scenarios will be performed in chapter 6.

First, let us consider the power spectra of the microwave background anisotropies, both temperature and polarization. They are expressed by the expansion coefficients of the two point correlation function into Legendre polynomials (see e.g. [163]) and admit the following expression in terms of the quantities defined in the previous sections:

$$C_l^T = 4\pi \int \frac{dk}{k} |\Delta_{Tl}(k, \tau_0)|^2 \quad , C_l^P = 4\pi \int \frac{dk}{k} |\Delta_{Pl}(k, \tau_0)|^2 \quad . \tag{4.106}$$

The adiabatic case is shown in figure (4.7). The presence of the scalar field (solid line) produces an increase of the power of the acoustic oscillations with respect to the CDM model (dashed line). This is due to the fact that the universe is not completely matter dominated at decoupling: thus at this time

the perturbations are growing faster than in the CDM models (we recall that density perturbations in adiabatic models grow as a^2 and a respectively in the radiation in the matter eras) and this produces an early integrated Sachs-Wolfe effect (ISW), found first in [51]. Also, the position of the first peak is slightly shifted toward smaller angular scales due to the increase of the distance of the last scattering surface (projection effect). Note how these features regard both the polarization and temperature peaks. Finally, the temperature spectra shows that the ISW is active on the smallest multipoles due to the dynamics of the scalar field in the present case; this is a distinctive feature with respect to the cosmological constant [51].

Figure 4.7 shows the spectrum from isocurvature perturbations. While the projection effect is the same as in the adiabatic case, now the situation regarding the amplitude of the acoustic oscillations is inverted: the peaks are lower than the ordinary models, both for polarization and temperature. This is due to the reduction of the matter/radiation ratio as we include ϕ by keeping $\Omega_{total} = 1$; in fact, the scalar field has *no* intrinsic dynamical effect at last scattering since matter and radiation components were largely dominant. The opposite behavior of the anisotropies in adiabatic and isocurvature models as one varies $\Omega_m h^2$ is well known (see e.g. [163]). To better see this point, we plot in figure 3 and 4 the power spectra for models having fixed $\Omega_b h^2$ and $\Omega_c h^2$ but varying $\Omega_m = \Omega_b + \Omega_c$ and h by means of different Ω_ϕ. Thus we expect the same amount of perturbations in the CMB except for the effects that are genuinely linked to the scalar field, being the projection effect and the ISW on the smallest multipoles. This is precisely what happens for the spectra in figure 3 and 4. The dashed lines represent again the curves for $\Omega_\phi = .6$ as in figures 1 and 2; the solid and thin lines represents $\Omega_\phi = .5$ and .7 respectively. The spectra show remarkably the same features for polarization and temperature, even if it should be noted how the former, arising from acoustic oscillations occurring just *at* decoupling, is not influenced by the ISW effect, since it comes from the line of sight integration. All this shows how the perturbation power at decoupling is not touched by the subdominant scalar field; the opposite behaviours in the adiabatic and isocurvature cases is explained by the decrease of matter in favor of scalar field.

More insight on the perturbation behaviour may be obtained by looking at the time evolution of some significant quantities; we look at one single scale, or wavenumber, roughly entering in the horizon between matter and radiation equality and decoupling:

$$k = 8 \times 10^{-2} \mathrm{Mpc}^{-1} \ . \tag{4.107}$$

Let us begin with the gravitational potential Ψ, shown in figure 5; the rapid increase (or decrease) is associated, in the isocurvature and adiabatic case respectively, to the horizon crossing of the scale examined. The amplitude of the gravitational potential variation at horizon crossing, in the scalar field models, is higher for the adiabatic case and lower for the isocurvature one when compared with the corresponding CDM models. These variations of the gravitational potential are the source of the CMB anisotropies on sub-horizon angular scales ($l \geq 200$) through the acoustic driving effect and the early ISW effect [110], and therefore follow the different behaviour in the two cases.

We concentrate now on two particularly significant quantities regarding both adiabatic and isocurvature regimes, the total entropy perturbation, defined below, and the curvature ζ defined in (2.105); we recall that these quantities are gauge invariant. The amplitude of the total entropy perturbation is given by

$$\begin{aligned} p\Gamma = p\Gamma_{int} + p\Gamma_{rel} &= \sum_a (\delta p_a - c_a^2 \delta\rho_a) + \sum_a (c_a^2 - c_s^2)\delta\rho_a = \\ &= \sum_a (\delta p_a - c_s^2 \delta\rho_a) \ , \end{aligned} \tag{4.108}$$

where p is the total pressure and the sound speed must take into account the scalar field contribution $c_\phi^2 = 1 - 2V'\dot{\phi}/\dot{\rho}_\phi$ in the summation

$$c_s^2 = \frac{\sum_a h_a c_a^2}{h} \ , \tag{4.109}$$

where

$$h_a = \rho_a + p_a \quad , \quad h = \sum_a h_a \ . \tag{4.110}$$

While the Γ_{int} term comes from the intrinsic entropy perturbation of each component, and it is ultimately sourced only by the scalar field component due to the spatial and temporal variations of the scalar field equation of state, the Γ_{rel} term arises from the different dynamical behaviours of the components, and it is related to the S_{ab} quantities defined in eq. (4.45) by the relation [133]:

$$p\Gamma_{rel} = \frac{1}{2}\sum_{a,b}\frac{h_a h_b}{h}(c_a^2 - c_b^2)S_{ab} \tag{4.111}$$

In figures 6 and 7 we plot Γ vs a (solid line and arbitrary units) using isocurvature CDM and adiabatic initial conditions respectively. We note that in both cases $\Gamma \to 0$ as $a \to 0$: in the last case, this is an obvious consequence of the definition of what adiabatic conditions are; on the other hand, taking isocurvature CDM initial conditions, we started with non-zero values of the S_{ab} relative to the CDM component and the other non-compensating components, but again $\Gamma \to 0$ as $a \to 0$. This is because at early times the cosmic fluid is radiation dominated, so that $p \propto 1/a^4$ in (4.108); this kills Γ for $a \to 0$, since no radiation perturbations are present initially. Instead, the initial value of the first time derivative of Γ is different from zero only selecting isocurvature initial conditions, since it takes contributions directly from the S_{ab} terms [133]. The behaviours of entropy perturbations in both cases have been compared with those in the standard Einstein-De Sitter model $\Omega_m = 1$ (dotted line), with the same choice of Ω_b and H_0. The entropy perturbations remain nearly constant before horizon crossing; at this time the perturbation starts its oscillations that are damped in amplitude when the scale is well below the effective horizon. As an expected feature, note that in the scalar-field model the peaks of the oscillations are shifted closer to the present when compared to the Einstein-De Sitter case, as the epoch of matter-radiation equality.

In figures 8 and 9 we plot the evolution of the gauge-invariant curvature perturbation ζ for isocurvature CDM and adiabatic initial conditions, respectively. At $a \ll 1$, this quantity is zero in the isocurvature case and non-zero in the adiabatic one, being an explicit indicator of the nature of the perturbations. Again the significant dynamics occurs in correspondence of the horizon crossing, and the latter occurs slightly later then in the CDM model due to the presence of the scalar field.

Finally, note how in the isocurvature cases (figures 6 and 8) the amplitude of the oscillations are lower than in the corresponding CDM models; as we mentioned above, this is due to the reduction of the matter component in favor of the scalar field energy density. Most important, these graphs show that this is the only possible cause of this effect, since at the times of oscillations for the scale examined, roughly between equivalence and decoupling, the scalar field is very subdominant with respect to the other components.

We may comment on the fact that isocurvature scenarios suffer from various problems; mainly, they give rise to an underproduction of large-scale structure relative to large-angle CMB anisotropies [70] and to small-angle acoustic peaks amplitude which is too small when compared with recent measurements of degree-scale anisotropies. However, entropy perturbations can arise in axion models [218, 195], and in phase transitions which produce topological defects, such cosmic strings [127].

Concluding, the hypothesis of a cosmic vacuum energy stored in the potential of a scalar field enlarges naturally the possibility to gain insight into high energy physics from the traces left in the cosmic radiation and in the matter distribution. With upcoming CMB experiments [155][156], it will be interesting to further study the cosmological imprints of these models, in the context of different theories attempting to describe the hidden sector of high energy physics.

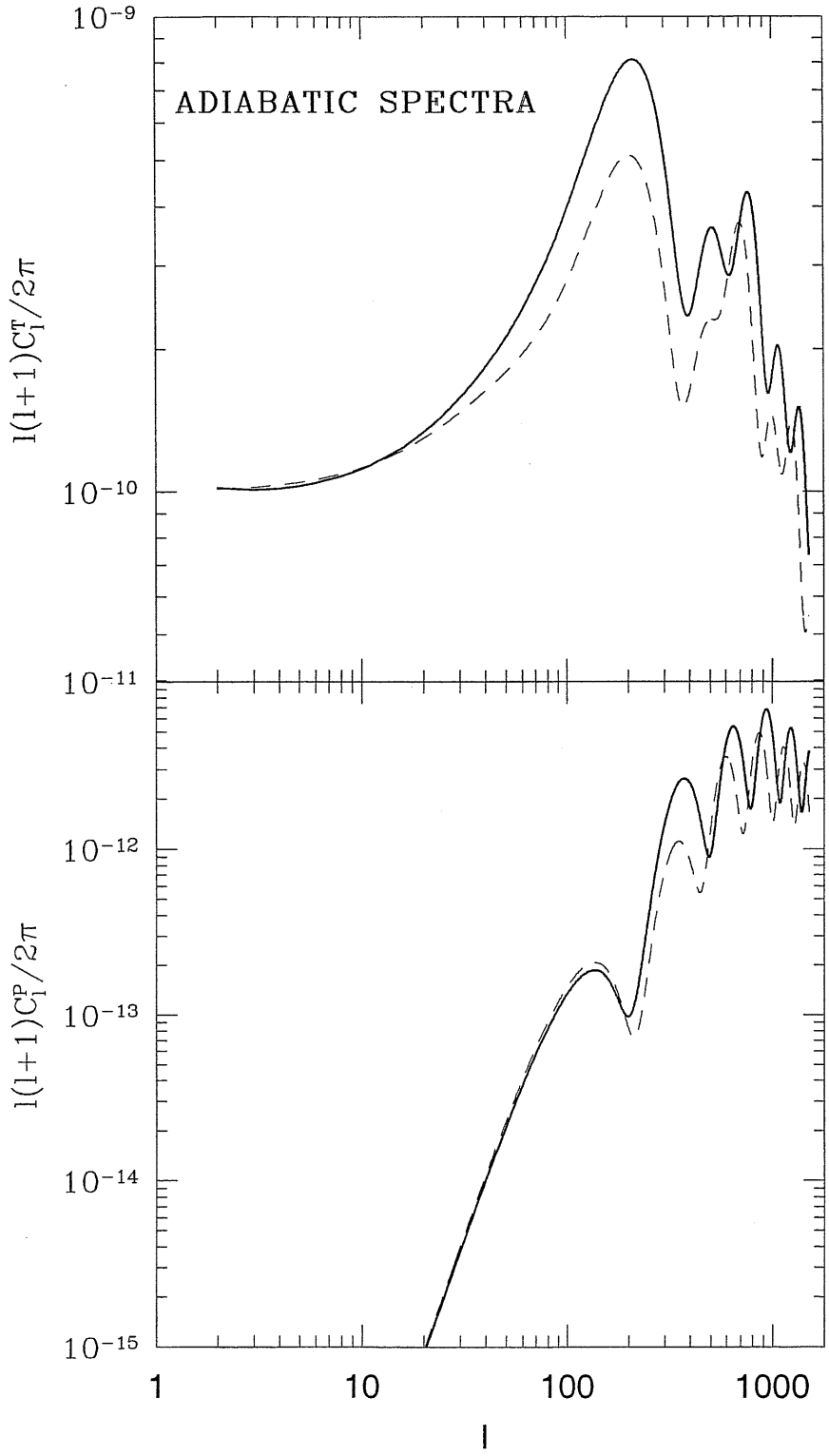

Figure 4.1: Power spectra of the CMB anisotropies from adiabatic initial conditions. The background parameters are $\Omega_b = .05$, $h = .7$, three massless neutrino families and $\Omega_\phi = .6, \Omega_c = .35$ (solid line), $\Omega_\phi = 0, \Omega_c = .95$ (dashed line). Note the increase of the acoustic peak power in the scalar field model.

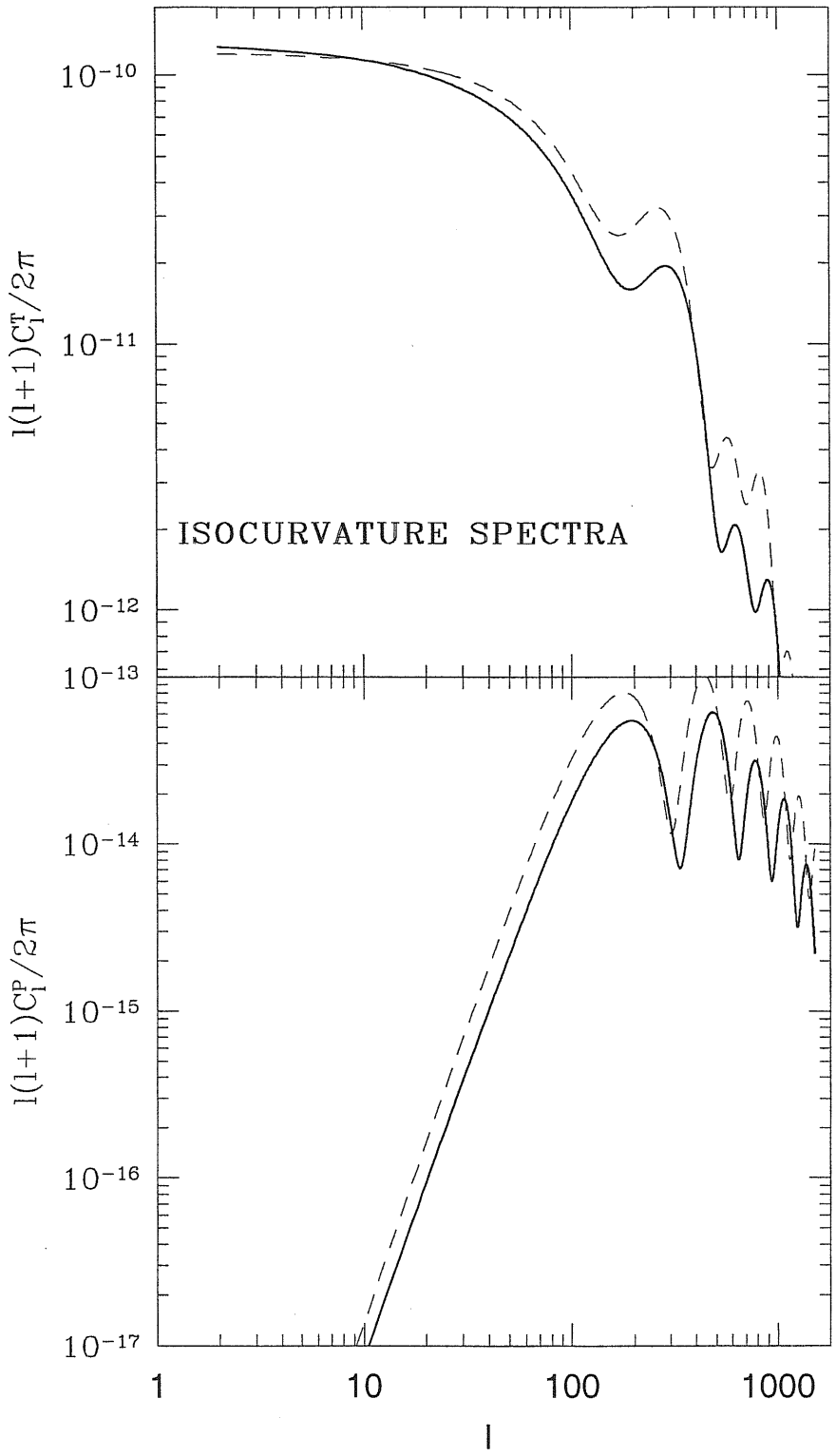

Figure 4.2: Power spectra of the CMB anisotropies from isocurvature initial conditions. The background parameters are $\Omega_b = .05$, $h = .7$, three massless neutrino families and $\Omega_\phi = .6, \Omega_c = .35$ (solid line), $\Omega_\phi = 0, \Omega_c = .95$ (dashed dotted line). Note the decrease of the acoustic peaks power in the scalar field model, an opposite behaviour with respect to the adiabatic case.

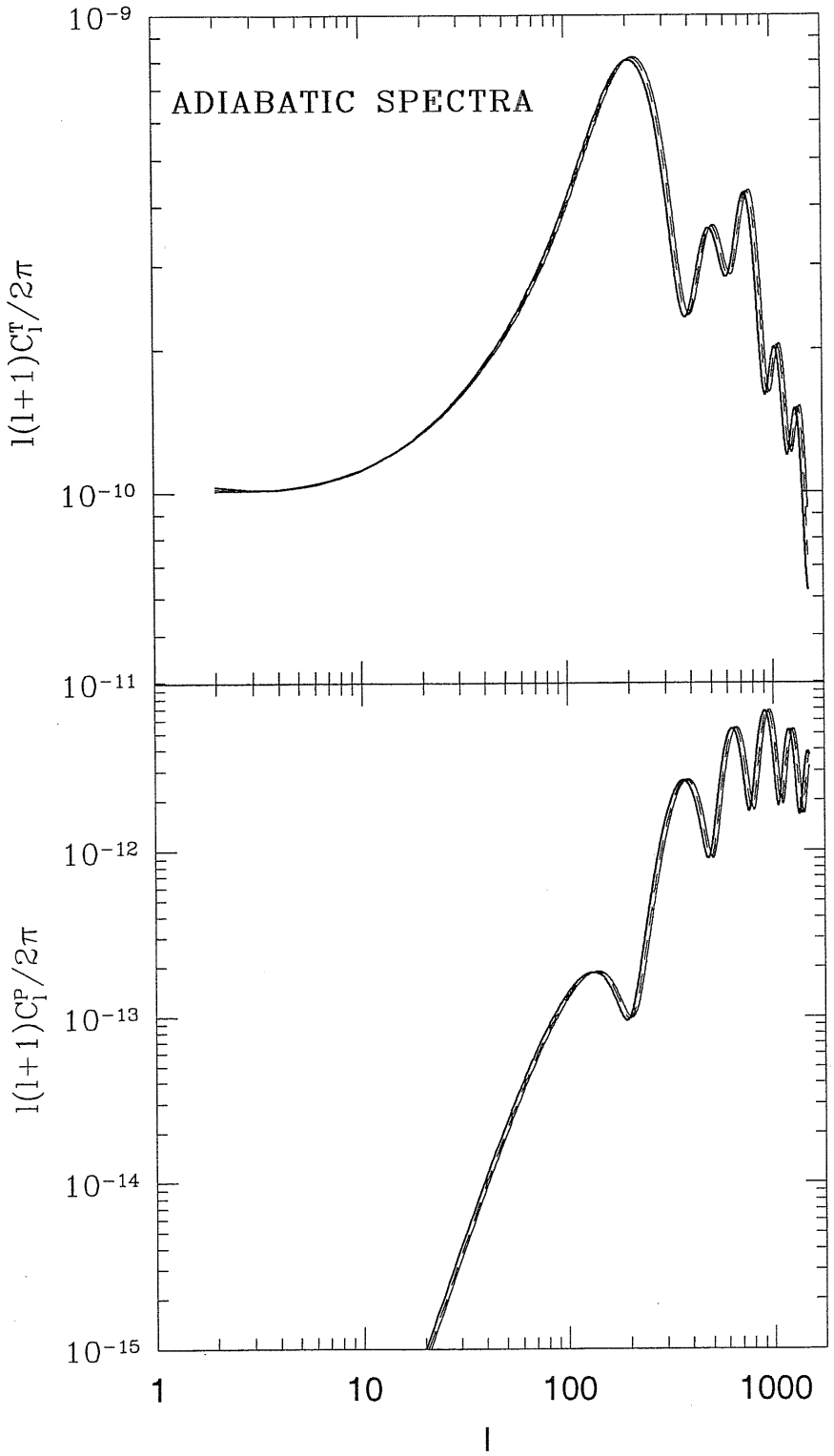

Figure 4.3: Power spectra of the CMB anisotropies from adiabatic initial conditions with different Ω_ϕ and fixed $\Omega_b h^2 = .0245$ and $\Omega_c h^2 = .1715$ ($\Omega_m h^2 = 0.196$) as in figures 4.7 and 4.7. The background parameters are $\Omega_m = .4, h = .7$ (dashed line), $\Omega_m = .3, h = .81$ (thin line), and $\Omega_m = .5, h = .63$ (thick line). The amplitude of the peaks is the same, while they are slightly shifted because of the projection effect.

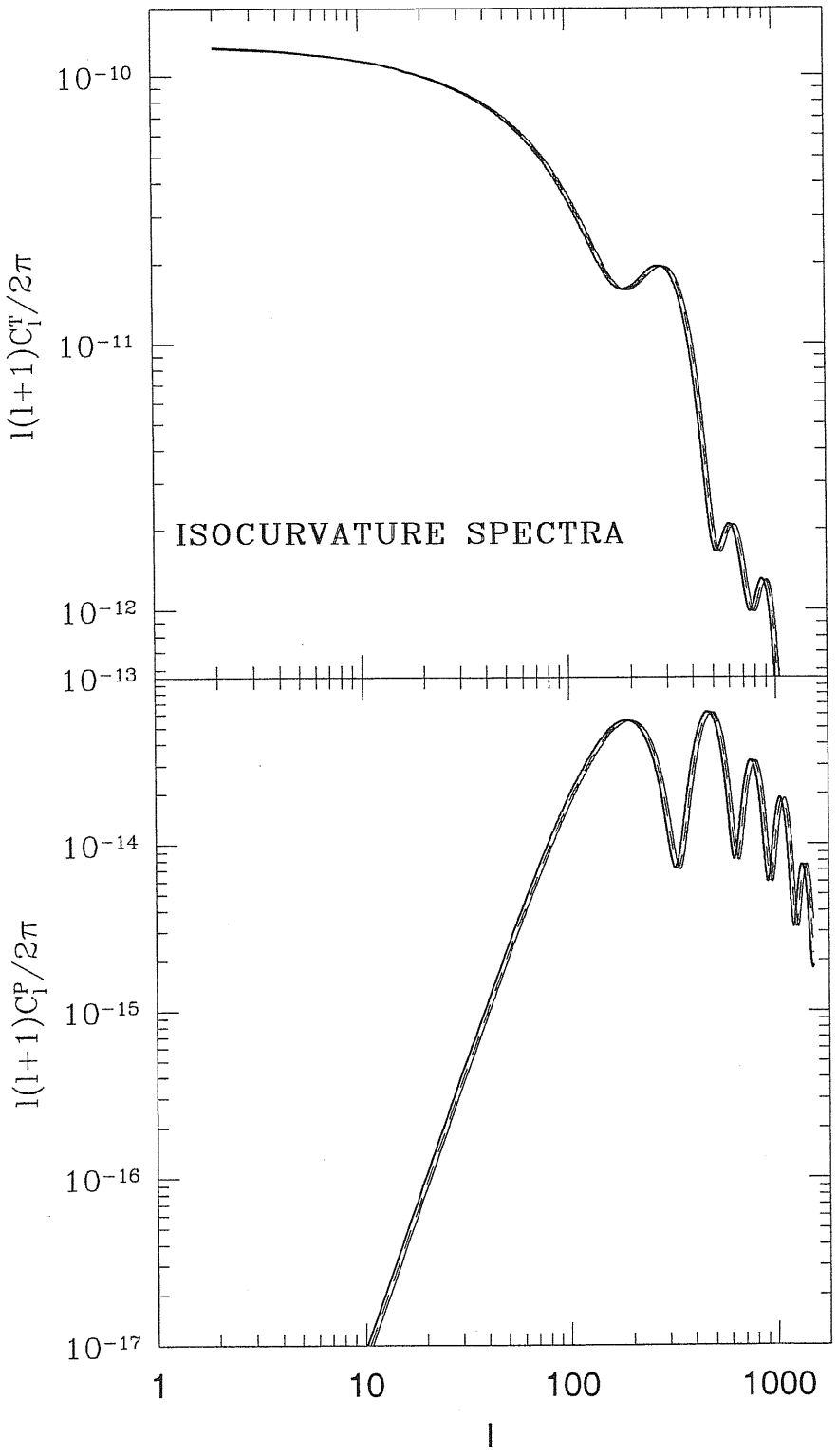

Figure 4.4: Power spectra of the CMB anisotropies from isocurvature initial conditions with different Ω_ϕ and fixed $\Omega_m h^2 = 0.196$. The spectra show the same behaviours for varying Ω_m as in figure 3.

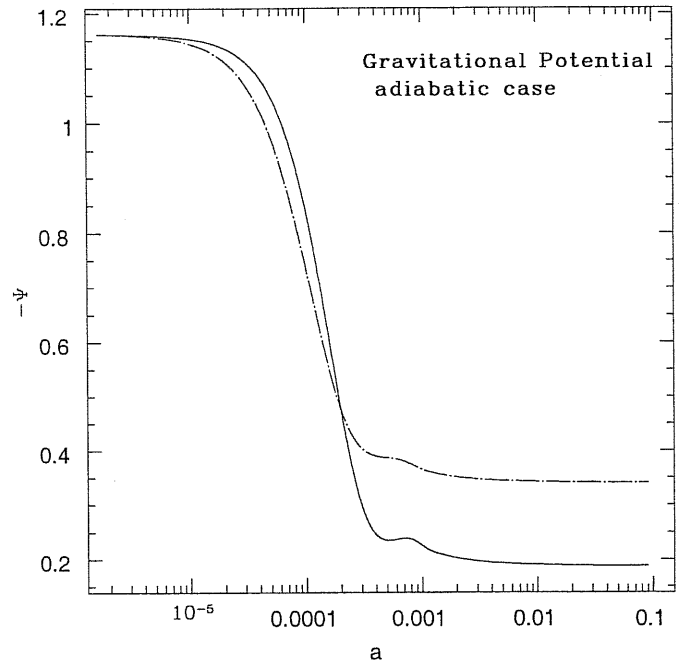

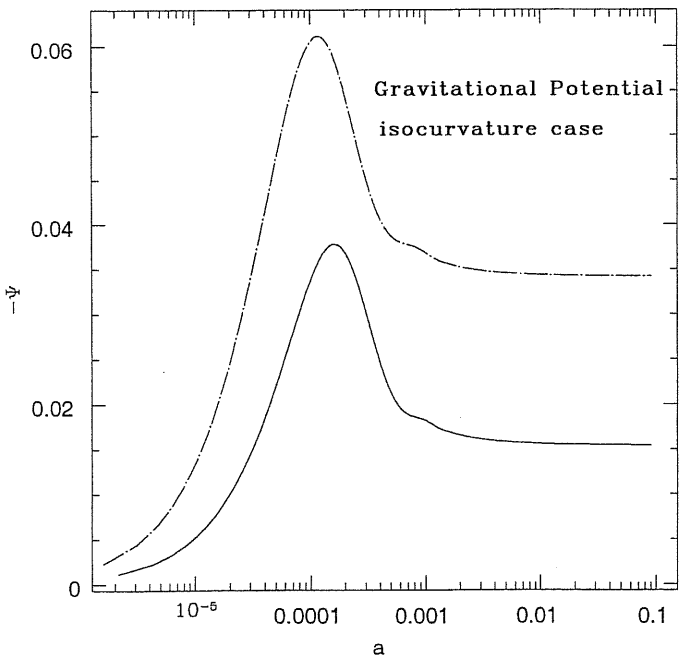

Figure 4.5: Gravitational potential (in arbitrary units) at the comoving wavenumber $k = 8 \times 10^{-2}$

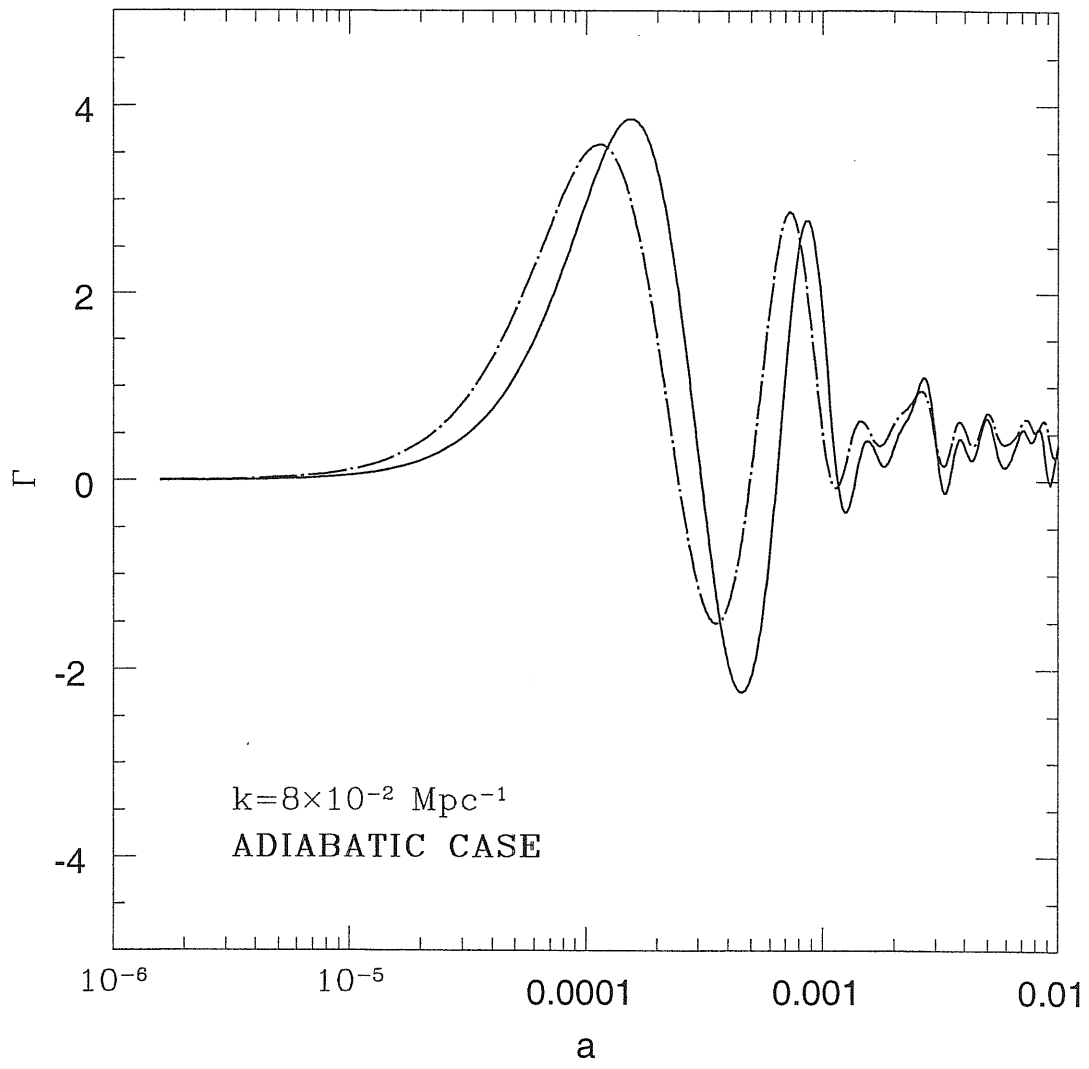

Figure 4.6: Gauge invariant entropy behaviour (in arbitrary units) as a function of the time in adiabatic models for scalar field (solid line) and pure CDM (dashed line) models. Note the shift of the horizon crossing (corresponding to the oscillations) toward late times due to the effective cosmological constant.

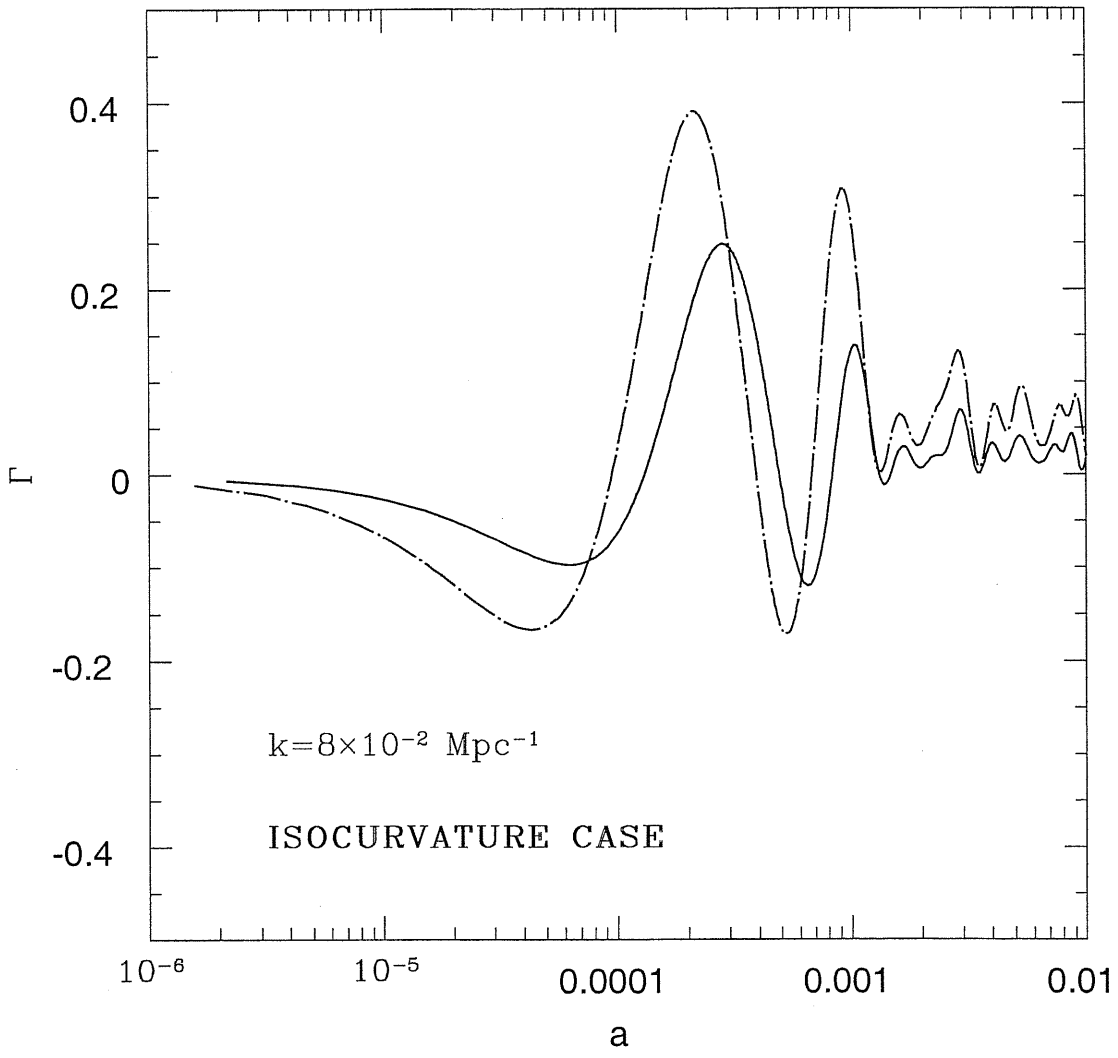

Figure 4.7: Gauge invariant entropy behaviour (in arbitrary units) as a function of the time in isocurvature models for scalar field (solid line) and pure CDM (dashed line) models. Note the decrease of the oscillation amplitudes in scalar field models, due to the lack of matter with respect to the pure CDM case.

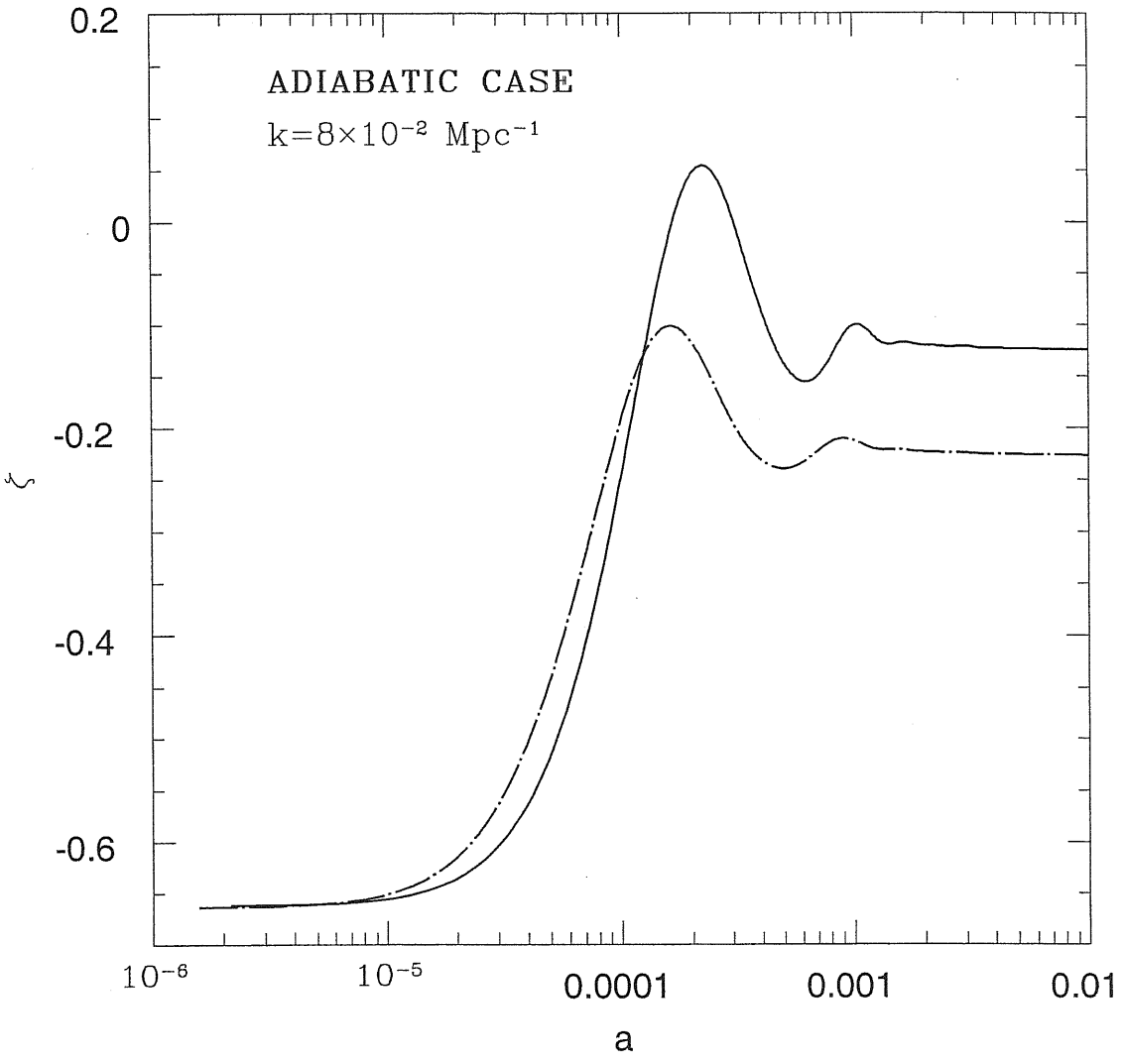

Figure 4.8: Gauge invariant curvature behaviour (in arbitrary units) as a function of the time in adiabatic models for scalar field (solid line) and pure CDM (dashed line) models. Note that the curvature is non-vanishing as $a \to 0$.

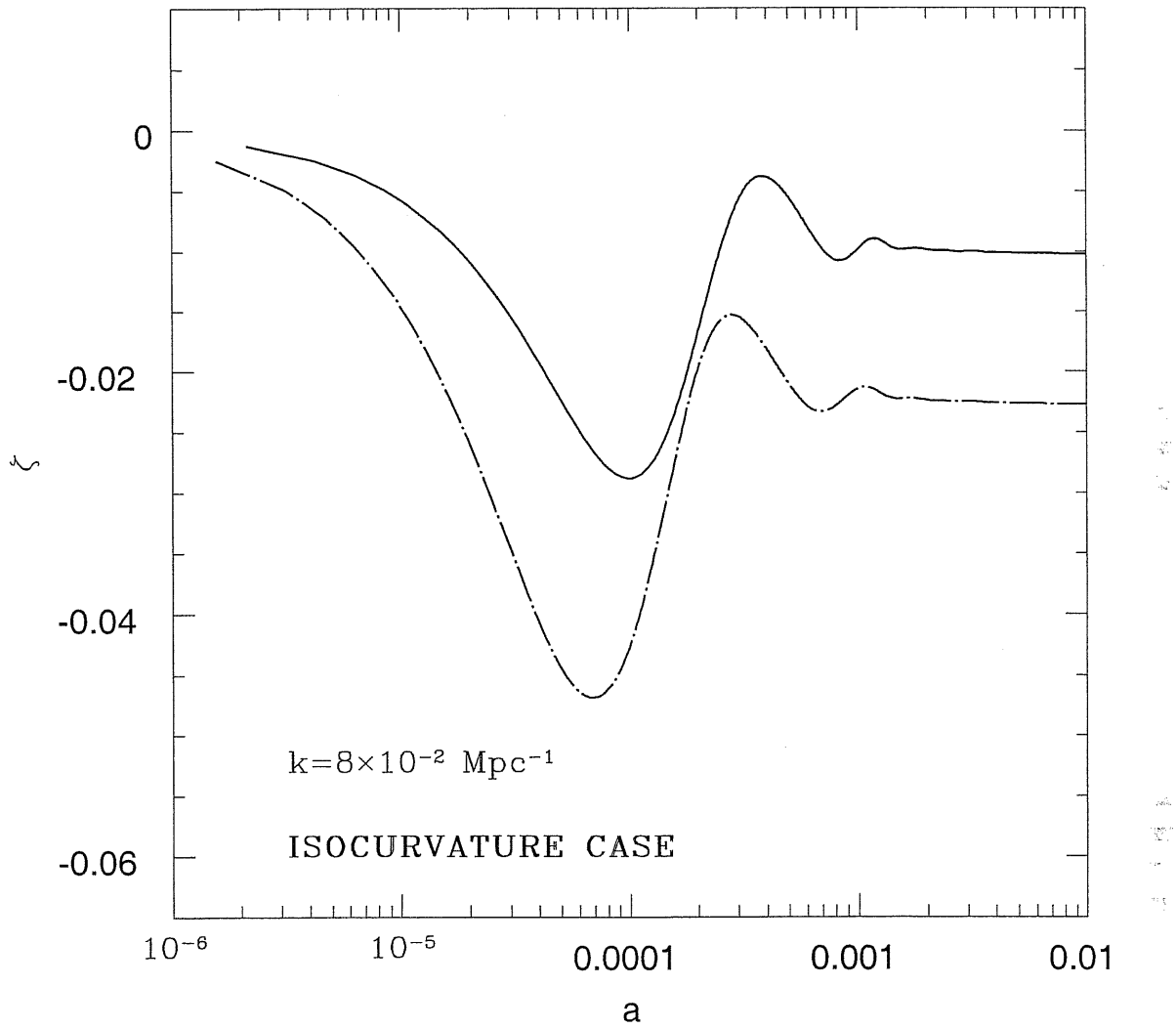

Figure 4.9: Gauge invariant curvature behaviour (in arbitrary units) as a function of the time in isocurvature models for scalar field (solid line) and pure CDM (dashed line) models. Note that the curvature is vanishing as $a \to 0$.

Chapter 5

Extended Quintessence

5.1 Introduction

In the previous chapter, a minimally coupled scalar field has been introduced as a candidate for the "missing energy" component of the universe. However, the choice of a minimally coupled field is largely arbitrary, and certainly it is not the most general possible field in which the eventual "vacuum energy" could reside. Indeed, in the context of generalized Einstein gravity theories, a coupling between the scalar field modeling the Quintessence component, and the Ricci scalar R is not to be excluded. In this chapter, we generalize Quintessence cosmologies to the large class of scalar-tensor theories of gravity; in order to do that, we assume that the Quintessence field is non-minimally coupled to the Ricci curvature scalar R.
Scalar fields coupled to gravity or matter are ubiquitous in particle-physics inspired models of unification, such as string theory. In many models, the scalar field is massive; if the Compton wavelength is of macroscopic scale, its effects are those of a "fifth force", characterized by the range λ of a Yukawa potential, $e^{-r/\lambda}/r$.
Of course, one is not completely free in choosing the coupling constants in the Lagrangian of the theory: indeed, the classical tests of gravity theories put severe constraints on the scalar field term arising in the action. By far, the strongest constraint is the Eötvös-Dicke experiment [186].
In order to be consistent with the classical test of General Relativity the theory should be cast as a metric theory with a scalar field of infinite range, or of long range compared to the scale of the solar system.

To avoid having to require a coincidental similarity between different Yukawa couplings, one must constrain to very small values any explicit coupling of the scalar field to ordinary matter [178].

The coupling between a Quintessence field and light matter has been explored in [41] and it is subject to restrictions from the constraints on the time variation of the constants of nature. Recently, the cosmological consequences of a coupling between Quintessence and matter fields have also been explored (see, e.g., [7]).
Due to the required flatness of its potential to achieve slow-rolling, the present mass-scale of the field is extremely small ($\leq H_0 \sim 10^{-33}$eV) and the force mediated by the scalar field is of long range ($> H_0^{-1}$). For this reason, a hypothetical coupling between Quintessence field and other physical entities gives rise to long-range interactions; in the case of coupling with the Ricci scalar, these long-range interactions are of gravitational nature, giving rise to time variation of the Newtonian constant, so that the coupling parameter is constrained by solar system experiments [49]. Recently, some authors [7], [220], [61], considered scalar-tensor theories of gravity in the context of Quintessence models, studying the existence and stability of cosmological scaling solutions.
Models in scalar-tensor theories of gravity involving scalar matter couplings have also been studied [19]. This chapter is based on the paper by Perrotta et al. [174], and it describes the evolution of cosmological perturbations in a subclass of these theories, where the scalar field coupled with R is proposed as the Quintessence candidate. The role of such a field on CMB anisotropies and on structure formation in the Universe is also discussed.

Following the original paper by Perrotta et al. [174], we name such models 'Extended Quintessence', in analogy with the 'extended inflation' models [137, 1, 227], proposed in the late eighties to rescue the original idea of inflation based on a first-order phase transition. In those models a Jordan-Brans-Dicke (JBD) scalar field [34] was added to the action to solve the 'graceful exit' problem of 'old inflation'. Of course, the similarity is not complete: in Extended Inflation a second scalar field - the 'Inflaton', undergoing a first-order phase transition, was the actual source of vacuum energy during inflation. Here, instead, we are supposing that our non-minimally coupled scalar field has its own potential which gives rise to a time (and space) varying cosmological constant term dominating the present-day energy density of the Universe.

The first proposal of using a non-minimally coupled scalar field to obtain a decaying cosmological constant dates back to 1983, when Dolgov [66] suggested to exploit the effective negative energy term contributed by the coupling of a massless scalar field with the Ricci scalar R to drive the overall vacuum energy density to zero asymptotically. The main problem with such a simple model is that the interesting dynamical range is achieved when the change in the effective Newton's constant strongly contradicts upper limits on solar system experiments (see [188]). Our model will differ from Dolgov's idea in that we will not assume that the non-minimal coupling term is the only cause of time variation for the effective vacuum energy contribution. This allows us to easily achieve consistency with the solar system experimental limits on the coupling constants.

In this chapter we present the background and perturbation equations in the most general form and we consider their evolution for Induced Gravity (IG) and Non-Minimally Coupled (NMC) scalar field models.

The Induced Gravity model was initially proposed by Zee in 1979 [246], as a theory for the gravitational interaction incorporating the concept of spontaneous symmetry breaking; it was based on the observation in gauge theories that dimensional coupling constants arising in a low-energy effective theory can be expressed in terms of vacuum expectation values of scalar fields. This model was subsequently incorporated in models of inflation with a slow-rolling scalar field [204]; in a modified form it was the key ingredient of the Extended Inflation [137],[1],[227] class of models. More recently, it has also been adopted in open inflation models [88]. In [246], a scalar field coupled to gravity by a term proportional to $R\phi^2$ in the Lagrangian, is anchored by a symmetry-breaking potential to a fixed value which eliminates the potential energy in the present broken-symmetric phase of the world. We propose here a different role for this scalar field, in the sense that we keep the same coupling with the Ricci scalar as [246], but we allow for a larger class of potentials than the Coleman-Weinberg one, also including potentials that do not possess a minimum and can therefore contribute to the present Quintessence energy density.

The second class of theories to which we apply our treatment is that of non-minimal coupling of a scalar field to the Ricci curvature, described extensively in curved space quantum field theory textbooks (e.g. [22]).

The work is organized as follows: in Sec. II we present the relevant equations, defining the dynamical system for the background as well as for the perturbations in non-minimally coupled scalar field cosmologies; Sec. III is devoted to the definition of the IG and NMC models and to the analysis of the background evolution; Sec. IV contains and discusses the results of the numerical integration. Finally, Sec. V contains a brief summary of the results and some concluding remarks.

5.2 Cosmological equations in scalar-tensor theories of gravity

Our purpose is to describe a class of scalar-tensor theories of gravity represented by the action

$$S = \int d^4x \frac{\sqrt{-g}}{\beta} \left[\frac{1}{2} f(\phi, R) - \frac{1}{2}\omega(\phi)\phi^{;\mu}\phi_{;\mu} - V(\phi) + \beta L_{fluid} \right] , \tag{5.1}$$

where R is the Ricci scalar, β is a constant needed to fix units and L_{fluid} is a classical multicomponent-fluid Lagrangian including also minimally coupled scalar fields, if any. We disregard any possible

coupling of our scalar field with ordinary matter, radiation and dark matter [57].

As in the previous chapter, we restrict ourselves to a flat FRW background; we are still using units where $c \equiv 1$, but the convention concerning $8\pi G$ will be stated later, since it will depend on the choice of a specific theory included in this general description. Instead, following [117], we will choose the relation $G_{\mu\nu} = T_{\mu\nu}$ to identify $T_{\mu\nu}$. Greek indices will be used for space-time coordinates, latin ones will label spatial ones. We use the signature $(-,+,+,+)$. By defining $F \equiv \partial f/\partial R$, the gravitational field equations derived by the action (5.1) are

$$G_{\mu\nu} = T_{\mu\nu} \equiv \frac{1}{F}\left[\beta T^{fluid}_{\mu\nu} + \omega\left(\phi_{,\mu}\phi_{,\nu} - \frac{1}{2}g_{\mu\nu}\phi_{,\sigma}\phi^{;\sigma}\right) + g_{\mu\nu}\frac{f - RF - 2V}{2} + F_{,\mu;\nu} - g_{\mu\nu}F^{;\sigma}_{;\sigma}\right] \quad (5.2)$$

Here $G_{\mu\nu}$ is the Einstein tensor, and all the other contributions have been absorbed in $T_{\mu\nu}$; as noted in refs. [116],[117], if one writes the gravitational field equation in this form, then $T_{\mu\nu}$ can be treated as an effective stress-energy tensor, which allows us to use the standard Einstein equations by simply replacing the fluid quantities with the effective ones. In particular, this is also true for the perturbed Einstein equations, here treated in the formalism of the synchronous gauge.
The background effective quantities following from the definition of $T_{\mu\nu}$ are

$$\rho = \frac{1}{F}\left(\beta\rho_{fluid} + \frac{\omega}{2a^2}\dot{\phi}^2 + \frac{RF - f}{2} + V - \frac{3\mathcal{H}\dot{F}}{a^2}\right); \quad (5.3)$$

$$p = \frac{1}{F}\left(\beta p_{fluid} + \frac{\omega}{2a^2}\dot{\phi}^2 - \frac{RF - f}{2} - V + \frac{\ddot{F}}{a^2} + \frac{\mathcal{H}\dot{F}}{a^2}\right), \quad (5.4)$$

where the overdot denotes differentiation with respect to the conformal time τ and $\mathcal{H} = \dot{a}/a$.

The background FRW equations read

$$\mathcal{H}^2 = \frac{1}{3F}\left(a^2\beta\rho_{fluid} + \frac{\omega}{2}\dot{\phi}^2 + \frac{a^2}{2}(RF - f) + a^2V - 3\mathcal{H}\dot{F}\right), \quad (5.5)$$

$$\dot{\mathcal{H}} = \mathcal{H}^2 - \frac{1}{2F}\left(a^2\beta(\rho_{fluid} + p_{fluid}) + \omega\dot{\phi}^2 + \ddot{F} - 2\mathcal{H}\dot{F}\right) \quad (5.6)$$

while the Klein-Gordon equation reads

$$\ddot{\phi} + 2\mathcal{H}\dot{\phi} = -\frac{1}{2\omega}\left(\omega_{,\phi}\dot{\phi}^2 - a^2 f_{,\phi} + 2a^2V_{,\phi}\right). \quad (5.7)$$

Furthermore, the continuity equations for the individual fluid components are not directly affected by the changes in the gravitational field equation, and for the $i-$th component

$$\dot{\rho}_i = -3\mathcal{H}(\rho_i + p_i). \quad (5.8)$$

In this background, the trace of (5.2) becomes

$$-R = \frac{1}{F}\left[\beta T_{fluid} + \omega\frac{\dot{\phi}^2}{a^2} + 2(f - RF - 2V) + 3\left(\frac{\ddot{F}}{a^2} + 2\frac{\mathcal{H}\dot{F}}{a^2}\right)\right], \quad (5.9)$$

recalling that $T_{fluid} = -\rho_{fluid} + 3p_{fluid}$. Note that R also appears in the right hand side of the equation, unless f is of the form $f(\phi, R) = F(\phi)R$. Let us express Ricci scalar in terms of the conformal expansion rate:

$$R = \frac{6}{a^2}(\dot{\mathcal{H}}^2 + \mathcal{H}^2). \quad (5.10)$$

Now, let us consider the perturbations to this background; as in chapter 4, we adopt the formalism of synchronous gauge.
In terms of the effective fluid, the perturbed quantities can be written as [174]:

$$\delta\rho = \frac{1}{F}\left[\beta\delta\rho_{fluid} + \omega\frac{\dot{\phi}\delta\dot{\phi}}{a^2} + \frac{1}{2}\left(\frac{\dot{\phi}^2\omega_{,\phi}}{a^2} - f_{,\phi} + 2V_{,\phi}\right)\delta\phi - 3\frac{\mathcal{H}\delta\dot{F}}{a^2} - \left(\frac{\rho + 3p}{2} + \frac{k^2}{a^2}\right)\delta F + \frac{\dot{F}\dot{h}}{6a^2}\right] \quad (5.11)$$

$$\delta p = \frac{1}{F}\left[\beta\delta p_{fluid} + \omega\frac{\dot\phi\dot{\delta\phi}}{a^2} + \frac{1}{2}(\frac{\dot\phi^2\omega_{,\phi}}{a^2} + f_{,\phi} - 2V_{,\phi})\delta\phi + \frac{\delta\ddot F}{a^2} + \frac{\mathcal{H}\delta\dot F}{a^2} + \left(\frac{p-\rho}{2} + \frac{2k^2}{3a^2}\right)\delta F - \frac{1}{9}\frac{\dot F\dot h}{a^2}\right] \tag{5.12}$$

$$(p+\rho)\theta = \frac{\beta(p_{fluid}+\rho_{fluid})\theta_{fluid}}{F} - \frac{k^2}{a^2}\left(\frac{-\omega\dot\phi\delta\phi - \delta\dot F + \mathcal{H}\delta F}{F}\right) \tag{5.13}$$

$$(p+\rho)\sigma = \frac{\beta(p_{fluid}+\rho_{fluid})\sigma_{fluid}}{F} + \frac{2k^2}{3a^2F}\left(\delta F + 3\frac{\dot F}{k^2}(\dot\eta + \frac{\dot h}{6})\right) . \tag{5.14}$$

The perturbed Klein-Gordon equation reads

$$\delta\ddot\phi + \left(3\mathcal{H} + \frac{\omega_{,\phi}}{\omega}\dot\phi\right)\delta\dot\phi + \left[k^2 + \left(\frac{\omega_{,\phi}}{\omega}\right)_{,\phi}\frac{\dot\phi^2}{2} + a^2\left(\frac{-f_{,\phi}+2V_{,\phi}}{2\omega}\right)_{,\phi}\right]\delta\phi = \frac{\dot\phi\dot h}{6} + \frac{a^2}{2\omega}f_{,\phi R}\delta R . \tag{5.15}$$

Note the presence of the Ricci curvature scalar R in the $f_{,\phi}$ term in the left hand side, as well as its perturbation δR in the right hand one.

All these ingredients have to be implemented in the perturbed Einstein equations 2.106-2.109, that can be integrated once initial conditions on the metric and fluid perturbations are given; we adopt here adiabatic initial conditions for the various components, as described in chapter 4, and we perform the numerical integration of the system above for two specific classes of scalar-tensor theories, that will be defined in the next section.

5.3 Induced gravity and non-minimally coupled scalar field models

We will consider two main classes of non-minimally coupled scalar field theories; both can be obtained by setting

$$f(\phi, R) = F(\phi)R \ , \ \ \omega(\phi) = 1 \ , \tag{5.16}$$

so that many of the formulas in the previous section simplify; also we take $\beta = 1$ requiring that F has the correct physical dimensions of $1/G$. Note that all this fixes the link between the value of F today and the Newtonian gravitational constant G:

$$F_0 = F(\phi_0) = \frac{1}{8\pi G} . \tag{5.17}$$

Also, this allows to define a time variation of the gravitational constant in non-minimally coupled theories,

$$\frac{G_t}{G} = -\frac{F_t}{F} , \tag{5.18}$$

(where the subscript t indicates differentiation w.r.t. the cosmic time t) that is bounded by local laboratory and solar system experiments [93] to be

$$\frac{G_t}{G} \leq 10^{-11} \text{ per year} . \tag{5.19}$$

There is another independent experimental constraint coming from the effects induced on photons trajectories [238]. As well known, by making the transformation $\phi \to \Phi_{JBD}$ such that

$$\frac{1}{2}F(\phi)R - \frac{1}{2}\phi^{;\mu}\phi_{;\mu} \to \Phi_{JBD}R + \frac{\omega_{JBD}}{\Phi_{JBD}}\Phi^{;\mu}_{JBD}\Phi_{JBD;\mu} , \tag{5.20}$$

the condition $\omega_{JBD} \geq 500$ has to be imposed at the present time. It is easy to see that in our case this takes the form

$$\omega_{JBD} = \frac{F_0}{F_{\phi 0}^2} \geq 500 , \tag{5.21}$$

where $F_{\phi 0}$ is the derivative of F w.r.t. ϕ calculated at the present time. As we shall see, this constraint turns out to be the dominant one for our models.

Now let us proceed to the definition of the IG and NMC models.

In Induced Gravity (IG) models the gravitational constant is directly linked to the scalar field itself, as originally proposed in the context of the Brans-Dicke theory. We treat here this case by setting

$$F(\phi) = \xi\phi^2 \ , \tag{5.22}$$

where ξ is the IG coupling constant. In this case equations (5.17,5.19,5.21) become respectively

$$\phi_0 = \frac{1}{\sqrt{\xi 8\pi G}} \ , \tag{5.23}$$

$$\frac{\phi_{t0}}{\phi_0} \leq 10^{-11} \text{ per year} \ , \ \xi \leq \frac{1}{2000} \ . \tag{5.24}$$

The minimally coupled case is recovered from IG models in the limit $\xi \to 0$; because of equation (5.24) this implies $\phi_0 \to \infty$, and it can be quite easily verified that these conditions reduce all the equations written in the previous case to ordinary general relativity.

In non-minimally coupled (NMC) scalar field models the term multiplying the curvature scalar R is made of two contributions: the dominant one, which is a constant, plus a term depending on ϕ; bearing in mind the constraint on F at the present time, from equation (5.17), this can be written in the most general way as

$$F(\phi) \equiv \frac{1}{8\pi G} + \widetilde{F}(\phi) - \widetilde{F}(\phi_0) \ . \tag{5.25}$$

Then, we choose $\widetilde{F}$ in equation (5.25) as

$$\widetilde{F}(\phi) = \xi\phi^2 \ , \tag{5.26}$$

where again ξ is a coupling constant [1] and the constraints (5.19,5.21) become

$$16\pi G\xi\phi_0\phi_{t0} \leq 10^{-11} \text{ per year} \ , \ 32\pi G\xi^2\phi_0^2 \leq \frac{1}{500} \ . \tag{5.27}$$

Contrary to the IG case, we are now free to set ϕ_0, and the ordinary GR case is recovered by taking $\xi \to 0$. Having no restrictions about this point, in our numerical integrations we fixed $\phi_0 = M_P \equiv G^{-1/2}$, the Planck mass (in natural units). We will only consider here for definiteness the case $\xi > 0$. The most general case, regarding the background evolution only, is discussed in [49].

Let us just mention here that one can always map this kind of scalar-tensor theories of gravity to canonical general relativity, by means of a conformal (Weyl) transformation, leading to the so-called Einstein frame (see, e.g. the recent review in [81]), where the gravity sector of the action takes the standard Einstein-Hilbert form. In the latter frame, the Quintessence field would be minimally coupled with gravity, but it would show explicit couplings with all the matter components. This mathematical technique is particularly useful if one is looking for scaling solutions [7]. We will not adopt this procedure here, but we will make all our calculations in the present physical frame, also called 'Jordan frame'.

Let us now elevate ϕ to the role of Quintessence. This requires giving it a non-zero potential $V(\phi)$. As mentioned in the previous chapter, several potentials have been proposed for the Quintessence. In [51], the authors analyzed a cosine potential motivated by an ultra-light pseudo Nambu-Goldstone boson, while in other works, trying to build a phenomenological link to supersymmetry breaking models, inverse power potentials have been considered [206], [249],[142],[75]. As pointed out in [21], inverse power potentials appear in supersymmetric QCD theories [208], [152]. Here we take the simplest potential of the second class,

$$V(\phi) = \frac{M^5}{\phi} \ , \tag{5.28}$$

[1] Note that we define here the coupling constant ξ with the opposite sign w.r.t. the standard notation for NMC models.

where the mass-scale M is fixed by the level of energy contribution today from the Quintessence.

We are now ready to make some preliminary investigation of the background model. We require that the present value of Ω_ϕ is 0.6, with Cold Dark Matter at $\Omega_{CDM} = 0.35$, three families of massless neutrinos, baryon content $\Omega_b = 0.05$ and Hubble constant $H_0 = 50$ Km/sec/Mpc; the initial kinetic energy of ϕ is not important since it is redshifted away during the evolution, so we can fix an equal amount of kinetic and potential energy at the initial time. Note that the physical meaning of our starting time is not that of the Big Bang. The validity of our discussions doesn' t applies to the initial singularity; rather, we make the scenario begin at a time deep in the radiation era, and after the end of the inflationary epoch, when each scale of cosmological interest was well beyond the horizon.

Let us introduce the next Section by fixing the compatibility of our models with the experimental constraints (5.19,5.21). A first version of these results, valid only for NMC models, can be found in [49].

First, we integrate equations (5.5,5.7) to compare with the experimental constraint of Eq.(5.19). The results are shown in Fig.5.1, where $|G_t/G|$ at the present time is shown as a function of ξ. Both for NMC and IG, the limit roughly is

$$\xi \leq 3 \times 10^{-2} \ . \tag{5.29}$$

However, as we anticipated, the stronger constraint comes from Eq.(5.21); it is simple to see that in our models Eqs.(5.24,5.27) become

$$\xi \leq 5 \times 10^{-4} \ \text{ IG case} \ , \tag{5.30}$$

$$\xi \leq 5 \times 10^{-3} (\sqrt{G}\phi_0)^{-1} \ \text{ NMC case} \ . \tag{5.31}$$

In the next section we will explore the effects on the cosmological perturbations spectra of EQ models, also considering values of ξ beyond the above constraints, in order to better illustrate its effect on the cosmological equations. Then, we will discuss how future CMB experiments like MAP and Planck will be able to detect features of the present models within the range allowed from Eqs.(5.30,5.31).

5.4 QR-effects on cosmological perturbations

Here we present the results coming from the integration of the complete set of equations of Sec. II. The numerical integration of this set of equations has not been performed before, and we obtain several new and interesting effects concerning cosmologies with a coupling between Quintessence and the Ricci curvature scalar R, that we name 'QR-effects'; we discuss them in the following subsections.

Let us now set initial conditions for the perturbation equations, referring to [173] for an extensive treatment. We adopt isoenthropic (i.e. adiabatic) initial conditions; in the minimal coupling case they are quite simple: everything is initially zero except for the metric perturbation η. It is easy to check that these conditions remain valid also in the present case. In fact, adiabaticity is imposed on each fluid separately, by requiring that the entropy perturbations is equal to zero initially for each pair of fluid components, including Quintessence [173]; these conditions do not depend on the coupling of a given component with R.

As we anticipated, the scalar-tensor theories of gravity that we consider leave several characteristic imprints on cosmological perturbations spectra. Also, both IG and NMC models, although for different coupling constant ranges, show a remarkably similar behavior. For clearness, we shall treat first the features related to the background evolution and successively the genuine QR-effects on perturbations.

5.4.1 QR-effects on the background: enhanced Hubble length growth and $\Omega_{\text{matter}} > 1$

Let us consider the Hubble length first. The integration of Eqs.(5.5,5.6) with the potential (5.28) shows that the time derivative of the Hubble length, $H_t^{-1}(z)$, *increases* at non-zero redshifts compared with the ordinary Quintessence case, both for NMC and IG models. Therefore, fixing the Hubble length

at present as we do implies that in the past it was smaller than in minimally coupled models. This effect is clearly displayed by Fig.5.2, where the comoving Hubble length as a function of z is shown (for simplicity we plot the IG case only, the NMC one being completely equivalent). This feature has been already noted in the context of pure Brans-Dicke theories [141]. The sharp change in the time dependence of H^{-1} at small redshifts is due to the Q-field, that dominates the cosmological evolution at later times.

The source of the enhanced Hubble length growth in our models is the last term in the Einstein equation (5.6); as we will show in a moment, this term is quite large and positive, being also responsible for most of the features that we shall see later concerning the cosmological perturbation spectra.

A related interesting point is that our model predicts a small change in H which mimics a change in the number of massless neutrinos at the Nucleosynthesis epoch (see [190] for an extensive overview). At this time Quintessence is very subdominant and the cosmological evolution is governed by the equation

$$H^2 \simeq \frac{\rho_{fluid}}{3F(\phi)} \; ; \tag{5.32}$$

since in our models $F(\phi) < F(\phi_0)$ at any past time, the shift in the value of H^2 due the time variation of the gravitational constant in EQ models is given by:

$$\frac{\Delta H^2}{H^2} = 1 - \frac{F(\phi)}{F(\phi_0)} \; . \tag{5.33}$$

As a function the shift ΔN of the number of relativistic species at Nucleosynthesis, the above quantity may be written as

$$1 - \frac{F(\phi)}{F(\phi_0)} = \frac{7\Delta N/4}{10.75 + 7\Delta N/4} \; . \tag{5.34}$$

Therefore, the shift ΔN^{QR} predicted in our models is

$$\Delta N^{QR} = -6.14 \times \frac{F(\phi_0) - F(\phi)}{F(\phi_0) - 2F(\phi)} \; . \tag{5.35}$$

It is worthwhile to note that for models satisfying Eq.(5.21), the predicted ΔN^{QR} is at the level of 10%, thus being well below the current experimental constraints from Nucleosynthesis.

Let us consider now the effects of our scenario on the cosmological equation of state. The $\mathcal{H}\dot{F}/F$ term appears also in the effective fluid pressure in Eq.(5.3), causing the following interesting feature in the behavior of the equation of state, shown in Fig.5.3. As it is evident, in the matter dominated era $p/\rho > 0$ up to $1 + z \approx 5$, when the Quintessence starts to dominate. Thereafter, the cosmic expansion starts to accelerate because of the vacuum energy stored in the Quintessence potential. Thus we have the apparent paradox that in the matter dominated era the total pressure is non-zero and positive: this is not surprising since it can be brought back to the dynamics of the scalar field itself in scalar-tensor theories of gravity. Corresponding to its positive value in the matter dominated era, the equation of state at present, when Quintessence dominates, is slightly above its value for Q models. In other words, we found that the Quintessence contribution to the equation of state in our models, p_ϕ/ρ_ϕ, does not change significantly in our case with respect to Q models; we found indeed

$$-1 \leq \frac{p_\phi}{\rho_\phi} \leq -0.9 \tag{5.36}$$

for all the cases considered. This is well within the range of values for which the Quintessence is mimicking a cosmological constant [69], [89].

Let us now come to the $\Omega_{matter} > 1$ effect. This interesting and very peculiar occurrence can be understood by looking at the behavior of the various components of the energy density in Eq.(5.5) and is obviously connected with the effect on the equation of state just described. After dividing both members by $\mathcal{H}^2$, the Friedmann equation takes the form

$$1 = \Omega_{matter}(z) + \Omega_{radiation}(z) + \Omega_\phi(z) \; , \tag{5.37}$$

where it must be noted that Ω_ϕ is actually made of three terms, namely

$$\Omega(z)_\phi = \Omega(z)_\phi^K + \Omega(z)_\phi^P + \Omega(z)_\phi^{QR} . \tag{5.38}$$

While Ω_ϕ^K and Ω_ϕ^P are the generalization of the kinetic and potential energy densities in scalar-tensor theories, the really new component is

$$\Omega_\phi^{QR} = -\frac{F_\phi \dot{\phi}}{F\mathcal{H}} , \tag{5.39}$$

which, as we already noted, is *negative* if $\dot{\phi} > 0$. Its amplitude is fixed essentially by the dynamics of the scalar field; as we anticipated, this term turns out to be important for the background evolution. The reason is the following. In all the cases considered, the scalar field evolution is slow, so that $\ddot{\phi}$ and the time variation of the potential in the Klein-Gordon equation can be neglected. Let us consider the radiation dominated era for simplicity: $a = \dot{a}_{rad}\tau$, where $\dot{a}_{rad}$ is a constant. Therefore, it is immediate to check that the approximate solution of the Klein Gordon equation is

$$\phi = \phi_{initial} - \frac{\dot{a}_{rad}^2 V_\phi}{20}(\tau^4 - \tau_{initial}^4) . \tag{5.40}$$

In the ideal case where the scalar field evolves for a large time so that only the term proportional to τ^4 is important, we see that $\dot{\phi}/\phi \propto 1/\tau \propto \mathcal{H}$; in this case the term in Eq.(5.39) would be of order unity. In the real case these arguments are weakened since the scalar field does not have a perfect slow-rolling dynamics, and it does not evolve enough to become much larger than its initial value; nevertheless this qualitatively explains why we found $\Omega_\phi^{QR} \sim 10^{-2}$ for models satisfying the constraints (5.21), and for a time interval covering almost all the post-equality cosmological history.

Fig.5.4 shows the various contributions to the cosmic density parameters as a function of redshift. The matter radiation equality epoch is clearly visible, as well as the matter dominated era, and, finally, the Quintessence dominated era at very small redshifts. Also, the sum (identically equal to 1) is shown, and it is immediately seen that in the matter dominated era one has

$$\Omega_{matter} > 1 . \tag{5.41}$$

As we already anticipated this is only an apparent paradox, because of the presence of the *negative* energy component in the Einstein equation (5.5), explicit in Eq.(5.39). Figure 5.5 shows the various contributions to the Quintessence energy density. As it can be seen, for the chosen value of the coupling constant ξ, Ω_ϕ^{QR} reaches values of a few percent and is responsible for the condition (5.41).

This completes a rapid survey of the features regarding the cosmological background evolution. Some of them have a relevant influence on the perturbation behavior, which is the subject of the next subsection.

5.4.2 QR-effects on the CMB: Integrated Sachs-Wolfe effect, horizon crossing delay and reduced acoustic peaks

The phenomenology of CMB anisotropies in EQ models is rich and possesses distinctive features.

In the top left panel of Fig.5.6, the effect of increasing ξ on the power spectrum of COBE-normalized CMB anisotropies is shown. Note that we plotted cases also exceeding the limit (5.21), to make clearer the perturbation behavior in EQ scenarios. The rise of ξ makes substantially three effects: the low ℓ's region is enhanced, the oscillating one attenuated, and the location of the peaks shifted to higher multipoles. Let us now explain these effects. The first one is due to the integrated Sachs-Wolfe effect, arising from the change from matter to Quintessence dominated era occurred at low redshifts. This occurs also in ordinary Q models, but in EQ this effect is enhanced. Indeed, in ordinary Q models the dynamics of ϕ is governed by its potential; in the present model, one more independent dynamical source is the coupling between the Q-field and the Ricci curvature R. As can be easily understood from the Lagrangian in equation (5.1), the scalar field ϕ evolves as dictated by the effective potential

$$V_{eff}(\phi) = V(\phi) - \frac{1}{2}F(\phi)R . \tag{5.42}$$

As is clear from equation (5.10), R is positive in the matter dominated era, ($a(t) \sim t^{2/3}$). Thus, from (5.42), after differentiating with respect to ϕ, both the forces coming from V_{eff} are *negative*, pushing together the field ϕ towards increasing values. In conclusion, the dynamics of ϕ is boosted by R together with its potential V. As a consequence, part of the COBE normalization at $\ell = 10$ is due to the Integrated Sachs-Wolfe effect; thus the actual amplitude of the underlying scale-invariant perturbation spectrum gets reduced. This is the main reason why the oscillating part of the spectrum, both for polarization and temperature, is below the corresponding one in Q-models.

There is however another effect that slightly reduces the amplitude of the acoustic oscillations. We have seen in Fig.5.2 that the Hubble length was smaller in the past in EQ than in Q models. This has the immediate consequence that the horizon crossing of a given cosmological scale is delayed. This is manifest in Fig.5.7, where we have plotted the photon density perturbation in the Newtonian gauge δ_γ^N; we choose this quantity since it is simply 4 times the dominant term of the CMB temperature fluctuations [108]. Its expression in terms of the quantities in the synchronous gauge is

$$\delta_\gamma^N = \delta_\gamma + \frac{\dot{h} + 6\dot{\eta}}{2k^2}\frac{\dot{\rho}}{\rho} . \tag{5.43}$$

The scale shown in Fig.5.7 is chosen so that it reenters the horizon between matter-radiation equality and decoupling. Both in the IG and NMC cases, it is evident that the oscillations start later than in ordinary Q models. As well known, the amplitude of the acoustic oscillations slightly decreases if the matter content of the universe at decoupling is increased [173, 51].

Finally, note how the location of the acoustic peaks, in terms of the multipole ℓ at which the oscillation occurs, is shifted to the right. Again, the reason is the time dependence of the Hubble length, which at decoupling, subtended a smaller angle on the sky. It is straightforward to check that the ratio of the peak multipoles in Fig.5.6 coincides numerically with the the ratio of the values of the Hubble lengths at decoupling in Fig.5.2 in EQ and Q models.
An interesting comparison could be done with the results of Chen and Kamionkowski [47], where the CMB temperature and polarization patterns produced by a pure JBD field in a standard Cold Dark Matter cosmology are proved to give rise to a similar dependence of the acoustic peak locations on the $\omega_{JBD} \propto 1/\xi$ parameter.
These considerations remains identical for NMC models: in a large range of values of ξ, IG and NMC models show remarkably similar features, yielding a genuine signature of scalar tensor-theories in the cosmological perturbations spectra.

Fig. (5.6) summarize the most important results of this chapter, concerning the features that appear in the CMB anisotropies and in the matter power spectrum in IG scenarios.
For a more detailed analysis of the power spectra consistent with the existing observational restrictions on ξ, we refer to the next chapter, where we will consider particular attractive solutions of the background dynamics called *tracking solutions*.

5.4.3 QR-effects on matter perturbations: power-spectrum decrease and peak shift

After decoupling, the different models considered in Fig.5.6 evolve until the present, when we snapshot the matter power-spectrum in the bottom left panel.

Soon after their introduction, Q-models were considered more appealing than those involving a cosmological constant term because of their capability to shift the power-spectrum toward larger scales without increasing its overall amplitude, which would have required an antibias mechanism. We find here that this effect is enhanced if a QR-coupling exists. This is evident in both the bottom right panel in Fig.5.6. The spectra are COBE-normalized as it is evident in the top panel. For increasing ξ, the spectra lose power. The reason for this behavior is that the CMB spectra include different effects together with the true perturbation amplitude; on the large scales measured by COBE, the matter perturbations add with the large Integrated Sachs-Wolfe effect; the greater is ξ, the stronger the Integrated Sachs-Wolfe effect, the weaker the true perturbation amplitude, as we pointed out in the previous subsection. This causes the power-spectrum decrease that is readily visible in the figure.

The other effect is the slight shift of the location of the peaks toward larger wavenumbers. Again, this is due to the time dependence of H^{-1}; since it is smaller in extended Quintessence models than in ordinary Quintessence ones, the horizon crossing is delayed for all the cosmological scales, for the given value of H_0.

These are the most prominent features concerning the power-spectrum. In principle however, there are terms in the cosmological perturbation equations that could make some relevant effects. We seek them as terms that do not multiply fluctuations in the scalar field, since the latter are negligible from the point of view of structure formation [173]. Looking indeed at Eq.(5.14), the last term in the r.h.s. could play some role: it is the shear perturbation associated with the Quintessence and it should be noted that it is not present in ordinary Q models. Looking at Eq.(2.109), it is immediate to verify that this term produces a sort of excess friction in the dynamics of the quantity $\dot{h}+6\dot{\eta}$ in addition to the cosmological Hubble drag term $2\mathcal{H}$ in the l.h.s.: we define it as

$$\mathcal{F}=\frac{\dot{F}}{F}\ . \tag{5.44}$$

Its relevance compared to $\mathcal{H}$ has been already discussed when we dealt with the Ω_ϕ^{QR} quantity of Eq.(5.39). As it is evident in Fig.5.8, $\mathcal{F}$ is not so important during the evolution since it is only a few percent of the Hubble drag during all the evolution. Although $\mathcal{F}$ clearly plays the role of a sort of integrated shear effect, it is less important than those described at the beginning of this subsection.

These effects change the matter power-spectrum today in a way that we will better explore in a future work. Here we make a first comparison with the known expectations concerning the spectrum normalization at $8h^{-1}$ Mpc, σ_8. Recently the cluster abundance in Q models has been analyzed [225]. An empirical formula for σ_8 in these models has been found as

$$\sigma_8=(0.5-0.1\Theta)\Omega_m^{-\gamma(\Omega_m,\Theta)}\ , \tag{5.45}$$

where

$$\Theta=(n-1)+(h-0.65)\ \ ,\ \ \gamma(\Omega_m,\Theta)=0.21-0.22\frac{p_\phi}{\rho_\phi}+0.33\Omega_m+0.25\Theta\ ; \tag{5.46}$$

n is the spectral index (1 in our scale-invariant case), h is the present Hubble constant in units of $100\mathrm{km\,s^{-1}\,Mpc^{-1}}$ and Ω_m the matter energy amount today. The existing experimental constraints (see [225]) may be expressed as follows:

$$\sigma_8\Omega_m^\gamma=0.5\pm0.1\ . \tag{5.47}$$

Our scenario is not significantly constrained by Eq.(5.47). For the models shown in Fig.5.6, we found

$$\sigma_8 = 0.525 \ \text{ for } \xi=2\times10^{-2}$$
$$\sigma_8 = 0.623 \ \text{ for } \xi=10^{-2} \tag{5.48}$$
$$\sigma_8 = 0.725 \ \text{ for ordinary Q models.} \tag{5.49}$$

It is easy to verify that the constraint in Eq.(5.47) is satisfied for $\xi\leq10^{-2}$; the same limit for NMC models is $\xi\leq2\times10^{-2}$. It is remarkable however that future experiments will be able to provide much more accurate measurements of the matter power spectrum [194].

5.5 Summary and conclusions

In this chapter, we investigated the possibility for the Quintessence field to be non-minimally coupled with the Ricci scalar.

When treating generalized theories of gravity, one must, first of all, ensure that the resulting theory is compatible with the bounds from solar system experiments: we found that these constraints are indeed satisfied if $\xi\leq5\times10^{-4}$, for IG, and $\xi\leq5\times10^{-3}(\sqrt{G}\phi_0)^{-1}$, for NMC models.

For these values of the coupling constant, we searched for the characteristic features that could distinguish these models from the "ordinary" Quintessence, described in chapter 4.
We found, in particular, that the Integrated Sachs-Wolfe effect, caused by the time variation of the gravitational potential between last scattering and the present time, is enhanced as compared with ordinary Q-models. This can be understood by considering the Klein-Gordon equation governing the time evolution of ϕ. It is easily seen that the coupling with R induces a new source of effective potential energy; the latter is ineffective in the radiation dominated era, when $R \approx 0$, but becomes important during matter and scalar field dominance, when it originates the effective potential

$$V_{QR} = -\frac{1}{2}F(\phi)R \ . \tag{5.50}$$

It is therefore immediate to realize that the force $dV_{QR}/d\phi$ in the Klein Gordon equation simply adds to the one coming from the true potential $dV/d\phi$, having the same sign and therefore enhancing the Integrated Sachs-Wolfe effect. As a consequence, part of the COBE normalization is now due to the latter effect and the cosmological perturbation amplitude, including also the oscillating region of the CMB spectrum, is reduced; this is evident in the CMB polarization and temperature patterns, as well as in the matter power-spectrum today. Moreover, the acoustic peaks and the power-spectrum turnover are displaced to smaller scales; the reason being that the Hubble length H^{-1} grows more rapidly in these theories than in ordinary Q-models, delaying - for a fixed value of H_0 - the horizon crossing of any scale larger than the Hubble radius at the matter-radiation equality, and slightly decreasing the amplitude of the acoustic oscillations.

Another effect of coupling comes from the change of the fluid shear σ arising in generalized Einstein theories. From the Einstein equations it turns out that the new terms in σ induce an additional friction to the growth of the gauge-invariant gravitational potential Ψ, besides that due to the Hubble drag. This makes the growth of Ψ weaker, and, since in adiabatic models the acoustic oscillations are essentially driven by this quantity, this results in a reduced amplitude for the acoustic peaks.

For what concerns large-scale structure formation, we also considered the effect of the extra term in the fluid shear arising from the QR-coupling. It produces a sort of friction in the dynamics of the metric perturbations, in addition to the genuine cosmological friction. Although interesting, we found that this effect is negligible compared to the effect due to the Integrated Sachs-Wolfe effect that changes the normalization to COBE data.

It is also remarkable that similar features occur both in IG and NMC models, suggesting the existence of an extended Quintessence phenomenology that is the signature of a large class of scalar-tensor theories in the cosmological perturbations.

This is a brief summary of the results we obtained in this class of Extended Quintessence models. Of course, this work does not answer all the questions nor does it explore all the aspects, but the results we obtained show distinctive and promising features at the point that we believe should be seriously taken into account, especially in favor of the hints on the existence of scalar fields and on their possible couplings with R coming from fundamental theories. An important problem to face is which effects are caused by the fact that we require that the field coupled with R is a Quintessence, and which instead come from the scalar-tensor theories themselves. The enhanced Integrated Sachs-Wolfe effect appears to be mostly determined by the extra effective potential coming from the non-minimal coupling; on the contrary, the effects at decoupling appear to be caused mostly by the true scalar field potential, since at that time the Ricci scalar R is much smaller than it is now. However, all these considerations, together for example with the exploration of other scalar field potentials and more general gravitational sectors in the Lagrangian, would deserve future work.

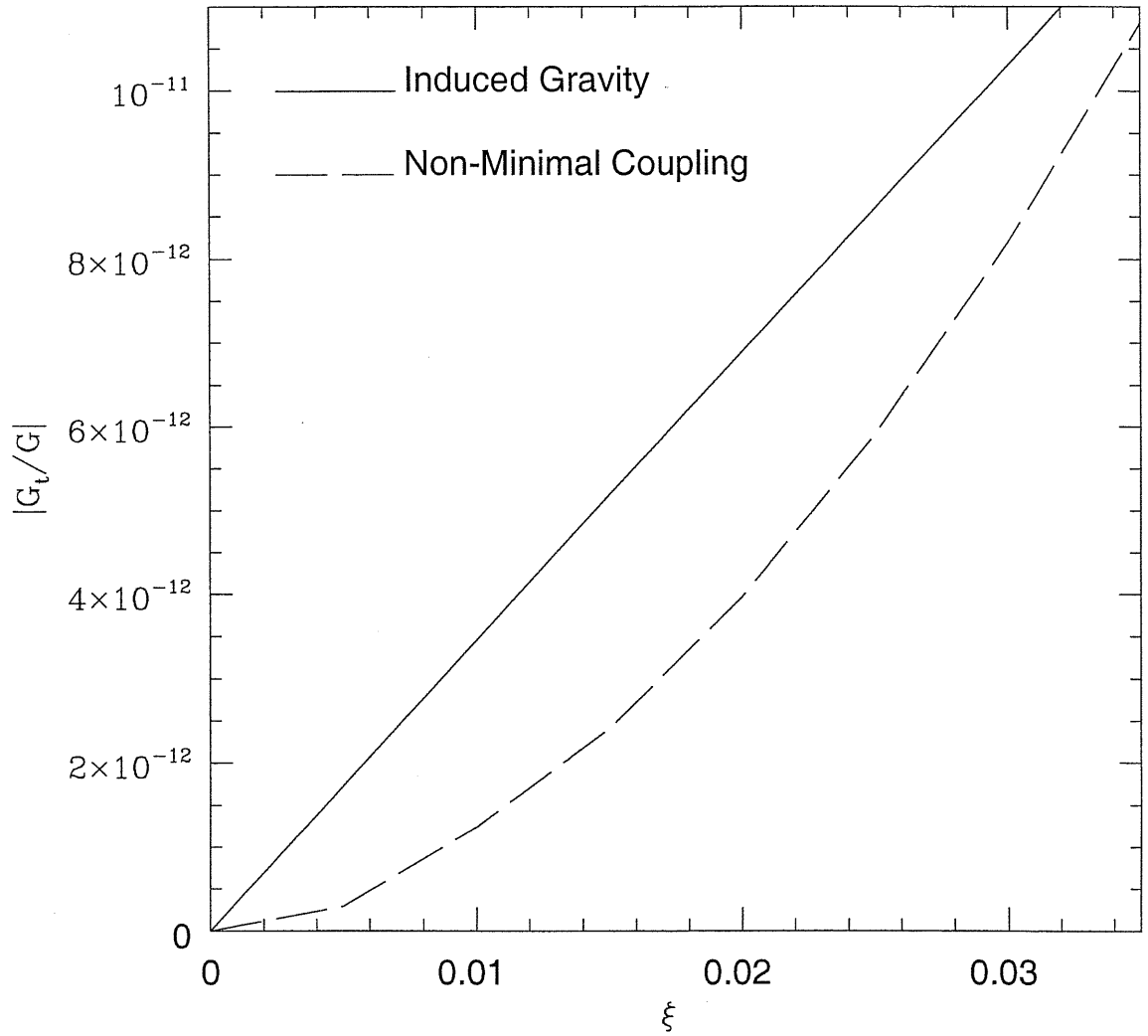

Figure 5.1: Numerical analysis of the time variation of the gravitational constant versus the QR coupling constant in EQ models.

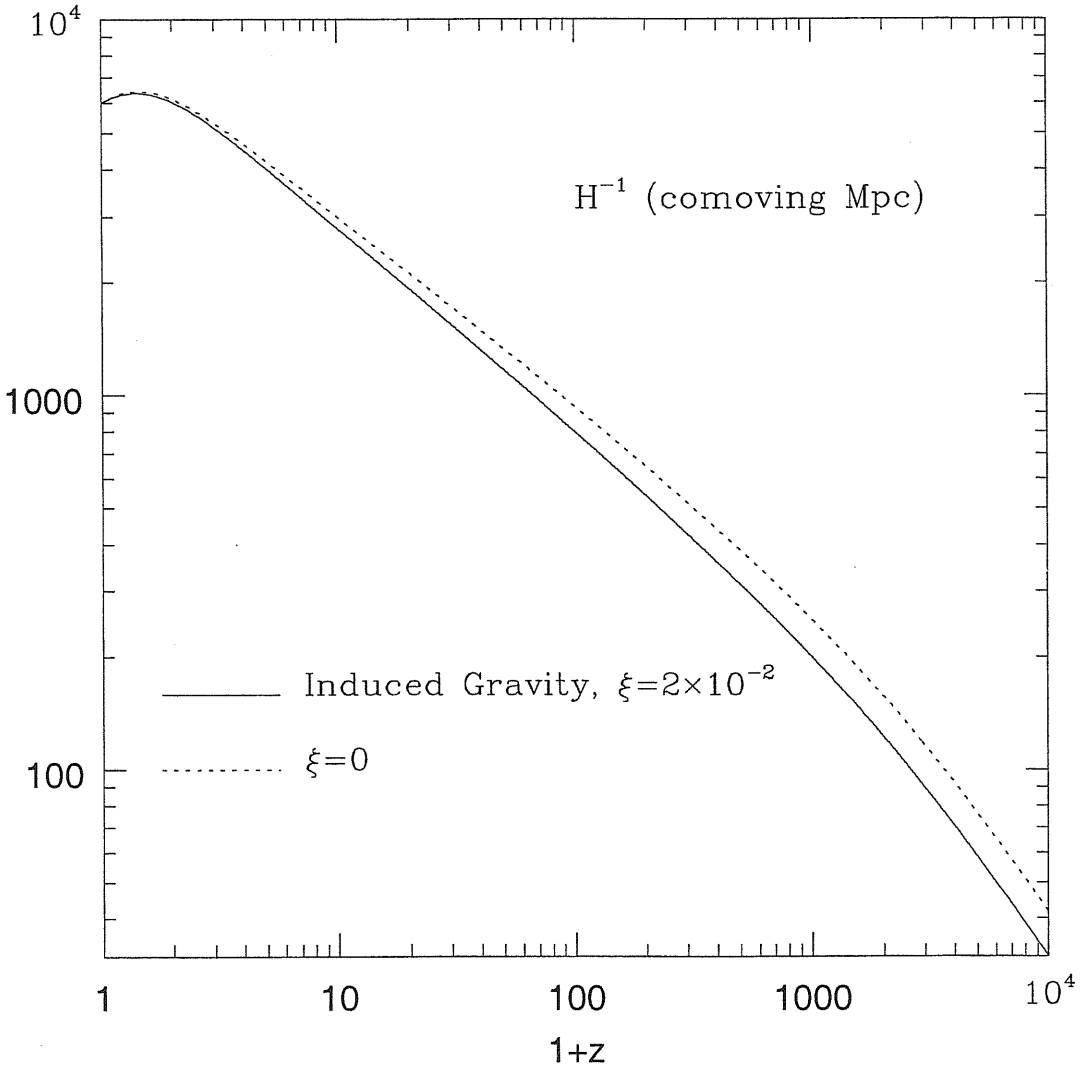

Figure 5.2: Time behavior of the Hubble length in EQ models versus ordinary Quintessence.

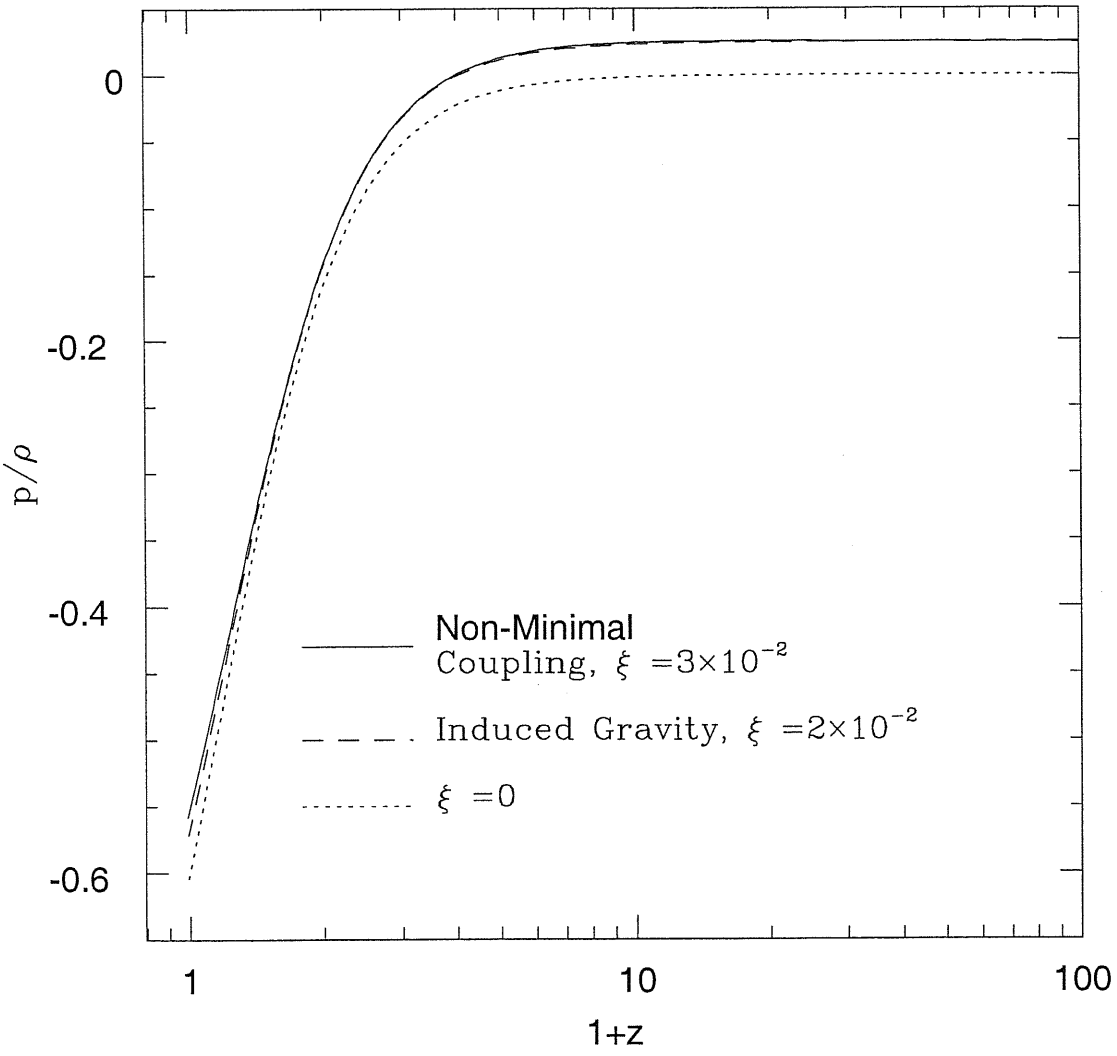

Figure 5.3: Time behavior of the cosmic equation of state in EQ models versus ordinary Quintessence.

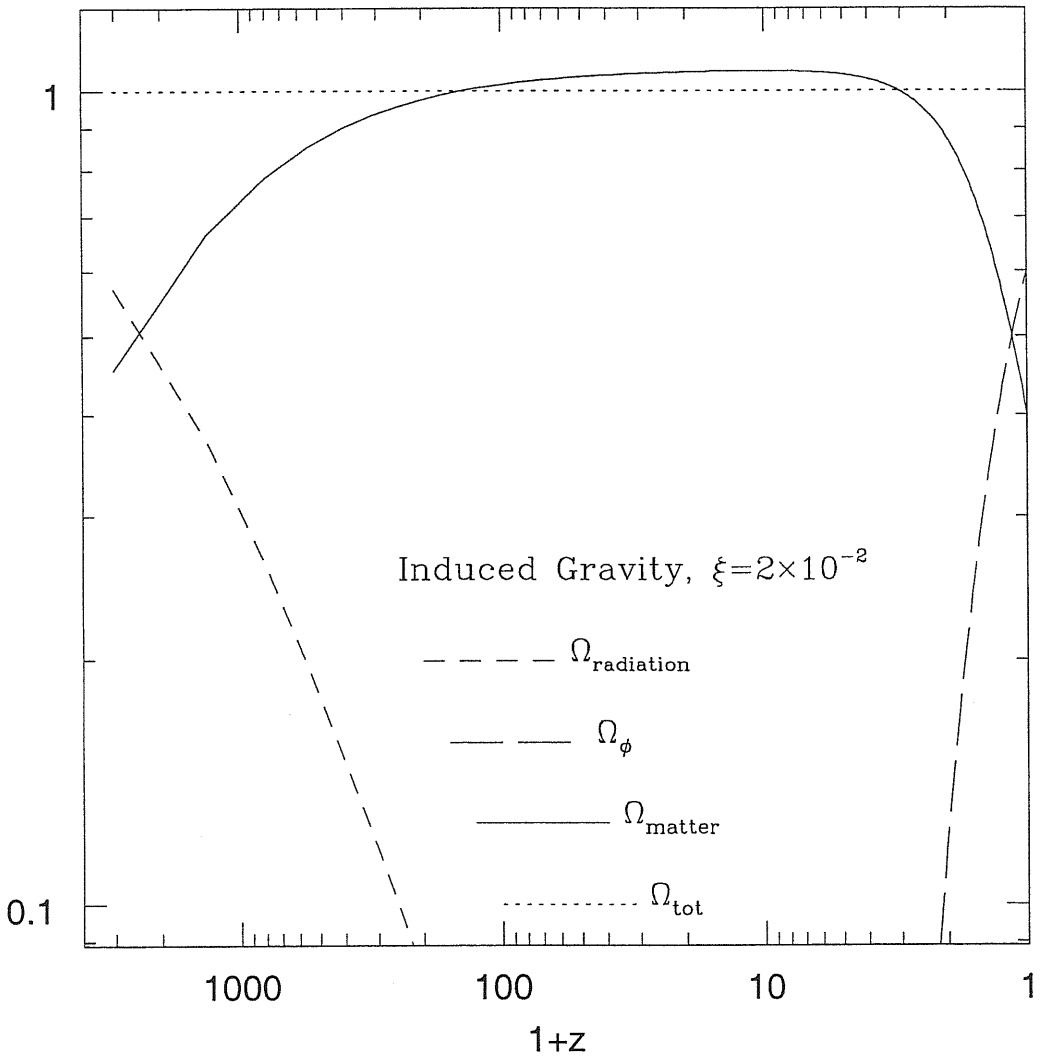

Figure 5.4: Time behavior of the Ω parameters relative to matter, radiation and Quintessence.

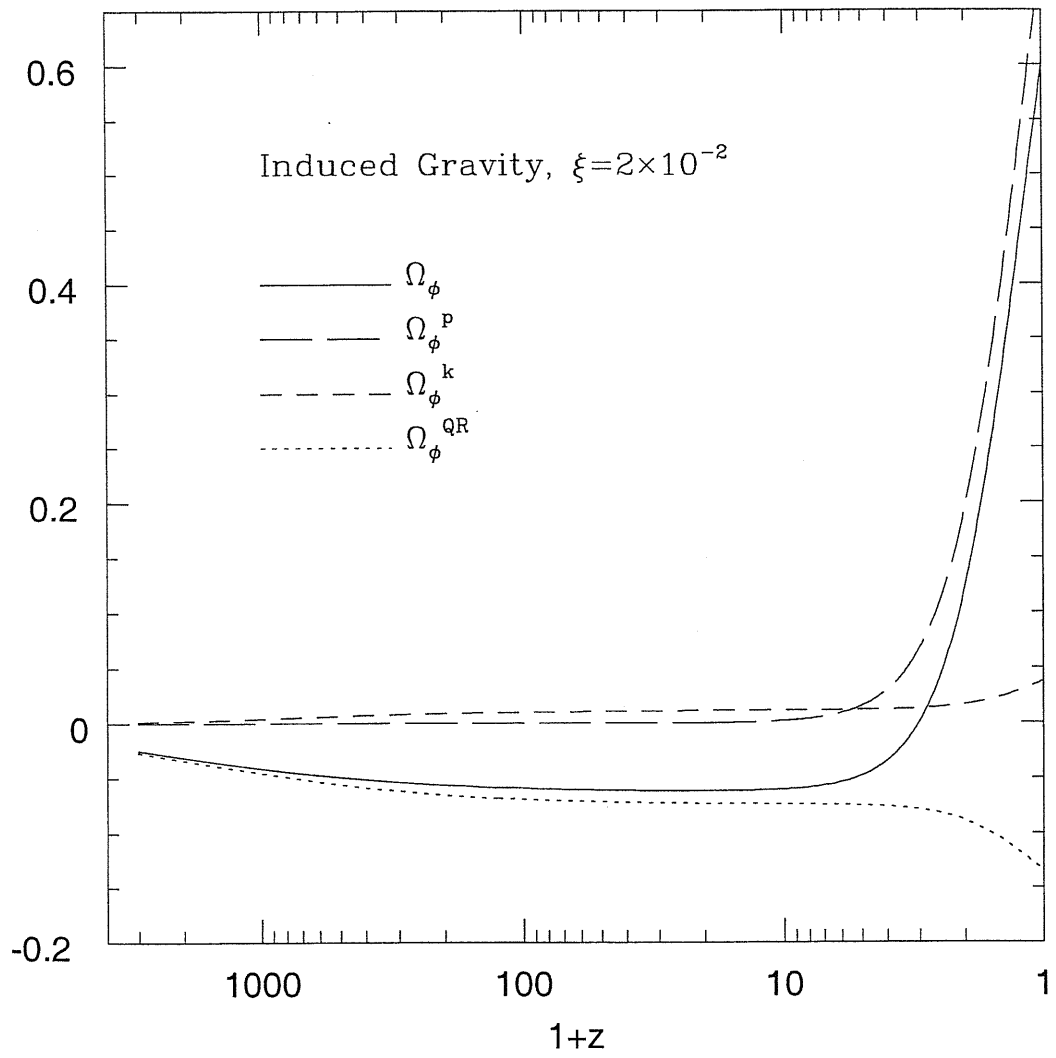

Figure 5.5: Time behavior of the Ω_ϕ parameters relative to the potential, kinetic and purely QR terms.

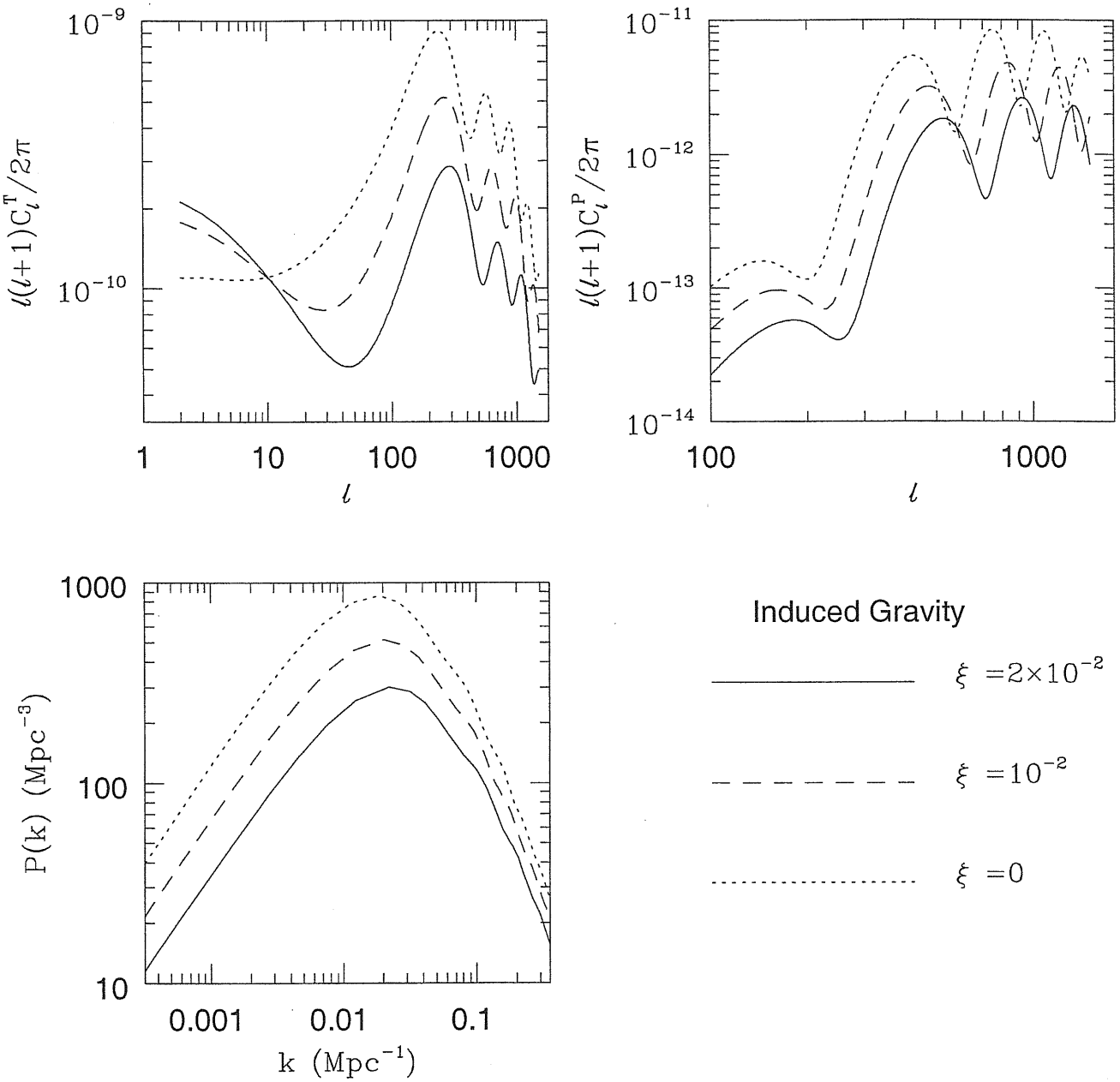

Figure 5.6: Perturbations for IG models for various values of ξ: CMB temperature (top left), polarization (top right), and matter power spectrum (bottom).

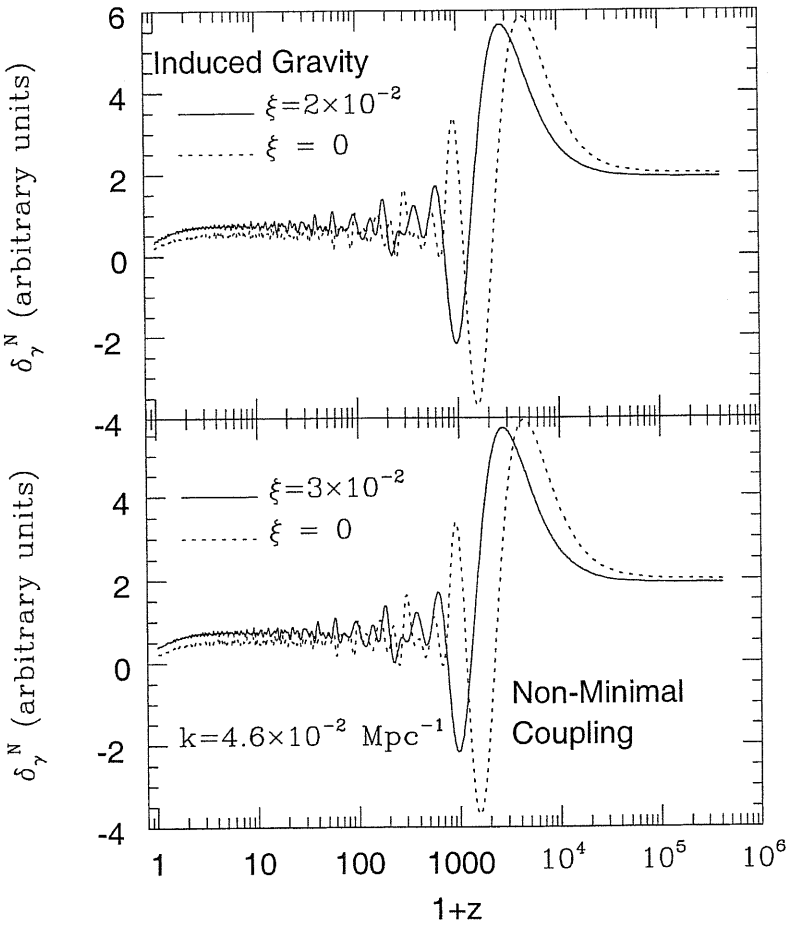

Figure 5.7: Comparison of the time behavior of the photon density fluctuations for the scale shown, for EQ and Q models.

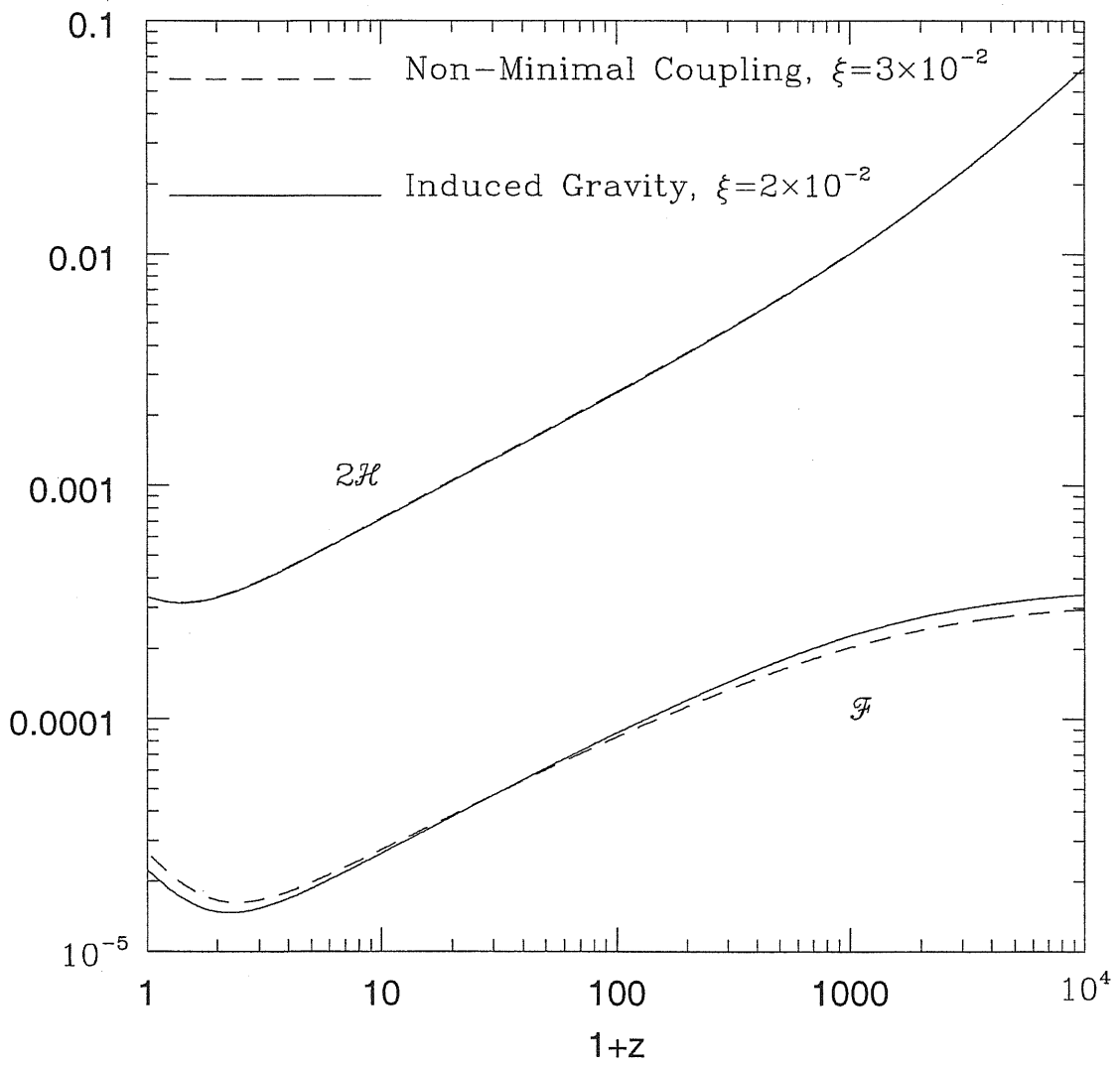

Figure 5.8: Time behavior of the friction term (in arbitrary units) arising from the shear perturbation in EQ models as compared with its cosmological counterpart.

Chapter 6

Tracking Extended Quintessence

The possible coupling between Q and the Ricci scalar R was the subject of chapter 5, where the observable impact of such a coupling was throughly investigated. Within this 'Extended Quintessence' (EQ) model two sets of theories were studied: Induced Gravity (IG, originally proposed in [246]) and Non-Minimal Coupling (NMC, see [22] for an extensive overview). In both models the term describing the coupling between the Ricci scalar R and the Quintessence field ϕ in the Lagrangian has the form $F(\phi)R/2$, where $F(\phi) = \xi\phi^2$; the difference between the two models is that in the NMC model the Lagrangian contains also the ordinary gravitational term $R/16\pi G$, that is instead absent in IG. Both models belong to the general class of scalar-tensor theories of gravity. The effects on Cosmic Microwave Background (CMB) anisotropies, as well as on Large Scale Structure (LSS), have been described and numerically computed for several values of $\xi > 0$; they turned out to be similar for IG and NMC, although for different values of the coupling constant. The main results were a modification of the low redshift dynamics, enhancing the Integrated Sachs Wolfe effect (ISW), as well as a shift of the CMB acoustic peaks and matter power spectrum turnover because of the dynamics of the Hubble length. Predicting in detail the shape and the position of the acoustic peaks in a given cosmological model is of course important in view of the formidable observations of the coming decade [151], but it is also of great importance at present, because of the strong evidence in favor of the existence of subdegree acoustic oscillations in the latest CMB data [60, 101].
Despite the fact that Quintessence models represent an improvement with respect to the theoretically puzzling cosmological constant, they still leaves many unresolved issues. The existence of a considerable amount of vacuum energy in the Universe, as observations seem to imply, brings together two main conceptual problems. The first is the so-called "coincidence" problem, namely the fact that we are right now in the phase in which the vacuum energy is starting to dominate over matter: if the densities of matter and vacuum decrease at different rates, it appears that the conditions in the early universe have to be set very carefully in order for the energy densities to be comparable just today. The second is a "fine-tuning" problem, which arises from the fact that if the vacuum energy is constant, as in the 'standard' cosmological constant scenario, then at the beginning of the radiation era the Q energy density should have been vanishingly small compared with both radiation and matter.

Important recent works demonstrated that the Quintessence scenario can avoid such fine tunings, while a cosmological constant fitting the data would be affected by both problems. Indeed, in the Quintessence scenario one can select a subclass of models which admit "tracking solutions" [206, 224, 142]: following early work by Ratra and Peebles [178] and Wetterich [231], it was shown how the observed amount of scalar field energy density today can be reached starting from a very wide set of initial conditions, covering tens of orders of magnitude. In particular, the Quintessence could have been initially at the level of the ordinary matter, thus being likely one of the products of the decay of the vacuum energy responsible for the inflation era.
This result is obtained with the peculiar dynamics of tracker fields: their equation of motion possesses attractor-like solutions which, nearly independently on the initial conditions, rapidly converge to a common, cosmic evolutionary track.
In order to avoid misunderstandings, it is useful to stress in which sense tracking solutions are attrac-

tors. We require that at present Ω_ϕ has the observed value. This is obtained by tuning the potential amplitude. Once this has been done, there is a huge set of initial conditions for the quintessence energy density for which its present value is unchanged.

Here we face the extension of tracking phenomenology in EQ; we find important results, both for background dynamics and perturbations, and we name this scenario Tracking Extended Quintessence (TEQ). We consider a NMC model for the coupling between Q and R. We first analyze the background evolution, accurately studying the Quintessence dynamics in the radiation dominated (RDE) and matter dominated (MDE) eras. Then, we compute the evolution of cosmological perturbations pointing out important observable effects on CMB and LSS. In this chapter, section 6.1 contains the analysis of tracking solutions; secs. 6.2 and 6.3 contain the description and a discussion of the effects on CMB and LSS, respectively; sec. 6.4 discusses how these effects change if we vary the form of the Q-field potential. Finally, sec. 6.5 contains a summary of our results and some concluding remarks. We adopt here inverse power-law potentials, as originally suggested by Ratra and Peebles [178], and found in some phenomenological supersymmetry breaking models [206, 224, 142, 75, 152]; with respect to the previous chapter, we now take a more general inverse-power law potential, namely

$$V(\phi) = \frac{M^{4+\alpha}}{\phi^\alpha} , \tag{6.1}$$

where the value of $\alpha > 0$ will be specified later and the mass-scale M is fixed by the level of energy contribution today from the Quintessence. Before going on, let us briefly define the quantities that represent the Q energy density and pressure. As it is evident from equations (5.3) and (5.4), the net energy density of the universe in scalar-tensor theories takes contributions from the scalar field, the matter fluid as well as from the Ricci scalar itself; the latter source of energy density, i.e. the last terms in the right-hand side of eqs. (5.3) and (5.4), could be included into the Q energy density and pressure, just because it comes directly from the scalar field coupling with R. Thus we define here the generalized Q energy density and pressure, including all the NMC terms:

$$\tilde{\rho}_\phi = \frac{1}{2a^2}\dot{\phi}^2 + V(\phi) - \frac{3\mathcal{H}\dot{F}}{a^2} . \tag{6.2}$$

$$\tilde{p}_\phi = \frac{1}{2a^2}\dot{\phi}^2 - V(\phi) + \frac{\ddot{F}}{a^2} + \frac{\mathcal{H}\dot{F}}{a^2} . \tag{6.3}$$

We will see how ρ_ϕ, p_ϕ may differ substantially from $\tilde{\rho}_\phi, \tilde{p}_\phi$, while in general they become nearly identical in the MDE.

6.1 Tracking Extended Quintessence

The existence of tracking solution trajectories was first pointed out by Ratra and Peebles [178] and Wetterich [231] independently. In [206, 224, 142], it was realized that they could be used to solve one of the two problems existing in Quintessence scenarios, namely the fine-tuning on the initial conditions; this is in favor of Quintessence compared with the ordinary cosmological constant models, which is affected by both the coincidence and fine tuning problems.

Following the paper by Baccigalupi et al. [10], we adopt here the following choice of the cosmological parameters: we require the present closure density of Quintessence to be $\Omega_\phi = 0.7$, with Cold Dark Matter at $\Omega_{CDM} = 0.253$, three families of massless neutrinos, baryon content $\Omega_b = 0.047$ and Hubble constant $H_0 = 100 h_{100}$ Km/sec/Mpc (with $h_{100} = 0.65$ thus keeping $\Omega_b h_{100}^2 = 0.020$). In section 6.4 we will explore the dependence of our results on the potential index α. Here we adopt $\alpha = 2$. Note that the case $\alpha = 1$ has been presented in the previous chapter, although the properties of tracking solutions were not analyzed; as we will see, however, the dynamical relevance of tracking solutions becomes more and more relevant, as the potential slope increases, so that the main results are not essentially modified. To get a preview of our results, we plot in Figure 6.1 the evolution of the energy density of the cosmic fluid components (radiation, matter and Quintessence) as a function of redshift,

in some models that we are going to describe. The plotted curves are ρ_r, ρ_m and ρ_ϕ. The high, dotted lines represent radiation and matter, which do possess the well known scalings $\rho_r \sim 1/a^4$, $\rho_m \sim 1/a^3$. Equivalence occurs roughly at $1 + z_{eq} \simeq 5 \times 10^3$. The other curves represent tracker solutions for the Quintessence energy density ρ_ϕ. We will describe in detail each curve in the next subsections; let us give here some general considerations. For each curve, the constant M in Eq.(6.1) has been chosen to produce the required Ω_ϕ today. The NMC dimensionless coupling constant is taken as

$$|\xi| = 1.5 \times 10^{-2} , \tag{6.4}$$

so as to satisfy the experimental constraints (5.21), because in all the cases shown in Fig.6.1 the present value of ϕ is $\phi_0 \simeq 0.35 M_P$, where $M_P = 1/\sqrt{G}$. Also we study both positive and negative values of ξ. The present value ϕ_0 is reached starting from initial conditions $\phi_{beg} \ll \phi_0$ and $\dot{\phi}_{beg}$ which can vary by several tens of orders of magnitude thanks to the capability of tracker solutions to remove any fine tuning of the initial conditions. In fact, it can be immediately noted from the curves in Fig.6.1 that, despite the huge range of initial values of the energy density, the Q component is going to dominate today at the chosen level. The final aspect we wish to point out before going to a detailed analysis of the dynamics in MDE and RDE, is that we plotted ρ_ϕ in the figure, which is always positive, as it is evident from its definition (4.4). This is not true for $\tilde{\rho}_\phi$ defined in (6.2), because the NMC terms may be negative, and in fact they overcome the kinetic and potential energy, as we will see below; this feature was first found and discussed in [174].

6.1.1 TEQ-trajectories in the Radiation Dominated Era: R-boost

To understand what happens, let us study the Klein-Gordon equation during the Radiation Dominated Era (RDE). The first feature to note is the behavior of the Ricci scalar R. The dominant fluid is radiation, so that $a \sim \tau$, and this could yield the wrong idea that $R = 0$ from Eq.(5.10). Actually this is not true as it is evident from Eq.(5.9): the first two terms $\rho_{fluid} - 3p_{fluid}$ take zero contribution from radiation, but there is a residual contribution ρ_m, from the subdominant matter component. Thus, there is a divergence $R \propto 1/a^3$ as $a \to 0$. Also, we will see in a moment that the other terms in Eq.(5.9), as well as the dynamics implied by the overall factor $1/F$ do not change this argument; in conclusion the behavior of R in the RDE is

$$R \simeq \frac{8\pi G \rho_{m0}}{a^3} = \frac{3H_0^2(\Omega_{CDM} + \Omega_b)}{a^3} \quad \text{for } a \to 0 . \tag{6.5}$$

This implies that on the RHS of the Klein Gordon equation (4.8) the term multiplying R diverges as $1/a$ and has the same sign of ξ since ϕ is assumed to be always positive. This generates a "gravitational" effective potential causing an enhancement of the dynamics of ϕ at early times, that we name "R-boost". The field accelerates until the friction term $2\mathcal{H}\dot{\phi}$ reaches a value that is comparable to the R-boost term on the RHS. After that, Q enters a phase of slow roll driven by the friction and the R-boost terms only:

$$2\mathcal{H}\dot{\phi} \simeq \frac{a^2 R F_\phi}{2} . \tag{6.6}$$

The slow roll holds until the true potential energy from V becomes important in the Klein Gordon equation. This dynamics is manifest in Fig.6.2, where the absolute values of the four terms in the Klein Gordon equation are plotted. The thin solid line is the potential term, that is subdominant until $1 + z \leq 1000$. The heavy dashed line is the friction term and the solid heavy one is the R-boost term. In a very short time the friction grows from zero (the initial Q velocity is here taken to be zero) until it reaches the R-boost term, setting the onset of the slow rolling regime. The thin dashed line is the Q acceleration, $\ddot{\phi}$, which is positive and decreasing initially; then, it becomes negative (deceleration) at the cusp corresponding to $1 + z \sim 10^7$, and again positive at $1 + z \sim 10^3$ when the potential energy becomes important and the tracker behavior in the MDE starts.

It is quite simple to write an accurate analytic form for the solution during the R-boost. By using Eqs.(6.5,6.6), and the behavior of a in the RDE, $a \simeq \sqrt{8\pi G \rho_r^0/3} \cdot \tau$, we easily get

$$\phi = \phi_{beg} \exp\left[\mathcal{C}(\tau - \tau_{beg})\right] , \tag{6.7}$$

where

$$\mathcal{C} = \frac{3H_0^2(\Omega_{CDM}+\Omega_b)}{2\sqrt{8\pi G\rho_r^0/3}}\xi \ . \tag{6.8}$$

With our choice of parameters, $\mathcal{C} \simeq 7\cdot 10^{-3}\xi$ Mpc^{-1}, which implies that the exponent in (6.7) remains much smaller than one at all relevant times. Therefore,

$$\phi \simeq \phi_{beg}[1+\mathcal{C}(\tau-\tau_{beg})] \ . \tag{6.9}$$

The behavior expressed by Eqs.(6.7, 6.9) corresponds to the dotted dashed line in Fig.6.1, which mimics very tightly the R-boost solution. Indeed in this phase the Q kinetic energy density dominates and Eq.(6.9) implies

$$\frac{1}{2}\phi_t^2 = \frac{1}{2}\frac{\dot\phi}{a^2} = \frac{1}{2}\frac{\phi_{beg}^2\mathcal{C}^2}{a^2} \ . \tag{6.10}$$

The dot-dashed line in Fig.6.1 has been obtained by inserting the value of $\mathcal{C}$ and ϕ_{beg} at the onset of the R-boost.

Note that the scaling as $1/a^2$ is significantly different from a truly kinetic dominated phase in minimally coupled models, for which we should have had $1/a^6$, from the continuity equation (4.6) with $p_\phi \simeq \rho_\phi$. The reason why we have a different scaling of ρ_ϕ is that the NMC terms in $\tilde\rho_\phi$ are not negligible during all the RDE and the first part of the MDE, as we will show in a moment. Let us conclude the description of the R-boost by estimating the time of its end. The latter occurs at a redshift z_{pot} when the true potential energy becomes comparable with the kinetic energy (6.10):

$$\frac{1}{2}\phi_{beg}^2\mathcal{C}^2(1+z_{pot})^2 = V[\phi(z_{pot})] \ . \tag{6.11}$$

Since the R-boost is a very high redshift process, it covers a very tiny time interval, and in practice ϕ does not move substantially from its initial condition ϕ_{beg} during this phase. Therefore we can take $V[\phi(z_{pot})] \simeq V(\phi_{beg})$ in Eq.(6.11). Moreover, for our inverse power-law potential we have $V(\phi_{beg}) = V(\phi_0)(\phi_0/\phi_{beg})^2$, and from the Friedmann equation today $8\pi GV(\phi_0)/3 = \Omega_\phi H_0^2$. Putting these ingredients together we can write an approximate formula for $1+z_{pot}$ giving the end of the R-boost:

$$1+z_{pot} \simeq \sqrt{\frac{6\Omega_\phi H_0^2\phi_0^2}{8\pi G\mathcal{C}^2\phi_{beg}^4}} \simeq 3000 \ , \tag{6.12}$$

where the precise number has been obtained by making use of the actual value of the parameters in our case: it correctly corresponds to the R-boost end in Fig.6.1. Note that the end of the R-boost actually occurs when the Universe has already become matter dominated.

Before concluding this subsection, let us return to the importance of the NMC terms in $\tilde\rho_\phi$ in equation (6.2); as we already anticipated, we show now that they are dominant with respect to kinetic and potential energy densities until the first part of the MDE. Indeed, the NMC term in $\tilde\rho_\phi$ is $-3\mathcal{H}F_\phi\dot\phi/a^2$ and scales roughly as $1/a^3$, since $\mathcal{H}$ goes like $1/a$; on the contrary, the true potential V is roughly constant and the R-boost kinetic energy scales like $1/a^2$; as we explained. Because of these scalings, we expect that there exists a time τ_{NMC} such that for $\tau < \tau_{NMC}$ the NMC term is larger than both the kinetic and potential energy, while it becomes subdominant after this time. In fact, assuming that the time dependence of the field is as in the R-boost solution (6.9), a simple calculation shows that the NMC energy density term $-3\mathcal{H}F_\phi\dot\phi/a^2$ dominates ρ_ϕ up to

$$\tau_{NMC} \simeq \left[\frac{3\xi\mathcal{C}\phi_{beg}^2}{\Omega_\phi\rho_{r0}H_0^3}\left(\frac{\phi_{beg}}{\phi}\right)^2\right]^{1/3} \quad \text{or } 1+z_{NMC} \simeq 850 \ , \tag{6.13}$$

that is long after matter radiation equivalence, as it is evident in Fig.6.1. Note however that this is only an approximation, since Eq.(6.12) tells us that the R-boost solution is no longer satisfied at these redshifts; anyway this clearly shows that the NMC terms become subdominant only after the onset of the matter domination, so that the distinction between ρ_ϕ and $\tilde\rho_\phi$ can be relaxed after τ_{NMC}. Our analysis is therefore approaching the MDE behavior of ϕ, subject of the next subsection.

6.1.2 TEQ-trajectories in the Matter Dominated Era

Tracking solutions have recently been obtained in the context of Induced Gravity models [220], whose only difference compared with NMC is the absence of a constant term multiplying the Ricci scalar in the gravitational sector of the Lagrangian, i.e. $F(\phi) = \xi\phi^2$. We make two claims here. The first is that the same tracker solutions also exist in NMC models, provided in the MDE the scale factor can be expressed as a power of τ. The second is that for $F(\phi) \propto \phi^\beta$ the same solutions exist only if $\beta = 2$, as assumed so far.

In fact, by looking at Eqs.(4.5, 4.8), it is immediately realized that the difference between the IG and NMC models resides only in the $1/3F$ term multiplying the RHS in (4.5), since all the other terms involving F are derivatives with respect to either time or ϕ. Tracking solutions in [220] have been obtained by assuming that the scale factor in the MDE is the square of the conformal time τ,

$$a(\tau) = a_* \left(\frac{\tau}{\tau_*}\right)^2 , \tag{6.14}$$

(τ_* is a generic time) so that Eq.(4.5) gets almost identically satisfied and disappears from the treatment. Indeed we show that in NMC models both Eq.(4.5) and Eq.(6.14) hold true, simply because matter is dominating and $F(\phi)$, playing the role of the gravitational constant in Eqs.(4.5, 5.6), is slowly varying. Since $\phi_{beg} \ll \phi_0 \simeq 0.35 M_P$, it is easy to see that the variation of the value of F throughout the whole cosmological trajectory is [1]

$$\left|\frac{F_0 - F_{beg}}{F_0}\right| \simeq 4.6 \times 10^{-2} . \tag{6.15}$$

To see this in another way, Fig.6.3 shows the behavior of $\mathcal{H}$, indicated on the vertical axis as $(1+z)H^{-1}$, where $H = a_t/a$, in three important moments of the cosmological evolution, namely present (top), decoupling (middle), and equivalence (bottom); the heavy, solid line represents TEQ with positive ξ, the thin solid line is TEQ with negative ξ, the short dashed line, instead, is ordinary Q, and the long dashed one is the cosmological constant, which is significantly different from Q and TEQ since it is not dynamical. As is evident, opposite signs of ξ imply opposite behaviors for $\mathcal{H}$, especially at small redshifts, compared with ordinary Q. At a given redshift, the shift in $\mathcal{H}$ is due to the behavior of $F(\phi)$, which is less or more than $1/8\pi G$ for positive or negative ξ, respectively, by an amount given by (6.15).

Therefore, Eq.(6.14) holds with good accuracy, and all the solutions obtained in [220] for IG models, as well as their stability properties, hold true also in our NMC case.

Let us come now to our second claim. We assume for a while a form $F(\phi) = \tilde{\xi}\phi^\beta$ and $F(\phi) = 1/(8\pi G) + \tilde{\xi}(\phi^\beta - \phi_0^\beta)$, respectively. We are searching for power law solutions for the Quintessence

$$\phi(\tau) = \phi_* \left(\frac{\tau}{\tau_*}\right)^\gamma ; \tag{6.16}$$

from (6.14) and (6.16), it is matter of simple algebra to check that Eq.(4.8) takes the form

$$\left(\gamma^2 + 3\gamma\right)\frac{\phi}{\tau^2} = \frac{a^2 R}{2}\beta\tilde{\xi}\phi^{\beta-1} + a^2\alpha\frac{M^{4+\alpha}}{\phi^{\alpha+1}} . \tag{6.17}$$

Also, from (5.10) the Ricci scalar in the MDE becomes $R = 12/(a \cdot \tau)^2$. It is easy to see that this is only satisfied if

$$\beta = 2 \quad \text{and} \quad \alpha = \frac{6}{\gamma} - 2 . \tag{6.18}$$

[1] It is also useful to point out here that, because of the small change in the value of $F(\phi)$ throughout the entire cosmological evolution, the well-known constraints on the variation of H at the epoch of nucleosynthesis are always satisfied in our models (see e.g. [174] and references therein).

This proves our second claim. If conditions (6.18) are satisfied, Eq.(6.17) gives ϕ_* in terms of γ, n, α; since it must be positive, the following additional condition is derived:

$$\gamma^2 - \gamma - 12\tilde{\xi} > 0 \ . \tag{6.19}$$

In this regime, the Quintessence energy density scales as

$$\rho_\phi = \rho_{\phi *} \left(\frac{a}{a_*}\right)^{-\epsilon} \quad , \quad \epsilon = \frac{3\alpha}{\alpha + 2} \ , \tag{6.20}$$

and its pressure is

$$p_\phi = -\rho_\phi \frac{2}{\alpha + 2} \ . \tag{6.21}$$

For what concerns the stability of these solutions, we report here only a remarkable result [220]; solutions satisfying (6.18) are stable under time dependent perturbations if and only if the following condition holds:

$$-1 - \frac{4}{\alpha + 2} < 0 \ , \tag{6.22}$$

holding for instance for any $\alpha > 0$. In summary, for the class of solutions we are interested in, namely those satisfying (6.14,6.17), the cases of interest here have been treated in [220]; we have shown here that such solutions apply both to NMC and IG cases.

Let us describe now in detail the solutions we see in Fig.6.1. Let us focus on the minimal coupling case first. The lowest, dashed line represents a minimally coupled case in which the behavior of the Q component during RDE is equivalent to a pure cosmological constant. The kinetic energy density is initially zero and remains largely subdominant with respect to the potential one. Thus ϕ "freezes" for almost all the RDE, and leaves this condition only when its energy density reaches a fraction of about 10^{-3} of the critical one. Thereafter, Q joins the tracker solution in the MDE regime corresponding to

$$\gamma = \epsilon = 1.5 \ , \tag{6.23}$$

that satisfies the constraint (6.19) with $\tilde{\xi} = 0$. The substantial motion of the field from the initial condition to its final value occurs in this last phase.

The thin long-dashed line represents a case in which the initial kinetic energy density is dominant with respect to the potential one, by 23 orders of magnitude. As it is evident, the field starts from an energy density comparable with the matter one. In this case the kinetic energy is redshifted away during the phase corresponding to the rapidly decreasing part of the trajectory in the figure; the scaling is easily found from the continuity equation, with $\rho_\phi \simeq p_\phi$. Then the field freezes again before joining the tracker solution at $1 + z \simeq 100$. Note that because of this early stage of kinetic energy dominance, the field freezes at a value slightly greater than the initial condition $\phi_{beg} = 10^{-2}$; that is the reason why the flat part of the curve lies slightly below that corresponding to the previous case. Although not plotted in the figure, a roughly equivalent trajectory might have been obtained by requiring that the initial potential energy density was comparable to the matter one. Note the very large set of initial energy values from which the field reaches the present state.

Let us come now to the analysis of the tracker solutions in the NMC case. The heavy solid line has been obtained for $\xi = 1.5 \times 10^{-2}$. The RDE is dominated by the R-boost: the field accelerates until the gravitational effective potential is reached by the cosmological friction term in the Klein-Gordon equation. The slow rolling sets in, and holds until the true potential becomes important, when the field freezes. After this early phase, $\tilde{\rho}_\phi$ and ρ_ϕ, after having been very different in magnitude and sign, become indistinguishable, and join the tracker solution in the MDE reaching the required value today.

The heavy dashed line corresponds to a case in which the initial kinetic energy density is larger by 23 orders of magnitude with respect to the potential one, thus starting from an energy comparable with the matter one. As for the Q case, in this condition the field undergoes an era of kinetic energy dominance until the latter is redshifted below the effective NMC potential energy and the R-boost is set also in this case. The evolution of the field from this time on is the same as in the zero initial kinetic energy case.

The dot-dashed line is in fact the R-boost approximate solution (6.7). Note that it describes very well the R-boost, and shows that the terms of order higher than the first in Eq.(6.9) become important only now, when the R-boost is no longer active.

The last point we want to stress is that the heavy solid line is actually superposed with a solid thin line, which describes a case identical, but for negative coupling constant, $\xi = -1.5 \times 10^{-2}$. The reason why these two trajectories agree so tightly is that during the R-boost the kinetic energy density, which dominates ρ_ϕ, is the same regardless of the sign of ξ, see Eqs. (6.7- 6.10). The only slight difference between the two trajectories is when the R-boost ends and the true potential starts to drive the dynamics of ϕ. For positive ξ, $\dot{\phi}$ is positive during the R-boost and later, while, for negative ξ, $\dot{\phi}$ is negative during the R-boost. Although the curves describing ρ_ϕ for positive and negative values of ξ look very similar, this is not true for the perturbations they generate, as will be discussed in the next section.

6.2 Cosmic Microwave Background spectra

In this section we analyze the CMB temperature and polarization spectra of our TEQ model.

Before to consider the "Extended" case, it is interesting to see what happens for tracker solutions with $\xi = 0$, i.e. for minimally-coupled scalar fields in tracking regime. In Fig. 6.4 the CMB angular power spectrum is plotted vs. the multipoles ℓ's and the present equation of state w_ϕ of a $\xi = 0$ tracking quintessence. This is simply related to the potential amplitude by Eq.(6.21), even if at present it is only approximatively true since the Quintessence is dominating cosmic expansion and the tracking regime is being abandoned.

The cosmological constant is recovered as $w_\phi = -1$. It is worth to note as the amplitude of the acoustic peaks is reduced as an effect of the COBE normalization at low ℓs and ultimately, of the ISW. In fact, for a given amount of vacuum energy density today ($\Omega_{vacuum} = 0.7$ for the plot in fig. 6.4), the "dynamical" vacuum energy comes to dominate at earlier times as compared with the cosmological constant, and the time variation of the gravitational potential is more severe, enhancing the ISW effect [51].

For the same reason, the distance to last scattering surface is reduced in the "dynamical" vacuum energy model, so that the same physical scale on the last scattering surface appears on larger angular scales (i.e., lower ℓ) as a projection effect, as described in Chap. 3. This explains the shift of the acoustic peaks toward smaller multipoles, with respect to the Λ model.

In Fig.6.5 we plot the CMB spectra for the models discussed in the previous section; the top panel describes temperature fluctuations; the bottom panel shows polarization spectra. The CMB spectrum coefficients are calculated from

$$C_\ell^T = 4\pi \int \frac{dk}{k} |\Delta_{T\ell}(k, \tau_0)|^2 \quad , \quad C_\ell^P = 4\pi \int \frac{dk}{k} |\Delta_{P\ell}(k, \tau_0)|^2 \, , \tag{6.24}$$

where the quantities $\Delta_{T\ell}(k, \tau_0)$ and $\Delta_{P\ell}(k, \tau_0)$ are functions of the photon and baryon perturbed quantities, see e.g. ref. [173] for detailed definitions. The spectra have been normalized at the COBE measurements at $\ell = 10$.

The heavy, solid line in Fig.6.5 describes CMB spectra for the model corresponding to the same line in Fig.6.1. The thin, solid line describes the same model, but for $\xi = -1.5 \times 10^{-2}$, again as the same line in Fig.6.1. The short-dashed line, in the left panels, represents a case of ordinary Quintessence with the same potential and $\Omega_\phi = 0.7$. The long-dashed line, in the right panels, describes a cosmological constant, Λ model, with $\Omega_\Lambda = 0.7$. Before entering into the description of the various effects we find, let us stress that the effects of TEQ are quite large, with respect to both ordinary Q and Λ models. Also, the models plotted respect the experimental constraints discussed in Section II, having $\omega_{JBD} \simeq 500$ and $G_t/G \simeq 10^{-12}$ yr^{-1}. We want to mention that the effects are here considerably larger than what we obtained in the previous chapter. The reason is twofold: in [174] we did not follow the tracker solution for the Q field, but for the shallower potential we considered there ($\alpha = 1$) the size of the effects we find here would have been smaller anyway (see the discussion in Section VI).

First of all, let us consider the dynamics of Q at low redshifts. By looking at Eq.(4.8), it is easily seen that at present Q obeys a sort of effective potential, caused by the true potential and by the curvature-coupling term:

$$V_{eff}(\phi, R) = V(\phi) - \frac{F(\phi)R}{2} \ . \tag{6.25}$$

At low redshifts when Q starts to dominate, the dynamics of the Hubble length is suppressed since the universe is approaching a de Sitter phase. Therefore, by neglecting $\dot{\mathcal{H}}$ in Eq.(5.10), we have $R \simeq 6H^2$. Also, from the Friedmann equation we get $(8\pi G/3)V \simeq \Omega_\phi H^2$, and for inverse power-law potentials of the form (6.1) we have $dV/d\phi = -\alpha V/\phi$. Thus the derivative of the effective potential (6.25) takes the following approximate form:

$$\frac{dV_{eff}}{d\phi} \simeq -\left(\frac{3\alpha\Omega_\phi}{8\pi G\phi} + 6\xi\phi\right) H^2 \ ; \tag{6.26}$$

for positive ξ, both terms push toward increasing values of ϕ, and we can immediately understand that the NMC term is comparable to the ordinary Quintessence one for

$$|\xi| = \frac{\alpha\Omega_\phi}{16\pi G\phi^2} \ . \tag{6.27}$$

Therefore, for $\xi = 1.5 \times 10^{-2}$ and $\alpha = 2$, we expect to have a 10% extra force coming from the NMC terms in Eq.(4.5). Just the opposite happens if ξ is negative, since the terms in (6.26) have opposite sign. Indeed what we see in Fig.6.3 is that for opposite signs of ξ, the change in the low redshift dynamics of $\mathcal{H}^{-1}$ is also opposite. Also, in Fig.6.2 it can be seen that at present roughly an order of magnitude separates the gravitational effective potential from the true one.

The Integrated Sachs Wolfe effect makes the CMB coefficients on large scales, or small ℓ's, change with the variation of the gravitational potential along the CMB photon trajectories. Since the gravitational potential is affected by the low redshift dynamics, we expect an increase or a decrease of the ISW for positive and negative ξ, respectively. Indeed this is precisely what we see in Fig.6.5, looking at the curves for $\ell \leq 10$: positive or negative ξ TEQ make the C_ℓ larger or smaller than ordinary Q, respectively.

The following simple calculation gives a good estimate of the amount of ISW in TEQ models. Take a cosmological scale comparable with the Hubble horizon today, so to be unaffected by acoustic oscillations. As it is known (see e.g. [108] and references therein), the ISW is simply given by the change, between decoupling and now, of the quantity $\Psi - \Phi$, where Ψ and Φ are the gauge-invariant expressions of the gravitational potential and of the intrinsic spatial curvature, respectively; it can be seen [108] that this results in a fraction of $\Psi - \Phi$ calculated at decoupling:

$$\left(\frac{\delta T}{T}\right)_{ISW} \propto (\Psi_{dec} - \Phi_{dec}) \ . \tag{6.28}$$

In NMC theories Ψ_{dec} and Φ_{dec} are slightly different from those calculated in minimally coupled theories, because they receive a contribution from the time variation of the gravitational constant; since Ψ and Φ are proportional to $G \propto 1/F$, in the limit $|F_{dec} - F_0| \ll F_0$ they change by an amount $(\Psi_{dec} - \Phi_{dec}) \cdot (1 - F_{dec}/F_0)$. This induces an ISW effect which is

$$\left(\frac{\delta T}{T}\right)_{ISW,NMC} \propto (\Psi_{dec} - \Phi_{dec}) \cdot \left(1 + \frac{F_0 - F_{dec}}{F_0}\right) \ . \tag{6.29}$$

Therefore, on the CMB power spectrum, the NMC contribution to the ISW can be estimated as

$$\frac{\delta C_{\ell\leq 10}}{C_{\ell\leq 10}} = \frac{C^{TEQ}_{\ell\leq 10} - C^{Q}_{\ell\leq 10}}{C^{Q}_{\ell\leq 10}} = \frac{(\delta T/T)^2_{ISW,NMC} - (\delta T/T)^2_{ISW}}{(\delta T/T)^2_{ISW}} \simeq 12 \cdot \frac{F_0 - F_{dec}}{F_0} \simeq 16\pi G\xi\phi_0^2 \ ; \tag{6.30}$$

the last equality has been obtained in our particular model, where at decoupling $\phi \ll \phi_0$, so that $1 - F_{dec}/F_0 \simeq 8\pi G\xi\phi_0^2$. Note again that, depending on the sign of ξ, the net effect can be an increase

or a decrease of the CMB power. Indeed in Fig.6.3 we see that the above estimate is fairly well respected: since in the present case $\phi_0 \simeq 0.35 M_P$ on large angular scales Eq.(6.30) predicts an effect of the order of 10%, as in the figure.

Let us come now to the evaluation of the effects on the acoustic peaks in the CMB spectrum. There are essentially two effects, peaks amplitude and position, that we describe now.

The amplitude changes in the opposite way for opposite signs of ξ. This feature can be understood as a normalization effect: we have seen that positive and negative ξ give rise to increased and decreased ISW in TEQ with respect to Q models; correspondingly, when the spectra are normalized at $\ell = 10$, a decrease and increase of the acoustic peak amplitude occurs. As a consequence, the magnitude of this effect is roughly at the level given by Eq.(6.30). For completeness, we report also another mechanism that changes the acoustic peaks amplitude, which occurs at decoupling, instead of at low redshifts. As is evident in Fig.6.3, the size of the Hubble horizon at a given redshift is different in TEQ with respect to Q models. As we noted in [174], this implies that the horizon reentry for a given comoving scale is delayed for positive ξ and anticipated for negative ξ; therefore, with respect to the ordinary tracking Quintessence, this implies a slight excess or deficit in CDM density when such scale crosses the horizon, corresponding to a deficit and an excess in the radiation energy density. This slightly suppresses the acoustic oscillations in the first case, and enhances them in the second.

Let us come now to the explanation of the acoustic peaks shift. The angular scales at which acoustic oscillations occur are directly proportional to the size of the CMB sound horizon at decoupling, that in comoving coordinates is roughly $\tau_{dec}/\sqrt{3}$, and inversely proportional to the comoving distance covered by CMB photons from last scattering until observation, that is $\tau_0 - \tau_{dec}$ [108]. Therefore, since the spectrum multipoles scale as the inverse of the corresponding angular scale, we have

$$\ell_{peaks} \propto \frac{\tau_0 - \tau_{dec}}{\tau_{dec}} \,. \tag{6.31}$$

In our models, τ_0 and τ_{dec} shift essentially because of two reasons, namely the change in τ_0 due to the domination of the Q component today, and the behavior the Hubble length H^{-1} in the past. The first feature mainly makes the Q and TEQ models different from a cosmological constant, since the latter does not have the kinetic degree of freedom. The second feature is related to the fact that, for a fixed value of the Hubble length today, in the past it possesses a behavior which is characteristic of the particular model at hand, because of the time evolution of the effective gravitational constant $1/F(\phi)$ (see Fig.3). Let us give a simple analytical formula for the acoustic peaks shift in TEQ models with respect to ordinary tracking Q. First, it can easily be seen that the conformal time τ can be conveniently written as a function of the scale factor as follows:

$$\tau = \int_0^a \frac{da}{a\dot{a}} \,. \tag{6.32}$$

However, from the Friedmann equation (4.5), $\dot{a}$ scales as the inverse of $\sqrt{F}$; therefore, small changes $\delta F \ll F$ induce a change $\delta\dot{a}/\dot{a} \simeq -(1/2)\delta F/F$, and consequently in the conformal time, which shifts by an amount

$$\delta\tau = \int_0^a \frac{da}{a\dot{a}[1-(1/2)\delta F/F]} - \tau \simeq \frac{1}{2}\int_0^a \frac{da}{a\dot{a}}\frac{\delta F}{F} \,, \tag{6.33}$$

where we have defined the time change of F as follows:

$$\frac{\delta F}{F} = \frac{F(\phi) - F_0}{F_0} \,. \tag{6.34}$$

Of course $\delta F/F$ at any given time depends on various details, but let us make the simplifying assumption that it is constant from the beginning until $z = 2$ and zero afterwards, empirically following what we see in Fig.3. It is then immediate to deduce that τ_{dec} changes as

$$\delta\tau_{dec} \simeq \tau_{dec} \cdot \frac{1}{2}\frac{\delta F}{F} \,. \tag{6.35}$$

Instead, for what concerns τ_0 we have

$$\delta\tau_0 \simeq \tau_{z=2} \cdot \frac{1}{2}\frac{\delta F}{F} \ , \tag{6.36}$$

because, according to our simplifying assumption, $\delta F/Fa \approx 0$ for $z \leq 2$. In conclusion, using Eq.(6.31), and after some algebra, we get the shift in the acoustic peaks as a result of the time variation of the effective gravitational constant:

$$\frac{\delta l_{peaks}}{l_{peaks}} = \frac{l^{TEQ}_{peaks} - l^{Q}_{peaks}}{l^{Q}_{peaks}} \simeq \frac{1}{2}\frac{\delta F}{F}\left(\frac{\tau_{z=2}}{\tau_0} - 1\right) \ . \tag{6.37}$$

Numerically we find $\tau_{z=2}/\tau_0 \simeq 75\%$; also, we already mentioned that the change of the value of F during all the cosmological evolution can be written as $\delta F/F \simeq -8\pi\xi G\phi_0^2$. Therefore, for our specific model Eq.(6.37) becomes

$$\frac{\delta l_{peaks}}{l_{peaks}} \simeq \pi\xi G\phi_0^2 \ . \tag{6.38}$$

Note that, for our values of $\xi = \pm 1.5 \times 10^{-2}$, the above shift is at the level of $\pm 6 \times 10^{-3}$, which is in quite good agreement with the results plotted in the left panels of Fig.4, that is $\pm 5 \times 10^{-3}$.

This completes our description of the TEQ features on the CMB angular power spectrum. We now turn to the analysis of what happens in the matter power spectrum today.

6.3 Matter power-spectrum

In Fig.6.6 we plot the matter power spectrum for the same cases shown in Fig.6.5. We can immediately note differences regarding both amplitude and turnover position.

The Λ model has the highest spectrum. The main reason is the different growth of density perturbations [51]. In both Q and Λ models the perturbation growth is suppressed at low redshifts due to the domination of the vacuum energy, that tends to keep H constant therefore enhancing the cosmological friction in the perturbation equations, where almost everywhere the terms involving the first time derivatives of the perturbations appear multiplied by the Hubble parameter. In Q and TEQ models this effect is considerably enhanced due to the magnitude of H which is greater than in Λ models at all redshifts, and in particular at the lowest ones, as it is evident from Fig.6.3. Another independent cause that contributes to push the Q spectrum down with respect to the Λ model is the COBE normalization. In fact, we have seen that the ISW effect is enhanced in Q models with respect to Λ ones, and the normalization to COBE implies subtraction of power to the true amplitude of the primordial cosmological perturbations.

Let us come now to the difference between Q and TEQ models. The dynamics of the field at low redshifts is almost the same as in Q models, as it is evident again by looking at Fig.6.1. Thus, the reason for the difference is to be sought in the COBE normalization. Indeed, by looking at the low wavenumber region, which is the zone of non-processed scales, we see that the amplitude shift is roughly at 10% and -18% level for TEQ with respect to Q for negative and positive ξ, respectively; these numbers roughly agree with the ISW corrections that we estimated to come from the NMC terms in the previous section.

Let us come now to the evaluation of the peaks shifts. As it is known (see for example [51]), the scale of the matter power spectrum turnover is essentially given by the scale entering the Hubble horizon at the matter-radiation equivalence. The latter age is the same for all our models:

$$1 + z_{eq} = \frac{\rho_{m0}}{\rho_{r0}} \approx 5500 \ . \tag{6.39}$$

However, we must take care of what was the Hubble horizon at the equivalence, since the Hubble radius follows different dynamics in the three cases that we are treating. In other words, the shift in

the power spectrum turnover is given by

$$\frac{\delta k_{turn}}{k_{turn}} = -\left(\frac{\delta H^{-1}}{H^{-1}}\right)_{eq} . \tag{6.40}$$

In Fig.6.3 the different values of the Hubble horizon are displayed at the equivalence (bottom). The Hubble horizon shift in Eq.(6.40) between the Q and Λ model is at the 18% level, which corresponds well to the power spectrum shift that we see in Fig.6.6, where $\delta k_{turn}/k_{turn} \simeq -20\%$. The same reasoning applies to explain the slight shift of the TEQ spectra turnover with respect to the Q one. The Hubble horizon shift in Fig.6.3 for positive ξ is 2.6%, in good agreement with what we get in Fig.6.6, 2.3%; for negative ξ we get 1.7% from both figures.

We can give a rough analytical estimate of this effect by reasoning as follows. At the equivalence the Q energy density, both in Q and TEQ models, is negligible with respect to matter and radiation as it is evident in Fig.6.1. Eq.(4.5) takes the form

$$\mathcal{H}^2 \simeq \frac{\rho_{fluid}}{3F(\phi)} . \tag{6.41}$$

Since in our model $F(\phi)$ is smaller or larger than $F(\phi_0)$ if ξ is positive or negative, respectively, this implies that the Hubble length H^{-1} at the equivalence was different in TEQ models with respect to ordinary Q. The amount and the sign of the difference can be estimated roughly as follows: from Eq.(6.41) we have

$$\left(\frac{\delta H^2}{H^2}\right)_{eq} \simeq \left(\frac{2\delta H}{H}\right)_{eq} = 1 - 8\pi G \cdot F_{eq}(\phi_{eq}) . \tag{6.42}$$

Therefore, the matter power spectrum turnover shifts due to the NMC terms by the following amount:

$$\left(\frac{\delta k_{turn}}{k_{turn}}\right)_{NMC} = -\left(\frac{\delta H^{-1}}{H^{-1}}\right)_{eq} = \frac{1 - 8\pi G F_{eq}(\phi)}{2} \simeq 4\pi G \xi \phi_0^2 , \tag{6.43}$$

simply by taking $\phi_{eq} \ll \phi_0$ as it is today. In our models, the quantity in Eq.(6.43) is roughly 2%, which agrees quite well with the numbers we obtain.

As concerns the shape of the power spectrum, there is no significant difference between the Q and TEQ models, since this could arise only when the scalar field becomes important at low redshifts, where however the dynamics in the two scenarios is very similar.

6.4 Variations in the potential slope

Varying the power α in the potential (6.1) implies varying the dynamics of ρ_ϕ according to Eq.(6.20). For increasing slopes of the potential, we expect that the low redshift effects are enhanced correspondingly.

In Fig.6.7 we show tracking solutions for different exponents: dot-dashed line for $\alpha = 1$, solid for $\alpha = 2$, long-dashed for $\alpha = 3$. It can be immediately seen how the low redshift tracker branch possesses different slopes, according to Eq.(6.20). Moreover, the R-boost is the same for all the slopes, again according to the arguments made in Section II. But, for increasing α, the R-boost is abandoned earlier. The reason is the mechanism that stops the R-boost itself, i.e. the fact that the Q potential energy starts to dominate. But, this happens earlier for larger exponents in Eq.(6.1), since the potential is steeper for $\phi < \phi_0$.

Another important aspect that we must address is the Q equation of state, $w_\phi = p_\phi/\rho_\phi$, since this is a parameter that is quite well constrained by the observations to be less than -0.6 today [172, 183, 89, 69]. In fact, from Eq.(6.21) we see that small α makes the equation of state similar to the pure cosmological constant case. The actual value that we find numerically is slightly different from what Eq.(6.21) would predict, because today the tracker regime has been abandoned, since Q

has started to dominate the cosmic evolution. For $\alpha = 1, 2, 3$, we find $w_\phi = -0.75$, -0.60 and -0.49, respectively, for positive ξ, and $w_\phi = -0.78$, -0.66 -0.59, respectively, for negative ξ.

Next, let us see what happens in the CMB. Fig.6.8 shows the behavior of the CMB temperature (top) and polarization (bottom) spectra for the same values of α as in Fig.6.7; the left and right panels are for positive and negative ξ, respectively. Solid lines, both heavy and thin, refer to the same cases as in Fig.6.5; the dotted and dot-dashed lines describe models with $\alpha = 3$ and 1, respectively. As we mentioned above, the low redshift ISW effect is enhanced by increasing α, merely because the low redshift dynamics is enhanced, as it is evident from Eq.(6.26). This is a known effect since it does not involve the NMC terms directly, but instead is a characteristic feature of dynamical vacuum energy models [166, 37, 82, 221]. The acoustic peaks region is suppressed correspondingly, by an amount that is roughly increasing linearly with α, due to the COBE normalization at low ℓ's. However, as can be easily noted in Fig.6.8, the strength of this effect is larger for positive ξ as compared with negative values. The reason is that negative ξ values tend to decrease the ISW effect, as it is evident both in the effective potential (6.26) and in our estimate of Eq.(6.30). For what concerns the shift in the position of the acoustic peaks, the different potential mainly influences the low redshift tracking behavior, thus affecting mostly τ_0 in (6.31); since large α enhances the low redshift dynamics, the peaks shift increases correspondingly, again as evident in Fig.6.8.

In conclusion, the increased dynamics obtained by increasing α has the indirect effect of enhancing all the NMC effects. To see this, let us stress the part of the effects that come from genuine NMC terms. To this aim we build tracking solutions corresponding to those that we show in Fig.6.7, but for the ordinary Q case, and calculate the CMB spectra for them. We take the ratios Eq.(6.30), now valid for all the ℓ's,

$$\frac{\delta C_\ell}{C_\ell} = \frac{C_\ell^{TEQ} - C_\ell^Q}{C_\ell^Q} \,, \tag{6.44}$$

to quantify in detail the pure NMC effects in the spectra. These quantities, for the different values of α treated in this Section, are displayed as a function of the multipole ℓ in Fig.6.9, temperature (top) and polarization (bottom). The meaning of the curves is the same as in Fig.6.8. The effects are larger for increasing values of α. In the upper box we can note the large ISW effect due to the NMC component only: it reaches roughly 30% by itself. Correspondingly, due to the normalization at small ℓ's, the acoustic peaks region is suppressed or enhanced for positive or negative ξ, respectively, even up to the 50% level. The enhancement of these effects, in particular the ISW one, for increasing α in in agreement with our formula (6.30), since for increasing α the field reaches larger values today: namely, for $\alpha = 1, 2, 3$, we have $\phi_0 = 0.2, 0.35$ and 0.5 Planck masses for positive ξ, and similar values for negative ξ.

The same phenomenology obtained for the temperature anisotropies is found for the polarization (bottom panels); we will not plot the low ℓ's region, since even if the NMC effect is large, the absolute value of the polarization multipole moments is significantly high only around degree angular scales.

6.5 Conclusions

In this chapter, we focused on the role of a Non-Minimally Coupled scalar field as a candidate for the "missing energy " component. It should enter in the Lagrangian of the world as

$$\frac{R}{16\pi G} + \xi\left(\phi^2 - \phi_0^2\right)\frac{R}{2} \,, \tag{6.45}$$

where ξ is a dimensionless coupling constant, ϕ is the Quintessence field, also indicated by Q, and ϕ_0 is its value today.

As a first step, we investigated the cosmological trajectories in this scenario, focusing on the redshift evolution of the Q energy density. The Q potential is modeled as an inverse power law, namely $V(\phi) = M^{4+\alpha}/\phi^\alpha$, where $\alpha > 0$ and M is the energy scale chosen to have the amount of Q energy today.

In the radiation dominated era we find that the divergence of R at early times generates an effective gravitational potential in the Klein Gordon equation, which drives the Q evolution in a sort of gravitational slow rolling. We named this era R-boost. The dominant component in ρ_ϕ during this epoch is the kinetic component. The R-boost ends when this kinetic energy becomes comparable with the true potential energy: we have estimated that this time corresponds to a redshift $1 + z_{pot} \simeq 3000$, i.e. the R-boost lasts also for the earliest part of the matter dominated era.

In the matter dominated era we obtained scaling solutions in NMC theories, which extend the validity of those studied in [220], for which ρ_ϕ and the Q pressure p_ϕ scale as follows:

$$\rho_\phi = \rho_{Q0} \left(\frac{a_0}{a}\right)^\epsilon \quad , \quad \epsilon = \frac{3\alpha}{\alpha + 2} \quad , \quad p_\phi = -\rho_\phi \frac{2}{\alpha + 2} \, . \tag{6.46}$$

This regime holds for almost all low redshifts, $1 + z \leq 100$. At recent times, however, $1 + z \leq 3$, the Quintessence component starts to dominate and the expansion accelerates.

These results show that the Extended Quintessence is a tracker field, in the sense of the original works on Quintessence tracker solutions [178, 206]. While the Quintessence potential energy density has to be chosen to produce the observed Ω_ϕ today, just as if Q was ordinary cosmological constant, the initial amount of ρ_ϕ can vary over a very wide range, covering more than 20 orders of magnitude.

We also investigate perturbation spectra in TEQ. The tracker dynamics imprints considerably larger effects compared with ordinary Tracking Quintessence and the cosmological constant, both on CMB and LSS. We gave quite accurate analytical formulas to describe these effects, that we summarize here.

We have shown that in TEQ models the low redshift dynamics of the field is either increased or decreased depending on whether ξ is positive or negative, respectively. This leaves its imprints on the large scale CMB angular power spectrum, where the signal is unprocessed by acoustic oscillations, and is affected by the dynamics of the gravitational potential (Integrated Sachs Wolfe effect, ISW). We derived a simple formula describing this effect, that allows us to compare the TEW effect on the CMB with the hypothetical effect of "ordinary" (minimally coupled) Quintessence; it has been possible to evaluate an effect running from 10 to 50% of that of a standard Q, as the potential slope α increases from 1 to 3. Note that for negative ξ the ISW is inverted, a feature that is quite unusual in Quintessence models.

The amplitude of the acoustic peaks varies because of the same ISW effect, if the overall power is normalized to COBE at $\ell = 10$. There exists also another mechanism that changes the acoustic peak amplitude, which occurs at decoupling rather than at low redshift. The Hubble horizon value at a given redshift is different in Extended vs. ordinary Quintessence models, as already noticed in [174]. This is because in order to reach the same value today the Hubble parameter followed a different dynamics in the past; we have shown here that the horizon reentry for a given comoving scale is delayed for positive ξ and anticipated for negative ξ. This implies a slight suppression of the acoustic oscillations in the first case, and an enhancement in the second, as a consequence of the different amounts of CDM when the baryon and photon densities are oscillating.

TEQ imprints also affect the position of the acoustic peaks. The angular multipoles at which CMB acoustic oscillations are occurring are inversely proportional to the comoving size of the CMB sound horizon at decoupling, proportional to τ_{dec}, and directly proportional to the comoving distance between last scattering and us, $\tau_0 - \tau_{dec}$. Both these quantities are affected by the TEQ dynamics. The CMB sound horizon is proportional to the Hubble horizon at decoupling, which, as we just mentioned is different in the various models. The comoving distance between last scattering and us is also affected by the TEQ low-redshift dynamics. We derived an analytical formula giving the shift in the positions of the acoustic peaks, towards smaller or larger angular scales.

For what concerns the LSS effects today, the first point to make is that since at the COBE scales, where we normalize our models, the CMB spectrum is affected by the ISW, the amplitude of perturbations on LSS scales is suppressed if $\xi > 0$ and increased if $\xi < 0$, by an amount that is approximately the opposite of the quantity in Eq.(6.30). Second, the turnover scale position k_{turn} is shifted, being inversely proportional to the Hubble horizon at the equivalence. The size of this effect

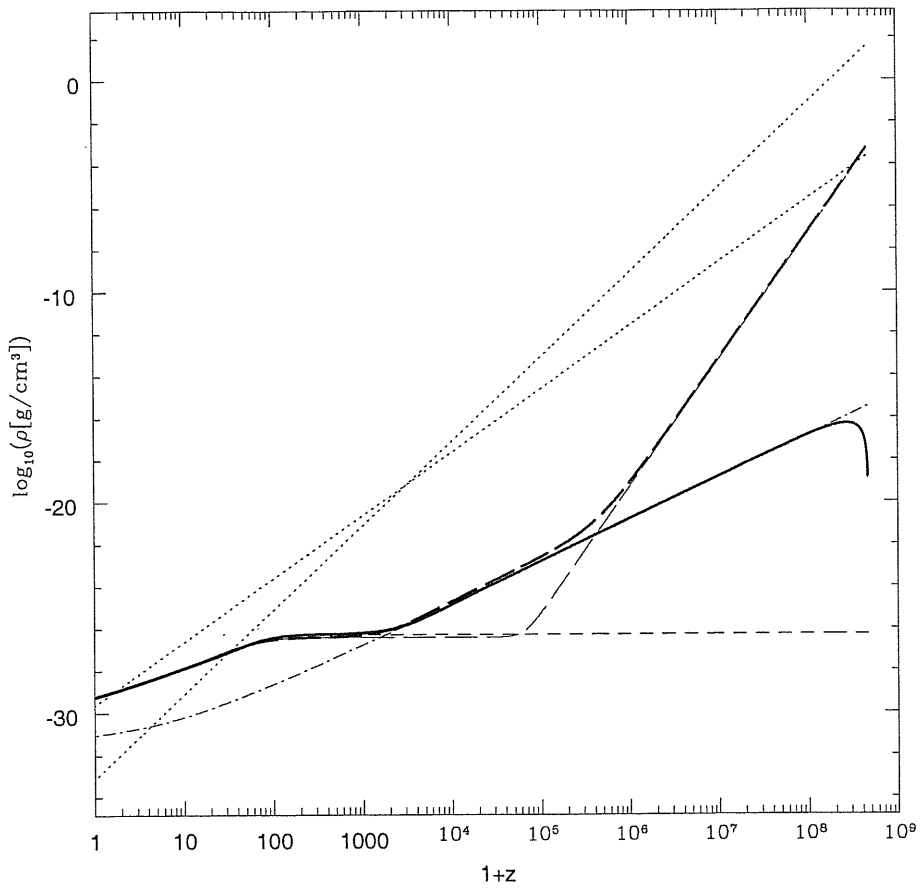

Figure 6.1: Matter, radiation, Quintessence energy densities as functions of redshift. Dotted lines: matter and radiation; heavy solid: Tracking Extended Quintessence; thin dashed: tracking minimally coupled Quintessence; heavy dashed: initially highly energetic Tracking Extended Quintessence; thin long-dashed initially highly energetic tracking Quintessence; dot-dashed: R-boost analytic.

can be simply estimated by the Friedmann equation, and it turns out to be sensitive to the tracking behaviour of the scalar field.

CMB anisotropies have been shown here to be considerably affected by the dynamical properties of the vacuum energy and by the Non-Minimal Coupling terms present in the Lagrangian. This is an important novelty in the literature on Quintessence models, which deserves as much attention as the dependence of the CMB spectra on the kind of dark matter, value of the primordial perturbation spectral index, etc.. This is made possible by the fact that the CMB itself is more than a snapshot of the early universe; its properties in fact are also determined by a line-of-sight integration over a very long part of the cosmic evolution, which is then able to tell us about the time variation of the gravitational constant and the dynamics of the vacuum energy.

With higher and higher accuracy achieved in CMB data, going from the encouraging present-day ones [60, 101] to the anticipated formidable performance of the Microwave Anisotropy Probe and Planck mission [151], we will be able to obtain exciting new insights into the structure of gravity as well as the nature of the vacuum energy.

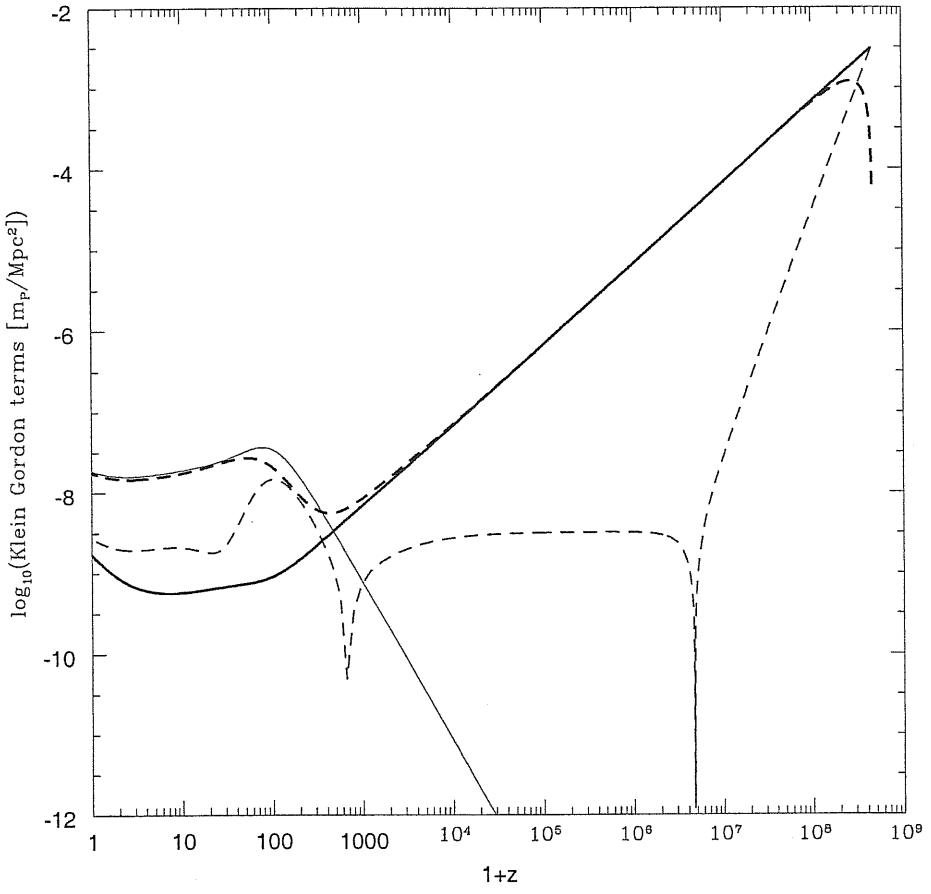

Figure 6.2: Absolute value of the Klein Gordon equation terms: heavy solid: gravitational effective potential; heavy dashed: friction; solid: potential; dashed: acceleration.

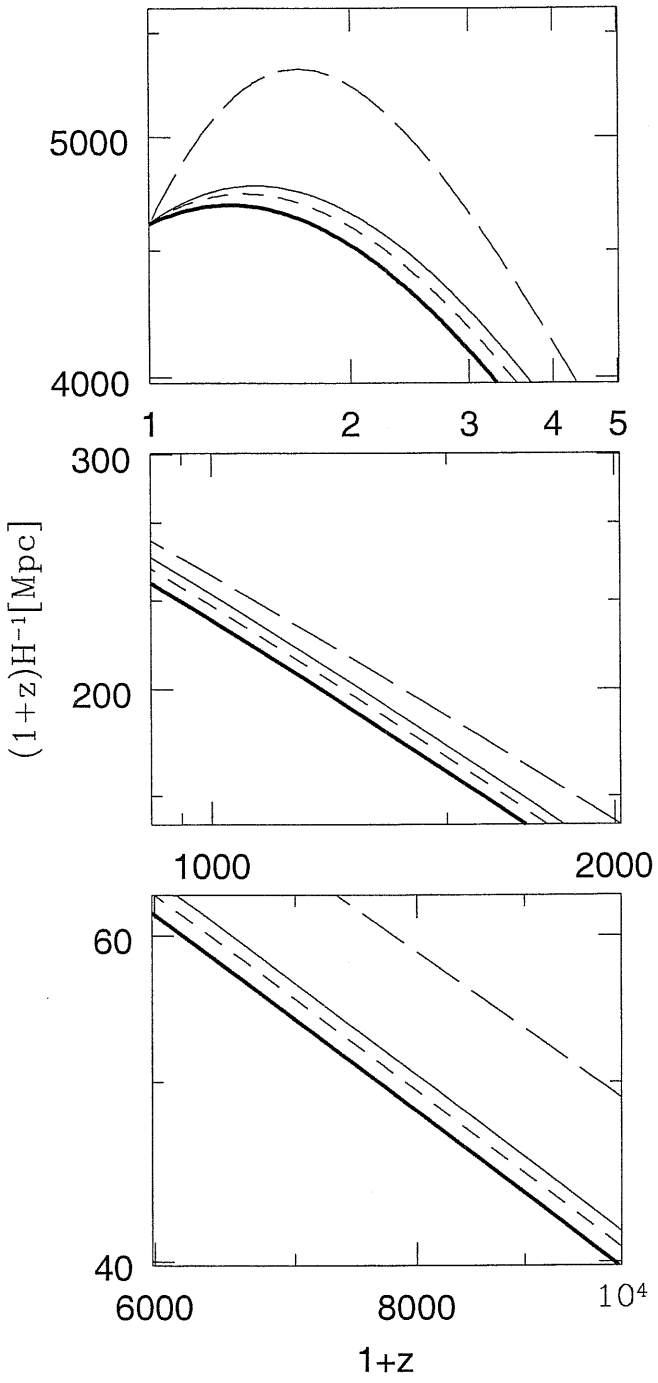

Figure 6.3: Snapshots of conformal Hubble horizon evolution. heavy solid: Tracking Extended Quintessence with positive ξ; short dashed: tracking minimally coupled Quintessence; thin solid: Tracking Extended Quintessence with negative ξ; long dashed: cosmological constant. Top: present; middle: decoupling; bottom: equivalence.

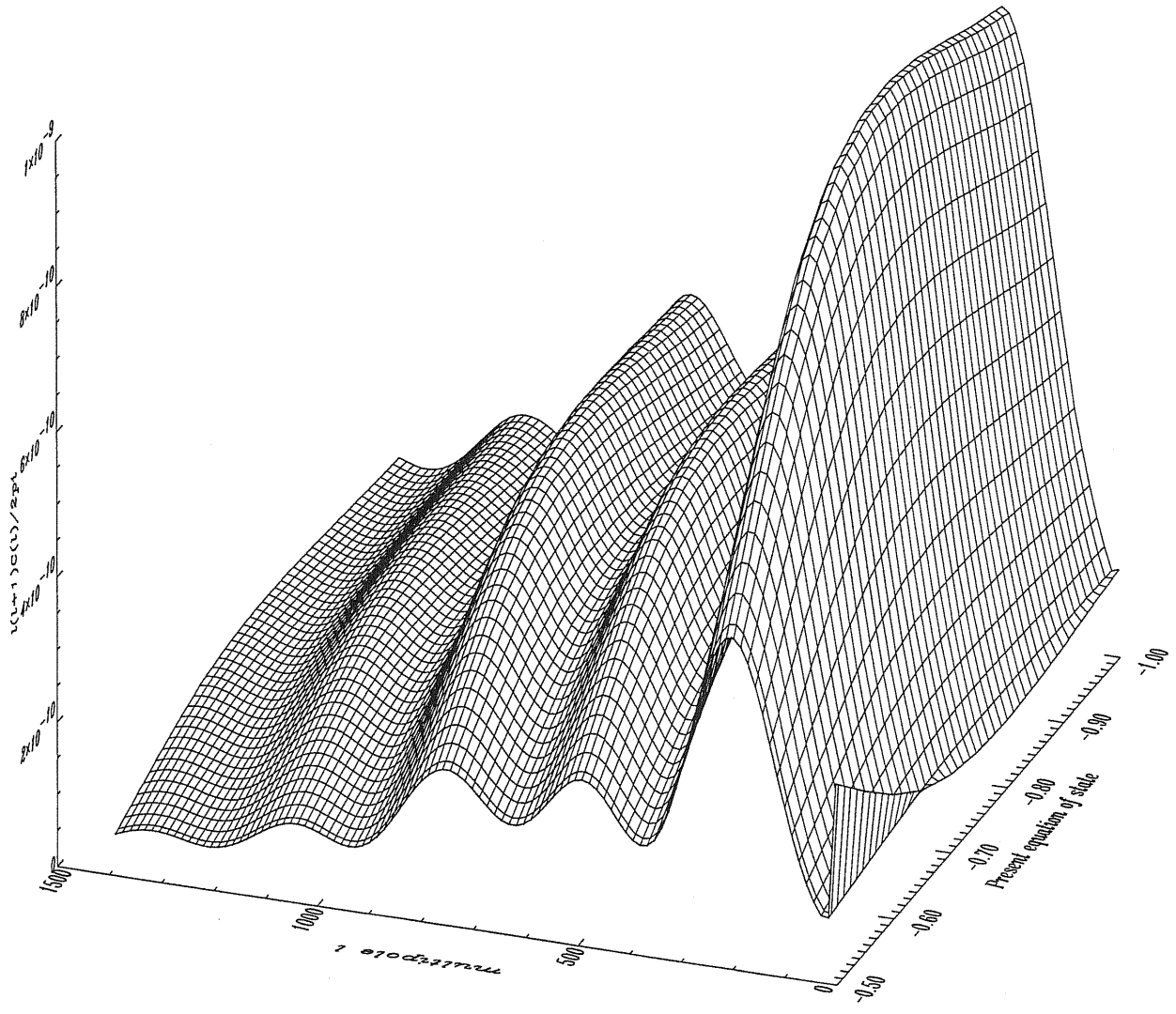

Figure 6.4: CMB angular power spectra for minimally-coupled ($\xi = 0$) quintessence with $\Omega_\phi = 0.7$. The power in the C_ℓ is plotted vs. the multipoles and the equation of state of the scalar field. The cosmological constant is recovered at $w_\phi = -1$.

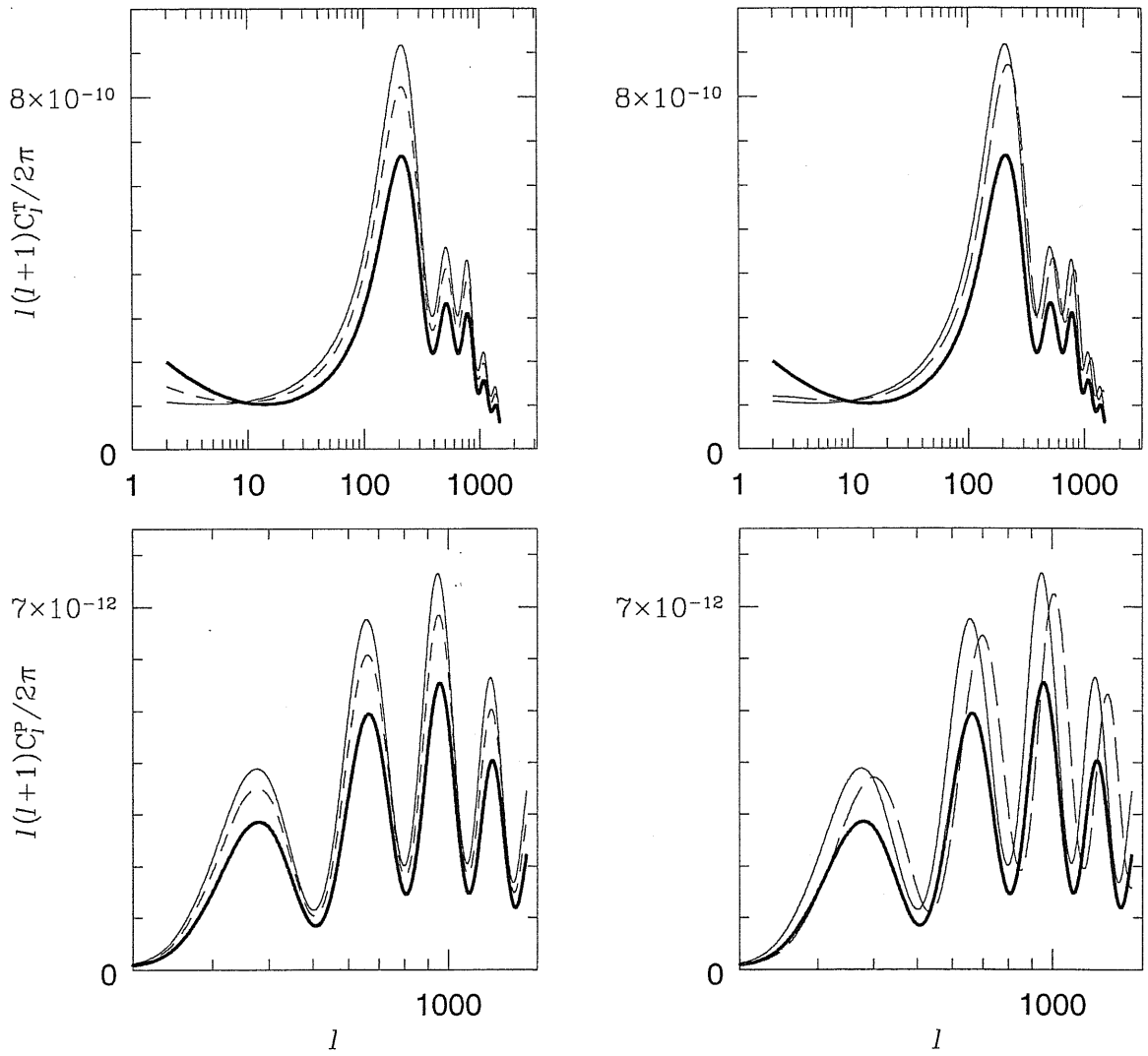

Figure 6.5: CMB angular power spectra. Top: temperature; bottom: polarization. Heavy solid: Tracking Extended Quintessence, positive ξ; thin solid: Tracking Extended Quintessence, negative ξ; short dashed: minimally coupled tracking Quintessence; long dashed: cosmological constant.

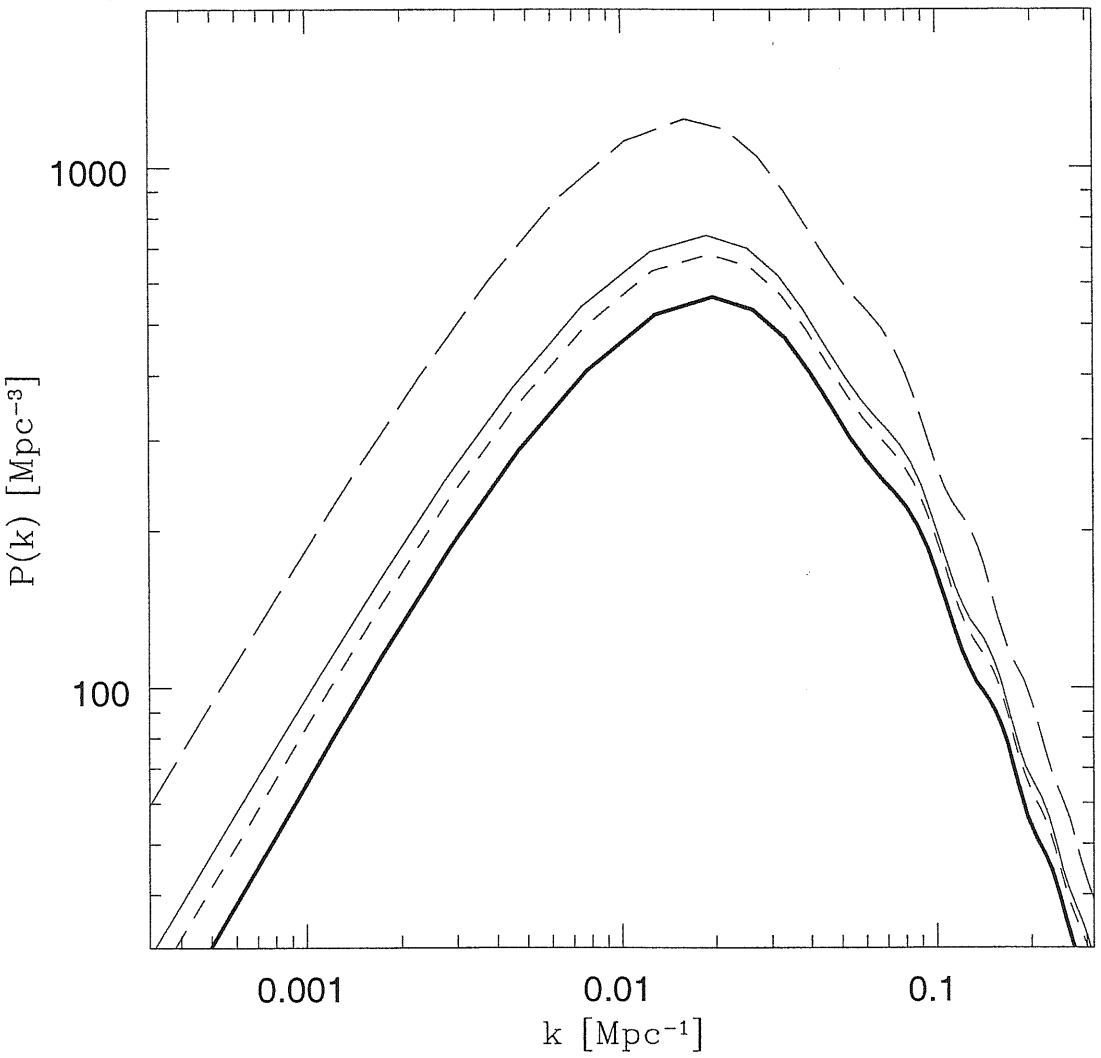

Figure 6.6: Present matter power spectra. Heavy solid: Tracking Extended Quintessence, positive ξ; thin solid: Tracking Extended Quintessence, negative ξ; short dashed: minimally coupled tracking Quintessence; long dashed: cosmological constant.

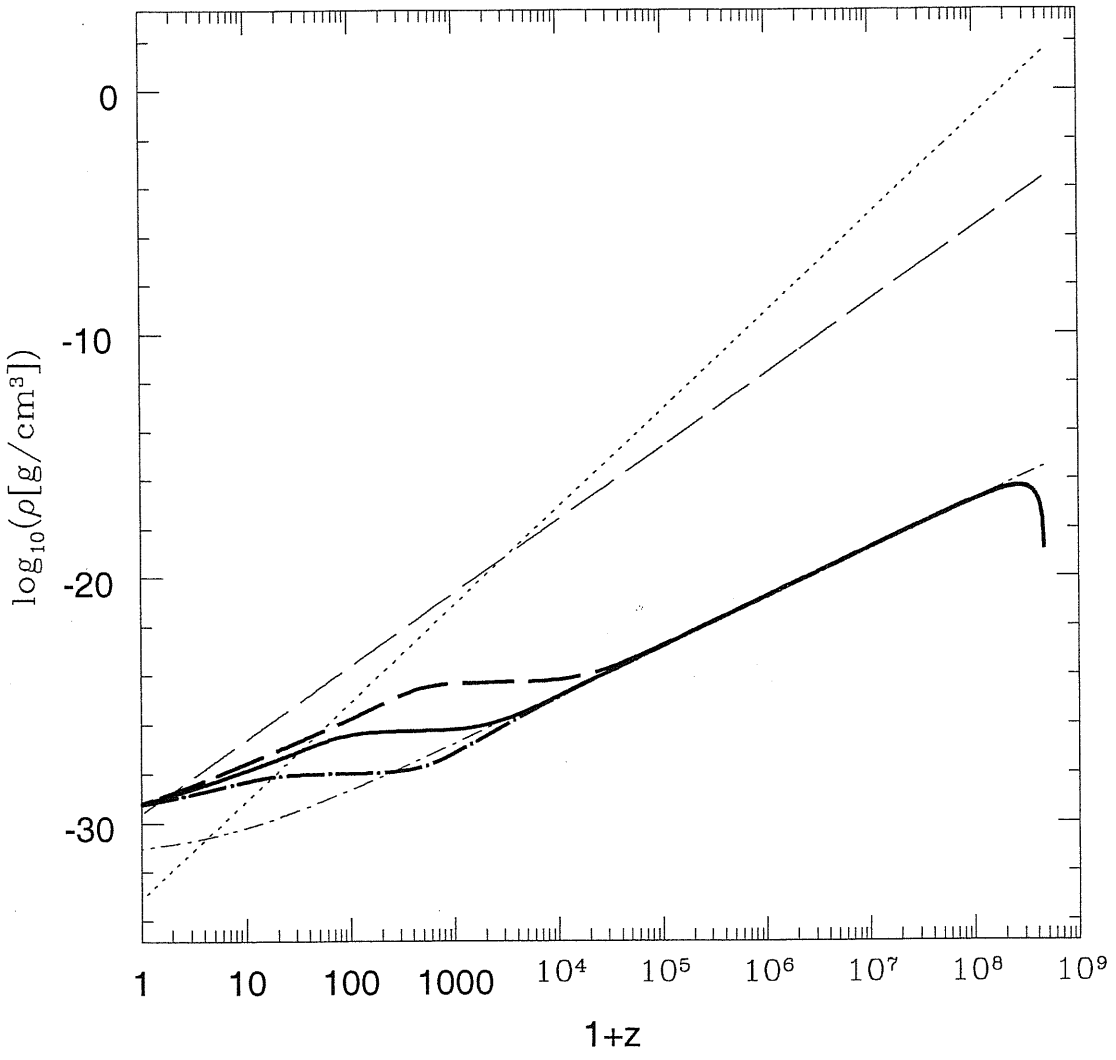

Figure 6.7: Matter, radiation and Quintessence energy densities for different potential slopes. Long dashed: matter; short dashed: radiation; heavy solid: Tracking Extended Quintessence, $\alpha = 2$; heavy dotted dashed: Tracking Extended Quintessence, $\alpha = 1$; heavy long dashed: Tracking Extended Quintessence, $\alpha = 3$.

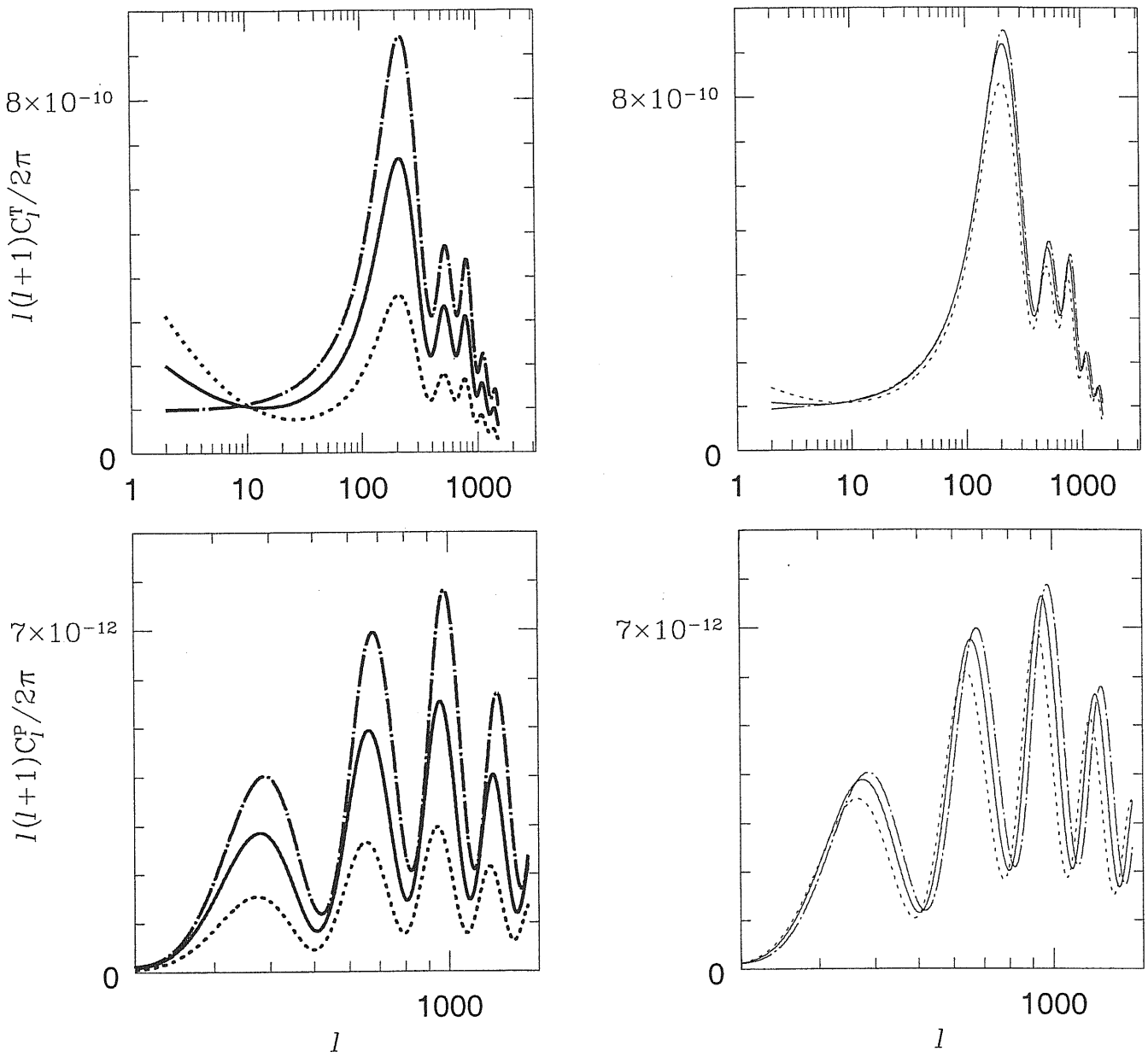

Figure 6.8: CMB angular power spectra for different potential slopes. Left (right): positive (negative) ξ. Solid: Tracking Extended Quintessence, $\alpha = 2$; dotted dashed: Tracking Extended Quintessence, $\alpha = 1$; short dashed: Tracking Extended Quintessence, $\alpha = 3$.

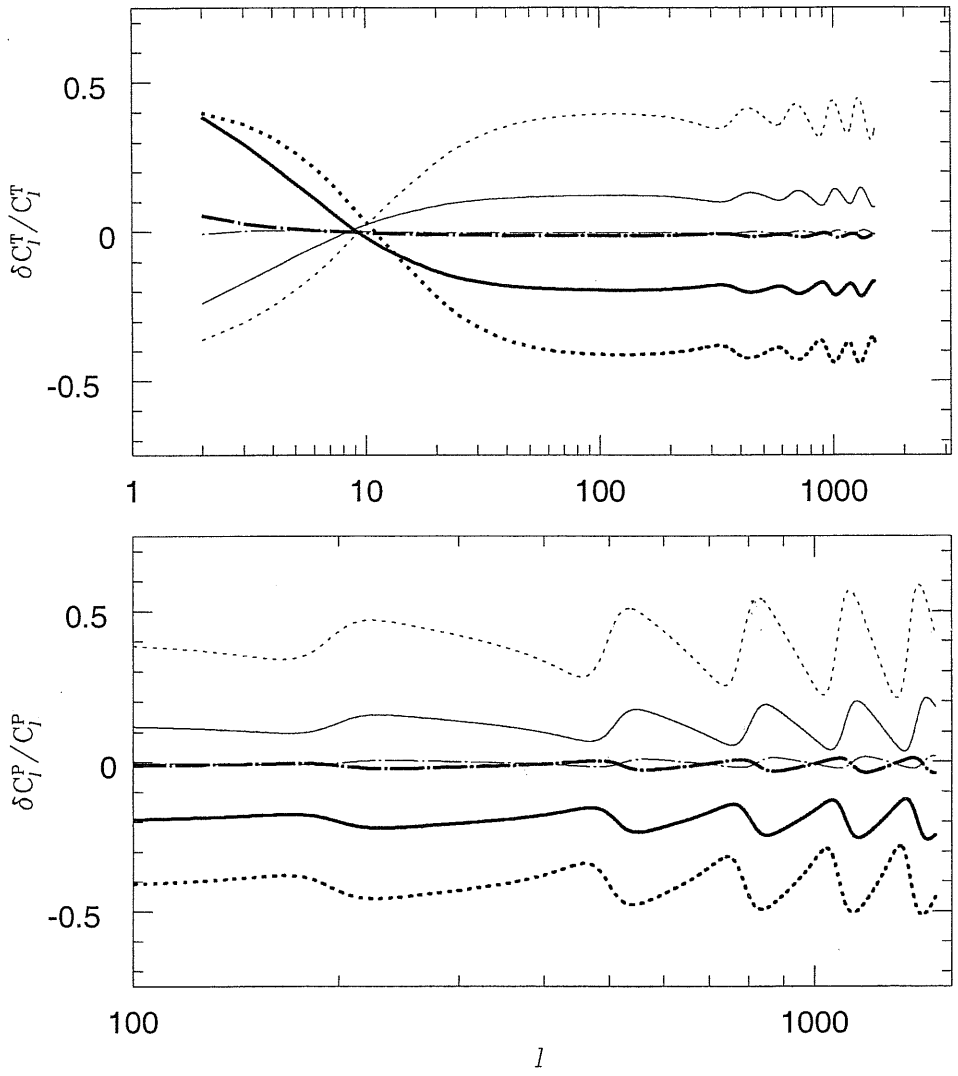

Figure 6.9: CMB angular power spectra: relative difference between Tracking Extended Quintessence and ordinary tracking Quintessence spectra ($\delta C_\ell/C_\ell = C_\ell^{TEQ}/C_\ell^Q - 1$) as a function of the inverse power of ϕ in the potential. Top (bottom): temperature (polarization); thick (thin) lines for positive (negative) ξ. Solid: extended vs. ordinary tracking Quintessence, $\alpha = 2$; dotted dashed for $\alpha = 1$, short dashed for $\alpha = 3$.

Chapter 7

Summary and conclusions

The main thread of the work presented in this thesis in the investigation of cosmological models involving a scalar field as a candidate for the "missing energy". Such scalar field, often called "quintessence", is proposed as an alternative to the cosmological constant scenario, which still retain many unsolved theoretical difficulties.
The motivation for such investigation mainly arises from the observed magnitude-redshift relation of type 1A supernovae, that recently opened the case for an accelerating universe.
In this thesis, we introduced quintessence scenarios by resuming, in chapter 1, the observational case for a substantial vacuum energy component.

In order to accelerate the overall expansion, it is generally sufficient that the equation of state of the dominant energy component is $w_{\rm vacuum} \lesssim -\frac{2}{3}$ at the present time: therefore, the scalar field proposed as a quintessence component can be described both by its energy density and negative pressure, related to the shape of the potential in which we assume the field evolves, or by an appropriate equation of state $-1 \lesssim w_{\rm vacuum} \lesssim -\frac{2}{3}$, given by the pressure/density ratio.
A key difference between the proposed quintessence scenarios and the cosmological constant, is that a scalar field evolves dynamically: therefore, in order to not violate the equivalence principle of General Relativity, a scalar field develops fluctuations, since the notion of a smooth component is gauge-dependent.
Therefore, we described in chapter 2 the formalism necessary for the description of perturbation evolution in General Relativity. Though the definition of most important quantities is given in a gauge-invariant formalism, the equations of interest are explicitly written in specific gauges, which is necessary for the development of the present work.

In most quintessence scenarios, the "missing energy" component is described as an ultra-light self-interacting scalar field, i.e. the scalar field is assumed to interact only gravitationally with matter. Furthermore, since a scalar field is too much relativistic to cluster on subhorizon scales, it can only influence the history of the universe through its dynamical effects on the background expansion, as well as on the perturbation growth. The effects of a "dynamical" vacuum energy component can be seek in the features of the observed CMB anisotropies; the relic radiation from the Big Bang is detectable as the photons that are reaching us today, after having propagated from the last scattering surface at redshift $z \sim 1000$. In their trajectories to us, the CMB photons are influenced by the geometry and the thermal history of the universe, so that it is possible to characterize the imprint that a quintessence component leaved on the last scattering surface by means of its geometrical and projection properties. Since primordial anisotropies are the seeds from which structures grew, the effect of a dynamical vacuum energy is also imprinted in the overall structure formation history, and is plausibly depicted in the present matter power spectrum.

In chapter 3, we described the main features of the Cosmic Microwave Background temperature and polarization anisotropies, and the physical mechanisms that gave rise to them.
In order to predict the CMB anisotropies spectra that a quintessence scenario would produce, a numerical machinery is needed. The numerical code produced by the author of this thesis, in collaboration with Carlo Baccigalupi, requires to specify initial conditions for the perturbations of the

various components of the cosmic fluid. We didn't face the problem of the *generation* mechanism for the perturbations: we simply assume that they are present after an inflationary period, needed to solve the horizon and flatness problems. In our treatment, the starting time doesn't coincides with the initial singularity associated to the Big Bang; rather, we consider initial conditions soon after the inflationary expansion, after the Universe reheated. The quintessence scalar field doesn't necessarily coincides with the inflaton field: it just survives inflation, participating to the initial conditions on the fluid, that hold deep in the radiation era, when all the scales of cosmological interest are well outside the horizon. Even if a general perturbation needs not to be purely adiabatic either isocurvature, the two situations can be studied separately: the introduction of a scalar field changes the standard scenarios, properly because a new component should participate in the correct distribution of energy between the fluid parts.

In the fourth chapter of this thesis, we analytically derived, in the synchronous and Newtonian gauges, the conditions that the scalar field perturbations should obey in order to result in adiabatic or entropy perturbations. In particular, in the isocurvature case, we considered models in which the initial perturbation arises from the matter as well as from the scalar field itself, provided that the initial value of the gauge invariant curvature is zero. Starting from these initial conditions, we evolved the background equations and the linearized Einstein equations, obtaining the signatures of a minimally coupled scalar field on the CMB anisotropies power spectrum. The so-obtained spectra have been compared with the standard Cold Dark Matter (CDM) model; it turned out that the acoustic peaks follow opposite behaviours in the adiabatic and isocurvature regimes: in the first case their amplitude is higher than in the corresponding pure CDM, while they make the opposite thing for pure isocurvature initial perturbations. The interpretation of these results has been discussed in terms of the effects that the introduction of a scalar field has on the matter/radiation ratio at recombination, since it turned out that the scalar field itself is not directly appreciable at very high redshifts.
The numerical integration allowed to obtain the time evolution of the entropy perturbations, of the curvature perturbation and of the gravitational potential, and a further comparison with the pure CDM model. Most of the differences arise because, in Quintessence models, the epoch of matter-radiation equality is shifted closer to the present when compared to the Einstein-De Sitter case. We showed as the hypothesis of a cosmic vacuum energy stored in the potential of a minimally-coupled scalar field enlarges naturally the possibility to gain insight into high energy physics from the traces left in the cosmic radiation and in the matter distribution.

However, restricting ourselves to scalar fields as candidates for the "dark energy", it is clear that a minimally coupled scalar field is not the most general possible field in which the eventual "vacuum energy" could reside. In the context of generalized Einstein gravity theories, it is possible to consider an explicit coupling between the scalar field, modeling the Quintessence component, and the Ricci scalar R in the gravitational sector of the Lagrangian of the system. We named such models 'Extended Quintessence', in analogy with the 'extended inflation' models where a Jordan-Brans-Dicke scalar field was added to the action to solve the 'graceful exit' problem of 'old inflation'.
'Extended Quintessence' cosmologies have the appealing feature that the same field causing the time (and space) variation of the cosmological constant is also the source of a time variation of the Newton's constant, as in the Jordan-Brans-Dicke theory.
We investigated two classes of models, in which the gravitational sector of the Lagrangian is $F(\phi)R$ with $F(\phi) = \xi\phi^2$ (Induced Gravity, IG) and $F(\phi) = 1 + \xi\phi^2$ (Non-Minimal Coupling, NMC), respectively.
In both classes, the potential of the scalar field has been chosen as simple inverse-power; we derived the corresponding constraints on ξ that satisfy the existing solar system experimental constraints. Using linear perturbation theory we then obtained the polarization and temperature anisotropy spectra of the Cosmic Microwave Background (CMB) as well as the matter power-spectrum.
The perturbation behavior possesses distinctive features, that we named 'QR-effects': the effective potential arising from the coupling with R adds to the true scalar field potential, altering the cosmic equation of state and enhancing the Integrated Sachs-Wolfe effect. As a consequence, part of the CMB anisotropy level on COBE scales is due to the latter effect, and the cosmological perturbation ampli-

tude on smaller scales, including the oscillating region of the CMB spectrum, has reduced power; this effect is evident on CMB polarization and temperature fluctuations, as well as on the matter power-spectrum today. Moreover, the acoustic peaks and the spectrum turnover are displaced to smaller scales, compared to ordinary Quintessence models, because of the faster growth of the Hubble length, which - for a fixed value today - delays the horizon crossing of scales larger than the horizon wavelength at matter-radiation equality and slightly decrease the amplitude of the acoustic oscillations.
The existence of a considerable amount of vacuum energy in the Universe, as observations seem to imply, brings together two fundamental problems, the "coincidence" problem and the "fine tuning" one. Contrarily to the cosmological constant, Quintessence scenarios can avoid the fine tuning problem: in particular, the Quintessence could have been initially at the level of the ordinary matter. In chapter 6, we extended the tracking phenomenology to non-minimally coupled scalar fields; it turned out that tracker solutions for these models, with inverse-power law potentials, possess an initial enhancement of the scalar field dynamics, named 'R-boost', caused by the effective potential generated by the presence of the Ricci scalar in the equation of motion of the field. After the initial gravitational boost, the field slowly evolves until the true potential becomes dominant. An accurate analytic formula, describing the scaling of the field energy density during the R-boost, has been given. At the end of the R-boost phase, the field trajectories matches the tracker solution in minimally coupled theories.
We analytically obtained the scaling solutions in the matter dominated era, extending the validity of those studied previously for theories without any coupling with the Ricci scalar.
We have shown that in tracking Extended Quintessence models the low redshift dynamics of the field is either increased or decreased depending on whether ξ is positive or negative, respectively. This leaves its imprints on the large scale CMB angular power spectrum, where the signal is unprocessed by the acoustic oscillations of the photon-baryon fluid before recombination, and is affected by the dynamics of the gravitational potential (Integrated Sachs Wolfe effect, ISW) at low redshifts.
In the context of linear perturbation theory, we integrated the full set of the equations for the evolution of linear fluctuations in scalar-tensor theories of gravity, assuming Gaussian scale-invariant initial perturbations. The Integrated Sachs Wolfe effect on the CMB angular spectrum causes a change in the spectrum amplitude at $\ell \leq 10$ as compared to the standard (minimally coupled) Quintessence. Furthermore, we showed that the ISW effect is sensitive to the sign of the coupling constant, so that the peaks amplitude in the CMB spectrum, compared to the simplest Quintessence models, changes in the opposite way for opposite sign of the coupling constant.
Besides the ISW effect, that influences also the peak amplitude through the normalization, the horizon cross for a given scale is delayed (anticipated) for positive (negative) values of the coupling constant, and the Hubble horizon at recombination changes correspondingly. This results in a shift in the location of the acoustic peaks, which we described analytically, towards smaller or larger scales depending on the sign of the coupling constant.
We showed that even large scale structure is sensitive to the coupling of the field to the Ricci scalar, in that the location of the turnover scale in the matter power spectrum is shifted by an amount that depends on the value of the Hubble constant at the matter-radiation equality, and, ultimately, on the value and sign of the coupling constant.
In this thesis, CMB anisotropies have been shown to be considerably affected by the dynamical properties of the vacuum energy and by the Non-Minimal Coupling terms that could be present in the Lagrangian. This is an important characteristic related to the fact that the CMB itself is more than a snapshot of the early universe; the features that we can observe today are are also determined by a line-of-sight integration over a very long part of the cosmic evolution, when the photon free-streamed towards us affected by the evolution of the gravitational potentials. For this reason, we expect that future high-precision measurements of the CMB anisotropies will reveal us much about the time variation of the gravitational constant and the dynamics of the vacuum energy, helping to highlight the nature of the vacuum energy that is pushing the universe in an accelerated expansion phase.

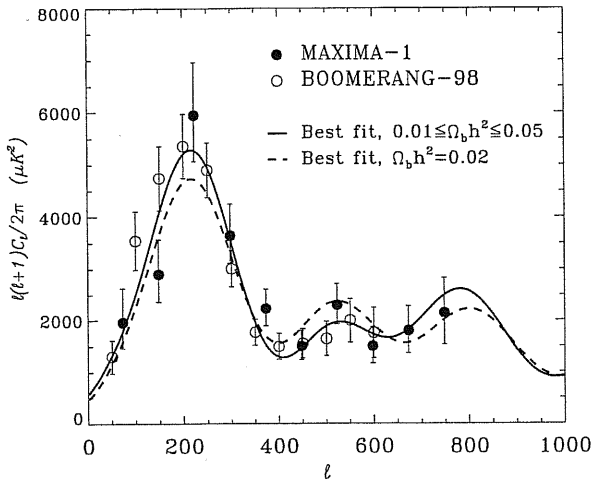

Figure 7.1: Data points used in the analysis. The curves correspond to the spectra predicted from quintessence models which best fit the combined data. The continuous line, obtained by marginalizing the likelihood over $\Omega_b h^2$, corresponds to $\Omega_\phi = 0.5$, $w_\phi = -0.75$ and $\Omega_b h^2 = 0.03$, while the dashed line is obtained by fixing $\Omega_b h^2$ at the Big Bang Nucleosynthesis value 0.02.

7.1 Observations and future perspectives

As shown in this thesis, the CMB anisotropy is powerful tool to discriminate between cosmological models, even including quintessence. The recent results from the first flight of the MAXIMA experiment [101] and from the long duration Antarctic flight of BOOMERANG (BOOMERANG-98, [60]) are in good agreement and have already been used to constrain a suite of cosmological parameters within the class of inflationary adiabatic models [118, 14, 138]. As seen in chapter I, these results strongly support a universe with a density very close to critical, making the case for a dark energy even stronger as these data are joined with those from large scale structure. In [15], a Bayesian likelihood analysis of data from MAXIMA and BOOMERANG-98 has been performed in order to see the implications on Quintessence models. This analysis applies to a minimally-coupled scalar field, described by its present equation of state w_ϕ and its energy density in units of the critical energy density today, Ω_ϕ. In [15], the attention is restricted to the simplest case of quintessence potentials having an inverse power-law form $V \propto \phi^{-\alpha}$, where α is related to the equation of state through eq. 6.21 in the tracking regime.

To rule out models in the 2-dimensional space of scalar field parameters (Ω_ϕ, w_ϕ), the probability distribution of these parameters has estimated by evaluating the likelihood of the data. The analysis is restricted to inflationary adiabatic models with a flat geometry and a scale-invariant spectrum of primordial fluctuations, neglecting reionization and without taking into account any massive neutrinos and gravitational waves.

The Hubble constant has been fixed at $H_0 = 65$ km s^{-1}Mpc^{-1}, while the physical baryon density $\Omega_b h^2$ is assumed to vary in the range $0.01 \leq \Omega_b h^2 \leq 0.05$: the results in [15] were obtained by marginalizing (integrating) the likelihood over $\Omega_b h^2$.

In fig. 7.1 the data points used in the analysis are shown, together with the best fitting spectra from quintessence models; the latter are obtained by marginalizing the likelihood over $\Omega_b h^2$ (solid line), or fixing it to the the Big Bang nucleosynthesis value $\Omega_b h^2 = 0.02$ (dashed line).

The best fit to data is given by a model with $\Omega_\phi = 0.5$, $w_\phi = -0.75$, $\Omega_b h^2 = 0.03$. Quite independently on the value of $\Omega_b h^2$, it turns out that pure cosmological constant models, although compatible with the CMB data used in [15], are slightly disfavored as compared with quintessence models; the likelihood contours in the $\Omega_\phi - w_\phi$ plane, plotted in fig. 7.1 give $-1 \leq w_\phi \leq -0.75$ and $0.35 \leq \Omega_\phi \leq 0.60$, at 1σ confidence level.

Obviously, we are not yet in the position to severely constrain quintessence parameters from pure CMB observations, nor to discard the cosmological constant in favor of quintessence, on observational grounds. In particular, it has been shown [115] that even an ideal, full-sky cosmic microwave background anisotropy experiment may not be able to remove the degeneracy between the two. The

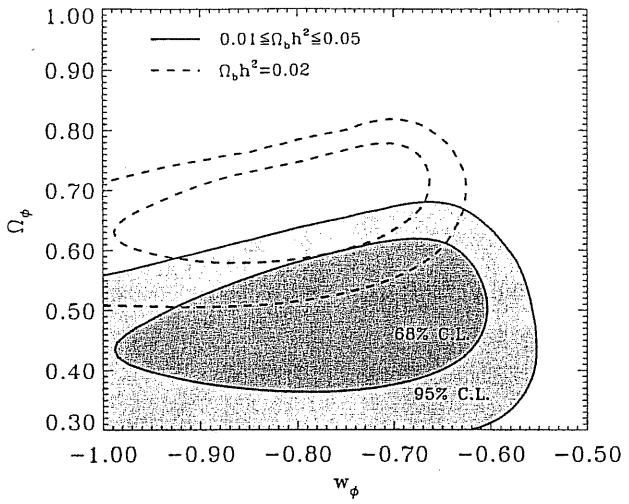

Figure 7.2: Likelihood contours at 68 % and 95% confidence level in the $\Omega_\phi - w_\phi$ plane. The shaded regions are obtained marginalizing over $\Omega_b h^2$ in the range $0.01 \leq \Omega_b h^2 \leq 0.05$. For comparison, the dashed contours show the bounds obtained imposing the BBN value $\Omega_b h^2 = 0.02$.

degeneracy problem between Λ and quintessence arises for a wide range of potentials and initial conditions; furthermore, degeneracy may remain even after considering classical cosmological tests and measurements of large scale structure. The degeneracy problem placed the accent on the necessity of combining various independent measures of the cosmological parameters; in particular, it will be important to probe the anisotropies in the CMB up to smaller angular scales and, most importantly, with increasing accuracy.

Plausibly, more information will be gained with future experiments, which will culminate with the Planck ESA's mission. It is now planned to launch Planck satellite in the first quarter of 2007. Planck satellite will carry on a telescope with an aperture of 1.5 m, which is designed to image the anisotropies of the CMB over the whole sky, with unprecedented sensitivity (temperature fluctuations will be determined with a precision of $\sim$ 2 parts in a million) and angular resolution $\sim 10'$, together with a very wide frequency coverage in order to remove foregrounds (see [9] for a recent method developed for the foreground removal). In fact, thanks to the receivers on board, the Low Frequency Instrument (LFI, tuned radio receiver array operated at 20K) and the High Frequency Instrument (HFI, 100 - 850 GHz bolometer arrays operated at 0.1K), Planck will produce calibrated maps of the whole sky on 10 frequency channels, running from 30 to 857 GHz.

In Fig. 7.1, the angular resolution of Planck is compared with COBE resolution: the same pattern of the CMB anisotropy is observed at the COBE/DMR (upper panel) and Planck (lower panel) resolution. The frequency channels of the two Instruments have FWHM running from $33'$ (for the lowest frequency channel at 30 GHz) to $4.5'$ (for the highest a7 857 GHz). The channels at 70 and 100 GHz are optimal to get the cleanest possible view of primordial CMB fluctuations: at 100 GHz, the LFI reaches an angular resolution of $10'$, allowing to determine the CMB power spectrum up to multipoles $l \simeq 1000$. Polarization measurements will be possible with an accuracy of a few μK, providing an independent estimate of the cosmological parameters and helping in removing the degeneracies.

Galactic emission, dominating the astrophysical foreground noise on scale $\leq 30'$, is minimum around 60 GHz; the noise due to extragalactic sources, dominating on smaller angular scales, is minimum in the range 100 – 200 GHz, where it is primarily due to radio sources. A combination of data from all LFI channels will allow an accurate subtraction of contaminating foreground signals; the removal of Galactic dust emission will be further improved using maps produced at higher frequencies by HFI. Besides the "primary science", i.e. the study of the CMB itself, the multifrequency maps will also allow to perform an accurate "secondary" science, relative to the study of the contaminating sources of radiation, such as Galactic and extragalactic emissions; the accurately calibrated maps of Galactic synchrotron and free-free will constitute a unique tool for investigating the distribution of the interstellar magnetic field, the relativistic electrons and the ionized components of the interstellar medium. At this point, it should be clear that Planck's CMB observations will provide a major source of in-

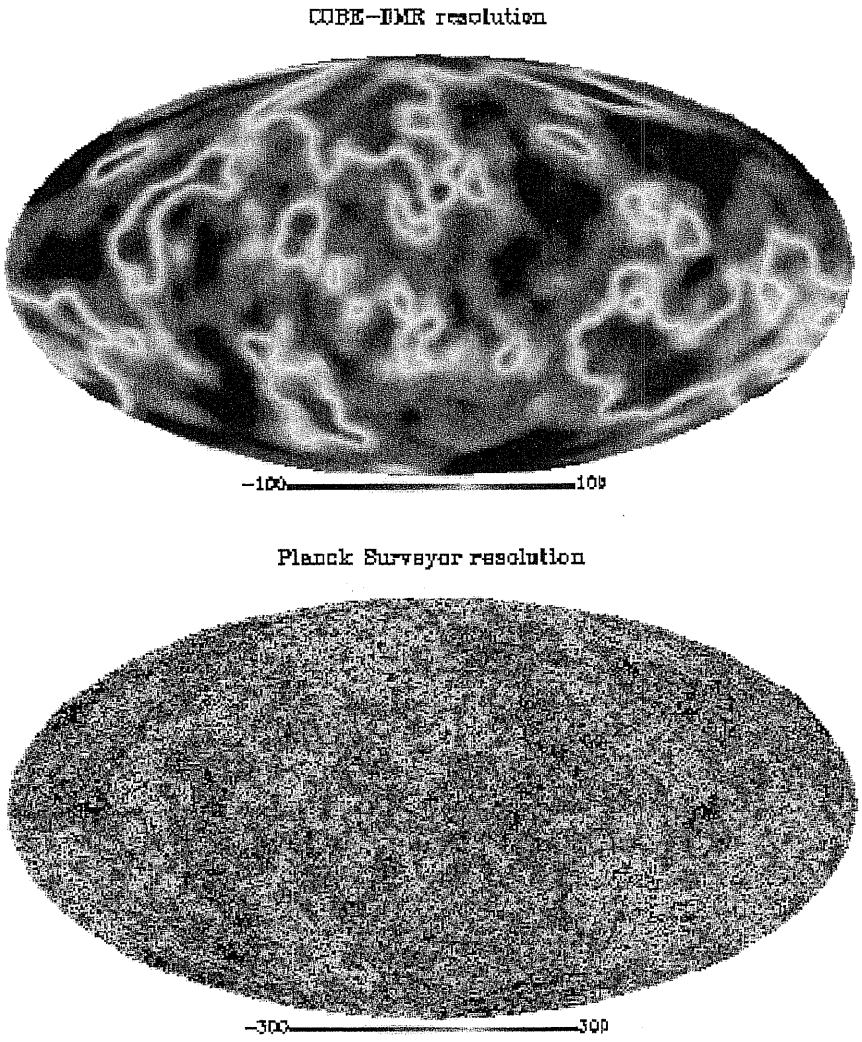

Figure 7.3: Comparison of COBE/DMR and Planck angular resolution: the same CMB pattern (here, a simulation of the Standard Cold Dark Matter Model) is observed at the COBE/DMR (upper panel) and Planck (lower panel) resolution.

formation relevant to several cosmological and astrophysical issues, such as testing theories of the early universe and the origin of cosmic structures. Other cosmological observations, such as the Sloan Digital Sky Survey [194] that will provide an improved measurement of the mass power spectrum, may not be as precise as those of the CMB anisotropies, but generally they do not share the same degeneracy.

Finally, we wish to mention a space mission which is now being considered, that would increase the discovery rate for Type Ia supernovae to about 2,000 per year, i.e. the SuperNova Acceleration Probe (SNAP) Satellite [203]. Discovery of so many more supernova would help eliminate possible alternative explanations, give experimental measurements of several other cosmological parameters, and put strong constraints on possible cosmological models. The SNAP satellite would be a space based telescope with a one square degree field of view with 1 billion pixels. Such a satellite would also complement the results of proposed experiments to improve measurements of the cosmic microwave background.

The work contained in this thesis is motivated by an observational evidence; if current observational trends continue, determining the nature of the missing energy may be the biggest challenge of the next decades. It is therefore fundamental, now as often in the past history of the Physics, that theory and many independent observations proceed together, and we all are impatiently looking ahead to a time when high precision measurements on different grounds will help to understand the mystery of this strange energy enclosed in the vacuum.

Bibliography

[1] Accetta F. S.,Trester J. J.,1989,Phys. Rev. D 39, 2854;

[2] Aguirre A.N., 1999, Ap. J., 512, L19

[3] Aguirre A.N.,1999, Ap. J., 525, 583

[4] Aguirre A.N., Haiman Z., 1999, astro-ph/9907039

[5] Albrecht A., Steinhardt P., 1982, Phys. Rev. Lett., 48, 1220

[6] Aldering G., Nugent R., Knop R.A., 2000, Astron. J., 119, 2110

[7] Amendola L., 1999, Phys.Rev.D60, 043501

[8] Anderson G.W. & Carroll S.M., 1997, 1997, astro-ph/9711288

[9] Baccigalupi C., Bedini L., Burigana C., De Zotti G., Farusi A., Maino D., Maris M., Perrotta F., Toffolatti L., Tonazzini A., 2000, MNRAS, in press, astro-ph/0002257

[10] Baccigalupi C., Matarrese S., Perrotta F., 2000, Phys.Rev.D in press, astro-ph/0005543

[11] Bahcall N.A., Fan X., 1998, Ap.J., 504, 1

[12] Bahcall N.A., Fan X., 1998, Proc.Nat.Acad.Sci., 95, 5956

[13] Bahcall N.A., Fan X., Cen R., 1997, Ap.J., 485, L53

[14] Balbi A. et al., 2000, submitted to Ap.J.Letters, astro-ph/0005124

[15] Balbi A., Baccigalupi C., Matarrese S., Perrotta F. Vittorio N., 2000, submitted to Ap.J.Letters

[16] Bardeen J.M. 1980, Phys.Rev.D 22, 1882

[17] Bardeen J.M., 1986, proceedings of the Inner Space/Outer Space, ed. E. W. Kolb, M. Turner, D. Lindley, K. Olive, D. Seckel, University of Chicago Press, 212

[18] Bartelmann M., Huss A., Colber J. M., Jenkins A., Pearce F., 1998, A& A, 330, 1

[19] Bartolo N. & Pietroni M., 2000, Phys.Rev. D, 61, 023518

[20] Bertschinger E., Dekel A., 1989, Ap.J., 335, L5

[21] Binétruy P., 1998, hep-ph/9810553

[22] Birrel N. D., Davies P.C., 1982, *Quantum Fields in Curved Spaces*, Cambridge Univ. Press

[23] Blanchard A. & Bartlett J.G., 1997, A& A, 322, L49

[24] Blanton M., Cen R., Ostriker J.P., Strauss M., 1998, Ap.J., 522, 590

[25] Blumenthal G.R., Faber S., Primack J.R., Rees M.J., 1994, Nature, 311, 517

[26] Bond J.R., Efstathiou G., 1987, MNRAS, 226, 655

[27] Bond J.R., Carr B.J., Hogan C.J., 1991, Ap.J., 367, 420; Franceschini A. et al., 1991, A& A Supp., 89, 285

[28] Bond J. R., Jaffe A. H., Phil.Trans.R.Soc.Lond.A, astro-ph/9809043

[29] Borgani S. et al. , 1999, astro-ph/9908155

[30] Born M, Wolfe E.,1980, *Principles of optics*, Pergamon Press

[31] Bouchet F.R., Prunet S., Sethi S.K., 1998, MNRAS, 302, 663, astro-ph/9809353

[32] Branch D., Tammann G.A., 1992, Ann.Rev.Astron.Astrophys., 30, 359

[33] Brandt W.N. et al., 1994, Ap.J., 424, 1

[34] Brans C. & Dicke R.H., 1959, Phys.Rev., 124, 925; Jordan P., 1959, Z.Phys., 157, 112

[35] Broadhurst T., Jaffe A.H., astro-ph/9904348

[36] Burles S. et al., 1999, Phys.Rev.Lett., 82, 4176

[37] Caldwell R.R., Dave R. & Steinhardt P.J., 1998, Phys.Rev.Lett. 80, 1582

[38] Carlberg R.G., Morris S.M., Yee H.K., Ellingson E., 1997, Ap.J., 479, L19

[39] Carlberg R.G. et al., 1996, Ap.J., 462, 32

[40] Carroll S.M., 2000, submitted to Living Reviews in Relativity, astro-ph/0004075

[41] Carroll S.M., 1998, Phys.Rev.Lett., 81, 15, 3097

[42] Carroll S.M., Press W.H., Turner E.L., 1992, Ann.Rev. Astron.Astrophys., 30, 499

[43] Carvalho J., Lima J., Waga I.,1992,Phys. Rev. D, 46, 2404

[44] Cen R., Ostriker J.P., 2000, Ap.J. 538, 83, astro-ph/9809370

[45] CHANDRA home page: http://chandra.nasa.gov/

[46] Chandrasekhar S., 1960, *Radiative Transfer*, Dover, New York Press

[47] Chen X., Kamionkowski M., 1999, Phys.Rev.D60, 104036, astro-ph/9905368

[48] Chen W., Wu Y., 1990, Phys.Rev. D, 41, 695

[49] Chiba T., 1999, Phys. Rev.D, 60, 083508

[50] Chiba M., Yoshii Y., 1999, Ap.J., 510, 42

[51] Coble K., Dodelson S. & Friemann J., 1997, Phys.Rev. D55, 1851

[52] Cohn J. D., 1998, Astrophys.S. Sci., in press, astro-ph/9807128

[53] Colafrancesco S., Mazzotta P., Vittorio N., 1997, Ap.J., 488, 566

[54] Copeland E.J., Liddle A.R. & Wands D. 1998, Phys.Rev.D 57, 4686

[55] Croft R.A.C., et al., 1998, Ap.J., 520, 1

[56] da Costa L.N. et al., 1998, MNRAS, 299, 425

[57] Damour T., Gibbons G.W. ,Gundlach C., 1990, Phys.Rev.Lett. 64, 123; Piccinelli G., Lucchin F., Matarrese S., 1992, Phys.Lett.B, 277, 58

[58] Davis M. et al., 1985, Ap.J., 292, 371

[59] Davis M., Nusser A., Willik J., 1993, Ap.J., 473, 22

[60] De Bernardis P. et al., 2000, Nature 404, 955

[61] De Ritis R., Marino A.A., Rubano C., Scudellaro P., 1999, submitted to Phys.Rev.D, hep-th/9907198

[62] Dekel A., Rees M.J., 1994, Ap.J., 422, L1

[63] Dekel A., Burstein D., White S.D., 1996, proceedings of the Princeton 250th Anniversary conference, June 1996, ed. Turok N., World Scientific Publishing, astro-ph/9611108

[64] Dickie R.H., Peebles P.J.E., Roll P.J., Wilkinson D.T., 1965, Ap.J., 142, 414

[65] Dolgov A. D., 1997, Lecture presented at the 4^{th} Colloque Cosmologie, Paris, astro-ph/9708045

[66] Dolgov A.D., 1983, proceedings of the meeting The Very Early Universe, eds. Gibbons G.W., Hawking S. W., Siklos S.T.C., Cambridge University Press, p.449.

[67] Dolgov A. D.,1989, Proceedings of the XXIVth Rencontre de Moriond; Series: Moriond Astrophysics Meetings, Les Arcs, France

[68] Drell P.S., Loredo T.J., Wasserman, 2000,Ap.J., 530, 593

[69] Efstathiou G., 1999, MNRAS 310, 842

[70] Efstathiou G., Bond J.R., 1986, MNRAS, 218, 103

[71] Einstein A., 1916, Annalen Der Physik,49,769

[72] Einstein A., 1917 Sitz.Preuss.Akad.d.Wiss.Phys.Math, 142

[73] Eke V.R., Cole S., Frenk C.S., Henry J.P., 1998, astro-ph/9802350

[74] Ellis G.F.R., 1971, proceedings of the XLVII International School of Physics Enrico Fermi, Varenna on Lake Como, edited by Sachs B.K..

[75] Ellis G.F.R. et al., 1984, Phys.Lett.B134, 429; Witten E., 1985, Phys.Lett.B155, 151; Nishino H., Sezgin E., 1984, Phys.Lett.B144, 187

[76] EMSS home page: http://www.tac.dk/lars_c/gammabox/doc/emss.html

[77] Evrard A.E., 1997, MNRAS, 292, 289

[78] Evrard A.E., Metzler C.A., Navarro F.J., 1996, Ap.J., 469, 494

[79] Falco E.E., Kochanek C.S., Munoz J.A., 1998, Ap.J., 494, 47

[80] Fan X., Bahcall N.A., Cen R., 1997, Ap.J., 490, L123

[81] Faraoni V., Gunzig E., Nardone P., 1998 Fund.Cosm.Phys., in press, gr-qc/9811047

[82] Ferreira P.G. & Joyce M. 1998, Phys.Rev.D58, 023503

[83] Fixsen D.J. et al., 1996, Ap.J., 473, 576

[84] Flores R.A., Maller A.H., Primack J.R., 1999, astro-ph/9909397

[85] Freese K., Adams F.C., Frieman J.A., Mottola E., 1987, Nucl.Phys.B, 287, 797

[86] Frenk C.S., White S.D.M., Efstathiou G., Davis M., 1990, Ap.J., 351, 10

[87] Fukugita M., Hogan C.J., Peebles P.J.E., 1997, Ap.J., 503, 518

[88] Garcia-Bellido J., 1997, Phys.Rev.D55, 4603

[89] Garnavich P.M. et al., 1998, Ap.J., 509, 74

[90] Garnavich P.M. et al., 1998, Ap.J., 493, L53

[91] Gaztanaga E., Frieman J., 1994, Ap.J., 437, L13

[92] Gell Mann M., Oakes R.J., Renner B., 1968, Phys.Rev., 175, 2195

[93] Gillies G.T., 1997, Rep.Prog.Phys., 60, 151.

[94] Golfand Y.A., Likhtman E.P., 1971, Pis'ma ZhETF, 13, 452

[95] Gouda N., Sugiyama N., Sasaki M., 1991, Prog.Theor. Phys., 85, 1023

[96] Gravitational Lens Data Base:
http://cfa-www.harvard.edu/glensdata

[97] Gross M.A.K., Somerville R.S., Primack J.R., Borgani S., Girardi M., 1997, proceedings of 12th Potsdam Cosmology Workshop, astro-ph/9708254

[98] Gunn J.E., Peterson B.A., 1965, Ap.J., 142, 1633

[99] Guth A., 1981, Phys.RevD23, 247

[100] Hamuy M. et al.,1996, Astron.J., 112, 2348

[101] Hanany S. et al., 2000, submitted to Ap.J.Lett., astro-ph/0005123

[102] Hatano K., Fisher A., Branch D., 1997, MNRAS, 290, 360

[103] Henry J.P., 1997, Ap.J., 489, L1

[104] Hill C. & Ross G., 1988, Nucl.Phys. B311, 253; Hill C. & Ross G., 1988, Phys.Lett.B203, 125; Friemann J., Hill C.T., Stebbins A. and Waga I., 1995, Phys.Rev.Lett.75, 2077; Estrada J., Masperi L., 1998, Mod.Phys.Lett. A13, 423, hep-ph/9710522

[105] Hobson M.P., Jones A.W., Lasenby A.N., Bouchet F.R., 1998, MNRAS, 3000, 1

[106] Holz D.E., Wald R.M., 1998, Phys.Rev.D58, 063501

[107] Hu W., 1998, Ap.J.506., 485, astro-ph/9801234

[108] Hu W., Seljak U., White M. & Zaldarriaga M., 1997, Phys.Rev.D56, 596, astro-ph/9709066

[109] Hu W., Sugiyama N., 1995, Phys.Rev.D, 51, 2599

[110] Hu W., Sugiyama N. & Silk J. 1997, Nature 386, 37; see also Hu W., 1996, proceedings of the meeting The Universe at High-z, Large Scale Structure and the Cosmic Microwave Background, eds. Martinez-Gonzalez E., Sanz J.L., Springer-Verlag, 207 astro-ph/9511130

[111] Hu W., White M., 1996, Ap. J., 471, 30

[112] Hu W., White M., 1997, Phys.Rev.D, 56, 596

[113] Hu W., White M., 1997, New Astron., 2, 323

[114] Hubble E.P., 1929, Proc.Natl.Acad.Sci., 15, 168

[115] Huey G., Wang L., Dave R., Caldwell R.R., Steinhardt P.J.,1999, Phys.Rev.D59, 063005

[116] Hwang J.C., 1991,Ap.J.375, 443; Hwang J.C., 1996, Phys.Rev.D53, 762

[117] Hwang J.C., 1990, Class.Quant.Grav.7, 1613

[118] Jaffe A. et al., 2000, submitted to Phys.Rev.Lett., astro-ph/0007333

[119] Jimenez R., 1998, IOP proc.series, in press astro-ph/9810311

[120] Jungman G., Kamionkowski M., Kosowsky A., Spergel D. N., 1996, Phys.Rev.Lett. 76, 1007

[121] Kaiser N., 1983, MNRAS, 202, 1169

[122] Kaiser N., 1986, proceedings of the Inner Space/Outer Space, ed. Kolb E.W., Turner M., Lindley D., Olive K., Seckel S. University of Chicago Press, 258

[123] Kamionkowski M., Kosowsky A., 1998, Phys.Rev.D67, 685

[124] Kamionkowski M., Kosowsky A., Stebbins A., 1997, Phys.Rev.D55, 7368

[125] Kamionkowski M., Spergel D.N., Sugiyama N., 1994, Ap.J.Lett., 426, L57

[126] Kantowski R., 1998, Ap.J., 507, 483

[127] Kibble T.W.B., 1976, J.Phys. A, 9, 1387

[128] Kirzhnits D.A., Linde A.D., 1972, Phys.Lett., 42B, 471

[129] Kirzhnits D.A., 1972, Pis'ma ZhETF, 15, 745

[130] Kochanek C.S., 1993, Ap.J., 419, 12

[131] Kochanek C.S., 1996, Ap.J., 466, 638

[132] Kochanek C.S., 1999, proceedings of the meeting After the Dark Ages, ed. S. S. Holt S.S. & Smith E.P., AIP Conf. Proc. 470, 163

[133] Kodama I. & Sasaki M., 1984 Progr.Theor.Phys.Supp. 78, 1

[134] Kolb E.W., Turner M.S., 1990, *The Early Universe*, Addison-Wesley, Redwood City, California

[135] Kosowsky A., 1996, Ann.Phys., 246, 49

[136] Krauss L. M., 1998, Proceedings of the Tropical Workshop on Particle Physics and Cosmology and Particle Physics, San Juan; WEIN 98, Santa Fe, hep-ph/9807376

[137] La D., Steinhardt P.J., 1989, Phys.Rev.Lett., 62, 376

[138] Lange A.E. et al., 2000, submitted to Phys.Rev.D, astro-ph/0005004

[139] Lawson K.D., Mayer C.J., Osborne J.L., Parkinson M. L., 1987, MNRAS, 225, 307; Hankock S. et al., 1994, Nature, 367, 333; Davies R.D. et al. 1996, MNRAS, 278, 883; Davies R.D., Watson R.A., Gutierres C.M., 1996, MNRAS, 278, 925

[140] Leibundgut B., proceedings of Supernovae and Cosmology, eds. Labhardt L., Binggeli B., Buser R., University of Basel, Basel., astro-ph/9801069

[141] Liddle A.R., Mazumdar A. & Barrow J.D., 1998, astro-ph/9802133

[142] Liddle A.R., Scherrer R.J., 1999, Phys.Rev.D59, 023509

[143] Lilly S. et al., 1995, Ap.J., 455, 108

[144] Linde A., 1982, Phys.Lett.B108, 389

[145] Lineweaver C.H., 1998, Ap.J., 505, L69

[146] Lubin L. et al., 1996, Ap.J., 460, 10

[147] Lyth D., 1985, Phys.Rev.D31, 1792

[148] Ma C.P. & Bertschinger E., 1995, Ap.J., 455, 7

[149] Maller A., Flores R., Primack J. R., 1997, Ap.J., 486, 681

[150] Maoz D., Rix H.W., 1993, Ap.J., 416, 425

[151] MAP home page: http://map.gsfc.nasa.gov/ ;
Planck Surveyor home page:
http://astro.estec.esa.nl/SA-general/Projects/Planck/

[152] Masiero A., Pietroni M., Rosati F., 2000, Phys.Rev.D61, 023504

[153] Melchiorri A., Vittorio N., 1997, proceedings of The Cosmic Microwave Background, Kluwer Academic Press, eds Lineweaver C.H., Bartlett J.G., Blanchard A., Signore M., and Silk J., 41

[154] Meneghetti M. et al., 2000, MNRAS, 314, 338, astro-ph/9907324

[155] Microwave Anisotropy Probe home page:
http://map.gsfc.nasa.gov;

[156] Planck Surveyor home page:
http://astro.estec.esa.nl/SA-general/Projects/Planck

[157] Mohr J.J., Mathiesen B., Evrard A.E., 1999, Ap.J., 517, 627

[158] Mohr J.J., Haiman Z., Holder G.P., 1999, contribution to PASCO99 meeting, astro-ph/0004244

[159] Mollerach S. 1990, Phys. Lett. 242B, 158

[160] Mukhanov V.F., Feldman H.A. & Branderberger R.H., 1992 Phys.Rep. 215, 203

[161] Oukbir J., Blanchard A., 1992, A & A, 262L

[162] Özer M., Taha M. O., 1987, Nucl.Phys. B, 287, 776

[163] Padmanabahn T. , 1993, *Structure formation in the Universe*, Cambridge University Press

[164] Peacock J., 1997, MNRAS, 284, 885

[165] Peacock J., Dodds S., 1994, MNRAS, 267, 1020

[166] Peebles P.J.E., Ratra B., 1988, Ap.J.352, L17

[167] Peebles P.J.E. & Yu, 1970, Ap. J.,162,815

[168] Peebles P.J.E.,1994, *Principles of Physical Cosmology*, Princeton University Press

[169] Penzias A.A., Wilson R.W., 1965, Ap.J., 142, 419

[170] Perlmutter S. et al., 1995, Ap.J.Lett., 440, L41

[171] Perlmutter S. et al., 1998, Nature 391, 51; Perlmutter S. et al., 1997, Ap.J. 483, 565

[172] Perlmutter S. et al., 1999, Ap.J., 517, 565;
Perlmutter S., Turner M.S. & White M., 1999, Phys.Rev.Lett.83, 670

[173] Perrotta F., Baccigalupi C., 1999, Phys.Rev.D 59, 123508

[174] Perrotta F., Baccigalupi C., Matarrese S., 2000, Phys.Rev.D61, 023507

[175] Phillips M.M., 1993, Ap.J.Lett., 413, L105

[176] Press W. & Vishniac E.T., 1980, Ap.J., 239, 1

[177] Ratra B., Quillen A., 1992, MNRAS, 259, 738

[178] Ratra B., Peebles P.J.E., 1988, Phys.Rev.D37, 3406

[179] Reichart et al., 1998, Ap.J., 518, 521, astro-ph/9802153

[180] Reynolds R.J., 1989, Ap.J.Lett., 339, L29; Valls-Gabaud D., 1998, Publications of the Astronomical Society of Australia, 15, 111; Kogut A., Banday A. J., Bennet C., Gorsky K.M., Hinshaw G., Smoot G.F., Wright E.I., 1996, Ap.J.Lett., 464, L5; L.Veeraraghavan, R. D. Davies, 1997, in proceedings of the PPEUC conference, University of Cambridge, available at http://www.mrao.cam.ac.uk/ppeuc/proceedings/cmb_prog.html;
Draine B. T., Lazarian A.,Ap. J. Lett., 494, L19; Rybicki G.B., Lightman A., 1979, *Radiative Processes in Astrophysics*, New York, Wiley.

[181] Reuter M., Wetterich C., 1987, Phys.Lett.B188, 38

[182] Riess A.G. et al., 1998, Astron.J., 116, 1009

[183] Riess A.G. et al., 2000, Ap.J., in press, astro-ph/0001384

[184] Riess A.G., Press W.H., Kirshner, 1996, Ap.J., 473, 88

[185] Riess A.G., Filippenko A.V., Li W., Schmidt B.P., 1999, Astron.J., 118, 2668

[186] Roll P.G., Krotkov R., Dicke R.H., 1964, Ann.Phys. 26, 442.

[187] Sachs R.K., Wolfe A.M., 1990, Ap.J., 360. 685

[188] Sahni V., StarobinskiA., 1999, Int.J.Mod.Phys.D, in press, astro-ph/9904398

[189] Santiago D.I., Silbergleit A., 2000, Phys.Lett.A268, 69, gr-qc/9811046

[190] Sarkar S., 1996, Rep.Prog.Phys.59, 1493

[191] Schade D. et al., 1996, Ap.J., 464, L63

[192] Schmidt B.P. et al., 1998, Ap.J., 507, 46

[193] Schramm D.N., Turner M.S., 1998, Rev.Mod.Phys., 70, 303

[194] SDSS home page: http://www.sdss.org/ ;
2dF home page: http://msowww.anu.edu.au/ c̃olless/2dF/

[195] Seckel D., Turner M., 1985, Phys.Rev.D, 32, 3178

[196] Seljak U., Zaldarriaga M., 1997, Phys.Rev.Lett., 78, 2054

[197] Seljak U.,Zaldarriaga M., 1996, ApJ, 469, 437

[198] Shifman M.A., Vainshtein A.I., Zakharov V.I., 1978, Nucl.Phys.B147, 385

[199] Silveira V., Waga I., 1997, Phys.Rev.D56, 4625

[200] Silveira V., Waga I., 1994, Phys.Rev.D50, 4890

[201] Simonsen J.T., Hannestad S., 1999, A & A, 351, 1

[202] Smoot G. F. et al., 1992, Ap.J.Lett., 396, L1; Bennet C. L. et al., 1996, Ap.J.Lett., 464, L1

[203] SuperNova Acceleration Probe SATellite web page, http://snap.lbl.gov/

[204] Spokoiny B.J., 1984, Phys.Lett. B147, 39; Accetta F.S., Zoller D.J., Turner M.S., 1985, Phys. Rev.D31, 3064; Pollock M.D., 1985, Phys.Lett.B156, 301; Lucchin F., Matarrese S., Pollock M.D., 1986, Phys.Lett.B167, 163

[205] Steidel C.C., Dickinson M., Persson S.E., 1994, Ap.J., 437, L75

[206] Steinhardt P.J., Wang L., Zlatev I., 1999, Phys.Rev.D59, 123504

[207] Sunyaev R.A., Zel'dovich Ya.B., 1972, Comm.Astroph.Sp.Phys., 2, 66

[208] Taylor T.R., Veneziano G., Yankielowicz S., 1983, Nucl.Phys.B218, 493; Affleck I., Dine M., Seiberg N., 1984, Phys.Rev.Lett., 51, 1026, Nucl.Phys.B241, 493

[209] Toffolatti L. et al., 1994, proceedings of the 1993 Capri Workshop on the cosmic microwave background, Astrophys.Lett. & Comm., in press, astro-ph/9410037

[210] Totani T., Kobayashi C., 1999, Ap.J., 526, L65

[211] Tegmark M., Eisenstein D., Hu W., 1998, proceedings of the meeting Fundamental parameters in Cosmology, astro-ph/9804168

[212] Tegmark M., Eisenstein D., Hu W., Kron R., 1998, submitted to Ap.J.Lett., astro-ph/9805117

[213] Tegmark M., Efstathiou G., 1996, MNRAS, 281, 1297

[214] Tegmark M., 1997, Ap.J.Lett., 480, L87

[215] Tegmark M., 1998, Ap.J., 502, 1

[216] Tegmark M., 1999, Ap.J.Lett., 514, L69

[217] Turner M. & White M., 1997, Phys.Rev.D56, 4439

[218] Turner M., Wilczek F., Zee A., 1983, Phys.Lett.B, 125, 35; Axenides M., Brandenberger R., Turner M., 1983, Phys.Lett.B126, 178

[219] Tytler D., Fan M., Burles S., 1996, Nature, 381, 207; Burles S., Tytler D., 1997, Ap.J., 499, 699; Burles S., Tytler D., 1997, Ap.J., 507, 732; Burles S., Tytler D., 1998, SSRv, 84, 65B

[220] Uzan J.P., 1999, Phys.Rev.D59, 123510

[221] Viana P.T.P. & Liddle A.R., 1998, Phys.Rev.D57, 674

[222] Viana P.T.P., Liddle A. R., 1999, MNRAS. 303, 535

[223] Volkov D.V., Akulov V.P., 1972, Pis'ma ZhETF, 16, 621

[224] Wang L., Caldwell R.R., Ostriker J. P., Steinhardt P.J., 2000, Ap.J., 530, 17

[225] Wang L., Steinhardt P.J., 1998, Ap.J., 508, 483

[226] Weinberg D.H. et al., 1999, Ap.J., 522, 563

[227] Weinberg E.J., 1989, Phys.Rev.D40, 3950

[228] Weinberg S., 1989, Rev.Mod.Phys., 61, 1

[229] Weiss N., 1989, Phys.Rev.D, 39, 1517

[230] Wess J., Zumino B., 1974, Phys.Lett.49, 52

[231] Wetterich C., A & A, 1995, 301, 321

[232] Wetterich C., 1988, Nucl.Phys.B, 302, 668

[233] White S.D.M. et al., 1993, Nature, 366, 429

[234] White S.D.M., Efstathiou G., Frenk C.S., 1993, MNRAS, 262, 1023

[235] White M., Scott D., 1996, Comm.Astrophys., 19, 289

[236] White M., Hu W., 1997, A& A, 321, 8

[237] White M., 1998, Astrophys.J., 506, 495, astro-ph/9802295

[238] Will C.M., 1984, Phys.Rep., 113, 345; Damour T., 2000, Nucl.Phys., 80, 41; Damour T., 1998, Eur.Phys.J. C3, 113; Damour T., 1990, proceedings of the meeting New and exotic phenomena '90, 280; Reasenberg R.D. et al., 1979, Ap.J. 234, L219

[239] Willick J. et al., 1997, Ap.J., 486, 629; Willick J. et al., 1999, Astrophys.J.S., 109, 333

[240] Willick J., Strauss M., 1998, Ap.J., 463, 404

[241] Wilson M.L., 1983, Ap.J., 273, 2

[242] Wilson M.L. & Silk J., 1981, Ap.J., 243, 14

[243] XMM home page: http://astro.estec.esa.nl/XMM/xmm.html

[244] Zaldarriaga M. & Seljak U., 1997, Phys.Rev.D55, 1830

[245] Zaroubi S. et al., 1997, Ap.J., 486, 21

[246] Zee F., 1979, Phys.Rev.Lett., 42, 417

[247] Zehavi I., Deckel A., 1999, Nature, 401, 252, astro-ph/9904221

[248] Zeldovich Y.B., 1967, JETP Lett., 6, 316

[249] Zlatev I., Wang L., Steinhardt P.J., 1998, Phys.Rev.Lett., 82, 896, astro-ph/9807002

Acknowledgements

I would like to thank all the people who helped and stimulated me during these years at SISSA.
The first special thought is for Carlo Baccigalupi, with whom much of the present work has been done. Carlo is one of the most motivated scientist I know. More, he has always been a guide for me, suffering with me in the hard task of understanding even a small piece of the Universe.
He has been, and is, the most important person for my work, and for my life.

The second special thought is for Sabino Matarrese, who introduced me to the study of an ambitious science like Cosmology. He has been a reference point during these years, and most importantly during the difficult period of the beginning of my research activity. Much that I know about Cosmology, I've learnt from Sabino. He has been one of the most forming persons for me.

Gianfranco De Zotti deserves a special thank; he is more than a collaborator, he is a capable, humble and indefatigable worker. Furthermore, he is always able to provide good suggestions advises and stimulate the people around him with his enthusiasm, and I think he should be taken as an example.

Many thanks are due to Gigi Danese and Reno Mandolesi, who gave me the chance to enter the fascinating scientific area aimed to detect and analyze the relic radiation from the Big Bang; I hope to give them back a compensation for having believed in me.

I am extremely grateful to Andrew Liddle, in particular for his careful reading of this thesis, that certainly improved it, and for the kind hospitality at the Brighton University. Discussions with him are always extremely highlighting, and to Andrew goes all my esteem and my friendship.

I' m happy to acknowledge Nicola Vittorio and Amedeo Balbi of the Tor Vergata University in Rome, and the people working at the Astronomical Observatory of Trieste and at the IEI-CNR in Pisa.

My view of the modern cosmology has been influenced and enriched by many people over these years. I wish especially thank Matthias Bartelmann, Luca Amendola, Lauro Moscardini, Cedric Lacey, Carlo Burigana, Davide Maino, Stefano Borgani, Riccardo Valdarnini, Marco Bruni, Bruce Bassett, Elena Pierpaoli, Ruggiero De Ritis, Ester Piedipalumbo, Roberta Paladini and Pasquale Panuzzo.

Finally, I thank all the people of the Astrophysics sector of SISSA and of the administrative staff, as well as the computer staff, in particular Davide Poccecai, Fabio Lonzar and Marina Picek, who efficiently helped the work performed during my period at SISSA.